ADVANCES IN CHEMICAL PHYSICS

VOLUME XVII

Advances in CHEMICAL PHYSICS

EDITED BY

I. PRIGOGINE

University of Brussels, Brussels, Belgium

AND

STUART A. RICE

Department of Chemistry
and
The James Franck Institute
The University of Chicago
Chicago, Illinois

VOLUME XVII

INTERSCIENCE PUBLISHERS

A DIVISION OF JOHN WILEY AND SONS
NEW YORK • LONDON • SYDNEY • TORONTO

Library of Congress Catalogue Card Number: 58-9935

SBN 471 69922 5

Printed in the United States of America

10 9 8 7 6 5 4 3 2 1

INTRODUCTION

In the last decades, chemical physics has attracted an ever-increasing amount of interest. The variety of problems, such as those of chemical kinetics, molecular physics, molecular spectroscopy, transport processes, thermodynamics, the study of the state of matter, and the variety of experimental methods used, makes the great development of this field understandable. But the consequence of this breadth of subject matter has been the scattering of the relevant literature in a great number of publications.

Despite this variety and the implicit difficult of exactly defining the topic of chemical physics, there are a certain number of basic problems that concern the properties of individual molecules and atoms as well as the behavior of statistical ensembles of molecules and atoms. This new series is devoted to this group of problems which are characteristic of modern chemical physics.

As a consequence of the enormous growth in the amount of information to be transmitted, the original papers, as published in the leading scientific journals, have of necessity been made as short as is compatible with a minimum of scientific clarity. They have, therefore, become increasingly difficult to follow for anyone who is not an expert in this specific field. In order to alleviate this situation, numerous publications have recently appeared which are devoted to review articles and which contain a more or less critical survey of the literature in a specific field.

An alternative way to improve the situation, however, is to ask an expert to write a comprehensive article in which he explains his view on a subject freely and without limitation of space. The emphasis in this case would be on the personal ideas of the author. This is the approach that has been attempted in this new series. We hope that as a consequence of this approach, the series may become especially stimulating for new research.

Finally, we hope that the style of this series will develop into something more personal and less academic than what has become the standard scientific style. Such a hope, however, is not likely to be completely realized until a certain degree of maturity has been attained—a process which normally requires a few years.

At present, we intend to publish one volume a year, and occasionally several volumes, but this schedule may be revised in the future.

In order to proceed to a more effective coverage of the different aspects of chemical physics, it has seemed appropriate to form an editorial board. I want to express to them my thanks for their cooperation.

I. PRIGOGINE

CONTRIBUTORS TO VOLUME XVII

B. J. BERNE, Columbia University, New York, New York

MICHAEL H. COOPERSMITH, Department of Physics, University of Virginia, Charlottesville, Virginia

WILLIAM L. GREER, National Bureau of Standards, Washington, D.C.

G. D. HARP, Columbia University, New York, New York

STUART A. RICE, The James Franck Institute, University of Chicago, Chicago, Illinois

G. M. SCHNEIDER, Institute of Physical Chemistry, The University, Karlsruhe, Germany

CONTENTS

ADVANCES IN CHEMICAL PHYSICS

VOLUME XVII

Advance in Chemical Physics, Volume XVII
Edited by I. Prigogine, Stuart A. Rice

PHASE EQUILIBRIA IN FLUID MIXTURES AT HIGH PRESSURES

G. M. SCHNEIDER

Institute of Physical Chemistry, The University, Bochum, Germany

CONTENTS

I. INTRODUCTION

With the rapid development of experimental techniques, it has become possible to investigate the phase behavior of pure substances and mixtures in more and more extreme ranges of temperature and pressure. In some cases the pressure dependence of liquid–solid and solid–solid phase equilibria has been determined up to several hundred kilobars in static experiments and up to several megabars in shock waves. The pressures used in the study of fluid systems, however, are much lower. Although temperature and pressure are, in principle, equivalent variables, the pressure dimension, say above several hundred bars, has hardly been considered

for many years. Experimental difficulties and special interest in low pressure work because of practical applications are the primary reasons why the pressure range hitherto investigated has been limited.

Whereas in fluid one-component systems only liquid–gas equilibria exist,* three different types of two-phase equilibria have to be considered in fluid mixtures: liquid–gas, liquid–liquid, and the so-called "gas–gas" equilibria. They all have the common feature of existing between two fluid phases of different densities separated by a meniscus.†

The pressure dependence and critical phenomena of these three kinds of phase equilibria will be reviewed in Section II. Since mainly high-pressure work, say above 300 bars, will be discussed, liquid–liquid and gas–gas equilibria in particular will be considered. The critical phenomena of pure substances have been extensively reviewed elsewhere[1-3] and the solubility of solids in compressed gases was treated by Rowlinson and Richardson[4] in Volume 2 of this Series.

New developments during recent years have shown that the limits between these three forms of phase equilibria in fluid mixtures are not well defined at high pressures and temperatures, and it seems that many phenomena can only be understood if continuous transitions between these three types of phase equilibrium in fluid systems occur. This continuity between liquid–gas, liquid–liquid, and gas–gas equilibria is deduced from recent results in Section III.

A discussion of the thermodynamic background and of some theoretical calculations, especially for gas–gas equilibria, will be given in Section IV.

II. CRITICAL PHENOMENA IN FLUID MIXTURES

The definition of a critical point for mixtures is essentially the same as that for a pure component: At a critical point the intensive properties of two phases in equilibrium become identical. Whereas pure substances are characterized by a critical point for the equilibrium liquid–gas,‡ binary systems exhibit a critical line in the three-dimensional T-p-x space (where x = concentration), and systems with n components an $(n-1)$-dimensional

* The pressure dependence of transition temperatures in liquid crystals,[80] of polymerization temperatures (e.g., for liquid sulfur [91,27]), of ceiling temperatures of polymers,[79] etc., have also been studied, but these phenomena are not in the scope of this article.

† Under certain conditions, however, the phases can even have the same density (isopycnic systems, barotropic phenomena) or the same refractive index (isooptic systems); in isooptic systems the meniscus can be invisible.

‡ No critical point liquid–solid has been found up to now.

critical surface in the $(n + 1)$-dimensional T-p-x_1-x_2-$\cdots$-x_{n-1} space for all kinds of fluid–fluid equilibria.

In binary systems the critical points of the mixtures are situated at the extreme values of all isobaric $T(x)$-cuts or all isothermal $p(x)$-cuts through the two-phase region in the T-p-x space. The line that connects the critical points of all binary mixtures is the critical curve; a very simple example for the equilibrium liquid–gas is schematically given in Figure 1.

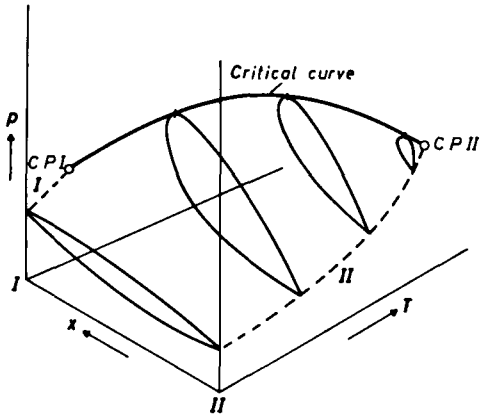

Fig. 1. p-T-x surface for the liquid–gas equilibrium of a simple binary mixture. (Dashed lines = vapor pressure curves of the pure components. CP = critical points of the pure components.)

The phase equilibria and the critical phenomena in fluid binary mixtures are most easily discussed with the aid of the $p(T)$-projections of these critical curves. The most important different types are schematically represented in Figures 2–8.* Most of them have already been discussed by Kuenen,[7] Büchner,[8] Ricci,[9] Zernike,[10] Rowlinson,[1] Kay,[11] Tsiklis and Rott,[12] Schneider,[5,6,104] Prausnitz[105] and others, and the reader is referred to these authors for details.

The formation of solid phases and the phenomena connected with the overlap of crystallization surfaces and critical liquid–gas regions are out of the scope of this review and will be considered only in some cases; the solubility of solids in critical and supercritical fluid phases (especially water) is extensively discussed elsewhere.[1,4,92,95]

* In all figures the critical curves are represented by solid lines, the phase diagrams of the pure components by dashed lines, and the three-phase lines by — · —; CP is the critical point of a pure component; A, B, C, D are critical end-points; and Q_1, Q_2 are quadruple points.

A. Liquid–Gas Equilibria

Because of their great industrial and scientific interest, liquid–gas equilibria have been extensively studied as a function of pressure up to the critical region,[1,7,9-11] and much work has been done for the related phenomena of the solubility of compressed gases in liquids.[82] The critical pressure of pure substances and mixtures is rarely higher than 200 bars, so that the pressure range necessary for these investigations is rather limited and was attainable by the experimental techniques available at the beginning of this century. Thus these phenomena are more or less out of the scope of this review and only a compilation of the different types of critical behavior as given in Figures 2 and 3 seems to be necessary.

The critical curves of all systems in Figure 2 correspond to liquid–gas

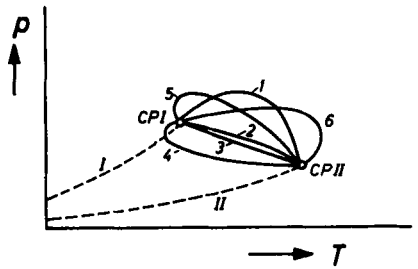

Fig. 2. $p(T)$-projection of the liquid–gas critical curves for binary systems (Schematic, see text)

equilibria and are continuous lines between the critical points of the pure components. Critical curves of Type 1 have a pressure maximum and have been found very often, e.g., ethane–*n*-heptane, CO_2–*n*-butane, ethane–acetone. For Type 2 the critical curve is monotonous, e.g., CO_2–propane, cyclopentane–cyclohexane, *n*-hexane–*n*-octane. The critical curve of Type 3 is a straight line; this type has been attributed to ideal systems and has been observed for binary mixtures with components differing only slightly in size, shape, and polarity, e.g., cyclohexane–methylcyclohexane, methylcyclopentane–*n*-hexane, benzene–toluene (see Kay[11]). The curves of Type 4 and 5 exhibit temperature minima either without an additional pressure maximum, e.g., acetone–*n*-hexane, ethane–CO_2 (Type 4) or with a pressure maximum, e.g., CO_2–N_2O (Type 5). Type 6 has a temperature maximum; only few examples are known (CH_3OCH_3–HCl[14], $CH_3OC_2H_5$–SO_2,[102] acetic acid-pyridine[100]). All types illustrated in Figure 2 have been extensively discussed in the literature[1,7,9-11] where references are also given; systems with azeotropes have also been considered.[15,1]

The critical curves for binary systems in which additional separation into two liquid phases occurs are schematically represented for several types in Figure 3. For these systems the critical curve can be interrupted and thereby consist of two branches. Only types known before 1963 are shown in Figure 3.[1] In Figure 3*a* the branch of the critical curve starting from the

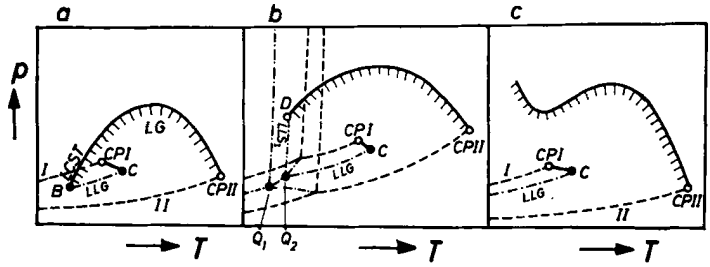

Fig. 3. $p(T)$-projections of the p-T-x surface of some binary systems showing liquid–liquid immiscibility. (Schematic, see text. B, C, D = critical end points. Q = quadruple points. $Q_1 = S_I S_{II} LG$, $Q_2 = S_I LLG$.) (*a*): Type found for *n*-hexane–methane,[16,17] etc. (*b*): Type resulting from 3*a* when B is displaced below the crystallization surface. (*c*): Type found for ethane–methanol.[7]

critical point of pure Component II runs through a pressure maximum and ends at a critical end-point B on the three-phase line LLG where two liquid and one gaseous phases are in equilibrium. The part of the critical curve near B corresponds to the pressure dependence of lower critical solution temperatures (LCST) for liquid–liquid immiscibility (LL) and merges directly into the critical curve liquid–gas (LG); the point B is normally situated near the critical point CP I of the pure Component I. Type 3b results when B is displaced to temperatures below the crystallization surface. Types 3a and 3b have been extensively studied and discussed by Kohn,[16] Rowlinson,[1,17] and others, and many examples are known for Type 3a (e.g., ethane–propanol, ethane–squalane, methane–*n*-hexane, methane–isooctane, propane–polyisobutene) and for Type 3b.* Type 3c was found by Kuenen[7] for the system ethane–methanol. This type of phase behavior will have a key position in the discussion in Section III.

B. Liquid–Liquid Equilibria

For the pressure dependence of liquid–liquid equilibria, only the classical work of Kohnstamm, Timmermans, and their co-workers[18–20] existed

* It has been shown that some examples cited for Type 3b[1,17] in reality belong to Type 3c[5,21e,61].

up to 1963. With only a few exceptions their measurements were limited to the pressure range below 200 bars; for only one system (triethylamine–H_2O) were results presented at pressures above 1300 bars, the maximum pressure being 2000 bars.[18] Further investigations up to 100 bars were performed by Hildebrand, Alder, Beams, and Dixon[81] and by Myers, Smith, Katz, and Scott.[28]

In spite of the limited pressure range of these measurements some general rules about the pressure dependence of immiscibility phenomena in liquid systems, particularly of critical solution temperatures (CST), were deduced from these results that are still to be found in books and review articles. According to Timmermans,[18] upper critical solution temperatures (UCST, T_c^{UCST}) may either rise with increasing pressure (Types 2–4 in Figure 4) or

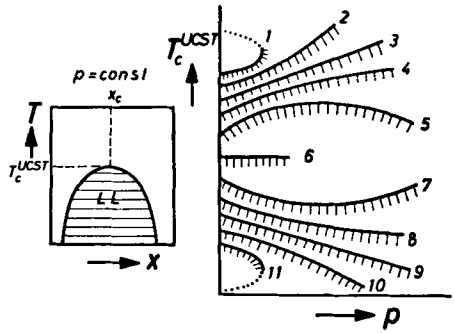

Fig. 4. Pressure dependence of upper critical solution temperatures UCST. (Isobaric $T(x)$-cut on the left. For Type 5 no example is known.)

remain constant within a limited pressure range (Type 6) or run through a temperature minimum (Type 7) or decline with increasing pressure (Types 8–10), whereas for lower critical solution temperatures (LCST, T_c^{LCST}) only an increase with increasing pressure was observed (Types 2–4 in Figure 5) and was said to be thermodynamically possible.[18] For almost all cases the pressure dependence of the CST is small and dT_c/dp only rarely exceeds $\pm 0.02°$/bar. An especially interesting pressure dependence was found by Kohnstamm and Timmermans[18] for some systems with closed solubility loops such as methyl ethyl ketone–H_2O: With increasing pressure the loop becomes smaller and smaller and finally disappears completely at a point HP in the T-p-x space where $dT_c/dp = \pm\infty$ (Type 1 in Figure 6, Type 11 in Figure 4; viz. 1 in Figure 5).[18,20,21a]

New measurements of the effects of high pressures on liquid–liquid immiscibility were started in 1963.[5,21–23] Pressures up to 7000 bars were

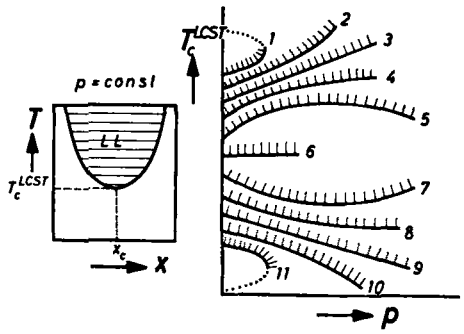

Fig. 5. Pressure dependence of lower critical solution temperatures LCST. (Isobaric $T(x)$-cut on the left. For Type 7 no example is known.)

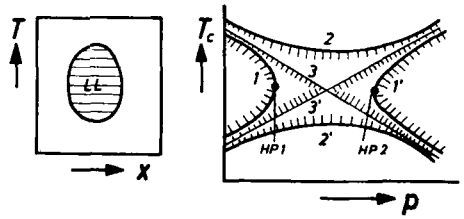

Fig. 6. Pressure influence on closed solubility loops. (Isobaric $T(x)$-cut on the left, see text.)

used and some types of the pressure dependence of immiscibility phenomena hitherto unknown were observed. In Figures 4–7 all types that are presently known are schematically represented. Examples exist for all types except for Type 5 in Figure 4 and Type 7 in Figure 5 (see Ref. 5).

$T_c^{\mathrm{LCST}}(p)$-curves running through temperature maxima, in contradiction to Timmerman's rule, were found for nicotine–H_2O, 4-methylpiperidine–H_2O, etc. (Type 5 in Figure 5).[21a] For triphenylmethane–sulfur dT_c^{LCST}/dp is already negative at normal pressure (Type 11 in Figure 5).[21d]

$T_c(p)$-curves of the types presented schematically in Figure 6 have been observed in methylpyridine–water systems.[21a,21b] Type 1-1′ in Figure 6 has been found for 2-methylpyridine–D_2O, the points HP1 and HP2 being situated at approximately 200 and 2000 bars, respectively.[21b] Binary mixtures of 2-, 3-, and 4-methylpyridine with H_2O and of 4-methylpyridine with D_2O exhibit $T_c(p)$-curves of Type 1′ in Figure 6, the Curve 1 being evidently displaced to negative pressures.[21a,21b] Type 2-2′ has been observed for 3-methylpyridine–D_2O and other systems.[21a,21b] Curves 3 and 3′

correspond to a transition type between 1-1′ and 2-2′. Recently similar systems have been studied by Steiner and Schadow[99] at pressures up to 1240 bars; immiscibility phenomena hitherto unknown were observed in the system methylisopropylketone-H_2O where $p(x)$-isotherms with two pressure maxima were found.

Type 1 in Figure 7 has been found for triphenylmethane–sulfur[21d] and Type 1′ is supposed to occur in hydrocarbon–methane systems.[5,21e,61]

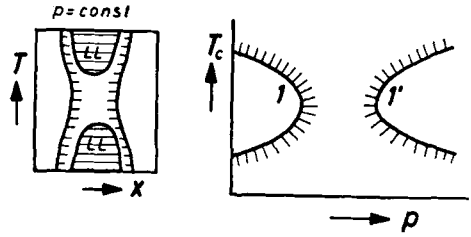

Fig. 7. Pressure influence on binary systems with two separate immiscibility regions where $T_c^{UCST} < T_c^{LCST}$. (Isobaric $T(x)$-cuts on the left.)

For further experimental material and a thermodynamic treatment of the results, the reader is referred to an article by Schneider[5] where a whole pattern of demixing phenomena in binary systems under pressure is derived and a review of the shapes of the immiscibility surfaces in the T-p-x space is given for binary systems. In this description allowance is made for the formation of solid[5,21e,22] and gaseous[5,6,21c,24-26] phases. Further investigations have shown that there are remarkable analogies in the influence of high pressures and of increasing amounts of an added third substance on the liquid–liquid equilibria of binary systems (e.g., of dissolved salts in aqueous mixtures of alcohols, organic bases, etc.).[23,27]

C. Gas–Gas Equilibria

The term "gas–gas equilibrium" or "immiscibility of gases" has been attributed to some phase separation effects in fluid systems at high pressures and temperatures, especially *above* the critical temperature of the less volatile substance.

The different types for binary mixtures are schematically given in Figure 8. The critical curve is interrupted and consists of two branches. The branch starting from the critical point of the more volatile Component I ends at a so-called critical end point C on the three-phase line LLG where two liquid and one gaseous phases are in equilibrium, whereas the branch

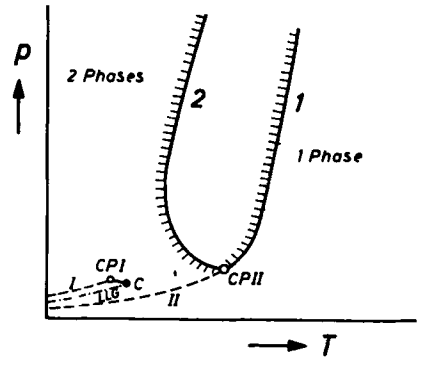

Fig. 8. $p(T)$-projections of the p-T-x surface for binary systems showing gas–gas equilibria of the first (Curve 1) or of the second (Curve 2) type.

beginning at the critical point of the less volatile Component II either immediately tends to higher temperatures and pressures (Curve 1 in Figure 8, so-called "gas–gas equilibrium of the first type") or goes through a temperature minimum first and then runs steeply to increasing pressures and temperatures even above the critical temperature of pure Component II (Curve 2 in Figure 8, so-called "gas–gas equilibrium of the second type"). In the following a temperature minimum on the branch of the critical curve that starts from CP II and a positive slope of the critical curve at high pressures are assumed to be characteristic for a gas–gas equilibrium of the second type irrespective of whether the initial slope at CP II is positive or negative.

These phase separation effects were predicted by van der Waals in 1894 from the fold theory[29] and were discussed in detail by Kamerlingh Onnes and Keesom in 1907[30]. Type 2 was found for the first time in 1940 by Krichevskii and co-workers[31] for the N_2–NH_3 system; their measurements were later extended to pressures up to 16 kbars by themselves and were reconfirmed by Lindroos and Dodge.[32] Type 1 was reported for the first time in 1952 by Tsiklis for the system He–NH_3.[34a] The existence of two separate fluid phases in these kinds of phase equilibrium was ultimately proved by the visual detection of a meniscus in 1953 by Tsiklis[34b] for the system He–C_2H_4 and by the determination of the surface tension between the two phases in 1963 by Tsiklis and Vasil'ev[33] for the systems He–C_2H_4 and He–CO_2.

In the meantime similar phase separation effects have been found in many other systems. Up to 1960 the Russian team headed by Krichevskii and Tsiklis was practically the only group in this field. At present gas–gas

equilibria are being investigated in several laboratories all over the world and the number of systems discovered is increasing continuously.

Gas–gas equilibria of the *first* type have been found in many binary mixtures of He, e.g., with NH_3, CO_2, C_2H_4, C_3H_8, C_6H_6, CH_3OH, SO_2, C_6H_{14}, some fluorinated compounds,[43] Xe (the most astonishing example being He–Xe[35]), and in the system Ar–H_2O[38a].* Gas–gas equilibria of the *second* type have been observed in binary mixtures of NH_3 with N_2, Ar, CH_4, etc.; of H_2O with CO_2, N_2, and numerous hydrocarbons; of CO_2 with *n*-hexadecane; of He with Ar and N_2; and in other systems. For He–CH_4 a critical $p(T)$-curve was observed that runs vertically to higher pressures[94] (see Figure 19); thus the gas–gas equilibrium found for this system is intermediate between the first and second type. At present approximately 40 systems are known that exhibit gas–gas equilibria. Most of them are cited in Table I, which owes much to an earlier published table[5] and to a recent compilation by Tsiklis and Rott[12]; the temperature range and the maximum pressure of the investigations and additionally the references are also given in Table I.

TABLE I

Systems in Which Gas–Gas Equilibria Have Been Found Experimentally

System	T(°C)	p_{max}(bar)	Ref.
A. Systems with Gas–Gas Equilibria of the First Type			
Helium–ammonia	125–175	10000	34*a*
Helium–carbon dioxide	25–100	10000	34*a*
Helium–ethylene	25–150	10000	34*b*
Helium–propane	100–150	7000	See 12,5
Helium–benzene	300	1000	,,
Helium–methanol	245	3000	,,
Helium–sulfur dioxide	175–200	7000	,,
Helium–*n*-hexane	245	3000	,,
Helium–xenon	5–65	2000	35
Helium–acetylene	36	64	See 12
Helium–ethane	32	51	,,
Helium–dinitrogen monoxide	37	74	,,
Helium–Freon 12	25–122	330	43
Helium–Freon 22	100	330	,,
Helium–Freon 114B_2	216–223	330	,,
Argon–water	270–440	3000	38*a*

* For Ar–H_2O Tsiklis and Prokhorov[38b] reported a gas–gas equilibrium of the second type whereas Lentz[38a] observed one of the first type.

TABLE I—*continued*

System	T(°C)	p_{max}(bar)	Ref.
B. Systems with Gas–Gas Equilibria of the Second Type			
Ammonia–nitrogen	90–175	16000	31*a*
Ammonia–methane	45–100	10000	See 12, 5
Ammonia–argon	70–140	10000	,,
Ammonia–nitrogen–hydrogen	90–120	5500	,,
Ammonia–nitrogen–methane	55–110	5500	,,
Sulfur dioxide–nitrogen	35–40	9000	,,
Helium–nitrogen	−196 to −151	830	93
Helium–argon	−182 to −126	650	36
Neon–krypton	−110 to − 63	1800	73
Carbon dioxide–*n*-hexadecane	20–100	1500	25
Water–nitrogen	300–350	6000	44*a*
Water–carbon dioxide	250–350	3500	42,83*b*
Water–ethane	200–400	3700	41
Water–*n*-butane	355–364	1100	41, 44*b*
Water–*n*-pentane	340–352	620	39
Water–2-methylpentane	330–355	500	39
Water–*n*-heptane	350–355	550	39
	350–420	1250	84
Water–propylene	325–350	2500	38*a*
Water–cyclohexane	130–363	200	58
	270–410	1800	84
Water–benzene	200–357	200	59
	287–300	735	39
	260–370	3700	26, 40
Water–toluene	305–310	455	39
	310–360	2000	40
Water–*o*-xylene	310–380	2000	40
Water-ethylbenzene	310–380	2000	40
Water–*n*–propylbenzene	320–400	2000	40
Water–1,3,5-trimethylbenzene	320–400	2000	40
C. Systems with Gas–Gas Equilibria Intermediate between First and Second Type			
Helium–methane	to − 82	170	84 (Fig. 19)

The critical $p(T)$-curves of many of the systems cited in Table I are plotted in Figures 9, 11, 12, 15, and 19. At elevated pressures all these curves run to higher temperatures and pressures, and no temperature maximum has been found for any of these systems even at the highest pressures; the most elevated pressure up to now is 16 kbars obtained in the measurements for

NH_3–N_2.[31a] Van der Waals originally proposed that the steeply ascending branch of the critical curve would run through a temperature maximum and a pressure maximum successively and should finally end on a three-phase line LLG with exhibition of LCST. No temperature maximum, much less any pressure maximum, has found to date, and thus his prediction seems to be incorrect; nevertheless, a temperature maximum is still possible but it would be situated at higher pressures where crystallization normally occurs.

The number of systems with gas–gas immiscibility will probably increase continuously in the future when progress in experimental techniques will allow the investigation of mixtures of compounds that differ more and more in size, shape and polarity, and the exhibition of gas–gas equilibria will be the rule rather than the exception for systems with relatively weak forces between unlike molecules (see Refs. 1, 36, 104).

Since high pressures are reached in these experiments, the molar volumes of the two phases are of the same order, and it depends on the average molecular weight of the separate phases if barotropic phenomena will be observed. Thus a barotropic behavior was frequently found in systems showing gas–gas immiscibility, especially if Component I consists of heavy and/or weakly interacting particles and Component II of comparatively light and/or strongly interacting molecules e.g., Ar–H_2O,[12,38] CO_2–H_2O,[42] CH_4–NH_3, N_2–NH_3, Ar–NH_3, He–H_2* (for references see Ref. 12). But barotropism is not necessarily combined with gas–gas immiscibility; barotropic phenomena have also been detected in binary and ternary systems with liquid–liquid equilibria.[90]

Gas–gas equilibria have been reviewed by Krichevskii,[31b] Rowlinson,[1] Streett,[36] Schneider,[5,6,104] and especially by Tsiklis and Rott.[12] The experimental techniques and equipments have been described by several authors.[12,13,24,26,35,39,40,41,42,61] Theoretical approaches have been presented by Rott,[45] Schäfer,[46] Kreglewski,[47] de Swaan Arons and Diepen,[35] Kaplan,[48] van Konynenburg and Scott,[49] Prausnitz,[105] and Zandbergen, Knaap, and Beenakker[50]; they will be reviewed in Section IV.

The origin and the nature of these gas–gas equilibria were obscure for many years. During recent years it has been shown that there are continuous transitions between liquid–gas, liquid–liquid, and gas–gas equilibria[1,5,6,37,40,61,104]; this continuity will be demonstrated in detail in Section III. A better understanding of these strange phase separation effects

* He–H_2 does not exhibit gas–gas immiscibility but only shows a tendency for a gas–gas equilibrium of the second type (see Figure 19). No barotropic behavior can be expected in other binary He systems such as those cited in Table I.[12,35]

is possible from this discussion which is also useful in resolving the problem of nomenclature. The terms "gas–gas equilibrium" or "immiscibility of gases" for phase separation effects of the types of Figure 8 have been proposed by Kamerlingh Onnes and Keeson[30] and are still used by some authors, especially the Russians. However, it has been criticized more and more as a misleading notation during recent years,[1,5,6,12,36,37,50,-52,89] and the discussion about this term contains polemics and misunderstandings. Lindroos and Dodge[32] were the first who proposed the term "fluid–fluid equilibrium" for phase separation phenomena of this kind; this notation has been adopted by many authors. Although this notation seems to be more logical the term "gas–gas equilibrium" will be nevertheless used throughout this article in order to retain a well defined and widely-used expression that is still preferred by the Russian pioneers in this field. However, it should be understood that the equilibrating phases in these kinds of phase equilibria are not gases in the common sense but highly compressed fluids of generally liquidlike densities; these effects are not restricted, however, to very high pressures but can be found at rather moderate pressures, e.g., for gas–gas equilibria of the first type just above the critical pressure of Component II (Type 1 in Figure 8).

III. RECENT RESULTS ON BINARY MIXTURES

In Section II the three possible types of two-phase equilibria in fluid systems, namely liquid–gas, liquid–liquid, and gas–gas, were briefly discussed. For years the limits between these different kinds of phase behavior appeared to have been well established. However, new measurements during recent years have shown that there are continuous transitions between these three types of phase equilibrium and that there is a real continuity between liquid–gas, liquid–liquid, and gas–gas equilibria.

In the present chapter this continuity will be demonstrated for some binary systems, e.g., for mixtures of hydrocarbons with substances of very different polarity, such as CH_4, CO_2, and H_2O,[6] and for mixtures of He with other condensed gases.[36]

A. Hydrocarbon–CO_2 Systems

The $p(T)$-projections of the critical curves of some binary mixtures of CO_2 with *n*-alkanes from methane through *n*-hexadecane are given in Figure 9 according to data taken from the literature. The curves presented exhibit a whole pattern of different types of critical behavior in binary systems and cover many of the types given schematically in Figures 2 and 3*c*.

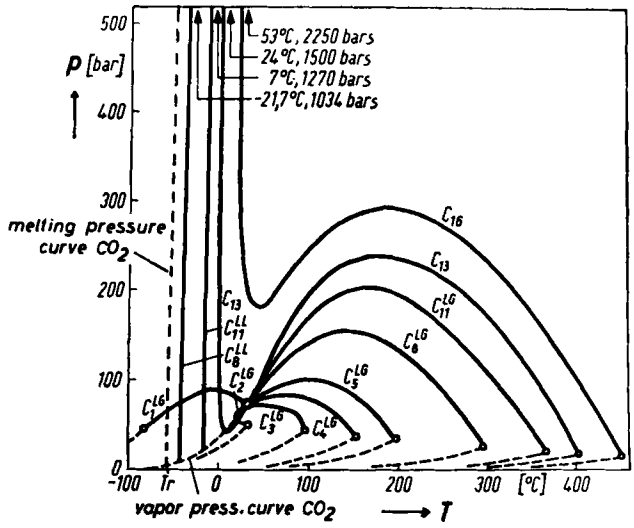

Fig. 9. Critical $p(T)$-curves for binary n-alkane–CO_2 mixtures.[25] ($C_n = n\text{-}C_nH_{2n+2}$; the temperatures and pressures at the curves indicate to what conditions the curves have been measured.)

Whereas the critical curve of ethane–CO_2 (C_2^{LG})[56] runs through a temperature minimum and that of propane–CO_2 (C_3^{LG})[54,55] is a monotonous line between the critical points of the pure components, the critical $p(T)$-curves for the equilibrium liquid–gas (LG) of methane–CO_2 (C_1^{LG}),[53] n-butane–CO_2 (C_4^{LG}),[54] n-pentane–CO_2 (C_5^{LG}),[54] n-undecane–CO_2 (C_{11}^{LG}),[24,25] and n-decane–CO_2[57] (not represented in Figure 9) run through pressure maxima; all these curves are continuous lines between the critical points of the pure components. The critical $p(T)$-curve of the system n-hexadecane–CO_2 (C_{16}),[24,25] however, has a much more complicated shape: Starting from the critical point of the pure hydrocarbon it first runs through the usual pressure maximum, and after that goes successively through a pressure minimum and a temperature minimum, and then tends steeply to higher temperatures and pressures.

In Figure 10 this unusual phase behavior is schematically deduced from a superposition of liquid–gas and liquid–liquid equilibria.[24,25] At temperatures far below the critical point of pure CO_2 the system n-octane–CO_2 separates into two liquid phases (see Figures 9, 10*a*, and 10*b*). The branch LL of the critical curve in Figure 10*b* (or the curve C_8^{LL} in Figure 9) corresponds to a pressure dependence of the UCST that is slightly raised with increasing pressure for the n-octane–CO_2 system.[24] For mixtures of CO_2

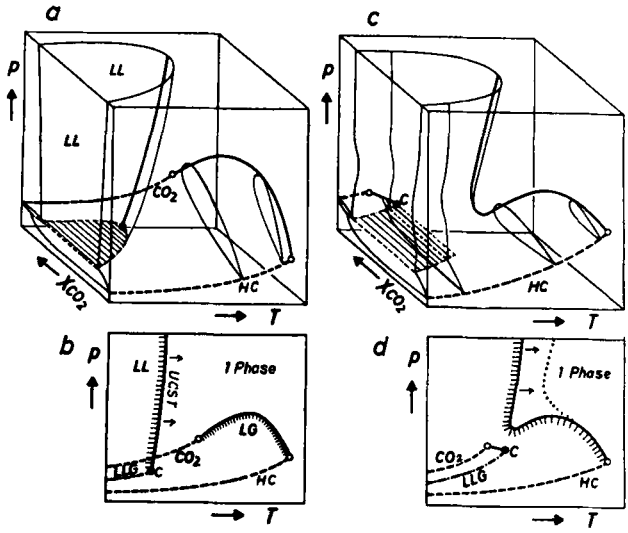

Fig. 10. p-T-x surfaces and $p(T)$-projections for binary n-alkane–CO_2 systems. (Schematic see text. HC = hydrocarbon.) (*a* and *b*): Type found for n-octane–CO_2.[25] (*c* and *d*): Type found for n-hexadecane–CO_2.[25]

with smaller n-alkanes the branch LL is situated below the crystallization surface.

The more the mutual miscibility of the two components decreases, the more the branch LL of the critical curve is displaced to higher temperatures. It can finally penetrate the ranges of temperature and pressure for the critical phenomena liquid–gas, and according to Figures 10*c* and 10*d*, it may pass continuously into the critical curve LG, whereas the branch of the critical curve starting from the critical point of the pure CO_2 ends at a critical end point on the three-phase line LLG. According to Figure 9 the system n-hexadecane–CO_2 belongs to this type, whereas the n-tridecane–CO_2 system corresponds to a transition type.

For even lower mutual miscibility of the components, critical $p(T)$-curves without a pressure maximum indicated by a dotted line in Figure 10*d* may be obtained. They are similar to those shown by systems with "immiscibility of gases" (see Figure 8).

B. Hydrocarbon–H_2O Systems

Because of their very low mutual miscibility, mixtures of hydrocarbons with water have not been investigated for many years, and for practical applications (e.g., steam distillation, extraction) complete immiscibility is

still commonly assumed. During recent years some measurements of the solubility of hydrocarbons in water were extended to ranges of temperature and pressure where hydrocarbons and water are miscible in all proportions and where parts of the critical curves could be determined (see Table I and Figures 11–13 and 15).

A simplified $p(T)$-diagram of the system benzene–H_2O is shown in Figure 11 according to measurements of Rebert and Kay,[59] Connolly,[39]

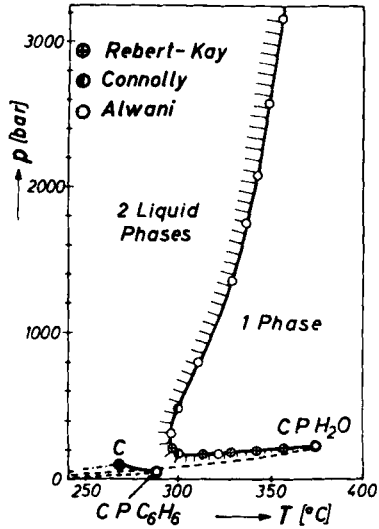

Fig. 11. $p(T)$-projection of the phase diagram of the benzene–H_2O system.[26,39,40,59] (C = critical end point.)

O'Grady,[60] and Alwani and Schneider.[26,40] The branch of the critical curve that begins at the critical point of pure water goes to lower temperatures and pressures, but bends near 300°C. It has a temperature minimum at 294°C and 200 bars and rises steeply with increasing temperatures and pressures[26,39,40] which correspond to a gas–gas equilibrium of the second type.

In Figure 12 some $p(T)$-curves for x = const $\approx$ 60 wt % H_2O are plotted for binary mixtures of H_2O with benzene, toluene, *o*-xylene, ethylbenzene, 1,3,5-trimethylbenzene, and *n*-propylbenzene[40]; the shape of these cuts can be assumed to be characteristic for the corresponding critical curves too. Figure 12 shows that the phase behavior of these systems is completely analogous to that of benzene–H_2O, but according to the lower mutual

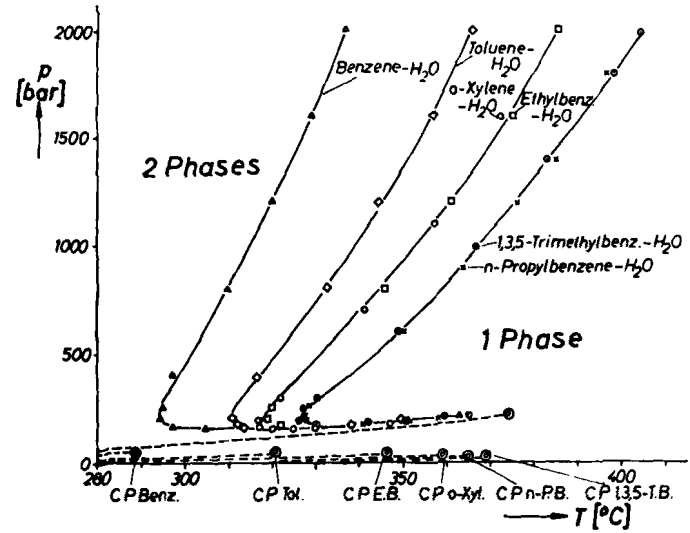

Fig. 12. $p(T)$-curves for x = constant for aqueous solutions of aromatic hydrocarbons. ($x \approx 60$ wt% H_2O.)

miscibility caused by the addition of CH_3-groups in the aromatic hydrocarbon, the temperature minima are shifted to higher temperatures. The influence of added salts was also studied.[40]

In Figure 14 this phase behavior is deduced from a superposition of liquid–liquid and liquid–gas equilibria, Figures 14*a* and 14*b* correspond to a

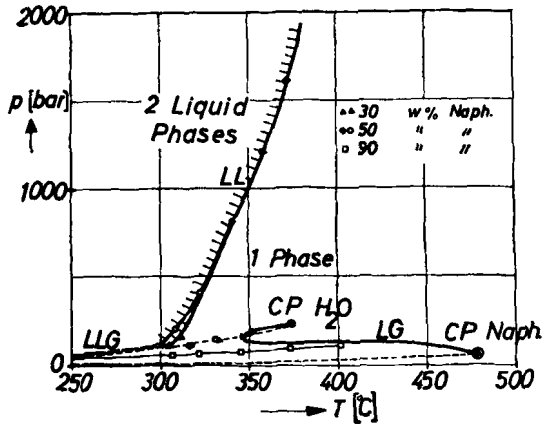

Fig. 13. Phase behavior of the naphthalene–H_2O system[40] (see text).

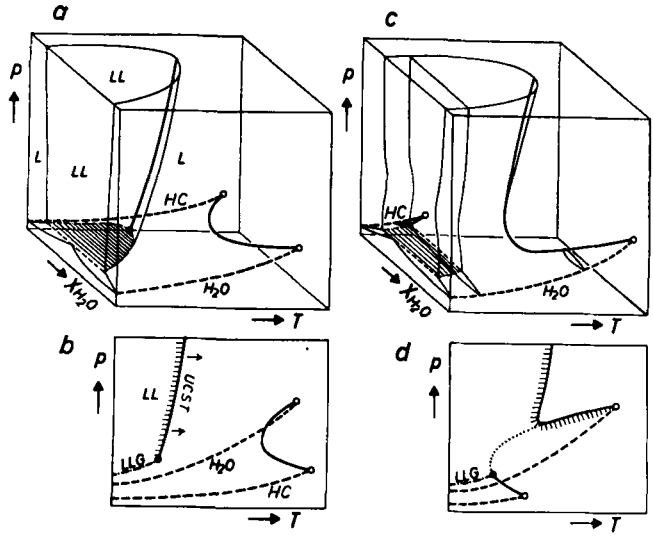

Fig. 14. p-T-x surfaces and $p(T)$-projections for binary mixtures of H_2O with aromatic hydrocarbons. (Schematic, see text. HC = hydrocarbon.) (*a* and *b*): Type found for naphthalene–H_2O.[40] (*c* and *d*): Type found for benzene–H_2O.[26,40]

binary system with a critical curve LG showing a temperature minimum and a phase separation into two liquid phases at lower temperatures, with the UCST rising with increasing pressure. The lower the mutual miscibility, the more the critical curve LL is displaced to higher temperatures, until finally the type of Figures 14*c* and 14*d* results, which corresponds qualitatively to the system benzene–H_2O and to similar systems in Figure 12.

This explanation is confirmed by measurements on the naphthalene–H_2O system. Some $p(T)$-cuts for x = const are plotted for this system in Figure 13 according to orientating measurements of Alwani.[40] The critical curve LG for the equilibrium liquid–gas is probably not interrupted and goes through a temperature minimum, whereas the critical curve LL for liquid–liquid equilibria is situated at much lower temperatures and has a positive slope. In this case, states *between* the two branches of the critical curves LG and LL can be attributed definitely to homogeneous *liquid* mixtures. Thus the naphthalene–H_2O system corresponds completely to the type of Figures 14*a* and 14*b*. The same type of phase behavior has been found for biphenyl-H_2O.[103] Thus naphthalene-H_2O and biphenyl-H_2O are the first hydrocarbon-H_2O systems where complete miscibility in all proportions has been found in ranges of temperature and pressure that belong definitely to the liquid state.

A compilation of experimental data on binary aqueous solutions taken from the literature is given in Figure 15. Only the vapor pressure curve of pure H_2O and the branches of the critical curves that start from CP H_2O are plotted for binary mixtures of H_2O with ammonia,[107] CO_2,[42] ethane,[41] *n*-butane,[41] cyclohexane,[84] benzene,[26,40] 1,3,5-trimethylbenzene,[40] N_2,[44a] Ar,[38a] and NaCl[83a] *; additionally, the branch of the critical curve that corresponds to liquid–liquid equilibria is given for the naphthalene–H_2O system.[40]

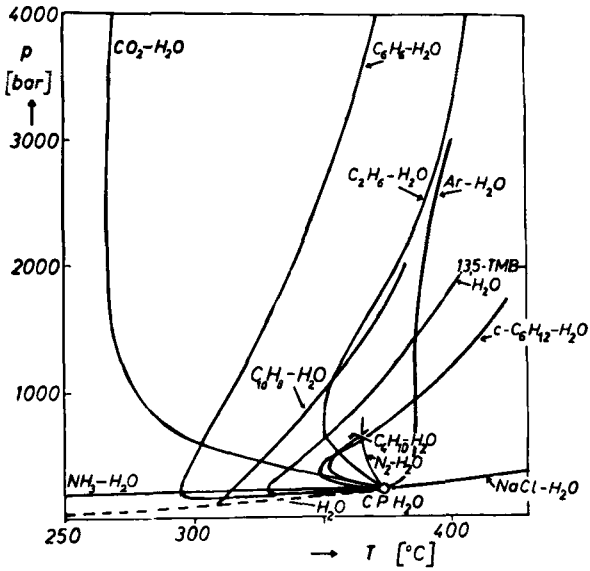

Fig. 15. $p(T)$-projections of the critical curves of aqueous binary systems. (Data taken from the literature, see text. TMB = trimethylbenzene.)

NH_3–H_2O and NaCl–H_2O have continous critical curves between the critical points of the pure components; no phase separation in the liquid phase occurs in these systems. For Ar–H_2O the critical curve tends directly to higher temperatures and pressures and corresponds to a gas–gas equilibrium of the first type. For all other systems in Figure 15 except for naphthalene–H_2O the critical curve has qualitatively the same shape, with a

* A gas–gas equilibrium of the first type was found for Ar–H_2O by Lentz,[38a] whereas the second type was reported by Tsiklis and Prokhorov.[38b] A gas–gas equilibrium of the first type was attributed to *n*-butane–H_2O by Tsiklis and Maslennikova,[44b] whereas Danneil, Tödheide, and Franck[41] showed that this system belongs to the second type (see Table I).

temperature minimum and a steep ascent to higher temperatures and pressures according to a gas–gas equilibrium of the second type. The curve for naphthalene–H_2O that belongs definitely to liquid–liquid equilibria fits remarkably well into the other curves. For benzene–H_2O and 1,3,5-trimethylbenzene–H_2O, the origin of the steeply ascending branches from liquid–liquid equilibria seems to be evident. The qualitatively similar shape of all curves above 1000 bars shows that there are continuous transitions between all types of critical curves as shown in Figure 15. Additionally, a marked extractive effect of H_2O on different hydrocarbons is demonstrated.

C. Hydrocarbon–CH_4 Systems

Liquid hydrocarbons of approximately the same size are in general completely miscible in all proportions, and the critical curves of their binary mixtures are continuous lines between the critical points of the pure components (Curves 1–3 in Figure 2).

This is no longer the case when the two hydrocarbons are very different in size. Whereas liquid methane is completely miscible with liquid ethane, propane, or butane, it has been shown by Kohn[16] and Davenport and Rowlinson[17] that liquid methane is completely miscible with hydrocarbons having 6 to 8 carbon atoms (e.g., *n*-hexane, isooctane) only *below* a definite temperature corresponding to a phase diagram of the type represented in Figure 3*a*. It was supposed that all other hydrocarbon–CH_4 systems belong to the same type (Figures 3*a* or 3*b*). Similar solution phenomena have been found for binary mixtures of ethane with C_{30}–C_{36} hydrocarbons (e.g. squalane)[97] and of hydrocarbon solvents such as *n*-heptane, cyclohexane, or benzene with polymers (e.g., polyisobutene).[96]

During recent years new measurements on hydrocarbon–CH_4 systems have been performed by several authors, e.g., Kohn,[16] and Kobayashi and co-workers.[74] Similar experiments were extended to approximately 3000 bars by Oeder and Schneider[21e,61]; some of their results are presented in Figure 16 together with data of Akers and co-workers[62] for the propane–CH_4 system. The curves plotted for propane–CH_4 and methylcyclopentane–CH_4 are the critical curves of these systems. The other curves in Figure 16 are $p(T)$-cuts for constant concentration in wt % methane; they are also typical for the shape of the critical $p(T)$-curves of these systems.

Whereas propane–CH_4 exhibits a continuous critical curve equivalent to Type 1 in Figure 2, the phase behavior of the system *n*-hexane–CH_4 corresponds to the type given in Figure 3*a*. The critical curve of the methylcyclopentane–CH_4 system, however, goes through a pressure minimum

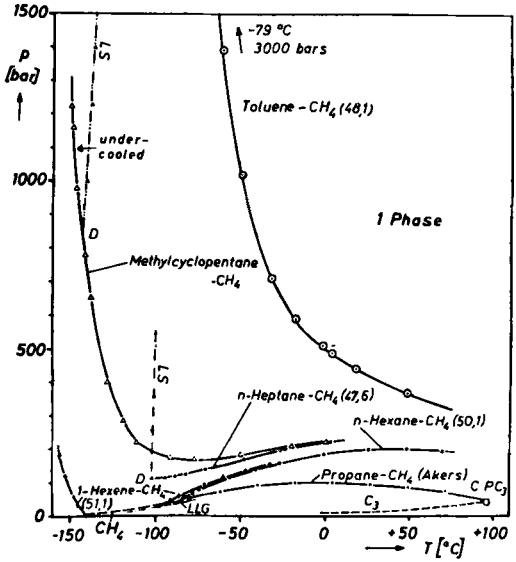

Fig. 16. Phase behavior of binary hydrocarbon–CH_4 systems. [For propane–CH_4[62] and methylcyclopentane–CH_4[61] the critical $p(T)$-curves are plotted. For all other systems[61] $p(T)$-curves for x = constant (in wt% CH_4) are given.]

and rises to higher pressures with decreasing temperatures. Since the curve becomes more and more steep, a temperature minimum on the curve seems to be possible. However, a solid phase appears at the point D (840 bars, −143°C)[61] before this hypothetical temperature minimum is reached. The line LS represents the pressure dependence of the freezing temperature of the critical mixture at the point D; because of undercooling the fluid–fluid curve could be measured down to approximately 15° below the crystallization curve. It has been shown[61] that the systems methylcyclohexane–CH_4, isoprene–CH_4, 1-heptene–CH_4, and toluene–CH_4 belong to the same type; however, no pressure minimum has been observed in the toluene–CH_4 system. *n*-Heptane–CH_4 would also correspond to this type of phase behavior, but a solid phase appears before the pressure minimum is reached[21e] (Figure 16). The phase behavior of the system 1-hexene–CH_4 in Figure 16 will be discussed below.

Figure 17 presents a schematic compilation of the $p(T)$-diagrams for the binary systems given in Figure 16. Type 3 in Figure 17*d* corresponds to the methylcyclopentane–CH_4 system: The critical curve of the binary mixtures starts at the critical point of Component II (= methylcyclopentane), runs successively through a pressure maximum and a pressure minimum, and

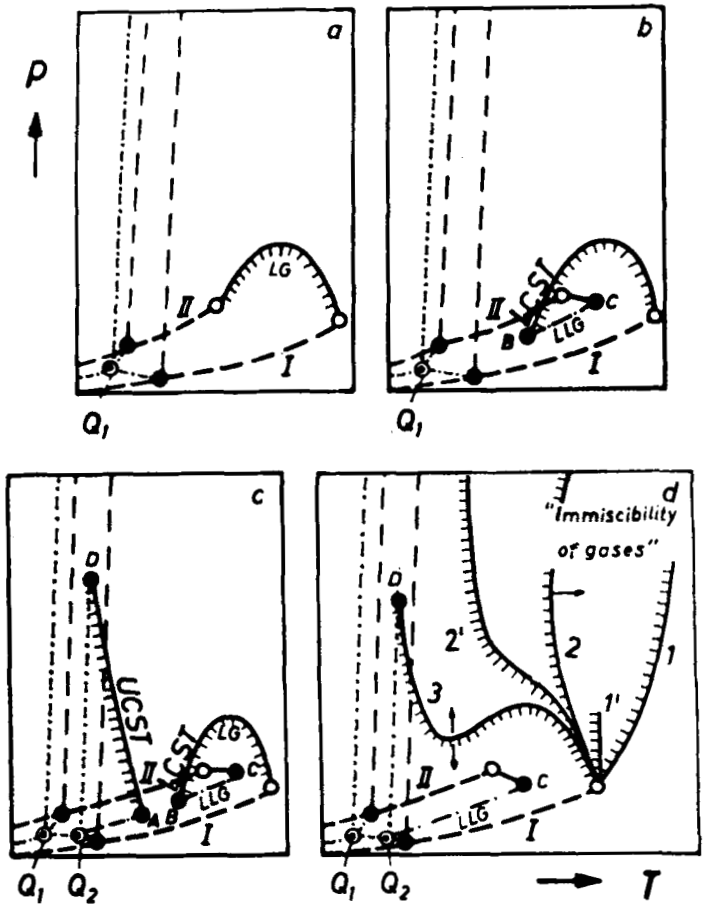

Fig. 17. $p(T)$-projections of the phase diagrams of binary hydrocarbon–CH_4 systems (schematic, see text. $Q_1 = S_I S_{II} LG$, $Q_2 = S_I LLG$) (*a*): Type found for propane–CH_4.[62] (*b*): Type found for *n*-hexane–CH_4, isooctane–CH_4.[16,17,21e] (*c*): Type found for 1-hexene–CH_4.[63,61] (*d*): Types found for methylcyclopentane–CH_4[21e,61] (Curve 3); toluene–CH_4[61] (Curve 2'); NH_3–H_2,[31] H_2O–CO_2,[42,83b] and H_2O-ethane[41] (Curve 2), and NH_3–He,[12,34a] Xe–He,[35] and H_2O–Ar[38a] (Curve 1).

ends at a critical end point *D* on a three-phase line *LLS*, where solid Component I and two liquid phases are in equilibrium.

For a binary system with even *lower* mutual solubility, the critical curve will be displaced to higher temperatures, and it may be possible that the critical curve no longer disappears below the crystallization surface, but may be supposed to run through a temperature minimum showing

successively different types of gas–gas equilibria (Types 2, 1′, and 1 in Figure 17*d*).

With *increasing* mutual miscibility, the critical curve of Type 3 in Figure 14*d* will be displaced to lower pressures and can cut the three-phase line LLG twice, e.g., at *A* and *B* in Figure 17*c*. The branch starting from *A* corresponds to UCST, whereas that starting from *B* first corresponds to LCST for a liquid–liquid equilibrium (LL) and merges then into the critical curve for the equilibrium liquid–gas (LG). Between *A* and *B* the liquid Components I and II are completely miscible in all proportions. According to Davenport, Rowlinson, and Saville[63] the system 1-hexene–CH_4 is an example of this type. This was confirmed by Oeder and Schneider,[61] who in addition measured the pressure dependence of the critical temperatures. Some of their results on this system are given in Figure 16. The same type of phase behavior has recently been found in the systems 2,3-dimethyl-1-butene-CH_4, 2-methyl-1-pentene-CH_4 and 3,3-dimethylpentane-CH_4.[49] If the branch of the critical curve starting from *A* in Figure 17*c* lies at very low temperatures or below the crystallization surface, Type 17*b* is found, e.g., *n*-hexane–CH_4, isooctane–CH_4.[21e,17] For a further increase in mutual miscibility, no regions of limited miscibility can exist in the liquid phase any longer and a phase diagram of the simple type of Figure 17*a* is found, e.g., propane–CH_4.

It is evident that there are continuous transitions between all types of phase behavior shown in Figures 17*a* through 17*d*. The most important types are represented three-dimensionally in Figure 18*a* and 18*b*.

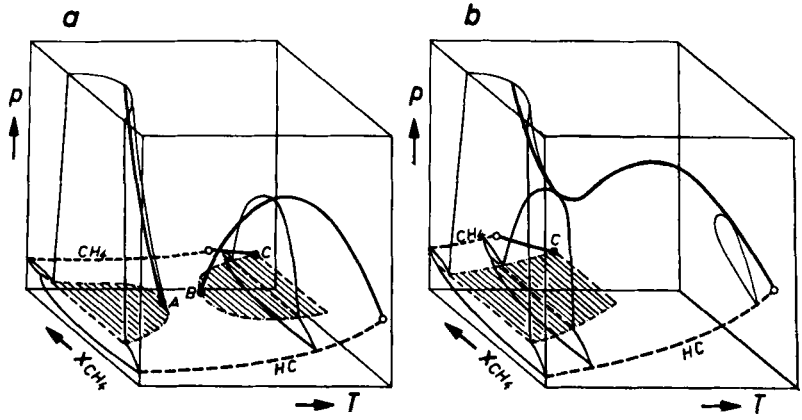

Fig. 18. Threedimensional representation of the *p-T-x* surfaces for systems of the types given in Figures 17*c* and 17*d*. (*a*): Type found for 1-hexene–CH_4.[63,61] (*b*): Type found for methylcyclopentane–CH_4 [21e,61]

D. Rare Gas Mixtures

Gas–gas separation effects have also been observed in binary mixtures of inert gases, especially in binary He-mixtures. In Figure 19 parts of the critical curves of the binary systems He–H_2, He–Ne, He–N_2,[93] He–Ar,[36] He–CH_4,[94] and He–Xe[35] and of the vapor pressure curves of the pure components are plotted according to a compilation by Streett.[36]

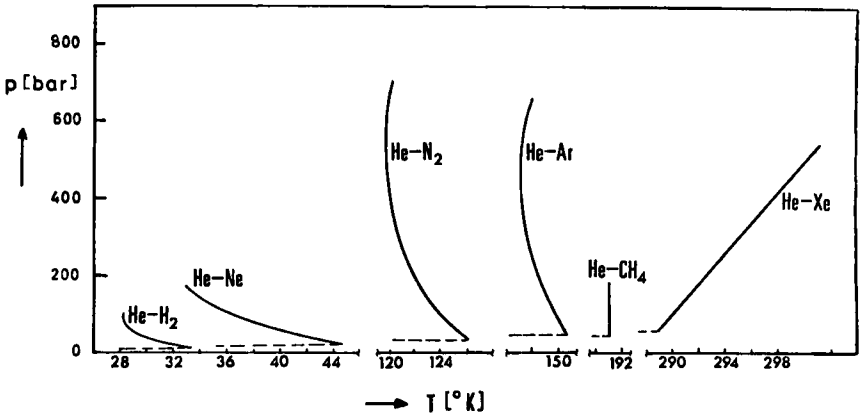

Fig. 19. Experimental critical $p(T)$-curves of some helium binary systems (according to Streett[36]).

Whereas He–N_2 and He–Ar exhibit gas–gas equilibria of the second type, and He–H_2* and He–Ne show a certain tendency for such a phase behavior, a gas–gas equilibrium of the first type has been found in the He–Xe system by de Swaan Arons and Diepen.[35] The system He–CH_4 belongs to an intermediate type. According to Streett[73] and to Trappeniers and Schouten[73] the critical curve of Ne–Ar resembles that of He–Ar; it exhibits a temperature minimum just before the crystallization surface is reached. It is evident that there are continuous transitions between all types of critical curves such as represented in Figure 19.

The existence of gas–gas equilibria in mixtures of nonpolar substances and even in rare gas mixtures is a very remarkable effect from the theoretical point of view because complete miscibility is normally assumed for mixtures of nonpolar components. Figure 19 shows that the greater the difference in the critical parameters of the pure components, the more

* The consequence of such a phase behavior for some planetary atmospheres (e.g., of Jupiter, Saturn) have been discussed by Streett.[36]

gas–gas equilibria of the second and after that of the first type are favored. Since mixtures of inert gases (especially rare gas systems) are particularly suited to theoretical treatment, some calculations that have been performed on these systems will be briefly reviewed in Section IV.

IV. THERMODYNAMIC AND THEORETICAL DESCRIPTION

A. Classical Thermodynamic Treatment

In Section III the continuity of all kinds of phase equilibria in fluid mixtures has been phenomenologically shown for some recent results on binary systems. This continuity is equally demonstrated by the fact that there is no real distinction in the thermodynamic description between a gas–liquid, a liquid–liquid, and a gas–gas critical point.

A classical description of the phase equilibria in fluid mixtures derives from the assumption that the Gibbs free energy $\bar{G}$ per mole mixture is an analytic function of the mole fractions x and the temperature T for a fixed pressure p at and near the critical point of the mixture. This treatment is completely analogous to the elementary and ultimately erroneous analysis of the behavior of a system of one component based on the equivalent assumption that the Helmholtz free energy $\bar{F}$ per mole is an analytic function of $\bar{V}$ and T at and near the critical point of the pure component.[3]

This classical treatment has been extensively described by several authors (e.g., van der Waals and Kohnstamm,[64] Prigogine and Defay,[65] Rowlinson,[1] Prigogine,[75] Haase,[66] and Rehage[86]). Therefore only the most important results for binary mixtures need to be cited (for multicomponent mixtures see Prigogine and Defay,[65] Storonkin,[67] Boberg and White,[68] Haase,[71] and others).

According to the criteria of material stability, the conditions for a critical point in a binary mixture are given by

$$\left(\frac{\partial^2 \bar{G}}{\partial x^2}\right)_c = 0 \tag{1}$$

$$\left(\frac{\partial^3 \bar{G}}{\partial x^3}\right)_c = 0 \tag{2}$$

where $\bar{G}$ is the Gibbs free energy per mole mixture and x is the mole fraction of one of the two components; the index c means that the derivatives have to be taken at the critical point. More derivatives of $\bar{G}$ with respect to x can be zero but the first nonvanishing derivative has to be positive and of even ($2n$) order (where $n = 2, 3, \ldots$).[1,65,66] From these conditions Eq. (3) can

be derived for the shape of the isobaric $T(x)$-coexistence curve near the critical point

$$(x - x_c) \sim (T - T_c)^{1/(2n-2)} \tag{3}$$

In Eqs. (1) and (2) mechanical stability is presumed at the critical point of the mixture. This assumption is not necessary for a description using the Helmholtz free energy $\bar{F}$ per mole mixture as a function of $\bar{V}$, T, and x Here the conditions of a critical point are, however, more complicated[1,75]

$$\left(\frac{\partial^2 \bar{F}}{\partial x^2}\right)_{T,V}\left(\frac{\partial^2 \bar{F}}{\partial \bar{V}^2}\right)_{T,x} - \left(\frac{\partial^2 \bar{F}}{\partial x\, \partial \bar{V}}\right)_T^2 = -\left(\frac{\partial p}{\partial \bar{V}}\right)_{x,T}\left(\frac{\partial^2 \bar{G}}{\partial x^2}\right)_{T,p} = 0 \tag{4}$$

A second condition is obtained from Eq. (2) with the use of Eq. (4).[1,75] Equation (4) shows that phase separation can occur by the system becoming either mechanically unstable $[(\partial p/\partial \bar{V})_{x,T} > 0]$ or materially unstable $[(\partial^2 \bar{G}/\partial x^2)_{p,T} < 0]$ [for further relations and a detailed discussion see Rowlinson (Ref. 1, pp. 203, 333) and Prigogine (Ref. 75, p. 236)]. It has, however, been shown that the condition for mechanical stability does not have to be considered for the discussion of a normal liquid–gas or liquid–liquid critical point[1,65,75] except for the coincidence of critical points and azeotropes [see Rowlinson (Ref. 1, p. 211)]. It follows from this that normally the conditions (1) and (2) suffice for the characterization of a critical point in a mixture.[1,65,75] Phase stability phenomena were initially discussed by van der Waals from such a three-dimensional isothermal $\bar{F}(\bar{V},x)$-surface, a critical point being the beginning of a "fold" in this surface.[64] *

These relations have been especially applied to liquid–liquid equilibria in binary systems. For $n = 2$ in Eq. (3) [that is, for $(\partial^4 \bar{G}/\partial x^4)_c > 0$)] the conditions (5)–(7) can be derived; here $\bar{H}$ and $\bar{H}^E$ are the enthalpy and the excess enthalpy per mole mixture, respectively.[1,65-67,86] Equation (6a) and (7a) allow the differentiation between UCST and LCST. The conditions (6b) and (7b) only hold approximately, with the assumption that the isothermal-isobaric $\bar{H}(x)$- or $\bar{H}^E(x)$-curves at $T = T_c$ = constant at a given pressure p are free of inflection points. These relations have been qualitatively confirmed by experiment.

$$(x - x_c) \sim (T - T_c)^{1/2} \tag{5}$$

* Often simplified cases are discussed such as $(\partial^2 \bar{F}/\partial x^2)_c = 0$ (characterizing the beginning of material instability and corresponding to a so-called "longitudinal fold" for phases with the same molar volume, e.g., approximately realized for liquid–liquid and gas–gas equilibria) or $(\partial^2 \bar{F}/\partial \bar{V}^2)_c = 0$ (characterizing the beginning of mechanical instability and corresponding to a so-called "transversal fold").

$$\text{UCST:}\quad \left(\frac{\partial^2 \bar{H}}{\partial x^2}\right)_c = \left(\frac{\partial^2 \bar{H}^E}{x^2}\right)_c < 0 \tag{6a}$$

$$\bar{H}_c^E > 0 \tag{6b}$$

$$\text{LCST:}\quad \left(\frac{\partial^2 \bar{H}}{\partial x^2}\right)_c = \left(\frac{\partial^2 \bar{H}^E}{\partial x^2}\right)_c > 0 \tag{7a}$$

$$\bar{H}_c^E < 0 \tag{7b}$$

For the pressure dependence of CST, Eq. (8a) has been deduced[1,65-67,5]

$$\frac{dT_c}{dp} = \frac{(\partial^2 \bar{V}/\partial x^2)_c}{(\partial^2 \bar{S}/\partial x^2)_c} = \frac{T_c(\partial^2 \bar{V}^E/\partial x^2)_c}{(\partial^2 \bar{H}^E/\partial x^2)_c} \tag{8a}$$

$$\frac{dT_c}{dp} \approx \frac{T_c \bar{V}_c^E}{\bar{H}_c^E} \tag{8b}$$

Here $\bar{S}$, $\bar{V}$, $\bar{V}^E$, and $\bar{H}^E$ are the entropy, the volume, the excess volume, and the excess enthalpy per mole mixture, respectively. Equation (8b) only holds if $\bar{V}^E$ and $\bar{H}^E$ have the same functional form of the types $\bar{V}^E = af(T,x)$ and $\bar{H}^E = bf(T,x)$,[28] e.g., for "regular solutions" where the excess Gibbs free energy $\bar{G}^E$ per mole mixture is given by $\bar{G}^E = A(T,p)x_1x_2$.[1,65-66,76]

According to Eqs. (8a) and (8b), some knowledge about the thermodynamic mixing functions can be deduced from the pressure dependence of CST at temperatures and pressures where nearly no direct measurements have been performed. Some of these thermodynamic conditions, based on a detailed discussion of Eqs. (8a) and (8b),[5] are schematically represented in Figure 20. The most interesting conclusions are:

(a) For $dT_c/dp = 0$ it follows from Figure 20 that $(\partial^2 \bar{V}^E/\partial x^2)_c = 0$ or that $\bar{V}_c^E \approx 0$. Here the first condition means that the isobaric-isothermal $\bar{V}^E(x)$-curve for $T = T_c$ = constant at the given pressure p has an inflection point at $x = x_c$.

With the simplifications mentioned above $\bar{V}_c^E$ would have to change its sign from minus to plus with increasing pressure for the types 7 in Figure 4, 5 in Figure 5, and 2-2′ in Figure 6. It is an interesting fact that no maximum value of an UCST (Type 5 in Figure 4) or minimum value of a LCST (Type 7 in Figure 5) as a function of pressure have been experimentally found. Thus the change of the sign of $\bar{V}_c^E$ from plus to minus with increasing pressure that corresponds to this type of pressure dependence seems to be rare or improbable; it is nevertheless thermodynamically possible.

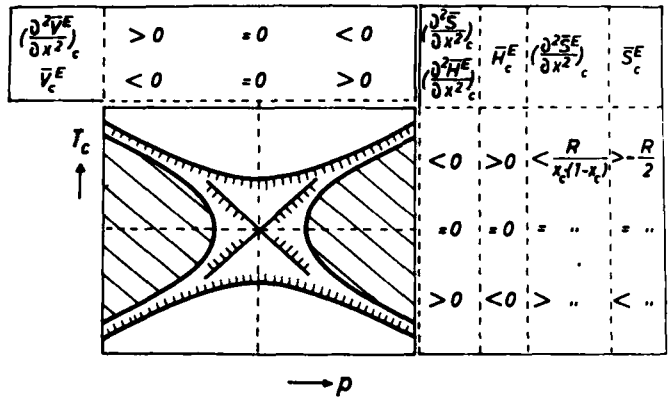

Fig. 20. Thermodynamic conditions for the different types of pressure dependence of critical solution temperatures. (Schematic, see text.)

(b) For $dT_c/dp = \pm\infty$ the result is that $(\partial^2\bar{H}^E/\partial x^2)_c = 0$ or that $\bar{H}_c^E \approx 0$. Here the first condition means that the isobaric-isothermal $\bar{H}^E(x)$-curve for $T = T_c = \text{constant}$ at the given pressure p has an inflection point at $x = x_c$ (see Types 1 and 11 in Figures 4 and 5, 1 and 1′ in Figures 6 and 7).

(c) For closed solubility loops of the types represented in Figure 6 and with the simplifications mentioned above, $\bar{H}^E$ has to change its sign from minus to plus with increasing temperature at constant pressure and $\bar{V}^E$ has to do the same with increasing pressure at constant temperature. The change of the sign of $\bar{H}^E$ has been confirmed at normal pressure,[1,5,65,66] but no direct determinations of $\bar{H}^E$ have been performed at high pressures up to now. Such experiments are very difficult because of the great heat capacity of the high pressure vessels. The change of the sign of $\bar{V}^E$ with increasing pressure has recently been verified for a system of Type 1—1′ in Figure 6 (3-methylpyridine–H_2O) by a direct method.[85]

(d) For gas–gas equilibria it follows from Eqs. (8a) and (8b) that on the steeply ascending branches of the critical curves of Types 1 and 2 in Figure 8

$$\left(\frac{\partial^2\bar{H}^E}{\partial x^2}\right)_c < 0 \qquad \text{and} \qquad \left(\frac{\partial^2\bar{V}^E}{\partial x^2}\right)_c < 0$$

or with the simplifications mentioned above that

$$\bar{H}_c^E > 0 \qquad \text{and} \qquad \bar{V}_c^E > 0$$

Here $\bar{H}^E$ and $\bar{V}^E$ are not excess functions in the common sense representing the deviations of the mixture from ideal solution behavior, because

at least one of the pure components is super-critical and no common reference state for both components can be defined. $\bar{H}^E$ and $\bar{V}^E$ are used in place of the mixing functions $\Delta\bar{H}$ and $\Delta\bar{V}$ with $\bar{H}^E$ and $\bar{V}^E$ defined by $\bar{H}^E \equiv \Delta\bar{H} = \bar{H} - (x_1 . \bar{H}_{01} + x_2 . \bar{H}_{02})$ and $\bar{V}^E \equiv \Delta\bar{V} = \bar{V} - (x_1 . \bar{V}_{01} + x_2 . \bar{V}_{02})$ where $\bar{H}$ and $\bar{V}$ are the molar enthalpy and the molar volume of the mixture and $\bar{H}_{01}$, $\bar{H}_{02}$, $\bar{V}_{01}$ and $\bar{V}_{02}$ are the molar properties of the pure components at the same temperature and pressure. It is in this sense that $\bar{H}^E$ and $\bar{V}^E$ are used in the remainder of Section IV.A and in Figures 21 and 22.

No $\bar{H}^E$ measurements have been performed for mixtures with gas–gas immiscibility, but for some systems $\bar{V}^E$ values have been determined from PVT data of the mixtures and of the pure components.*

$\bar{V}^E$ values obtained by this method are plotted in Figure 21 for the benzene–H_2O system according to measurements of Alwani.[40] Figure 21 shows that the predictions of the signs of $\bar{V}^E_c$ and $(\partial^2\bar{V}^E/\partial x^2)_c$ are confirmed by the experimental results. $\bar{V}^E$ data have been reported by Lentz[38a] for the Ar–H_2O system. For his experimental results in this system Lentz[38a] claims that $\bar{V}^E$ equals zero at the inflection points of the $p(T)$-isopleths and that at these points the molar volume of the mixture equals

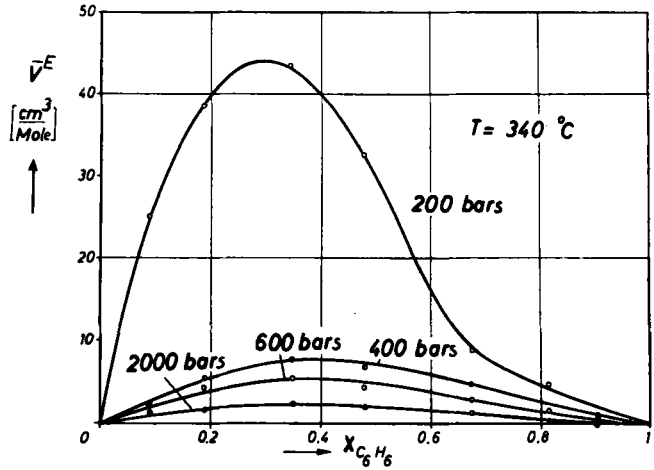

Fig. 21. Volume change in mixing in the benzene–H_2O system: $\bar{V}^E$ (x)-curves at 340°C for different pressures (x = mole fraction).[40]

* With direct methods $\bar{V}^E$ has been determined in gas mixtures at low pressures by several authors and in liquid mixtures up to 400 bars by Jeener and Lambert[87] viz. up to 3000 bars by Engels.[85]

approximately the constant b in the van der Waals equation for the more volatile component.

The volumetric behavior has also been studied for some other systems, e.g., hydrocarbon–CH_4 systems.[16,61] In Figure 22 $\bar{V}^E$ values obtained from PVT data are plotted for the methylcyclopentane–CH_4 system according to measurements of Oeder.[61] Since $dT_c/dp < 0$ at low temperatures and high pressures for this system (Figure 16), it follows from Eqs. (8a) and (8b) and Figure 20 that $(\partial^2 \bar{V}^E/\partial x^2)_c > 0$ or that $\bar{V}_c^E < 0$ near the critical curve. Figure 22 shows that these predictions are confirmed experimentally in the concentration range of the critical mixture on this branch of the critical curve ($x_c \approx 84$ mol % CH_4).

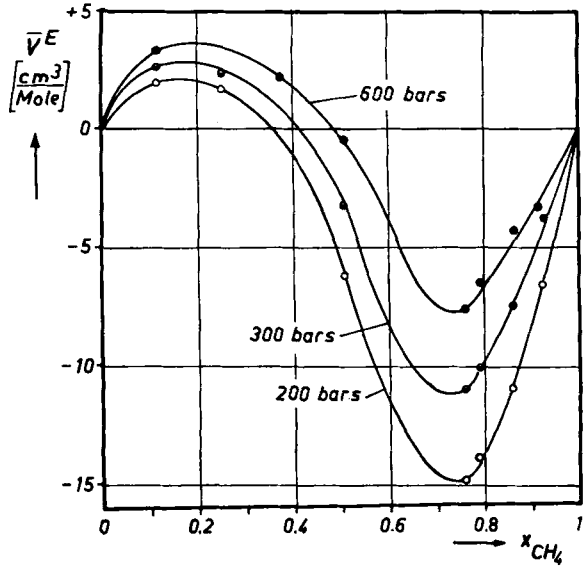

Fig. 22. Volume change in mixing in the system methylcyclopentane–CH_4: $\bar{V}^E(x)$-curves at −50°C for different pressures (x = mole fraction).

B. Extension of the Classical Description

It has been shown in Section IV.A that the agreement between the classical theory and the experimental results is qualitatively good. However, there is some evidence that the classical theory seems to be quantitatively inadequate, in analogy to the failure of the classical theory of the critical point of a single component system.[1,3]

Up to now the comparison of theory with experimental data was only possible for liquid–liquid equilibria at normal or moderate pressure because measurements at higher pressures are not yet accurate enough. It has

been shown from very precise experiments (e.g., by Thompson and Rice[72] on the CCl_4–c–C_7E_{14} system withing 10^{-4} degree of the UCST) that the isobaric $T(x)$-coexistence curve is very well represented by $(x' - x'') \sim (T - T_c)^{1/3}$ near the CST (where x' and x'' are the mole fractions of the two liquid phases in equilibrium) whereas the classical theory gives $(x' - x'') \sim (T - T_c)^{1/(2n-2)}$ (with $n = 2, 3, \ldots$); light scattering experiments gave an exponent 1/3 too.[1,3,106] Discrepancies have also been found for the heat capacities near the CST.[1] The conclusion is that $\bar{G}$ is non-analytic in these cases.

It has been assumed by several authors[3,28] that $(\partial^2 \bar{V}^E/\partial x^2)_{p,T}$ and $(\partial^2 \bar{H}^E/\partial x^2)_{p,T}$ both vanish at the critical solution point.* Equation (8a) must then be replaced by

$$\frac{dT_c}{dp} = \lim_{\substack{T \to T_c \\ x \to x_c}} \frac{(\partial^2 \bar{V}/\partial x^2)_{p,T}}{(\partial^2 \bar{S}/\partial x^2)_{p,T}} = \lim_{\substack{T \to T_c \\ x \to x_c}} \frac{T(\partial^2 \bar{V}^E/\partial x^2)_{p,T}}{(\partial^2 \bar{H}^E/\partial x^2)_{p,T}} \tag{9}$$

Since $\bar{V}^E$ and $\bar{H}^E$ themselves do not vanish at the critical point, even if the second derivatives do so, Myers and co-workers[28] claimed that Eq. (8b) is still approximately applicable. Reasonable agreement of some experimental results on binary systems up to 100 bars with Eq. (8b) was found.

The discussion in Section IV.A has shown that nevertheless Eq. (8a) remains approximately valid and useful for the qualitative evaluation of the thermodynamic mixing functions from $T_c(p)$-curves. More experimental and theoretical work, which has to include the new types of phase behavior recently found at high pressures (see Sections II and III),† seems to be necessary in order to attain further progress on these problems.

C. Theoretical Treatment of Gas–Gas Equilibria

The objective of an equilibrium theory of fluid mixtures is the determination of the thermodynamic equilibrium properties of the mixture (e.g., phase equilibria, critical properties, mixing functions) from the properties of the pure substances, particularly from the molecular interaction parameters of the pure components. In spite of extensive work this objective has only been imperfectly reached even for mixtures of very simple molecules. The situation is fully described in excellent monographs by Guggenheim,[78] Prigogine,[75] Rowlinson,[1] and Hildebrand and Scott[76] where the theory of

* Evidently this does not correspond to inflection points in the isobaric–isothermal $\bar{V}^E(x)$- and $\bar{H}^E(x)$-curves but to small non-analytic parts in these curves at the critical concentration.

† E.g., the exhibition of very small and infinitely small closed solutility loops (near and at the points HP in Figure 6), the transition Type 3–3′ in Figure 6, the exhibition of extreme values for T_c in $T_c(p)$-curves (Figures 4–6, 8), etc.

phase separations in fluid systems is also considered. In the present section some approaches that have been made to predict or explain gas–gas equilibria will be briefly discussed.

1. Solubility Parameter Approach

Hildebrand's solubility parameter $D = (\bar{E}/\bar{V})^{1/2}$ (where $\bar{E}$ originally equals the vaporization energy per mole, and $\bar{V}$ is the molar volume of a pure liquid component) was used by Kreglewski[47] for the prediction of gas–gas immiscibility. With the additional assumption that $\bar{E} = 3RT_c/2$ at the critical point, with the result that $D = (3RT_c/2\bar{V}_c)^{1/2}$, he claimed that the greater the difference in the D-values of the pure components the more probable will be the existence of a gas–gas equilibrium in a binary mixture.

Kreglewski's method, which allowed some useful predictions, was modified by Kaplan.[48] He arranged the components in a table in order of increasing D^2 values toward the right and toward the bottom, the binary systems being represented by the intersecting horizontal rows and vertical columns. From experimental findings in each row, more reliable predictions of whether a system will exhibit a gas–gas equilibrium or not were possible.

This semi-empirical method has proved to be quite successful. Exhibition of a gas–gas equilibrium is predicted for binary mixtures of H_2O with He, Xe, H_2, O_2, CH_4, C_2H_4, C_3H_8; of SO_2 with H_2, C_6H_{14}, etc.; of CH_3OH with H_2, N_2, etc.*; and of NH_3 with H_2, C_6H_{14} etc.; all these systems have not yet been studied experimentally. A shortcoming of the method in its original state was that it did not predict what type of gas–gas equilibrium will occur; but this restriction could be eliminated to some extent by recent improvals of the method.[48]

2. Approaches Based on an Equation of State

Some approaches start from the Helmholtz free energy $\bar{F}$ calculated by an integration of $(\partial\bar{F}/\partial\bar{V})_{T,x} = -p$ using one of the well-known semi-empirical equations of state.† With $\bar{F}$ as a function of $\bar{V}$, T, and x obtained from this integration, the critical concentration and the critical temperature of a mixture for a given volume can be calculated from the corresponding thermodynamic conditions (see Section IV.A). Similar approaches have been used for the determination of liquid–gas critical curves, e.g., by Redlich and Kister[70] and Joffe and Zudkevitch.[69]

* A gas–gas equilibrium in the system CH_3OH–C_6H_{14} was also predicted,[48] but it seems to be rather improbable.

† The determination of $\bar{G}$ from $(\partial\bar{G}/\partial p)_{T,x} = \bar{V}$ is more difficult since the well-established equations of state are more easily solved with respect to p than to $\bar{V}$.

Temkin[52] based his discussion on the van der Waals equation for binary mixtures

$$\left(p + \frac{a}{\bar{V}^2}\right)(\bar{V} - b) = RT \tag{10a}$$

with

$$a = a_{11}x_1^2 + 2a_{12}x_1x_2 + a_{22}x_2^2 \tag{10b}$$

and

$$b = b_{11}x_1^2 + 2b_{12}x_1x_2 + b_{22}x_2^2 \tag{10c}$$

With the assumption of a longitudinal fold [that is $(\partial^2\bar{F}/\partial x^2)_c = 0$*] and $b_{12} = 0.5(b_{11} + b_{22})$ he deduced the criteria (11a) and (11b) for the exhibition of gas–gas equilibrium at or above the critical temperature of the less volatile component (that is, of a gas–gas equilibrium of the first type). With the additional assumption that $a_{12} = (a_{11}a_{22})^{1/2}$, Eq. (11b) can be simplified to give Eq. (11c)

$$b_{11} \geqslant 0.42b_{22} \tag{11a}$$

$$a_{12} < \tfrac{1}{2}(a_{11} + a_{22}) - \tfrac{8}{27}a_{22} \tag{11b}$$

$$a_{11} < 0.053a_{22} \tag{11c}$$

The conditions (11a)–(11c) show that in Temkin's theory the exhibition of gas–gas equilibria of the first type is more a consequence of large differences in intermolecular forces (e.g., found for He with most other components) rather than in size. Temkin successfully predicted gas–gas equilibria of the first type in mixtures containing He, and even of H_2O with nonpolar gases—no example being known at that time (see Table I). De Swaan Arons and Diepen[35] also predicted a gas–gas equilibrium of the first type for the He–Xe system from Temkin's theory; this phase behavior was confirmed experimentally by the same authors.

Essentially the same method was used by van Konynenburg and Scott[49] for the theoretical representation of critical phenomena in hydrocarbon mixtures. With $\bar{F}(\bar{V},T,x)$ calculated from the van der Waals equation for

* The validity of Eq. (10a) was also assumed by Ostrovskii,[51] but a purely transversal fold [that is $(\partial^2\bar{F}/\partial\bar{V}^2)_c = 0$] was used. Such a fold apparently does not correspond to a gas–gas equilibrium in a binary mixture since phase separation from mechanical and not from material instability is assumed.

binary mixtures, and assuming the usual mixing rules for a and b, a whole pattern of different types of critical curves (approximately corresponding to the type given in Figures 17*a*–17*d*) could be obtained from the criteria of material stability by variation of the parameters a and b of the pure components.

Schäfer (Ref. 46, pp. 243–250) used a virial expansion for the equation of state of the mixtures and of the pure components with the form

$$p\bar{V} = RT + Bp + Cp^2 \tag{12a}$$

Here B and C are the second and third virial coefficients respectively and are given by

$$B = x_1^2 B_{11} + 2x_1 x_2 B_{12} + x_2^2 B_{22} \tag{12b}$$

$$C = x_1^3 C_{111} + 3x_1^2 x_2 C_{112} + 3x_1 x_2^2 C_{122} + x_2^3 C_{222} \tag{12c}$$

From this equation of state Schäfer calculated the Gibbs free energy $\bar{G}$ as a function of p, T, and x and deduced from the criteria (1) and (2) that phase separation will be found for

$$\frac{18|\delta|RT}{\alpha^2} \leqslant 3 - 2\left(\frac{\beta}{\delta} + 1\right) - 2\left[\left(\frac{\beta}{\delta} + 1\right)^2 - 3\left(\frac{\beta}{\delta} + 1\right)\right]^{1/2} \tag{13a}$$

with $\alpha < 0$ and $[(\beta/\delta) + 1] < 0$ where

$$\alpha \equiv B_{11} + B_{22} - 2B_{12} \tag{13b}$$

$$\beta \equiv \tfrac{1}{2}(C_{111} - C_{112}) + (C_{111} + C_{222} - 2C_{112}) \tag{13c}$$

$$\delta \equiv \tfrac{1}{2}(C_{111} - 3C_{112} + 3C_{122} - C_{222}) \tag{13d}$$

Schäfer showed that such phase separations qualitatively correspond to gas–gas equilibria. For a quantitative description, however, higher virial coefficients have to be considered.

3. Corresponding States Treatment

In 1967 Zandbergen, Knaap, and Beenakker[50] published a theoretical calculation of the critical curve of the He–Xe system based on a corresponding states treatment originally developed by Prigogine[75] and Scott.[77] The calculations were performed both with the so-called "single-liquid" and with the "three-liquid" model. The validity of a Lennard-Jones 6-12 potential with the parameters ε and σ for all pair interactions and of the

usual combination rules $\varepsilon_{12} = (\varepsilon_{11}\varepsilon_{22})^{1/2}$ and $\sigma_{12} = 0.5(\sigma_{11} + \sigma_{22})$ for all 1-2 pair interactions was assumed.

The *single-liquid* model favors a certain liquid-like character of the mixture. The change of the Gibbs free energy in mixing, per mole of the mixture, $\Delta\bar{G}$, is given by

$$\Delta\bar{G} = \bar{G}_m^{res} - x_1\bar{G}_{01}^{res} - x_2\bar{G}_{02}^{res} + RT(x_1 \ln x_1 + x_2 \ln x_2) \qquad (14)$$

where $\bar{G}_m^{res}$, $\bar{G}_{01}^{res}$, and $\bar{G}_{02}^{res}$ are the residual values of the Gibbs free energy per mole of the mixture and of the pure components 1 and 2, respectively, at temperature T and pressure p. The determination of the residual Gibbs free energy for pure components, $\bar{G}_0^{res}$, is described in the literature.[1] Zandbergen, Knaap, and Beenakker[50] obtained $\bar{G}_m^{res}$ from a corresponding states treatment according to

$$\bar{G}_m^{res}(x_1,p,T) = \frac{\langle\varepsilon\rangle}{\varepsilon_{RR}}\bar{G}_{0R}^{res}\left[\frac{\langle\varepsilon\rangle}{\varepsilon_{RR}}\left(\frac{\sigma_{RR}}{\langle\sigma\rangle}\right)^3 p; \frac{\langle\varepsilon\rangle}{\varepsilon_{RR}}T\right] \qquad (15)$$

Here $\bar{G}_{0R}^{res}$ is the residual Gibbs free energy of a reference substance (generally Component 1 or 2) that has to be known as a function of temperature and pressure. ε_{RR} and σ_{RR} are the Lennard-Jones parameters of this reference substance. $\langle\varepsilon\rangle$ and $\langle\sigma\rangle$ are averaged values of these parameters for the mixture and can be obtained from

$$\langle\varepsilon\rangle = \frac{c^2}{d} \qquad (16a)$$

$$\langle\sigma\rangle = \left(\frac{d}{c}\right)^{1/6} \qquad (16b)$$

with

$$c \equiv x_1^2\varepsilon_{11}\sigma_{11}^6 + 2x_1x_2\varepsilon_{12}\sigma_{12}^6 + x_2^2\varepsilon_{22}\sigma_{22}^6 \qquad (16c)$$

$$d \equiv x_1^2\varepsilon_{11}\sigma_{11}^{12} + 2x_1x_2\varepsilon_{12}\sigma_{12}^{12} + x_2^2\varepsilon_{22}\sigma_{22}^{12} \qquad (16d)$$

For the calculation of the critical curve, $\Delta\bar{G}$ is evaluated as a function of x_1 for different temperatures at a given pressure p. When phase separation occurs these isobaric–isothermal $\Delta\bar{G}(x_1)$-curves are double s-shaped and the common tangent determines the mole fractions x_1' and x_1'' of the coexisting phases. The isotherm where $x_1' = x_1'' = x_{1c}$ corresponds to the critical temperature T_c at the given pressure. This procedure is repeated for other pressures. From this, the critical curve in the p-T-x space can be calculated.

The *three-liquid* model favors a certain gaslike character of the mixture.[50,77] For this model $\Delta\bar{G}$ is given by

$$\Delta\bar{G} = Wx_1x_2 + RT(x_1 \ln x_1 + x_2 \ln x_2) \tag{17}$$

with

$$W \equiv 2[\bar{G}_{12}^{res} - 0.5(G_{01}^{res} + \bar{G}_{02}^{res})] \tag{18}$$

$\bar{G}_{12}^{res}$ for a hypothetical liquid interacting in 1-2 pairs only is again obtained from a corresponding states treatment

$$\bar{G}_{12}^{res} = \frac{\varepsilon_{12}}{\varepsilon_{RR}} \bar{G}_{0R}^{res}\left[\frac{\varepsilon_{12}}{\varepsilon_{RR}}\left(\frac{\sigma_{RR}}{\sigma_{12}}\right)^3 p; \frac{\varepsilon_{12}}{\varepsilon_{RR}} T\right] \tag{19}$$

When $\Delta\bar{G}$ from Eq. (17) is introduced into the conditions (1) and (2) for a critical point, Eqs. (20a) and (20b) for T_c and x_c are obtained

$$T_c = \frac{W}{2R} \tag{20a}$$

$$x_{1c} = x_{2c} = 0.5 \tag{20b}$$

The simplest method to determine T_c at a given pressure p is to calculate W from Eqs. (18) and (19) for different temperatures T at this pressure, and to plot these values of W against T. According to Eq. (20a), T_c is given by the intersection point of this curve with the straight line $W = 2RT$. This procedure is repeated for other pressures and T_c is obtained as a function of p.

In Figure 23 the values that were calculated from these two models by Zandbergen, Knaap, and Beenakker[50] are compared with the experimental results of de Swaan Arons and Diepen[35] for the He-Xe system that is especially suited for such calculations. Whereas the slope of the critical curve is very well represented by the three liquid model, the corresponding absolute values for the critical temperatures are too low. Only one point was calculated for the single-liquid model, and it showed a critical temperature that is too high. The authors claim that the two-liquid model would probably give the best results.[50] Similar approaches were presented by Patterson and Delmas[98] and reviewed by Leland and Chappelear.[101]

4. Correlation Function Treatment

A fundamental theoretical treatment of phase transitions would be based on certain singularities of the configuration integral. Unfortunately, the configuration integral cannot be solved explicitly.[1,75]

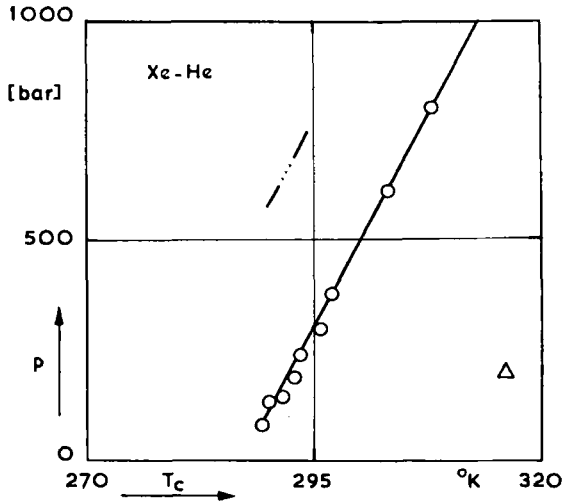

Fig. 23. Critical $p(T)$-curve of the He–Xe system: Comparison of experimental results (○)[35] with values calculated from the single- (△) and the three-liquid (-···-) model[50] (see text).

From an approximate treatment using the so-called two-index correlation functions, a criterium for the exhibition of gas–gas equilibria of the first type was deduced by Rott.[12,45] In this theory a parameter β is defined by Eq. (21)

$$\beta = \frac{3.31 \frac{\varepsilon}{k} \sigma^4}{T r_0^4} \tag{21}$$

where r_0 is the radius of the molecular volume $v = 4\pi r_0^3/3$, ε and σ are the parameters of the L.J. potential, k is Boltzmann's constant, and T is the temperature. For many substances $\beta \approx 4$–5 at the critical temperature. For a binary system the parameter β is calculated according to Rott[45,12] by inserting T_c and r_0 for the less volatile substance (e.g., H_2O) in the denominator of Eq. (21) and ε and σ for the more volatile component in the numerator. If the resulting value of β is greater than that of the pure less volatile component at its critical point, exhibition of gas–gas equilibria of the first type is said to be possible.

This criterion, however, does not seem to be very reliable. Gas–gas equilibria of the *first* type have been predicted by Tsiklis and Rott[12] for binary mixtures of H_2O with propane, *n*-butane, *n*-octane, and benzene. On the other hand, gas–gas equilibria of the *second* type have already been found experimentally for *n*-butane–H_2O[41] and benzene–H_2O[26,40] (see

Table I and Figure 15), and the same can be expected for propane–H_2O and *n*-octane–H_2O since ethane–H_2O,[41] *n*-butane–H_2O,[41] and *n*-heptane–H_2O[84] all show gas–gas equilibria of the second type. For Ar–H_2O, no gas–gas equilibrium of the first type was predicted by Rott but, however, it was found experimentally.[38a]

V. CONCLUSIONS

Whereas phase equilibria in fluid systems have been intensively studied over a large temperature range for many years, a systematic investigation of the pressure range above several hundred bars has become possible only during recent years through the rapid development of experimental techniques. Up to now, the results obtained from such experiments under high pressure are still rather sparse; they have been briefly reviewed in Sections II and III. There is no doubt that the so-called gas–gas equilibria, only rarely found previously, will become more and more important, and it is quite probable that the exhibition of gas–gas equilibria will be the rule rather than the exception for systems with relatively weak forces between unlike molecules.[1,36]

In the future, the number of such investigations at high pressures will certainly increase considerably—the experiments being extended both to lower and to higher temperatures. Investigations of condensed gas mixtures at low temperatures and high pressures will be interesting from a theoretical point of view, since mixtures of small and highly symmetrical molecules that are suitable for a theoretical treatment can be studied (see Sections III.A, III.C, III.D, and IV.C). Measurements at low temperatures may also have a certain practical and technical interest for the petroleum and gas industry, for cryogenic applications, separation problems, space research, etc.

The experimental techniques for the investigation of phase equilibria in fluid systems at high temperatures, high pressures, and possibly under strong corrosion should also be further developed in order to allow the study of mixtures with components which differ more and more in volatility, structure, size, and polarity up to supercritical conditions (e.g., water with gases, organic compounds, molten salts, solids, etc.). There is much evidence that phase equilibria, miscibility relations, solubilities, and even critical phenomena will also be increasingly studied in molten salts, slags, minerals, fluid metals, etc., at high temperatures and pressures, All these experiments may additionally present a certain practical or technological interest for mineralogy, geo-chemistry, and earth sciences (especially for problems connected with hydrothermal syntheses and with the formation

and migration of oil), for separation processes (particularly extraction), reactor research, high pressure chemistry (especially for the application of these mixtures as reaction media), wet air oxidation,[88] etc. These studies on phase relationships have to be completed by measurements of the thermodynamic functions of fluid mixtures under high pressure.

It was the aim of this review to show that there are continuous transitions between liquid–gas, liquid–liquid, and gas–gas equilibria in fluid systems under high pressures. This concept of a continuity between all kinds of phase equilibria in fluid mixtures should also be helpful for further investigations because it will aid in understanding the great variety of phase relationships and in giving a certain order to many different types of critical behavior in fluid systems.

References

1. J. S. Rowlinson, *Liquids and Liquid Mixtures*, Butterworths, London, 1959 (2nd ed. 1969).
2. K. A. Kobe and R. E. Lynn, *Chem. Rev.*, **52**, 117 (1953); L. P. Kadanoff and co-workers, *Rev. Mod. Phys.*, **39**, 395 (1967); J. V. Sengers and A. L. Sengers, *Chem. Eng. News* **46** (25), 104 (1968); H. Richtering, *Naturwiss.*, **54**, 481 (1967); M. Fixman, *Advan. Chem. Phys.*, **6**, 175 (1964).
3. J. S. Rowlinson, "Critical States of Simple Fluids and Fluid Mixtures," in *Critical Phenomena* (M. S. Green and J. V. Sengers, Eds), proceedings of a Conference held in Washington, D.C., April 1965, *Natl. Bur. Std.* (U.S.), *Misc. Publ.*, **273** (1966).
4. J. S. Rowlinson and M. J. Richardson, *Adv. Chem. Phys.*, **2**, 85 (1959).
5. G. Schneider, *Ber. Bunsenges. phys. Chem.*, **70**, 497 (1966).
6. G. Schneider, *Chem. Eng. Prog. Symp. Ser.*, **64**, (88), 9 (1968),
7. J. P. Kuenen, *Die Theorie der Verdampfung und Verflüssigung von Gemischen*, Barth, Leipzig, 1902.
8. E. Büchner, "Systeme mit zwei flüssigen Phasen," in *Die heterogenen Gleichgewichte*, Vol. II, Part II, (H. W. Roozeboom, Ed.), Vieweg, Braunschweig, 1918.
9. J. E. Ricci, *The Phase Rule and Heterogeneous Equilibrium*, Van Nostrand, Toronto, New York, London, 1951.
10. J. Zernike, *Chemical Phase Theory*, Kluwer, Deventer, Antwerp, Djakarta, 1955.
11. W. B. Kay, *Accounts Chem. Res.*, **1**, 344 (1968); W. B. Kay and D. Hissong, paper presented at the 32nd Midyear Meeting of the API, Los Angeles, May 1967.
12. D. S. Tsiklis and L. A. Rott, *Usp. Khim.*, **36**, 869 (1967); *Russ. Chem. Rev.*, **1967**, 351.
13. D. S. Tsiklis, *Handbook of Techniques in High Pressure Research and Engineering*, Plenum, New York, 1968.
14. J. P. Kuenen, *Z. Physik. Chem.*, **37**, 485 (1901).
15. W. B. Kay, *J. phys. Chem.*, **68**, 827 (1964).
16. J. P. Kohn, *A. I. Ch. E. J.*, **7**, 514 (1961); J. P. Kohn and co-workers, *J. Chem. Eng. Data*, **7**, 3 (1962); **9**, 5 (1964); 11, 176 (1966); **12**, 189 (1967).
17. A. J. Davenport and J. S. Rowlinson, *Trans. Faraday Soc.*, **59**, 78 (1963).
18. J. Timmermans, *J. Chim. Phys.*, **20**, 491 (1923).
19. J. Timmermans, *Physico-chemical Constants of Binary Systems*, Interscience, New York, London, 1960; *Les Solutions Concentrées, Masson, Paris*, 1936.

20. G. Poppe, *Bull. Soc. Chim. Belges*, **44**, 640 (1935).
21. G. Schneider, *Z. Phys., Chem. (Frankfurt)*, (*a*) **37**, 333 (1963); (*b*) **39**, 187 (1963); (*c*) **41**, 327 (1964); (*d*) **41**, 110 (1964); (*e*) **46**, 375 (1965).
22. K. Roth, G. Schneider and E. U. Franck, *Ber. Bunsenges phys. Chem.*, **70**, 5 (1966).
23. G. Schneider and C. Russo, *Ber. Bunsenges. Phys. Chem.*, **70**, 1008 (1966); J. P. Novak and G. M. Schneider, *Ber. Bunsenges. Phys. Chem.*, **72**, 791 (1968).
24. G. Schneider, *Ber. Bunsenges. Phys. Chem.*, **70**, 10 (1966).
25. G. Schneider, Z. Alwani, W. Heim, E. Horvath, and E. U. Franck, *Chem. Ingr. Tech.*, **39**, 649 (1967).
26. Z. Alwani and G. Schneider, *Ber. Bunsenges. Phys. Chem.*, **71**, 633 (1967).
27. G. Schneider and co-workers, unpublished results.
28. D. H. Myers, R. A. Smith, J. Katz, and R. L. Scott, *J. Phys. Chem.*, **70**, 3341 (1966).
29. J. D. van der Waals, *Zittinsversl. K. Akad. Wet. Amst.*, Nov. 1894, 133.
30. H. Kamerlingh Onnes and W. H. Keesom, *Commun. Phys. Lab. Univ. Leiden, Suppl. No.* **15** (1907); *Proc. Roy. Acad. Sci. Amst.* **9**, 786 (1907); **10**, 231 (1907).
31. (*b*) I. R. Krichevskii, *Acta Phys. Chim. URSS*, **12**, 480 (1940); I. R. Krichevskii and P. E. Bol'shakov, *Zh. Fiz. Khim.*, **15**, 184 (1941); I. R. Krichevskii and D. S. Tsiklis, *Zh. Fiz. Khim.*, **15**, 1059 (1941); **17**, 126 (1943); D. S. Tsiklis, *Dokl. Akad. Nauk. SSSR*, **86**, 993 (1952). (*b*) I. R. Krichevskii, *Phase Equilibria in Solutions at High Pressures* (in Russian), Goskhimizdat, Moscow, 1946 and 1952.
32. A. E. Lindroos and B. F. Dodge, *Chem. Eng. Prog. Symp. Ser.* **48**, 10 (1952).
33. D. S. Tsiklis and Yu. N. Vasil'ev, in *The Physics and Chemistry of High Pressures*, Soc. Chem. Ind., London, 1963, p. 25; *Russ. J. Phys. Chem.*, **1963**, 720.
34. D. S. Tsiklis, *Dokl. Akad. Nauk SSSR*, (*a*) **86**, 1159 (1952); (*b*) **91**, 1361 (1953).
35. J. de Swaan Arons and G. A. M. Diepen, *J. Chem. Phys.*, **44**, 2322 (1966).
36. W. B. Streett, *Trans. Faraday Soc.*, **65**, 696 (1969).
37. J. S. Rowlinson, in *The Physics and Chemistry of High Pressures*, Soc. Chem. Ind., London, 1963, p. 5.
38. (*a*) H. Lentz and E. U. Franck, Ber. Bunsenges. Phys. Chem. **73**, 28 (1969); H. Lentz, Ph.D. Thesis, University of Karlsruhe, Germany, 1967; (*b*) D. S. Tsiklis and V. M. Prokhorov, *Russ. J. Phys. Chem.* **1966**, 1257; *Zh. Fiz. Khim.*, **40**, 2335 (1966).
39. J. F. Connolly, *J. Chem. Eng. Data*, **11**, 13 (1966).
40. Z. Alwani and G. M. Schneider, Ber. Bunsenges. Phys. Chem. **73**, 294 (1969); Z. Alwani, Ph.D. Thesis, University of Karlsruhe, Germany, 1969.
41. A. Danneil, K. Tödheide, and E. U. Franck, *Chem. Ingr. Tech.*, **39**, 816 (1967).
42. K. Tödheide and E. U. Franck, *Z. Phys. Chem. (Frankfurt)*, **37**, 387 (1963).
43. V. Ya. Maslennikova, N. P. Gorjunova and D. S. Tsiklis, Dokl. Akad. Nauk SSSR **178**, 886 (1968); D. S. Tsiklis, V. Ya. Maslennikova and N. P. Gorjunova, Zhur. Fiz. Khim. **41**, 1804 (1967).
44. D. S. Tsiklis and V. Ya. Maslennikova, *Dokl. Akad. Nauk SSSR*, (*a*) **161**, 645 (1965); (*b*) **157**, 426 (1964).
45. L. A. Rott, *Russ. J. Phys. Chem.*, **1962**, 1205; **1964**, 286; *Dokl. Akad. Nauk SSSR*, **160**, 1138 (1965).
46. K. Schäfer, *Statistische Theorie der Materie*, Vol. 1, Vandenhoek and Ruprecht, Göttingen, Germany, 1960.
47. A. Kreglewski, *Bull. Acad. Polon Sci., Classe III*, **5**, 662 (1957).
48. R. Kaplan, *A. I. Ch. E. J.*, **13**, 186 (1967); **14**, 821 (1968).
49. P. van Konynenburg, Ph.D. Thesis, University of California, Los Angeles, 1968.
50. P. Zandbergen, H. F. P. Knaap, and J. J. M. Beenakker, *Physica*, **33**, 379 (1967).

51. I. A. Ostrovskii, *Russ. J. Phys. Chem.*, **1963,** 501, 503.
52. M. I. Temkin, *Russ. J. Phys. Chem.*, **1959,** 275.
53. G. Donnelly and D. L. Katz, *Ind. Eng. Chem.*, **46,** 511 (1954).
54. H. Poettmann and D. L. Katz, *Ind. Eng. Chem.*, **37,** 847 (1945).
55. H. H. Reamer, B. H. Sage, W. N. Lacey, *Ind. Eng. Chem.*, **43,** 2515 (1951).
56. J. P. Kuenen, *Z. Phys. Chem.*, **24,** 667 (1897).
57. H. H. Reamer and B. H. Sage, *J. Chem. Eng. Data*, **8,** 508 (1963); **10,** 49 (1965).
58. C. J. Rebert and K. E. Hayworth, *A. I. Ch. E. J.*, **13,** 118 (1967).
59. C. J. Rebert and W. B. Kay, *A. I. Ch. E. J.*, **5,** 285 (1959).
60. T. M. O'Grady, *J. Chem. Eng. Data*, **12,** 9 (1967).
61. D. Oeder and G. M. Schneider, Ber. Bunsenges. Phys. Chem. **73,** 229 (1969); D. Oeder, Ph.D. Thesis, University of Karlsruhe, Germany, 1969.
62. W. W. Akers, J. F. Burns, and W. R. Fairchild, *Ind. Eng. Chem.*, **46,** 2531 (1954).
63. A. J. Davenport, J. S. Rowlinson, and G. Saville, *Trans. Faraday Soc.*, **62,** 322 (1966).
64. J. D. van der Waals and Ph. Kohnstamm, *Lehrbuch der Thermodynamik*, Vol. II, Barth, Leipzig, 1912.
65. I. Prigogine and R. Defay, *Chemische Thermodynamik*, Verlag für Grundstoffindustrie, Leipzig, 1962.
66. R. Haase, *Thermodynamik der Mischphasen*, Springer, Berlin, Göttingen, Heidelberg, 1956.
67. A. V. Storonkin, *Thermodynamics of Heterogeneous Systems* (in Russian), Leningrad, 1967.
68. T. C. Boberg and R. R. White, *Ind. Eng. Chem. Fundam.*, **1,** 40 (1962).
69. J. Joffe and D. Zudkevitch, *Chem. Eng. Prog. Symp. Ser.*, **63,** (81), 43 (1967).
70. O. Redlich and A. T. Kister, *J. Chem. Phys.*, **36,** 2002 (1962).
71. R. Haase, *Z. Naturforsch.*, **5A,** 109 (1950).
72. D. R. Thompson and O. K. Rice, *J. Am. Chem. Soc.*, **86,** 3547 (1964).
73. N. J. Trappeniers and J. A. Schouten, Physics Letters **27a,** 340 (1968); W. B. Streett, *J. Chem. Phys.* **46,** 3282 (1967).
74. H. L. Chang and R. Kobayashi, *J. Chem. Eng., Data*, **12,** 517, 520, (1967).
75. I. Prigogine, A. Bellemans, and V. Mathot, *The Theory of Solutions*, North-Holland, Amsterdam, 1957.
76. J. H. Hildebrand and R. L. Scott, *The Solubility of Non-Electrolytes*, Dover, New York, 1964; J. H. Hildebrand and R. L. Scott, *Regular Solutions*, Prentice-Hall, Englewood Cliffs, N.J., 1962.
77. R. L. Scott, *J. Chem. Phys.*, **25,** 193 (1956).
78. E. A. Guggenheim, *Mixtures*, Clarendon Press, Oxford, 1952.
79. K. E. Weale, *Chemical Reactions at High Pressures*, Spon, London, 1967.
80. J. Robberecht, *Bull. Soc. Chim. Belg.*, **47,** 597 (1938); N. A. Puschin and I. V. Grebenschtschikow, *Z. Phys. Chem.*, **124,** 270 (1926).
81. J. H. Hildebrand, B. J. Alder, J. W. Beams, and H. M. Dixon, *J. Phys. Chem.*, **58,** 577 (1954).
82. R. Battino and H. L. Clever, *Chem. Rev.*, **66,** 395 (1966).
83. (*a*) S. Sourirajan and G. C. Kennedy, *Nucl. Explos. Peaceful Applic.*, UC 35, TID-4500, Report, UCRL-6175 (1960); (*b*) S. Takenouchi and G. C. Kennedy, *Amer. J. Sci.*, **262,** 1055 (1964).
84. K. Peter, Diplomarbeit, University of Karlsruhe, Germany, 1968.
85. P. Engels, Ph.D. Thesis, University of Karlsruhe, Germany, 1970.
86. G. Rehage, *Z. Naturforsch.*, **10a,** 300 (1955).

87. J. Jeener and M. Lambert, *Discussions Faraday Soc.*, **22,** 85 (1956).
88. G. H. Teletzke, *Chem. Eng. Prog.*, **60,** 33 (1964)
89. W. Yu. Urbakh, *Zh. Fiz. Khim.*, **32,** 1163, 1407 (1958).
90. A. W. Francis, *Ind. Eng. Chem.*, **45,** 2789 (1953).
91. G. Schneider and M. Kuballa, paper presented at a IUPAC Symposium on Thermodynamics, Heidelberg, Germany, Sept, 1967; M. Kuballa, Ph.D. Thesis, University of Karlsruhe, Germany, 1970.
92. E. U. Franck, *Angew. Chem.*, **73,** 309 (1961).
93. W. B. Streett, *Chem. Eng. Prog. Symp. Ser.* **63,** (81), 37 (1967).
94. J. C. Mullins and W. T. Ziegler, *Advan. Cryog. Eng.*, **10,** 171 (1965).
95. J. A. M. van Hest and G. A. M. Diepen, in *The Physics and Chemistry of High Pressures*, Soc. Chem. Ind., London, 1963, p. 10.
96. P. I. Freeman and J. S. Rowlinson, *Polymer*, **1,** 20 (1960).
97. J. S. Rowlinson and P. I. Freeman, *Pure appl. Chem.*, **2,** 329 (1961).
98. D. Patterson and G. Delmas, *Trans. Faraday Soc.*, **65,** 708 (1969).
99. R. Steiner and E. Schadow, *Z. Phys. Chem.* (Frankfurt), **63,** 297 (1969).
100. W. Swietoslawski and A. Kreglewski, *Bull. Acad. Pol. Sci.*, Classe III, **2,** 77 (1954).
101. T. W. Leland Jr. and P. S. Chappelear, *Ind. Eng. Chem.*, **60,** (7), 15 (1968).
102. S. Glowka and A. C. Zawisza, paper presented at the 1st International Conference on Calorimetry and Thermodynamics, Warsaw, Aug. 31-Sept. 4, 1969.
103. K. Bröllos, University of Karlsruhe, unpublished results.
104. G. M. Schneider, *Fortschr. chem. Forsch.*, **13,** 559 (1970).
105. J. M. Prausnitz, *Adv. Chem. Eng.*, **7,** 139 (1968); J. M. Prausnitz, *Molecular Thermodynamics of Fluid-Phase Equilibria*, Prentice-Hall, Inc., Englewood Cliffs, N.J., 1969.
106. B. H. Zimm, *J. Phys. Chem.*, **54,** 1306 (1950); *J. Chem. Phys.*, **20,** 538 (1952).
107. D. S. Tsiklis, L. R. Linshitz, and N. P. Gorjunova, *Zh. Fiz. Khim.*, **39,** 2978 (1965).

Advance in Chemical Physics, Volume XVII
Edited by I. Prigogine, Stuart A. Rice

THE THERMODYNAMIC DESCRIPTION OF PHASE TRANSITIONS

MICHAEL H. COOPERSMITH

Department of Physics,
University of Virginia,
Charlottesville, Virginia 22903

CONTENTS

I. INTRODUCTION

Despite recent heroic attempts to construct microscopic models whose exact solutions show phase transitions, there remains a peculiar gap between the equations of state which arise from these models and the experimentally defined relationships among the thermodynamic parameters. This gap is all the more striking due to the fact that good quantitative agreement with experiment can be obtained for a wide range of parameters but there is a decided lack of qualitative agreement near just those values of the parameters which appear to be most interesting. These are the values near a critical point of the system.

That the neighborhood of a critical point is indeed the most interesting place to look at a phase transition is not only a latter-day phenomenon but also an historical fact. In looking over the literature pertaining to changes of state, one is immediately struck by the concern of early workers in the field with the fact that, above certain critical values of the parameters, no

change of state of the system can be observed. Thus, as early as 1822, one Baron de la Tour[1] observed that various gases including CO_2 and water vapor exist in only one phase when the temperature is above the value now commonly known as the critical temperature. We might remark here that even with the meager experimental devices available to him (he made only what amounted to qualitative viscosity measurements), the Baron was able to delineate the entire critical region and even observe critical opalescence in a glass tube before it shattered from the excessive internal pressure. Later experiments confirmed these results more quantitatively[2] but de la Tour's work had already uncovered the basic phenomenon described by van der Waals[3] in his now classic equation of state. This "continuity of liquid and vapor states" (as van der Waals referred to it) or the ability of a system to avoid showing a phase transition when taken along a suitable thermodynamic path represents the most outstanding feature of the critical region and may, in fact, be thought of as the essence of a critical point. It is a sad fact that our understanding and description of this feature has progressed very little from the time when van der Waals proposed his semiphenomenological explanation.

Although this last statement appears to be at odds with the myriad "results" which have come out in the last few years,[4] we shall demonstrate its validity in the course of this paper. In the process, we shall offer a way of looking at the problem which reconciles the various conflicting views. These views will be taken up individually in the proceeding sections.

II. THE SEMIPHENOMENOLOGICAL VIEW

The idea of offering a semiphenomenological explanation for the continuity of states originated, as already mentioned, with van der Waals, was continued by Weiss[5] for an explanation of the Curie point of ferromagnetism, and reached its culmination in the generalization of van der Waals' equation of state proposed by Widom[6] a few years ago. The prefix "semi" is justified because one can concoct microscopic models which yield the van der Waals' and Weiss' equations of state in some approximation. These models have been discussed extensively in the literature[7] and will not be taken up here. We shall only note that the physical basis of these equations of state comes about from the competition between energy and entropy in the Helmholtz free energy, $F = E - TS$, the one arising from the weak, long range attraction between the particles and the other from the strong, short range repulsion (generally taken as a hard core). Widom's homogeneous equations of state do not have such a simple explanation[8] but if we accept the idea of homogeneity as at least an approximation to

some general physical principle, then these equations too may be described as semiphenomenological.

In order to put this viewpoint in its proper perspective, we refer to an analysis of free energies (i.e., thermodynamic potentials) which show the phenomenon of the critical point as given by the author.[9] This treatment relies on the sole assumption of analytic continuation of the thermodynamic potential in both its variables, a point which we shall comment upon further in Section VIII. We quote here the main results which are

(1) In the neighborhood of the Curie (critical) point, the Weiss theory free energy $F(H,T)$ can be represented by an algebraic function of third degree. The chemical potential corresponding to van der Waals' equation of state in the neighborhood of the critical point has the same form when regarded as a function of reduced pressure and temperature after a transformation which makes the reduced vapor pressure equal to zero for all temperatures. (We use the word "reduced" to denote the difference between a variable and its critical value.)

(2) Magnetic free energies which are algebraic functions homogeneous in the applied field and reduced temperature form a special case of the analog of Widom's homogeneous functions.

The assumption that a thermodynamic potential is an algebraic function of its natural variables is clearly an approximation since (*a*) the critical exponents must be rational and (*b*) no logarithmic behavior can be obtained. However, we shall see that algebraic functions act as a framework on which to hang the more general description which will include logarithmic behavior as well as other singularities.

III. MODEL BUILDING—THE "RIGOROUS" APPROACH

The ability to obtain an analytic solution to the two-dimensional Ising model problem in the absence of a magnetic field[10] and the related square ice problem[11] are monumental mathematical achievements. Nevertheless, it seems increasingly clear that a simple closed analytic expression for the full ferromagnetic problem with applied field or the related problem of a fluid is by its very nature impossible to obtain. The reason boils down to a question of representation of a function. We have seen in Ref. 9 that even the simplest algebraic functions which show the characteristic behavior of a critical point cannot be represented in closed form but are defined as implicit functions by a polynomial equation. The representation is then realized by expanding the individual terms in the polynomial about any point of interest, thus obtaining a representation of the function about that point. This representation is in the form of an ordinary Taylor expansion

if the point is nonsingular and a Taylor expansion in the variable $\zeta = z^{1/n}$ if the point is a singular one. Here z is the original variable, n is the degree of the defining polynomial (more accurately, the order of the singular point) and the expansion may start with a negative but finite power of ζ. In the neighborhood of a critical point we are dealing with a function of two variables, and the points of interest lie on either the coexistence curve or the critical isotherm. The critical point itself is excluded. For the magnetic case, the expansions are of the form

$$F(H,T) = \sum_{n=0}^{\infty} a_n(T - T_c)H^n \tag{1}$$

for the first case and

$$F(H,T) = \sum_{n=0}^{\infty} b_n(H)(T - T_c)^n \tag{2}$$

for the second. The coefficients a and b are themselves expandable in the form required for a singular (branch) point in one variable, so that we have

$$a_n(z) = \sum_{i=r_n} A_{ni} z^{i/t_n} \tag{3}$$

and

$$b_n(z) = \sum_{i=s_n}^{\infty} B_{ni} z^{i/u_n} \tag{4}$$

where r and s are positive or negative integers and t and u are the orders of the branch points. The numbers r_n/t_n and s_n/u_n (referred to as α_n and β_n in Ref. 9) are the leading exponents and are commonly known as the critical exponents for the nth derivative of the free energy with respect to H and T, respectively. For the two-dimensional Ising model, only the asymptotic forms of the leading terms of $a_0^{\pm}(T - T_c)$ and $a_1^{-}(T - T_c)$ have been found analytically. (The plus and minus signs refer to whether T is greater than or less than T_c; that is, whether we are above or below the critical point.) Onsager's well-known solution gives $a_0^{+}(T - T_c)$ and $a_0^{-}(T - T_c)$ both asymptotically equal to $(T - T_c)^2 \ln(|T - T_c|)$ while the published solution of Yang[12] for the spontaneous magnetization gives the asymptotic form of $a_1^{-}(T - T_c)$ as $(T_c - T)^{1/8}$. None of the other a's and b's are known even asymptotically.[13] It is in this sense that our understanding of critical phenomena has progressed very little in the last 70 years for of all the microscopic models, van der Waals' or the equivalent molecular field types are the only ones whose analytic properties are completely known. Nevertheless, the mean field theories together with some recent work on perturbation expansions to be discussed in the next section contain what we believe to be the essential features of phase transitions.

IV. PERTURBATION EXPANSIONS—MAYER REVISITED

The idea of starting with an ideal gas and working ones way up to a liquid seemed particularly attractive in the early part of this century. Thus it was that after the initial development of the formal structure of the density power series for the pressure of a fluid,[14] Mayer[15] attempted to find the place at which the formal power series broke down, that is, its radius of convergence. Of course, if one does not know the (virial) coefficients, one cannot hope to predict the singularities of the function. Nonetheless, Mayer was able to present arguments for the existence of a finite radius of convergence when the temperature was below a certain (critical) value. He then argued that what existed at higher densities was a liquid whose pressure could not be reached by perturbation theory starting from the ideal gas pressure. We now know that it is, in fact, possible to develop a perturbation expansion which includes both high and low densities if one starts, not from the ideal gas pressure, but from the pressure of a hard core gas. Various authors have found this result in the recent past either inadvertantly or by design. Thus, Brout[16] developed a cluster expansion for the Ising model starting from what is recognizable as the analog of a hard core gas, a system of non-interacting spins, no more than one of which can occupy a lattice site. The author, in conjunction with Brout,[17] then extended the method to include the related lattice gas and finally to develop a formal cluster expansion for a real gas with interactions including a hard core and attractive tail. This expansion has been reworked recently by Jalicki, Siegert, and Vezzetti.[18] For quantum mechanical systems, a similar formal development was attempted by Huang[19] following the work of Yang and Lee[20] on the non-interacting hard core Bose system.

Expansions of this type have the feature of being essentially power series in $\rho(\rho_0 - \rho)$ where ρ_0 is the close packed density. They are therefore convergent for large as well as small values of the density. Whenever any particular classes of terms in the expansion are picked out, however, the result is always of the mean field type.[21] Although a physical explanation of phase transitions is thereby obtained (entropy of hard cores versus energy of attractive tails), as an analytical tool these expansions have provided no further insight than the original density expansion.

The expansion about the ideal gas pressure, this time with the fugacity as the variable, has been returned to recently by a number of authors, among them Andreev,[22] Langer,[23] and Fisher.[24] It is shown that if one considers an expansion in the fugacity of real droplets (as opposed to mathematical clusters), one is led to a series which represents a function which has an

essential singularity on the real axis for all temperatures. Thus the conjecture[25] that there will be a singularity at the condensation point (as opposed to the critical point) has been verified in a physically appealing approximation. Furthermore, Fisher[24] has also analyzed a one-dimensional model which shows these properties.

At this point there may be some temptation to develop a polarization of attitudes regarding the singular behavior observed near the critical point. On the one hand it is clear that algebraic functions contain a number of essential features of thermodynamic potentials in the neighborhood of the critical point. On the other hand it appears that many people are somewhat upset by a multiple valued free energy, coming as it does from the infinite volume limit of an apparently single valued free energy of a finite system, and would prefer it to be single valued with a bifurcation point (discontinuity in the density) coming from a singularity. In the Appendix we show precisely how the limit of a sequence of single valued functions can be multiple valued. Using this fact, the two views may be easily reconciled in the following way.

We consider the Riemann surface of an algebraic function of the type proposed in Ref. 9. On a neighborhood of this Riemann surface not containing a branch point, one may define a single valued function.[26] We now imagine a function defined on the Riemann surface which has an essential singularity at the crunode (see Ref. 9) and is linear in a neighborhood of the crunode. If the essential singularity is chosen so that its value and the values of all its derivatives approaching from the real axis are zero (the most common example is e^{-1/z^2}), then we will have a function of the type which has been found for the droplet model.[24] A specific example is the following. Let the algebraic function of two variables be denoted by $f(z,T-T_c)$ where z is the variable appropriate to the physical system (reduced chemical potential for a fluid, magnetic field for a ferromagnet). Let $g(z)$ be a function which has an essential singularity of the type previously mentioned. The function $f(g(z)+z,T-T_c)$ then has all the properties ascribed by Fisher to the grand potential of his one-dimensional model. Furthermore, the line of essential singularities is continued above the transition temperature as in that model.

This description of the thermodynamic potential has the property of containing all the features of the algebraic functions of Ref. 9 as well as the conjectured singularity at the condensation point which "warns" of the impending change of state. One could then argue that the essential features of the critical region are contained in the behavior of the Riemann surface of the algebraic function while the essential singularity is not "essential" at all but, rather, aesthetically pleasing.

V. THE THEORY ACCORDING TO YANG AND LEE

In 1952 Yang and Lee[27] published two, by now, famous papers dealing with the analytic properties of the grand partition function in the vicinity of a critical point. The first paper dealt with the general qualitative properties of the isotherms of the grand potential as a function of the fugacity, while the second paper was concerned with specific properties of the grand potential for the lattice gas equivalent of the Ising model.

The point of view expressed in Ref. 27 appears to be entirely at odds with the representation of a thermodynamic potential as a function defined on the Riemann surface of an algebraic function. In particular, it appears to imply that the thermodynamic potential must be single valued and that any peculiar behavior is caused by certain barriers of singularities. We shall now demonstrate that this is not so. First, note that in Ref. 27, no mention is made of the analytic properties of the grand partition function in both the temperature and fugacity but, rather, only the analytic properties along an isotherm are considered. A lot of information is thereby lost.

Now, the Yang–Lee theory is based on the fact that the analytic behavior of the pressure is determined by the limiting distribution of roots of the grand partition function in the complex fugacity plane as the volume becomes infinite. The crucial point here is that this distribution arises as a limit. Because of the peculiar nature of the limiting process, the final distribution of roots has nothing directly to do with the singularities of the thermodynamic potential but is merely a means of representing the desired branches of the limit function. The validity of the last statement is directly connected with the fact noted in the last section that the limit of a sequence of polynomials may be a multiple valued function.

Let us then return to algebraic functions for the moment and define an isotherm of the thermodynamic potential to be that function which is single valued and identical to the branches of the algebraic function which have the smallest real value. When the temperature is below the critical value, this function is non-analytic at the point where reduced fugacity equals zero since the derivative is discontinuous. Note that the general analytic function of which this limit function is a part has no singularity at the origin but a crunode, which is a place where the values of the function on two different branches are accidentally equal. According to the Yang–Lee theory, however, there must be a singularity there. We now see that the origin of the difficulty lies in the attempt to discover the analytic properties of a limit function (the thermodynamic potential) by analyzing the singularities of finite volume partition functions. That this should not be done was, in fact, intimated by Yang and Lee themselves, since, as they point out

in I of Ref. 26, the convergence of the polynomials is not uniform when the temperature is below the critical temperature.

The point can be driven home further when cognizance is taken of a paper by Hemmer and Hauge[28] in which the Yang-Lee distribution of zeros for a van der Waals gas is calculated. Since we know that the van der Waals (or any molecular field theory) thermodynamic potential is given in the neighborhood of the critical point by an algebraic function of third order (see Ref. 9), we know that there is no singularity at the crunode and, indeed, we know precisely what the singularities are in the neighborhood of the critical point (two branch points of order two). We see in this calculation explicitly that the so-called distribution of zeros has nothing directly to do with the singularities of the limit function but arises because the limiting process picks out just those branches of the multiple valued limit function which we are interested in for thermodynamic reasons. The distribution of zeros is then only a means of representing the single valued function defined by those branches and has no other direct thermodynamic significance.

VI. ANALYSIS OF THE CRITICAL REGION

A method of approach to critical phenomena which has become somewhat fashionable recently is the analysis of thermodynamic potentials in terms of relations between the coefficients a and b of Eqs .(1) and (2). These take the form of inequalities which come about because certain partial derivatives of the free energy are positive definite in order to have thermodynamic stability.[29] Following the conjecture by Essam and Fisher,[30] based on homogeneous functions, that the leading exponents governing the behavior of the a's satisfy the relation $\alpha_n - \alpha_{n-1} = \alpha_1 - \alpha_0$ for all n, it was shown by Rushbrooke[31] that the equality sign for $n = 2$ should be replaced by an inequality sign, $\leqslant$. More recently, Griffiths[32] has written down a large number of inequalities involving the exponents of low order (up to $n = 2$) a_n's and b_n's. The method used by Griffiths to obtain these inequalities is that of comparing various thermodynamic functions on two curves approaching a critical curve and using known convexity conditions. Thus, for example, to obtain Rushbrooke's inequality, one looks at the thermodynamic potential $A(M,T)$ on two isotherms with the same value of M and uses the convexity of A in M.

These inequalities are very useful for checking the consistency of experimental data but, unfortunately, are of little help in determining the analytic character of the thermodynamic potential. It we think in terms of algebraic functions and their expansions given by Eqs. (1) and (2), then it

seems quite reasonable in view of the analysis of Ref. 9 that any equality signs can only hold in general in relations among exponents of the same type, i.e., those governing the behavior of the a_n's or the b_n's. We have already referred to such relations as unmixed.[9] It is difficult to see how the restriction to algebraic functions provides any conditions on the mixed relations so that we must be content for the time being with the inequality signs coming from thermodynamic stability requirements. The idea that mixed equalities exist for more general conditions than homogeneity is not precluded, however. The analysis simply hasn't been done yet.

VII. METASTABILITY

In formulating any theory or description of the critical region, one always comes up against the experimental fact that a system does not always choose to exist in the state which minimizes the appropriate thermodynamic potential but can sometimes be coaxed into a state which does not satisfy the ordinary rules of thermodynamics. Such states are not stable, since the system will go back very rapidly to the equilibrium configuration if a slight disturbance is made or if it is carried too far from this equilibrium state. The term metastability has been used to describe such a situation, and there seems to be some difficulty in fitting this concept into the ordinary statistical mechanical calculation for the partition function since, as we have seen, for hard cores in a finite volume, this partition function is single valued. This value must be the thermodynamically stable one if we are to believe in the formalism of statistical mechanics at all. Nevertheless, metastability is a fact of life and must be accounted for.

If we take the concept of a multiple valued thermodynamic potential at face value, then we already have states of the system which are, at least, candidates for metastability. To see whether these states may be the ones which are experimentally observed, we now inquire into their origin in terms of finite volume limits. The discussion will be restricted to the ferromagnetic case for simplicity in drawing diagrams.

For the free energy F in a finite volume, we have already argued that the isotherms for $T < T_c$ are polynomials which look like the dashed portion of Figure 1. The corresponding free energy $A (= F + MH)$ then looks like the dashed portion of Figure 2. In the infinite volume limit, these functions develop a discontinuous derivative and a flat portion, respectively (solid portions of Figures 1 and 2). We have maintained that the limiting function F is a combination of certain branches of a multiple valued function. If the other real valued branches are to represent metastable states, then they should also arise out of finite volume limits. The finite volume

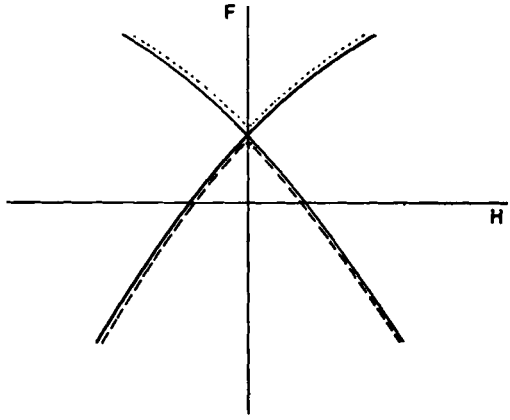

Fig. 1. An isotherm of $F(H,t)$ for $t < 0$. The dashed line represents a system with finite volume while the solid line represents the infinite volume limit. The dotted line shows possible metastable states.

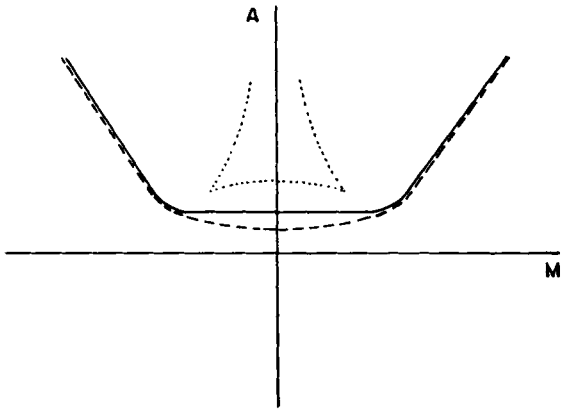

Fig. 2. An isotherm of $A(M,t)$ for $t < 0$. The dashed, solid, and dotted lines have the same meaning as in Figure 1.

metastable values of F would presumably look like the dotted curve in Figure 1 with the corresponding values of A being given by the dotted curve in Figure 2.

How do these states arise? One would expect that certain portions of the (microcanonical) constant energy surface on which the system may be confined for long periods of time compared with the experimental measurement time may be relatively large. The entropy, being a measure of these portions, might then be analytically related to the total entropy of the

system in the sense that, in the infinite volume limit, it would become the analytic continuation of the total entropy. In the canonical and grand canonical ensembles, this would lead to the above pictures for A and F.

There are two essential problems. One is to demonstrate the existence of states with relatively larger probability than neighboring states. This was attempted by Siegert[33] for the finite two-dimensional Ising model but the results were only conclusive for low temperatures (i.e., far from the critical point). The second problem involves an examination of the dynamics of the system to see whether a relatively more probable group of states has a relaxation time which is long compared with the experimental measurement time. To the author's knowledge, this has never been investigated.

VIII. DESCRIPTION OF EQUILIBRIUM PHENOMENA

In the preceding sections, we have attempted to show the relationship between the currently accepted views of critical phenomena and the picture presented by the author in Ref. 9. In that paper, explicit use was made of algebraic functions as a representation of that thermodynamic potential whose natural variables are intensive. But we have already seen in Section II, that algebraic functions cannot provide all the observed behavior. We now pose the following question. What class of functions can exhibit all the known behavior and yet is elementary in the sense that it has already been studied?

Before discussing this problem, we might remark that there is a natural analog of this situation in the description of decay of physical states. That problem might be thought of in the same light as the present one; that is, we have available an elementary function (the decreasing exponential) whose properties are obviously well known and which describes the qualitative physical behavior. Nevertheless, as in the present case, the connection between the underlying microscopic dynamics and the observed macroscopic behavior has never been completely established.[34]

What then are the elementary functions describing critical phenomena? We have already seen that algebraic functions alone are capable of describing many aspects of the two phase region. The main feature of algebraic functions of two variables which is most useful for the present situation is the breaking up of the Riemann surface into two disjoint pieces when one of the variables has the particular value which corresponds physically to the critical value of the thermodynamic variable. This feature may be kept by working with functions defined on the Riemann surface of the appropriate algebraic function. Since the only missing aspect of the

equilibrium situation is the possible logarithmic behavior of the coefficients $a_n(T - T_c)$ defined in Eq. (1), we need only assume that the functions defined on the Riemann surface are Abelian integrals or products of analytic functions and Abelian integrals. Such functions are elementary in the sense defined above. Since an Abelian integral is defined as the integral of a rational function of an algebraic function and its variable on the Riemann surface of that algebraic function, then its singularities include poles and logarithmic singularities, but no essential singularities.[35] With these functions, we may now have $a_0(T - T_c) \sim (T - T_c)^2 \ln (T - T_c)$ as in the two-dimensional Ising model. Also, since the singularities of an Abelian integral (in one variable) are isolated, we preserve the property of analytic continuation in two variables from one side of the two phase region to the other. Finally, as in Section IV, we can add an essential singularity at the crunode by forming the function $F[g(z) + z, T - T_c]$ where $F(x,y)$ is an Abelian integral defined on the Riemann surface of an algebraic function of x and y, and $g(z)$ is a function with an essential singularity of the type $\exp(-1/z^2)$ at the origin.

IX. AN ILLUSTRATION

The following serves to illustrate the method of description of free energy in the preceding section. It was chosen to fit the known critical indices for the two-dimensional Ising model and may be considered to be an example of a conjectured form for the free energy near the critical point of that celebrated problem. We begin with the algebraic function defined by

$$P(f;H,t) = (f + t^2)^8 f^4 (f - t^2)^3 + 2tH^8 f^7 + H^{16} + t^{15} H^8 = 0 \quad (5)$$

Before defining the Abelian integral, we note that for the two-dimensional Ising model, $a_0^+ \sim t^2 \ln t$ and $a_0^- \sim t^2 \ln (-t)$. Since an Abelian integral can have at most logarithmic singularities, we see that what is needed is t^2 times an Abelian integral. Consequently, we work with the function $f/t^2 \equiv g$ whose Riemann surface is identical to that of the function f. This Riemann surface is, of course, very complicated and we shall characterize it here in the following way only. For fixed real t, regard f as a function of H alone. Then, near $H = 0$, f has fifteen sheets, eight of which are given by

$$a_0 = -t^2 \text{ (eight times)} \quad (6a)$$

$$a_1 = (1/8)^{1/8}(-t)^{1/8} \quad (6b)$$

$$a_2 = -8^{3/4}(17/128)(-t)^{-7/4} \quad (6c)$$

four of which are given by

$$a_0 = 0 \text{ (four times)} \tag{7a}$$

$$a_1 = 0 \tag{7b}$$

$$a_2 = t^{-7/4} \tag{7c}$$

while the remaining three belong to a cycle with a third-order branch point at the origin. The physical (real) values of f are given for positive t by the negative fourth root in Eq. (7c) and for negative t by the two real (positive and negative) eighth roots in Eq. (6b) which correspond to the real and positive fourth root in Eq. (6c).

The determination of the other branch points in the neighborhood of the origin involves the computation of the roots of the discriminant of the polynomial defined by Eq. (5) and is too difficult to be attempted here. Rather, we shall infer the positions of these branch points from our knowledge of the structure of the Riemann surface near the origin. Since $P(f;H,t)$ is homogeneous, the relevant independent variable is $z \equiv H^8/t^{15}$. The function f will have branch points at $z = 0$, $z = z_1$, $z = z_2$, etc. Each of these branch points (except the first) represents eight branch points in H with H_i being given as a function of t by $H_i = z_i^{1/8} t^{15/8}$. All of these branch points converge on the origin as t approaches zero, and we may suppose that two of them lie on the extensions of the physical branches above the crunode for $t < 0$ as in the molecular field theory. The Abelian integrals are then constructed by putting a logarithmic singularity at each of these two branch points (one branch point in the t-plane). We shall actually need the sum of two integrals in order to obtain the symmetric logarithmic singularity for the specific heat. These are

$$\frac{F}{t^2} = \int_{t_0}^{t} \frac{g - g_-(H)}{t - t(H)}\, dt - \int_{-t_0}^{t} \frac{g - g_+(H)}{t + t(H)}\, dt \tag{8}$$

where $t(H)$ is the position of the nearest branch point on the real axis and $g_-(H)$ and $g_+(H)$ are the physical values of g for $t = t(H)$ and $t = -t(H)$, respectively. The lower limit of the integrals, t_0, is an arbitrary positive real constant. The Riemann surface is shown schematically in Figure 3. For $H \neq 0$, it is evident that F/t^2 has no singularities on the physical branches of g since $g(t,H)$ is linear in t near $t(H)$ and $-t(H)$. There will be a logarithmic singularity in F/t^2 on the non physical branch which contains the branch point at $t(H)$ since the integrand of the first integral has a pole there. For $H = 0$, the Riemann surface becomes disjoint and we get two distinct logarithmic singularities when we approach $t = 0$ along the negative and positive real axes separately. The first integral vanishes for

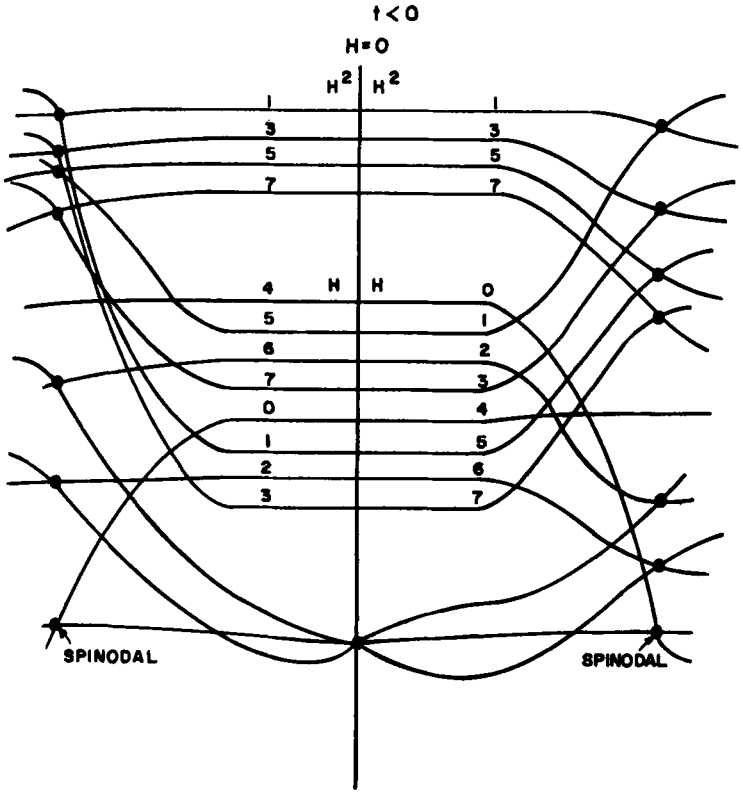

Fig. 3. Possible structure for the Riemann surface of the two-dimensional Ising model free energy for $t < 0$. H and H^2 refer to the dependence of the isotherm on H near $H = 0$. The numbers give the powers of the eighth root of unity and represent the coefficients of H and H^2.

negative t, while the second integral vanishes for positive t since $g(t < 0, H) \xrightarrow[H \to 0]{} -1 = g_-(H = 0)$ and $g(t > 0, H) \xrightarrow[H \to 0]{} 0 = g_+(H = 0)$. We therefore get

$$\frac{F}{t^2} = \begin{cases} \ln\left(\frac{t}{t_0}\right) & \text{for } t > 0 \\ \ln\left(\frac{-t}{t_0}\right) & \text{for } t < 0 \end{cases} \tag{9}$$

as desired. The free energy F will be seen to have the same critical exponents as f when the expansions of Eqs. (1) and (2) are used in the integral of Eq. (8). The expansions for the a_n's may contain terms of the form $t^i \ln t$ but these terms will not affect the leading (critical) exponent for each a_n.

The branch points in the neighborhood of the origin illustrate another aspect of the critical region which has become popular recently, mainly with the experimentalists. Since the two physical branches of f which form the crunode for $t < 0$ must be connected to the other nonphysical branches, there must be a branch point on each of them which approaches the origin of the H-plane as $t \to 0$. The trajectory of these branch points in the t-H manifold is the spinodal line originally referred to by van der Waals.[36] Since the spinodal line lies on a nonphysical (perhaps, metastable) sheet, it is unreachable by an equilibrium experiment. Nevertheless, by measuring a thermodynamic quantity along, say, an isotherm close to the critical isotherm, one may approach the branch point on the spinodal line and thus measure the associated exponent. The most obvious thing to measure along an isotherm is the magnetization as a function of H.[37] In the molecular field theory, this behaves as

$$M \sim (H - H(t))^{1/2} \tag{10}$$

where $H(t)$ is the trajectory of branch points. One may also approach the spinodal line along other curves; typically, for a liquid, C_V may be measured along a noncritical isochore. Note, however, that one cannot reach the spinodal branch point by moving along an isochamp. The reason is that when f is regarded as a function of t alone for fixed $H \neq 0$, the physical sheet contains no singularities, the spinodal branch point

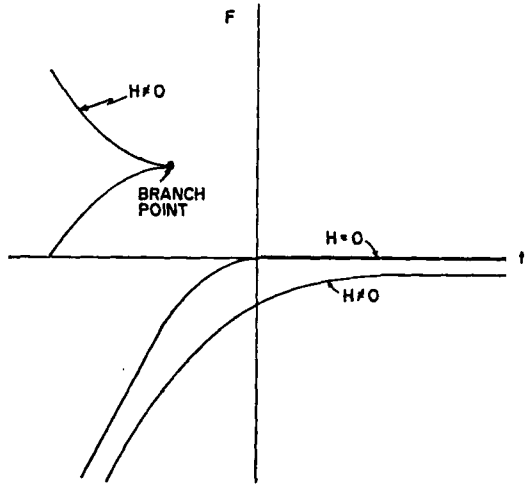

Fig. 4. Isochamps of $F(H,t)$ for the molecular field theory. Note that the branch point which is the intersection of the spinodal line with an isochamp, cannot be reached by continuation along the lower (equilibrium) line $H \neq 0$.

lying on another (nonphysical) sheet as shown in Figure 4 for the molecular field theory.

It is a curious fact that, to the author's knowledge, this is the only instance in which information about nonphysical singularities may be obtained by direct experimental measurement. In the still uncertain light in which we view the critical region, it is important that this be done.

X. CONCLUSION

We have attempted to take some of the mystery out of the mathematical description of themodynamic potentials near a critical point by showing that there are elementary functions which posess all the properties normally ascribed to these potentials in the vicinity of such a point. For the thermodynamic potential whose natural variables are naturally intensive, these properties may be summarized as follows. The thermodynamic potential is denoted by F and its reduced natural variables by z and t.

1. F is a single valued function of z and t with a singularity in z and t separately at $z = t = 0$ (critical point).

2. $(\partial F/\partial z)_t$ has a discontinuity along the line $z = 0$ for $t < 0$ (coexistence curve).

3. F has no singularity in t along the line $t = 0$ and $z \neq 0$ (critical isotherm) nor anywhere else in a (real) neighborhood $(0 < z < z_0, 0 < t < t_0)$ of the critical point.

The elementary analytic function which has the above properties is a single valued analytic function defined on the Riemann surface of an algebraic function. The algebraic function $f(z,t)$ has the following characteristics.

1. f has a branch point in z and t separately at $z = t = 0$.

2. The two smallest real branches of f form a crunode (crossing point) in the z-plane along the line $z = 0$ for $t < 0$.

3. The sheets of f contain branch points whose trajectories in the z-t manifold pass through the origin $(z = t = 0)$. That part of the Riemann surface of the true thermodynamic potential which is relevant in the neighborhood of the critical point is given by the Riemann surface of f. None of the other sheets of the true thermodynamic potential affect the critical exponents.

This last characteristic of f is illustrated by the molecular field theory. The equation of state $\tanh[(H + M)/kT] = M$ has an infinite number of solutions (sheets of M as a function of H) but only the three sheets which contain the two branch points (cusps) which come together at the origin determine the critical behavior. Thus, the relevant part of the Riemann

surface for the molecular field theory is given by the Riemann surface of the appropriate third-order algebraic function.[38] This Riemann surface is seen to be connected in the t-plane for $z \neq 0$ (the defining polynomial is irreducible in t for $z \neq 0$) but becomes disjoint when $z = 0$ (the polynomial factorizes when $z = 0$).

The property of convexity of the thermodynamic potential has been left out of the above list since it plays no direct role in determining the qualitative properties of the Riemann surface. It is, rather, a feature which must be taken into account when constructing specific examples of thermodynamic potentials and will, of course, play a role in determining the relationships among the critical exponents, the so-called scaling laws.

One point which we have studiously avoided in the foregoing discussion is the question of whether the critical exponents are rational or not, that is, whether the number of sheets of the Riemann surface with branch points which close down on the origin is finite or infinite. From the point of view of numerical estimates and experimental determination of critical exponents, the question is purely academic; any finite decimal is a rational number. Our present motive is to describe critical phenomena in terms of elementary functions and to this end we have employed the Riemann surface of algebraic functions. Since an algebraic function has, by its very definition, a finite number of sheets, we have ruled out the possibility of irrational critical exponents from this discussion. However, all the presently known features of the critical region are accounted for by these elementary functions so that until a given microscopic model is shown to have irrational exponents, we must continue to assume that the free energies we are looking for have the character defined above.

APPENDIX

An arbitrary holomorphic function can be written as the limit of a sequence of polynomials.[39] For the magnetic case, we look at the isotherms of $F(H,t)$ which are symmetric. We want to show that the sequence of polynomials can be symmetric.

To do this, pick an arbitrary point, say $H = +1.$ and expand the limit function about this point.

$$F = F_0 + F_1(\Delta H) + F_2(\Delta H)^2 + \cdots \tag{11}$$

where $\Delta H = H - 1$. Now choose the polynomial to be

$$\begin{aligned} P_{2n} &= P_0 + P_2 H^2 + P_4 H^4 + \cdots + P_{2n} H^{2n} \\ &= P'_0 + P'_1(\Delta H) + P'_2(\Delta H)^2 + \cdots + P'_{2n}(\Delta H)^{2n} \end{aligned} \tag{12}$$

where

$$\begin{aligned} P_0' &= P_0 + P_2 + \cdots + P_{2n} \\ P_1' &= 2P_2 + 4P_4 + \cdots + 2nP_{2n} \\ P_2' &= P_2 + 6P_4 + \cdots + n(2n-1)P_{2n} \\ &\cdots \end{aligned} \tag{13}$$

are not all linearly independent.

We can match n derivatives of F at the point $H = +1$ and obviously at $H = -1$ as well with P_{2n} since there are n independent coefficients. In the limit $n \to \infty$, the sequence converges to the function F uniformly in the punctured disk $0 < H < H_0$ where H_0 is arbitrary. Therefore, the imposition of symmetry on the polynomial does not represent a restriction on the original theorem.

For $H = 0$, the sequence does not converge to F since $(\partial P_{2n}/\partial H)_{H=0} = 0$ for all n. The situation is similar to the step function representing the Fermi distribution of free particles at zero temperature regarded as the limit of a sequence of finite temperature Fermi distributions. The sequence converges uniformly in the punctured disk $0 < E - E_F < E_0$ where E_F is the Fermi energy and E_0 is arbitrary but does not converge to the step function at $E = E_F$.

References

1. C. de la Tour, *Ann. Chim. Phys.* [2] **21**, 127 (1822). This rather obscure work was made known to the author in an article by M. H. Andrews and W. C. Woodbury, *Phys. Rev.* **129**, 1911 (1963).
2. See, for example, T. Andrews, *Trans. Roy. Soc.* **A178**, 45 (1887).
3. J. D. van der Waals, unpublished dissertation (Leiden).
4. An almost complete list of references to experimental and theoretical results appears in L. P. Kadanoff et al., *Rev. Mod. Phys.* **39**, 395 (1967), and M. E. Fisher, *J. Math. Phys.* **5**, 944 (1964).
5. P. Weiss, *J. de Phys.* **6**, 667 (1907).
6. B. Widom, *J. Chem. Phys.* **43**, 3898 (1965).
7. See, for example, M. Kac, G. E. Uhlenbeck, and P. C. Hemmer, *J. Math. Phys.* **4**, 216 (1963).
8. L. P. Kadanoff has shown how one can derive the condition of homogeneity for the Ising model in *Physics* **2**, 263 (1966).
9. M. H. Coopersmith, *Phys. Rev.* **172**, 230 (1968).
10. L. Onsager, *Phys. Rev.* **65**, 117 (1944).
11. E. Lieb, *Phys. Rev.* **162**, 162 (1967).
12. C. N. Yang, *Phys. Rev.* **85**, 808 (1952).
13. Various numerical calculations for the a_n's and b_n's up to $n = 8$ have been made. See, for example, C. Domb and D. L. Hunter, *Proc. Phys. Soc.* **86**, 1147 (1965), and G. A. Baker et al., *Phys. Lett.* **22**, 69 (1955).
14. See, for example, H. D. Ursell, *Proc. Cambridge Phil. Soc.* **23**, 685 (1927).

15. J. Mayer, *J. Chem. Phys.* **5**, 67 (1937).
16. R. Brout, *Phys. Rev.* **118**, 1009 (1960).
17. M. H. Coopersmith and R. Brout, *Phys. Rev.* **130**, 2539 (1963).
18. J. B. Jalickee, A. J. F. Siegert, and D. J. Vezzetti, preprint.
19. K. Huang, *Phys. Rev.* **119**, 1129 (1960).
20. The famous series of papers concludes with T. D. Lee and C. N. Yang, *Phys. Rev.* **117**, 897 (1960).
21. See Ref. 17 and also H. E. Stanley, Critical Phenomena in Heisenberg Models of Magnetism, in *Solid State Physics, Nuclear Physics, and Partical Physics: Ninth Latin American School of Physics* (W. A. Benjamin, Inc., New York, 1968).
22. A. F. Andreev, *Soviet Phys. JETP* **18**, 1415 (1964).
23. J. S. Langer, *Ann. Phys. (N.Y.)* **41**, 108 (1967).
24. M. E. Fisher, *Physics* **3**, 255 (1967).
25. S. F. Streeter and J. E. Mayer, *J. Chem. Phys.* **7**, 1025 (1939), conjectured this feature.
26. For a description of the precise method of defining a holomorphic function on the Riemann surface of an algebraic function, see F. A. Bliss, *Algebraic Functions* (Dover Publications, Inc., New York, 1966), Section 29.
27. C. N. Yang and T. D. Lee, *Phys. Rev.* **87**, 404 (1952), and T. D. Lee and C. N. Yang, *Phys. Rev.* **87**, 410 (1952).
28. P. C. Hemmer and E. H. Hauge, *Phys. Rev.* **133A**, 1010 (1964).
29. For a review of stability requirements on thermodynamic systems, see H. B. Callen, *Thermodynamics* (John Wiley and Sons, New York, 1960).
30. J. W. Essam and M. E. Fisher, *J. Chem. Phys.* **38**, 802 (1963).
31. G. S. Rushbrooke, *J. Chem. Phys.* **39**, 842 (1963).
32. R. B. Griffiths, *J. Chem. Phys.* **43**, 1958 (1965).
33. A. J. F. Siegert, *Phys. Rev.* **97**, 1456 (1955).
34. An example of this is the decay of an arbitrary state of a system to its thermodynamic equilibrium value. Although various approximation schemes enable one to calculate the relaxation time (i.e., the normalization of the exponent governing the time dependence), its actual existence has never been rigorously demonstrated.
35. Since we do not make any computational use of Abelian integrals here, we merely catalogue some of their properites. The interested reader is referred to G. A. Bliss, *op. cit.*, for the precise definition of Abelian integrals as well as theorems relating to them.
36. See J. S. Rowlinson, *Liquids and Liquid Mixtures* (Butterworths, London, 1959), p. 205, for a description of van der Waals' spinodal lines.
37. M. H. Coopersmith, *Phys. Lett.* **30A**, 192 (1969).
38. The particular form of this algebraic function is given in Ref. 9.
39. See R. C. Gunning and H. Rossi, *Analytic Functions of Several Complex Variables* (Prentice-Hall, Inc., Englwood Cliffs, N. J., 1965), p. 42, for a proof of the polynomial approximation to holomorphic functions.

Advance in Chemical Physics, Volume XVII
Edited by I. Prigogine, Stuart A. Rice

ON THE CALCULATION OF TIME CORRELATION FUNCTIONS

B. J. BERNE
and
G. D. HARP

CONTENTS

I. INTRODUCTION

A large number of experimental methods are currently used to probe the dynamics of molecular motions in solids, liquids, and gases. These include lineshape studies of electronic,[1] infrared, and Raman spectra[2]; studies of the shape of the spectral density function obtained from light- and neutron-scattering experiments[3-6]; lineshape studies in dielectric relaxation[7]; spin relaxation experiments[8]; acoustic attenuation[9]; as well as studies of static and frequency-dependent transport coefficients.[10]

All of these experimental methods share one characteristic in common. They all use as a probe an external field which is weakly coupled to the system and they all study the response of the physical system to the probe. This is to be expected since a more strongly coupled probe would influence the dynamical behavior of the system and would thereby obscure the fundamental molecular processes taking place.

The experiments can be divided into two categories according to whether the probe is mechanical or thermal. For example, light scattering falls into the first category whereas the measurement of the thermal conductivity falls into the second. The reason for making this division is the fact that the response of systems to mechanical probes is much easier to treat than their response to thermal probes. The interaction between a mechanical probe and the physical system can be described by an interaction Hamiltonian, whereas thermal probe system interactions must be handled differently.

The basic theoretical problem is to describe the response of an equilibrium system to a weak force field be it mechanical or thermal in nature. The solution to this problem is by now well known and there exist many excellent reviews on the subject.[11-17] A particularly informative account of this work together with historical comments has been given by Zwanzig.[12]

The major conclusions of this theory, which is known as linear response theory, can be simply stated as follows. Whenever two systems are weakly coupled to one another such as radiation weakly coupled to matter, or molecular vibrations weakly coupled to molecular motion, it is only necessary to know how both systems behave in the absence of the coupling in order to describe the way in which one system responds to the other. Furthermore, the response of one system to the other is completely describable in terms of time correlation functions of dynamical properties.

Time-dependent correlation functions have been familiar for a long time in the theory of noise and stochastic processes. In recent years they have become very useful in many areas of statistical physics and spectroscopy. Correlation functions provide a concise method for expressing the degree to which two dynamical properties are correlated over a period of time.

The correlation function $C_{\alpha\beta}(t)$ for two dynamical properties α and β is defined mathematically as

$$C_{\alpha\beta}(t) = \langle \alpha(0)\beta(t) \rangle$$

where the bracket indicates an equilibrium ensemble average. When α and β are different properties of the system, $C_{\alpha\beta}$ is called a cross-correlation function, and when they are the same property it is called an autocorrelation function. The dynamical property $\beta(t)$ can be computed in the following way. Consider a Gibbsian ensemble. Each replica system in the ensemble is in an initial state characterized by a point in phase space. As time progresses each replica system point traverses a trajectory in phase space which is uniquely determined by its initial state and by the canonical equations of motion. The function β varies on each trajectory due to its dependence on the phase. Thus corresponding to each replica system there is an initial point in phase space, a corresponding trajectory, and a corresponding time variation of the property β. Thus for each replica system the product $\alpha(0)\beta(t)$ depends only on the initial state of that system and the time. Averaging this product over all replica systems is equivalent to averaging it over a distribution of initial states consistent with the constraints on the ensemble. The bracket in the above expression merely indicates this averaging procedure. In the applications that are discussed here only the equilibrium canonical ensemble is used. In other applications different equilibrium and non-equilibrium ensembles are used. There is, of course, a corresponding quantum-mechanical definition which we will discuss later.

Because the response of a system to a specific weak probe is directly related to a correlation function, many experiments have been devised to determine specific correlation functions. Only a few such experiments will be mentioned here. The interested reader should consult the excellent reviews on the subject.[12-16]

The most important experiment of this type is thermal neutron scattering. A complete determination of the differential scattering cross section for the scattering of neutrons from liquids completely determines the Van Hove scattering function.[18] This function is related through a space-time Fourier transform to the autocorrelation function of the number density at two

different space-time points in the liquid. In principle, this function contains all relevant information concerning the structure and dynamics of liquids that is necessary to describe liquid equilibrium and transport properties. There are still many experimental difficulties preventing the complete realization of this experimental program.

With the advent of lasers, light scattering has become a convenient and powerful tool for the determination of liquid properties.[19,20] Brillouin scattering experiments involve the spectral resolution of light scattered at various angles from a liquid or solid system. The differential scattering cross section obtained from this inelastic light-scattering experiment is directly related to the long wavelength and low frequency behavior of the Van Hove scattering function. It supplements the information gained from neutron scattering experiments but is not capable of giving short wavelength and high frequency information. Nevertheless, it is useful for the determination of hydrodynamic and transport properties,[21,22] and recently it has been shown how it can be used to determine rate constants in very fast chemical reactions.[23-25]

The shape of the vibration-rotation bands in infrared absorption and Raman scattering experiments on diatomic molecules dissolved in a host fluid have been used to determine[2,15] the autocorrelation functions $\langle \mathbf{u}(0) \cdot \mathbf{u}(t) \rangle$ and $\langle P_2(\mathbf{u}(0) \cdot \mathbf{u}(t)) \rangle$ where $\mathbf{u}$ is a unit vector pointing along the molecular axis and $P_2(x)$ is the Legendre polynomial of index 2. These correlation functions measure the rate of rotational reorientation of the molecule in the host fluid. The observed temperature- and density-dependence of these functions yields a great deal of information about reorientation in solids, liquids, and gases. These correlation functions have been successfully evaluated on the basis of molecular models.[15]

Another experimental method that has been used to determine orientational correlation functions in macromolecular systems is based on measurements of the time-dependence of the depolarization of fluorescence.[26] From these measurements rotational diffusion coefficients and the shape of the rotating macromolecule have been determined.[27]

Microwave spectroscopy and dielectric relaxation studies probe the autocorrelation function of the total electrical polarization of the system and thereby also provide information about molecular reorientation. This information is difficult to interpret.

All of these methods yield information about the time evolution of the specific correlation functions. What is usually measured, except in the case of the depolarization of fluorescence, is the power or frequency spectrum of the respective correlation functions over a wide range of frequencies.

There are many experiments which determine only specific frequency components of the power spectra. For example, a measurement of the diffusion coefficient yields the zero frequency component of the power spectrum of the velocity autocorrelation function. Likewise, all other static coefficients are related to autocorrelation functions through the zero frequency component of the corresponding power spectra. On the other hand, measurements or relaxation times of molecular internal degrees of freedom provide information about finite frequency components of power spectra. For example, vibrational and nuclear spin relaxation times yield finite frequency components of power spectra which in the former case is the vibrational resonance frequency,[28,29] and in the latter case is the Larmour precessional frequency.[8] Experiments which probe a range of frequencies contribute much more to our understanding of the dynamics and structure of the liquid state than those which probe single frequency components.

There are several compelling reasons to interpret experiments in terms of correlation functions. The most important among these is that the results of several different experiments can often be correlated and used to clarify the basic underlying dynamical processes in the liquid. For example, infrared absorption and Raman spectroscopy, as well as dielectric relaxation and the depolarization of fluorescence studies, provide information about molecular reorientation through the correlation functions $\langle \mathbf{u}(0) \cdot \mathbf{u}(t) \rangle$ and $\langle [\frac{3}{2}[\mathbf{u}(0) \cdot \mathbf{u}(t)]^2 - 1] \rangle$. These different measurements can be used to fill in gaps in the frequency-dependence of the power spectra, thereby providing a complete picture of the particular dynamical processes involved. Furthermore, correlation functions provide a useful link between theory and experiment. Any theoretical model which stands up to an exhaustive comparison with the full experimental frequency-dependence of the power spectra of the various correlation functions reflects more strongly on the nature of the liquid state than does one which only gives the transport coefficients or equivalently the zero frequency components of the power spectra. Thus a set of quite different experiments can be used to test a given model of a liquid and to assess the validity of certain *ad hoc* assumptions which unavoidably go into any theoretical model of liquids.

It can be stated that time correlation functions have done for the theory of time-dependent processes what partition functions have done for equilibrium theory. The time-dependent problem has become well defined, but no easier to solve. One now knows which correlation function corresponds to a given time-dependent phenomenon. Nevertheless, it is still extremely difficult to compute the correlation function. This is analogous to equilibrium theory where one knows that to compute any equilibrium property

of a system, one must compute a well-defined partition function—a very difficult task.

At present the complete time dependence of only a few time-correlation functions have been determined experimentally. Furthermore, the theory of time-dependent processes is such that we know in principle which experiments can be used to determine specific correlation functions, and in addition certain general properties of these correlation functions. However, one of the major difficulties encountered in developing a theory of time-correlation functions arises from the fact that there seems to be, at least at present, no simple way of bypassing the complex many-body dynamics in a realistic fashion. Consequently both theoretically and experimentally there are difficult obstacles impeding progress towards a satisfactory understanding of the dynamic behavior of liquids, solids, and gases.

In the case of monatomic fluids digital computers have recently been employed to cope with the mathematical difficulties encountered above. Two methods have been used and both have been reviewed by Nelson.[30] The first method is used to determine the equilibrium properties of fluids by Monte Carlo techniques. This method does not, however, provide dynamical information. The second method, molecular dynamics, is a brute force solution to the N-body problem. Alder and Wainwright[31] have used this latter method to study fluids of "hard sphere" atoms, and "square well" atoms. These authors originally pointed out the potential applications and limitations of this method. Rahman demonstrated that it is feasible to do dynamics studies on fluids having more realistic two-body interaction potentials.[32] He studied the dynamical properties of liquid argon with a Lennard-Jones interaction potential. Rahman was primarily interested in the time-dependent correlation functions which enter into the theory of neutron scattering. Among other things, his time-correlation functions show that the motion of argon atoms in the fluid is more complicated than that assumed earlier in simplified model calculations. According to Zwanzig,[12] "Rahman's calculations provide what is probably the most detailed 'experimental' information currently available about dynamical processes in liquids."

Until now there have been no simulations done on liquids whose constituents possess internal degrees of freedom. We have therefore undertaken a series of computer studies of the simplest liquids of this type: liquids made up of the diatomic molecules carbon monoxide and nitrogen. There were a number of compelling reasons for making these studies:

(1) To obtain a realistic and detailed picture of how individual molecules rotate and translate in these classical fluids.

(2) To examine in detail some of the time-correlation functions that enter into the theories of transport, light absorption, and light scattering and neutron scattering.

(3) To see how well simulations based on various proposed potentials reflect physical reality.

(4) To test various stochastic assumptions for molecular motion that would simplify the N-body problem if they were valid. Molecular dynamics is far superior to experiment for this purpose since it provides much more detailed information on molecular motion than is provided by any experiment or group of experiments.

These studies are to be regarded as "experiments" which probe time-correlation functions. They provide the raw data against which various dynamical theories of the liquid state can be checked. These studies provide insight into the microscopic dynamical behavior of real diatomic liquids for both the experimentalist and theoretician alike.

There have been a number of attempts to calculate time-correlation functions on the basis of simple models. Notable among these is the non-Markovian kinetic equation, the memory function equation for time-correlation functions first derived by Zwanzig[33] and studied in great detail by Berne et al.[34] This approach is reviewed in this article. Its relation to other methods is pointed out and its applicability is extended to other areas. The results of this theory are compared with the results of molecular dynamics.

Linear response theory is reviewed in Section II in order to establish contact between experiment and time-correlation functions. In Section III the memory function equation is derived and applied in Section IV to the calculation of time-correlation functions. Section V shows how time-correlation functions can be used to guess time-dependent distribution functions and similar methods are then applied in Section VI to the determination of time-correlation functions. In Section VII a succinct review is given of other exact and experimental calculations of time-correlation functions.

II. LINEAR RESPONSE THEORY

A. Linear Systems

When a system of molecules interacts with a weak radiation field the interaction Hamiltonian in the dipole approximation is

$$H' = -\int_v d^3r \mathbf{M}(\mathbf{r}) \cdot \mathbf{E}(\mathbf{r}, t) \tag{1}$$

where $\mathbf{E}(\mathbf{r}, t)$ is the classical electric field at the space-time point (r, t) and $\mathbf{M}(\mathbf{r})$ is the electric polarization at the point $\mathbf{r}$.

$$\mathbf{M}(\mathbf{r}) = \sum_m \boldsymbol{\mu}_m \, \delta(\mathbf{r} - \mathbf{r}_m)$$

Here $\boldsymbol{\mu}_m$ is the electric dipole operator and $\mathbf{r}_m$ the center of mass position of molecule m. The Hamiltonian can also be written as

$$H' = -\sum_m \boldsymbol{\mu}_m \cdot \mathbf{E}(\mathbf{r}_m, t)$$

There is a completely analogous development for a system of nuclear spins interacting with a time-dependent magnetic field polarized along the x axis.

It is a fact that when a system interacts with a weak probe the interaction Hamiltonian can often be written as

$$H' = -\int d^3\mathbf{r} \hat{B}(\mathbf{r}) F(\mathbf{r}, t) \tag{2}$$

Here

$$\hat{B}(\mathbf{r}) = \sum_m \tfrac{1}{2}[\hat{B}_m, \delta(\mathbf{r} - \mathbf{r}_m)]_+ \tag{3}$$

with $\hat{B}_m$ a molecular property and $\mathbf{r}_m$ the position of particle m. $F(\mathbf{r}, t)$ is a field which acts on the property $\hat{B}(\mathbf{r})$ at the space-time point $(\mathbf{r}, t)$, much as the electric field at the space-time point $(\mathbf{r}, t)$ acts on the dipole moments in the neighborhood of the point $\mathbf{r}$. $F(\mathbf{r}, t)$ depends only on the properties of the probe. $[\,]_+$ denotes the anticommutator.

More generally there may be a set of different forces $F_i((\mathbf{r}, t)$ acting on the molecular system so that

$$H' = -\sum_i \int d^3r \hat{B}_i(\mathbf{r}) F_i(\mathbf{r}, t)$$

This form of the interaction potential between a system and a probe is quite ubiquitous. We shall therefore restrict our attention to the study of how a system responds to the adiabatic turning on of a Hamiltonian of the form given by Eq. (2).

It is convenient to assume from the outset that in the absence of the probing field F the expectation value of the observable $\hat{B}$ is zero. In the presence of the probe F, $\langle B \rangle$ is in general not zero, because the system is "driven" by the force F. This also applied to other properties of the system which in the absence of the probe are expected to be zero. The perturbation thus "induces" certain properties of the system to take on nonzero expectation values. If the perturbation is sufficiently weak it produces a

linear response in the system. In the linear regime, doubling the magnitude of F simply doubles the magnitude of the induced responses. A simple example of linear response is Ohm's law.

$$\mathbf{J} = \sigma \cdot \mathbf{E}$$

according to which the current induced in a medium is linear in the electric field $\mathbf{E}$ (although not necessarily in the same direction as $\mathbf{E}$ because of possible anisotropies in the conductivity tensor σ).

The expectation value of the property $\hat{A}$ at the space-time point $(\mathbf{r}, t)$ depends in general on the perturbing force F at all earlier times $t - t'$ and at all other points $\mathbf{r}'$ in the system. This dependence springs from the fact that it takes the system a certain time to respond to the perturbation; that is, there can be a time lag between the imposition of the perturbation and the response of the system. The spatial dependence arises from the fact that if a force is applied at one point of the system it will induce certain properties at this point which will perturb other parts of the system. For example, when a molecule is excited by a weak field its dipole moment may change, thereby changing the electrical polarization at other points in the system. Another simple example of these nonlocal changes is that of a neutron which when introduced into a system produces a density fluctuation. This density fluctuation propagates to other points in the medium in the form of sound waves.

It is consequently quite natural to write

$$\langle A(\mathbf{r}, t)\rangle = \int_{-\infty}^{t} dt' \int d\mathbf{r}' \Phi_{AB}(\mathbf{r}, \mathbf{r}'; t, t') F(\mathbf{r}', t') \tag{4}$$

where it is assumed that the force has been turned on in the past. Note that the induced response $\langle A(\mathbf{r}, t)\rangle$ is linear in the applied force F and furthermore depends on the values F at all earlier times t, and at all points in the system. Causality is built into the above equation since the response follows and does not precede the application of the force. $\Phi_{AB}(\mathbf{r}, \mathbf{r}'; t, t')$ is called the "after-effect function" because it relates the response $\langle A(\mathbf{r}, t)\rangle$ at the space-time point $(\mathbf{r}, t)$ to the disturbance at the space-time point $(\mathbf{r}', t')$. Note that the response to a delta function force,

$$F(\mathbf{r}, t) = \delta(\mathbf{r} - \mathbf{r}_0)\, \delta(t - t_0) \tag{5}$$

is

$$\langle A(\mathbf{r}, t)\rangle = \Phi_{AB}(\mathbf{r}, \mathbf{r}_0; t, t_0)\, \eta(t - t_0) \tag{6}$$

where $\eta(t)$ is the Heaviside function. Thus $\Phi_{AB}(\mathbf{r}, \mathbf{r}_0, t, t_0)$ is the response $\langle A(\mathbf{r}, t)\rangle$ to a unit delta function pulse applied at the space-time point

$(\mathbf{r}_0, t_0)$. If in the absence of the perturbation the system is a large uniform system in thermodynamics equilibrium, then the response should be invariant to an arbitrary shift in the origin of the space-time coordinate system by $(\mathbf{a}_0, t_0)$. Consequently for such systems the condition

$$\langle A(\mathbf{r} + \mathbf{a}_0, t + t_0)\rangle = \langle A(\mathbf{r}, t)\rangle$$

must hold. This condition can only be met if the after-effect function has the form

$$\Phi_{AB}(\mathbf{r}, \mathbf{r}_0; t, t_0) = \Phi_{AB}(\mathbf{r} - \mathbf{r}_0, t - t_0) \tag{7}$$

Thus the response of a spatially uniform system in thermodynamic equilibrium is always characterized by translationally invariant and temporaly stationary after-effect functions. This article is restricted to a discussion of systems which prior to an application of an external perturbation are uniform and in equilibrium. The condition expressed by Eq. (7) must be satisfied. Caution must be exercised in applying linear response theory to problems in double resonance spectroscopy where non-equilibrium initial states are prepared. Having dispensed with this caveat, we adopt Eq. (7) in the remainder of this review article.

The response can thus be written as

$$\langle A(\mathbf{r}, t)\rangle = \int_{-\infty}^{t} dt' \int dr' \Phi_{AB}(\mathbf{r} - \mathbf{r}', t - t') F(\mathbf{r}', t') \tag{8}$$

Once the after-effect function has been determined the response to any form of $F(\mathbf{r}, t)$ can be predicted. The after-effect function is an intrinsic dynamical property of the system, which is independent of the precise magnitude and form of the applied force, and which succinctly summarizes the way in which the constituent particles in a many-body system cooperate to give the observed response of the system to the external perturbation.

That the after-effect function $\Phi_{AB}(\mathbf{r}, t)$ is a real function of the space-time coordinates $(\mathbf{r}, t)$ can be deduced from the fact that, since A is an observable, the response $\langle A(\mathbf{r}, t)\rangle$ to a real force must be real.

The force $F(\mathbf{r}, t)$ is in general a very complicated real function of the position and time. Any such force can be regarded as a superposition of monochromatic components,

$$F_{k\omega} e^{-i[k\cdot r - \omega t]} e^{-\varepsilon|t|} \qquad \varepsilon > 0$$

The factor $e^{-\varepsilon|t|}$ has been introduced so that the field vanishes in the infinite past. Furthermore a field which is left on for an infinite time, no matter how weak it is, will tend to heat the system. To avoid this eventuality the response is calculated in the limit that $\varepsilon \to 0+$. Since the response is

linear in the force it suffices to compute the response of the system to each one of the monochromatic waves separately and then to superpose the results to find the total response. Therefore without loss of generality we consider only the response to a single monochromatic force. Introducing the above force into Eq. (8) yields

$$\langle A(\mathbf{r}, t)\rangle = \chi_{AB}(\mathbf{k}, \omega)F_{k\omega}\, e^{-i[k\cdot r-\omega t]} \tag{9}$$

where $\chi_{AB}(\mathbf{k}, \omega)$ is the frequency and wave vector-dependent complex susceptibility governing the linear response of $\langle A(\mathbf{r}, t)\rangle$ to the monochromatic perturbation. The susceptibility is obviously the Fourier-Laplace transform of the after-effect function.

$$\chi_{AB}(k, \omega) = \lim_{\varepsilon\to 0}\int_0^\infty dt \int d\mathbf{r}\Phi_{AB}(\mathbf{r}, t)\, e^{i[\mathbf{k}\cdot\mathbf{r}-\omega t]}e^{-\varepsilon t} \tag{10}$$

Since the after-effect function is a real function of $(\mathbf{r}, t)$, the susceptibility can be written in terms of its real, $\chi'_{AB}(\mathbf{k}, \omega)$, and imaginary, $\chi''_{AB}(\mathbf{k}, \omega)$ parts,

$$\chi_{AB}(\mathbf{k}, \omega) = \chi'_{AB}(\mathbf{k}, \omega) + i\chi''_{AB}(\mathbf{k}, \omega) \tag{11}$$

Comparison of Eqs. (10) and (11) yields

$$\begin{aligned}\chi'_{AB}(\mathbf{k}, \omega) &= \lim_{\varepsilon\to 0}\int_0^\infty dt \int d\mathbf{r}\Phi_{AB}(\mathbf{r}, t)\cos[\mathbf{k}\cdot\mathbf{r} - \omega t]\, e^{-\varepsilon t}\\ \chi''_{AB}(\mathbf{k}, \omega) &= \lim_{\varepsilon\to 0}\int_0^\infty dt \int d\mathbf{r}\Phi_{AB}(\mathbf{r}, t)\sin[\mathbf{k}\cdot\mathbf{r} - \omega t]\, e^{-\varepsilon t}\end{aligned} \tag{12}$$

The field applied to the system must in general be real, so that the full monochromatic force should be the superposition,

$$\tfrac{1}{2}[F_{k,\omega}\, e^{-i[\mathbf{k}\cdot\mathbf{r}-\omega t]} + F^*_{k,\omega}\, e^{i[\mathbf{k}\cdot\mathbf{r}-\omega t]}]\, e^{-\varepsilon|t|}$$

and the total response is the superposition of responses from each component, or

$$\langle A(\mathbf{r}, t)\rangle = \tfrac{1}{2}[\chi_{AB}(\mathbf{k}, \omega)F_{k\omega}\, e^{-i[\mathbf{k}\cdot\mathbf{r}-\omega t]} + \chi_{AB}(-\mathbf{k}, -\omega)F^*_{k\omega}\, e^{i[\mathbf{k}\cdot\mathbf{r}-\omega t]}] \tag{13}$$

The following properties follow directly from these definitions,

$$\begin{aligned}&\text{(i)} && \chi'_{AB}(-\mathbf{k}, -\omega) = \chi'_{AB}(\mathbf{k}, \omega)\\ &\text{(ii)} && \chi''_{AB}(-\mathbf{k}, -\omega) = -\chi''_{AB}(\mathbf{k}, \omega)\\ &\text{(iii)} && \chi^*_{AB}(\mathbf{k}, \omega) = \chi_{AB}(-\mathbf{k}, -\omega)\end{aligned} \tag{14}$$

These properties result from the fact that the sin and cos are respectively odd and even functions of their arguments. Condition (iii) can also be deduced directly from Eq. (10) by demanding that the induced response be real (that is $\langle A \rangle = \langle A \rangle^*$). Condition (iii) allows Eq. (13) to be expressed as

$$\langle A(\mathbf{r}, t) \rangle = \mathrm{Re}\, \chi_{AB}(\mathbf{k},\omega) F_{k,\omega}\, e^{-i[k\cdot r - \omega t]}$$

The response of the system to the external monochromatic perturbation of Eq. (9) is accompanied by the absorption and emission of energy. This follows because under the influence of the external perturbation the system changes state. The difference between the energy absorbed and emitted is the energy dissipation. The energy dissipated per second $Q(\mathbf{k}, \omega)$, can be related to a susceptibility of the system. The time rate of change of the system's energy is simply $\partial \hat{H}'/\partial t$ where H' is given by Eq. (2) $Q(\mathbf{k}, \omega)$ is obtained from the expectation value of $\partial \hat{H}'/\partial t$ by averaging it over one period of the monochromatic field. Thus

$$Q(\mathbf{k}, \omega) = \frac{\omega}{2\pi} \int_0^{2\pi/\omega} dt \int_v d\mathbf{r} \langle B(\mathbf{r}, t) \rangle \frac{\partial F}{\partial t}(\mathbf{r}, t) \tag{15}$$

Substitution of Eq. (13) results in

$$Q(k, \omega) = V \frac{\omega}{2} \chi''_{BB}(\mathbf{k}, \omega) |F_{k,\omega}|^2 \tag{16}$$

where V is the volume of the system.

The imaginary part of the susceptibility $\chi_{BB}(\mathbf{k},\omega)$ is therefore related to the net energy dissipated per unit time by the system. It is obvious that all real processes are always accompanied by some energy dissipation* so that $Q(\mathbf{k}, \omega) \geq 0$. It then follows from Eq. (16) that

$$\chi''_{BB}(\mathbf{k}, \omega) = \begin{cases} >0 & \omega > 0 \\ <0 & \omega < 0 \end{cases}$$

The susceptibility can in principle be determined in the following way: A force,

$$F(\mathbf{r}, t) = F_{k,\omega} \cos [\mathbf{k} \cdot \mathbf{r} - \omega t] \tag{17}$$

is switched on and the response $\langle A(\mathbf{r},t) \rangle$ is measured as a function of time. From Eq. (10) it is seen that

$$\langle A(\mathbf{r}, t) \rangle = F_{k,\omega} \{\chi'_{AB}(\mathbf{k}, \omega) \cos [\mathbf{k} \cdot \mathbf{r} - \omega t] + \chi''_{AB}(\mathbf{k}, \omega) \sin [\mathbf{k} \cdot \mathbf{r} - \omega t]\} \tag{18}$$

* According to the Weiner-Khinchin theorem $\chi''_{BB}(k, \omega) \geq 0$ so that it can be proved quite generally that $Q(k,\omega) \geq 0$ and consequently a linearly driven system always dissipates energy.

If phase-sensitive detection is used then χ'_{AB} can be found from the part of $\langle A \rangle$ that oscillates in phase with the applied field (dispersion) and χ''_{AB} can be found from the part of $\langle A(\mathbf{r},t) \rangle$ that oscillates 90° out of phase with the applied field (absorption). In practice it is unnecessary to measure both χ' and χ'' because there exists a theoretical relationship between χ' and χ'' so that a determination of one member of the pair uniquely determines the other member of the pair. It follows from this fact that the complex function, $\chi(\mathbf{k}, \omega) - \chi''(\mathbf{k}, \infty)$, is analytic and vanishes on an infinite semicircle in the lower half of the complex frequency plane (z-plane) and that χ'_{AB} and χ''_{AB} are related through the Kramer's Kronig relations

$$\begin{aligned} \chi'_{AB}(\mathbf{k}, \omega) - \chi'_{AB}(\mathbf{k}, \infty) &= \frac{1}{\pi} P \int_{-\infty}^{+\infty} d\omega' \chi''_{AB}(\mathbf{k}, \omega') \frac{1}{\omega' - \omega} \\ \chi''_{AB}(\mathbf{k}, \omega) &= -\frac{1}{\pi} P \int_{-\infty}^{+\infty} d\omega' [\chi'_{AB}(\mathbf{k}, \omega) - \chi'_{AB}(\mathbf{k}, \infty)] \frac{1}{\omega' - \omega} \end{aligned} \tag{19}$$

where P denotes the Cauchy principle part. Thus to compute χ'_{AB} at one frequency, one has to know χ''_{AB} at all frequencies and vice versa.

In spectroscopy the Kramer's Kronig relations are often used. For example the optical rotatory dispersion (ORD) is related to the circular dichroism (CD) through such a pair of transforms.[36] Workers in the area usually measure the (CD) and determine the (ORD) through Kramer's Kronig inversion of the (CD).

B. The Statistical Theory of the Susceptibility

There are a number of different ways to determine the quantum mechanical formulas for the susceptibilities $\chi_{AB}(\mathbf{k}, \omega)$. Perhaps the simplest and most elegant procedure is due to Kubo.[11] We follow this procedure here.

The total Hamiltonian of our system $\hat{H}$ consists of two parts: H:, the unperturbed Hamiltonian of the system and $\hat{H}'(t)$, the perturbation

$$\hat{H}'(t) = -\int d\mathbf{r} \hat{B}(\mathbf{r}) F(\mathbf{r}, t) \tag{20}$$

This perturbation, as we have seen, can also be written as

$$\hat{H}'(t) = -\sum_m \tfrac{1}{2}[\hat{B}_m, F(\mathbf{r}_m, t)]_+ \tag{21}$$

Since the responses that we are trying to calculate are linear in the force, it suffices to develop $F(\mathbf{r}_m, t)$ in a spatial Fourier series and then to compute

the response to each term separately. The total response is found by superposing each of these terms. Thus without loss of generality we consider only the response to the simple Hamiltonian

$$\begin{aligned} \hat{H}'(t) &= -\sum_m \tfrac{1}{2}[\hat{B}_m, e^{-i\mathbf{k}\cdot\mathbf{r}_m}]_+ F_k(t) \\ &= -\hat{B}_{-k} F_k(t) \end{aligned} \tag{22}$$

The density matrix, $\hat{\rho}$, characterizing the state of the responding system obeys the Liouville equation

$$\frac{\partial \hat{\rho}}{\partial t} = \frac{1}{i\hbar}[\hat{H}, \hat{\rho}]_- \tag{23}$$

The procedure that we adopt here is to:

(1) Solve the Liouville equation for the density matrix $\hat{\rho}(t)$ at time t, given that the system is initially in thermodynamic equilibrium.

(2) Linearize the solution in the field F.

(3) Compute the response $\langle A(\mathbf{r}, t)\rangle$ with the linearized solution.

The formal solution of the Liouville equation is

$$\hat{\rho}(t) = \hat{\rho}(-\infty) + \frac{1}{i\hbar}\int_{-\infty}^{t} dt' U_0(t-t')[H'(t'), \hat{\rho}(t')]_- U_0^{-1}(t-t') \tag{24}$$

where $[\ ]_-$ denotes the commutator and $U_0(t-t')$ is the unitary time-displacement operator $\exp[-(i/\hbar)H_0(t-t')]$ which transforms the state of the system at t',$\psi(t')$, into the state $\psi(t)$. In the Heisenberg picture of quantum mechanics the basis states are time independent, and the dynamical operators contain all of the time dependence. These operators depend on time in such a way that the arbitrary properly A at time t is generated from $\hat{A}(t')$ by the unitary transformation, $U_0(t-t')$

$$\hat{A}(t) = U_0^{-1}(t-t')\hat{A}(t')U_0(t-t')$$

or

$$\hat{A}(t) = \exp\left[\frac{i}{\hbar}\hat{H}_0(t-t')\right]\hat{A}(t')\exp\left[-\frac{i}{\hbar}\hat{H}_0(t-t')\right] \tag{25}$$

That Eq. (24) formally solves Eq. (23) is easily verified.

It is assumed that the system is in a state of thermodynamic equilibrium at temperature T prior to the application of the forces F_j. $\hat{\rho}(-\infty)$ must consequently be the canonical density matrix, $\hat{\rho}_0$,

$$\hat{\rho}_0 = Q^{-1} e^{\beta \hat{H}_0}$$

where $\beta^{-1} = KT$ and Q is the canonical partition function. After the forces F are adiabatically turned on, the density matrix $\hat{\rho}(t)$ varies with the time.

The deviation of the density matrix $\hat{\rho}(t)$ from its initial value $\hat{\rho}_0$ grows as the force grows so that

$$\hat{\rho}(t) = \hat{\rho}_0 + 0(F)$$

The commutator in Eq. (24) depends on the applied forces through the perturbation Hamiltonian $\hat{H}'(t')$ and through the density matrix $\hat{\rho}(t')$. To describe the linear response of the system it is sufficient to replace $\hat{\rho}(t')$ in the commutator by $\hat{\rho}_0$ so that

$$\hat{\rho}(t) = \hat{\rho}_0 + \frac{1}{i\hbar}\int_{-\infty}^{t} dt' U_0(t-t')[\hat{H}'(t'), \hat{\rho}_0]_- U_0^{-1}(t-t') + 0(F^2) \quad (26)$$

In order to proceed with the method outlined above let us note, by taking the spatial Fourier transform of Eq. (8), that

$$\langle A_k(t)\rangle = \int_{-\infty}^{t} dt' \Phi_{AB}(k, t-t') F_k(t') \quad (27)$$

where $\Phi_{AB}(\mathbf{k}, t)$ is the spatial Fourier transform of the after-effect function. To proceed we compute $\langle A_k(t)\rangle$ with the density matrix of Eq. (26). The resulting response is then compared with the preceding equation in order to find a closed formula for $\Phi_{AB}(\mathbf{k}, t)$. $\langle A_k(t)\rangle$ computed in this fashion is

$$\langle A_k(t)\rangle = \frac{1}{\hbar}\int_{-\infty}^{t} dt' \mathrm{tr} A_k U_0(t-t')[\hat{H}'(t'), \hat{\rho}_0]_- U_0^{-1}(t-t') \quad (28)$$

where tr denotes a trace. Note that $U_0^{-1}(t-t') = U_0(t')U_0^{-1}(t)$, and $U_0(t-t') = U_0(t)U_0^{-1}(t')$. Furthermore, the trace of a product of operators is invariant to a cyclic permutation in the order of appearance of the operators. This allows Eq. (28) to be written as

$$\langle A_k(t)\rangle = \int_{-\infty}^{t} dt' < \frac{i}{\hbar}[A_k(t-t'), B_{-k}]_- > F_k(t') \quad (29)$$

after substitution of the perturbation Hamiltonian of Eq. (22). The after-effect function, $\Phi_{AB}(\mathbf{k}, \mathbf{t})$, follows directly from a comparison of Eqs. (29) and (27),

$$\Phi_{AB}(\mathbf{k}, t) = \left\langle \frac{i}{\hbar}[A_k(t), B_{-k}] \right\rangle \quad (30)$$

The properties A_k and B_{-k} were defined previously as

$$\begin{aligned} A_k &= \sum_m \tfrac{1}{2}[\hat{A}_m, e^{i\mathbf{k}\cdot\mathbf{r}_m}]_+ \\ B_{-k} &= \sum_m \tfrac{1}{2}[\hat{B}_m, e^{-i\mathbf{k}\cdot\mathbf{r}_m}]_+ \end{aligned} \quad (31)$$

Let us assume that the single particle properties $\hat{A}_m$ and $\hat{B}_m$ have definite symmetry under coordinate inversion, $\hat{P}$, so that

$$\hat{P}\hat{A}_m = \varepsilon_A \hat{A}_m$$
$$\hat{P}\hat{B}_m = \varepsilon_B \hat{B}_m$$

where the signatures ε_A and ε_B of $\hat{A}_m$ and $\hat{B}_m$ are $+1$ or -1 depending on whether the corresponding operators are even or odd on inversion. Thus

$$\hat{P}\hat{A}_k\hat{P} = \varepsilon_A \hat{A}_{-k}\hat{P}^2 = \varepsilon_A \hat{A}_{-k}$$
$$\hat{P}B_{-k}\hat{P} = \varepsilon_B \hat{B}_k \hat{P}^2 = \varepsilon_B \hat{B}_k$$

It should now be noted that the expectation value is invariant under an inversion transformation. This follows directly from the invariance of a trace to similarity transformation. Thus*

$$\Phi_{AB}(\mathbf{k}, t) = \left\langle \frac{i}{\hbar}[A_k(t), B_{-k}]_- \right\rangle = \mathrm{tr}\,\frac{i}{\hbar}\hat{P}[A_k(t), B_{-k}]_-\hat{\rho}\hat{P}$$

Now if the Hamiltonian is invariant under inversion, that is, if the potential is symmetric,

$$\hat{P}\hat{A}_k(t)\hat{P} = \hat{P}e^{iHt/\hbar}\hat{A}_k e^{-iHt/\hbar}\hat{P}$$
$$= \varepsilon_A e^{iHt/\hbar}\hat{A}_{-k}e^{-iHt/\hbar}$$

Thus we see that

$$\Phi_{AB}(\mathbf{k}, t) = \varepsilon_A\varepsilon_B\left\langle \frac{i}{\hbar}[A_{-k}(t), B_k]_- \right\rangle = \varepsilon_A\varepsilon_B\Phi_{AB}(-\mathbf{k}, t) \qquad (32)$$

It can be concluded that if $\varepsilon_A = \varepsilon_B$ the after-effect function is an even function of the wave vector whereas if $\varepsilon_A = -\varepsilon_B$ it is an odd function of the wave vector.

Now that we have determined the quantum-mechanical form of the after-effect function for an equilibrium system, we can determine the response to a monochromatic field. This response has the same frequency

* It can be demonstrated that the after-effect function $\Phi_{AB}(\mathbf{k}, t)$ can also be written as

$$\Phi_{AB}(\mathbf{k}, t) = \int_0^\beta d\lambda \,\langle e^{\lambda\hat{H}}B_{-k}e^{-\lambda\hat{H}}A_k(t)\rangle$$

or

$$= \int_0^\beta d\lambda \,\langle B_{-k}(-ih\lambda)A_k(t)\rangle$$

where $\dot{B}_k = (1/ih)[B_{-k}, \hat{H}]_-$ is the time rate of change of B_{-k}. The formula above is called the Kubo transform of the time-correlation function $\langle B_{-k}(0)A_k(t)\rangle$. That $\Phi_{AB}(\mathbf{k}, t)$ is given by this formula can be demonstrated by expanding $\langle (i/h([A_k(t), B_{-k}]\rangle$ in terms of the energy eigenstates of $\hat{H}$.

and wave vector as the field, and is entirely prescribed by the complex susceptibility $\chi_{AB}(\mathbf{k}, \omega)$ of Eq. (11) which becomes

$$\chi_{AB}(\mathbf{k}, \omega) = \int_0^\infty dt e^{+i\omega t} \left\langle \frac{i}{\hbar} [A_{+k}(t), B_{-k}]_- \right\rangle \tag{33}$$

The inversion symmetry of Φ_{AB} implies that,

$$\chi_{AB}(\mathbf{k}, \omega) = \varepsilon_A \varepsilon_B \chi_{AB}(-\mathbf{k}, \omega) \tag{34}$$

$$\Phi_{BB}(\mathbf{k}, t) = \Phi_{BB}(-\mathbf{k}, t)$$

and

$$\chi_{BB}(\mathbf{k}, \omega) = \chi_{BB}(-\mathbf{k}, \omega) \tag{35}$$

Another important property of the after-effect function $\Phi_{AB}(\mathbf{k}, t)$ can be derived. Note that

$$\Phi_{AB}(-\mathbf{k}, -t) = \left\langle \frac{i}{\hbar} [A_{-k}(-t), B_k]_- \right\rangle$$

Since the trace is invariant to a cyclic permutation of the operators, it follows that

$$\Phi_{AB}(-\mathbf{k}, -t) = -\left\langle \frac{i}{\hbar} [B_k(t), A_{-k}]_- \right\rangle = -\Phi_{BA}(\mathbf{k}, t) \tag{36}$$

and

$$\Phi_{BB}(-\mathbf{k}, -t) = -\Phi_{BB}(\mathbf{k}, t)$$

C. The Reciprocal Relations

The operators $\hat{A}_k$ and $\hat{B}_k$ are

$$\hat{A}_k \equiv \sum_m \tfrac{1}{2}[\hat{A}_m, e^{i\mathbf{k}\cdot\mathbf{r}_m}]_+$$

$$\hat{B}_k \equiv \sum_m \tfrac{1}{2}[\hat{B}_m, e^{i\mathbf{k}\cdot\mathbf{r}_m}]_+$$

The single particle properties $\{\hat{A}_m\}$ and $\{\hat{B}_m\}$ are Hermitian. $\hat{A}_{-k}$ and $\hat{B}_{-k}$ are consequently the Hermitian conjugates of $\hat{A}_k$, $\hat{B}_k$. Observables can quite generally be classified as time-even or time-odd depending on whether they do or do not change sign on time reversal. All even time derivatives of the coordinates are even under time reversal while all odd derivatives are odd under time reversal. Thus the Hamiltonian is time even, the angular momentum is time odd and the linear momentum is time odd. Time-even properties are represented by real Hermitian operators, while time-odd properties are represented by imaginary Hermitian operators.

The properties $\hat{A}_m$ and $\hat{B}_m$ have the property that

$$\hat{A}^*_m = \gamma_A \hat{A}_m$$
$$\hat{B}^*_m = \gamma_B \hat{B}_m$$

where γ_A and γ_B are the time reversal signatures of the observables. Thus if $\hat{A}_m$ is time-even $\gamma_A = 1$, whereas if it is time-odd $\gamma_A = -1$. The same holds true for γ_B.

From the definitions of A_k and B_k it follows that

$$\hat{A}^*_k = \gamma_A \hat{A}_{-k} = \gamma_A \hat{A}^+_k$$
$$\hat{B}^*_k = \gamma_B \hat{B}_{-k} = \gamma_B \hat{B}^+_k$$

where $\hat{A}^+_k$ and $\hat{B}^+_k$ denote the Hermitian conjugates of $\hat{A}_k$ and $\hat{B}_k$.

In the absence of external magnetic fields, or for that matter any external pseudovector field, the exact energy eigenstates of a system can only be degenerate with respect to the total angular momentum of the system. This source of degeneracy can be removed if we assume that the body is enclosed in a container with rigid walls. It is always possible in this case to choose the energy eigenstates to be real. Consider the matrix elements of $\hat{A}_k$ and B_k in the energy representation in which the eigenstates are real. From the preceding relation it is seen that

$$(n\,|\hat{A}^*_k|\,m) = \gamma_A (n\,|\hat{A}^+_k|\,m) \tag{37}$$

Since the states are real

$$(n\,|\hat{A}^*_k|\,m)^* = (n\,|\hat{A}_k|\,m) = \gamma_A (n\,|\hat{A}^+_k|\,m)^* = \gamma_A (m\,|\hat{A}_k|\,n) \tag{38}$$

The last equality follows from the definition of the Hermitian conjugate. Consequently

$$(n\,|\hat{A}_k|\,m) = \gamma_A (m\,|\hat{A}_k|\,n)$$

and similarly (39)

$$(n\,|\hat{B}_k|\,m) = \gamma_B (m\,|\hat{B}_k|\,n)$$

The operators $\hat{A}_k$ and $\hat{B}_k$ are seen to be symmetric or antisymmetric depending on their symmetry in time.

Let us now consider the time dependence of the one-sided correlation function,

$$\langle A_k(t) B_{-k}(0)\rangle \equiv \mathrm{Tr}\ \hat{\rho}\, e^{i\hat{\mathcal{H}}t/\hbar}\, \hat{A}_k\, e^{i\hat{\mathcal{H}}t/\hbar}\, \hat{B}_{-k}$$

Because the trace is invariant to a cyclic permutation in the order of the operators,

(i) $$\langle A_k(t) B_{-k}(0)\rangle = \langle A_k(0) B_{-k}(-t)\rangle$$

The trace can be expanded in the complete set of energy eigenstates described above. Then

$$\langle A_k(t)B_{-k}(0)\rangle = \sum_{nm} \hat{\rho}_n(n\,|\hat{A}_k|\,m)(m\,|\hat{B}_{-k}|\,n)\,e^{i\omega_{nm}t}$$

where $\omega_{nm} = (E_n - E_m)/\hbar$. Substitution from Eq. (39) shows that

$$\langle A_k(t)B_{-k}(0)\rangle = \gamma_A\gamma_B \sum_{nm} \hat{\rho}_n(n\,|\hat{B}_{-k}|\,m)(m\,|\hat{A}_k|\,n)\,e^{i\omega_{nm}t}$$

so that

(ii) $$\langle A_k(t)B_{-k}(0)\rangle = \gamma_A\gamma_B\langle B_{-k}(0)A_k(-t)\rangle$$

The complex conjugate of the one-sided function is

(iii)
$$\begin{aligned}\langle A_k(t)B_{-k}(0)\rangle^* &= \sum_{nm} \rho_n(n\,|\hat{A}_k|\,m)^*(m\,|\hat{B}_{-k}|\,n)^*\,e^{-i\omega_{nm}t}\\ &= \sum_{nm} \rho_n(n\,|\hat{B}_k|\,m)(m\,|\hat{A}_{-k}|\,n)\,e^{i\omega_{mn}t}\\ &= \gamma_A\gamma_B \sum_{nm} \rho_n(n\,|\hat{A}_{-k}|\,m)(m\,|\hat{B}_k|\,n)\,e^{i\omega_{mn}t}\end{aligned}$$

The second equality follows from the definition of the Hermitian conjugate and is $\langle B_k(0)A_{-k}(t)\rangle$. The third equality follows from the reality of the states and is $\langle A_{-k}(0)B_k(t)\rangle$. Consequently

$$\langle A_k(t)B_{-k}(0)\rangle^* = \langle B_k(0)A_{-k}(t)\rangle = \gamma_A\gamma_B\langle A_{-k}(0)B_{+k}(t)\rangle$$

Analogous relations follow for the one-sided correlation function $\langle B_{-k}(0)A_k(t)\rangle$,

(i) $$\langle B_{-k}(0)A_k(t)\rangle = \langle B_{-k}(-t)A_k(0)\rangle$$

(ii) $$\langle B_{-k}(0)A_k(t)\rangle = \gamma_A\gamma_B\langle A_k(-t)B_{-k}(0)\rangle$$

and

(iii) $$\langle B_{-k}(0)A_k(t)\rangle^* = \langle A_{-k}(t)B_k(0)\rangle = \gamma_A\gamma_B\langle B_k(t)A_{-k}(0)\rangle$$

Consider now the after-effect function

$$\begin{aligned}\Phi_{AB}(k,t) &= \left\langle \frac{i}{\hbar}\,[A_k(t), B_{-k}(0)]_- \right\rangle\\ &= \frac{i}{\hbar}\,\{\langle A_k(t)B_{-k}(0)\rangle - \langle B_{-k}(0)A_k(t)\rangle\}\end{aligned}$$

From the properties (i), (ii), and (iii) for $\langle A_k(t)B_{-k}(0)\rangle$ and $\langle B_{-k}(0)A_k(t)\rangle$ it is easily seen that

$$\text{(i)} \qquad \Phi_{AB}(\mathbf{k}, t) = -\Phi_{BA}(-\mathbf{k}, -t)$$

$$\text{(ii)} \qquad \Phi_{AB}(\mathbf{k}, t) = +\gamma_A\gamma_B\Phi_{BA}(-\mathbf{k}, t) \tag{40a}$$

$$\text{(iii)} \qquad \Phi^*_{AB}(\mathbf{k}, t) = \Phi_{AB}(-\mathbf{k}, t) = \gamma_A\gamma_B\Phi_{BA}(\mathbf{k}, t)$$

These relationships can be combined with the transformation properties of $\Phi_{AB}(\mathbf{k}, t)$ under reflection summarized in Eq. (32)

$$\text{(iv)} \qquad \Phi_{AB}(-\mathbf{k}, t) = \varepsilon_A\varepsilon_B\Phi_{AB}(\mathbf{k}, t)$$

Conditions (i) and (ii) together give

$$\Phi_{AB}(\mathbf{k}, t) = -\gamma_A\gamma_B\Phi_{AB}(\mathbf{k}, -t) \tag{40b}$$

Conditions (iii) and (iv) together give

$$\Phi^*_{AB}(\mathbf{k}, t) = \varepsilon_A\varepsilon_B\Phi_{AB}(\mathbf{k}, t) = \gamma_A\gamma_B\Phi_{BA}(\mathbf{k}, t) \tag{40c}$$

and

$$\Phi_{AB}(\mathbf{k}, t) = \lambda_A\lambda_B\Phi_{BA}(\mathbf{k}, t) \tag{40d}$$

where $\lambda_A = \gamma_A\varepsilon_A$ and $\lambda_B = \gamma_B\varepsilon_B$ are the signatures of the properties $\hat{A}_k$ and $\hat{B}_k$ under combined inversion and time reversal.

It should be noted that

$$\Phi_{BB}(\mathbf{k}, t) = -\Phi_{BB}(\mathbf{k}, -t)$$
$$\Phi^*_{BB}(\mathbf{k}, t) = \Phi_{BB}(\mathbf{k}, t) \tag{40e}$$

and

$$\Phi_{BB}(\mathbf{k}, t) = \Phi_{BB}(-\mathbf{k}, t)$$

so that $\Phi_{BB}(\mathbf{k}, t)$ is a real odd function of the time and a real even function of $\mathbf{k}$.

From Eq. (33) it follows that

$$\chi_{AB}(\mathbf{k}, \omega) = \lambda_A\lambda_B\chi_{BA}(\mathbf{k}, \omega) \tag{40f}$$

The same arguments can be developed for a system which is in a uniform external magnetic field, B. The eigenvectors cannot be made real in this case and the wave functions have the property $\psi^*(B) = \psi(-B)$. It then follows that

$$\chi_{AB}(\mathbf{k}, \omega, \mathbf{B}) = \lambda_A\lambda_B\chi_{BA}(\mathbf{k}, \omega, -\mathbf{B}) \tag{41}$$

These symmetry relations are called the Onsager reciprocal relations. Their meaning is best illustrated by reference to the following problem. Suppose the interaction Hamiltonian is

$$H'(t) = -\sum_i \int d\mathbf{r} \hat{B}_i(\mathbf{r}) F_i(\mathbf{r}, t)$$

It then follows from completely equivalent arguments that

$$\langle B_{jk}(t) \rangle = \sum_l \int_{-\infty}^{t} dt' \Phi_{jl}(\mathbf{k}, t - t') F_{lk}(t')$$

where $\Phi_{jl}(\mathbf{k}, t)$ is the after-effect function that relates the jth response at time t to the lth field at all previous times. The reciprocal relations then give

$$\Phi_{jl}(\mathbf{k}, t) = \lambda_j \lambda_l \Phi_{lj}(\mathbf{k}, t)$$

or

$$\chi_{jl}(\mathbf{k}, \omega) = \lambda_l \lambda_j \chi_{lj}(\mathbf{k}, \omega)$$

According to these relations the response $\langle B_j \rangle$ produced by a unit pulse of F_i is identical except for sign to the response $\langle B_i \rangle$ produced by a unit pulse of F_j.

D. The Fluctuation–Dissipation Theorem

The lineshape of the power dissipation function, $Q(\mathbf{k}, \omega)$, is determined by the imaginary part of the susceptibility, $\chi''_{BB}(\mathbf{k}, \omega)$ as was shown in the previous section.

$$Q(\mathbf{k}, \omega) = V \frac{\omega}{2} \chi''_{BB}(\mathbf{k}, \omega) |F_{k\omega}|^2$$

Since many important dynamical properties of a many-body system are explored through precise lineshape measurements, it is worth studying some of the properties of $\chi''_{BB}(\mathbf{k}, \omega)$.

According to Eq. (14)

$$\chi^*_{BB}(\mathbf{k}, \omega) = \chi_{BB}(-\mathbf{k}, -\omega) = \int_0^\infty dt\, e^{-i\omega t} \Phi_{BB}(-\mathbf{k}, t)$$

Transforming from t to $-t$ and substitution of Eq. (14) leads to

$$\chi^*_{BB}(\mathbf{k}, \omega) = -\int_{-\infty}^{0} dt\, e^{i\omega t} \Phi_{BB}(\mathbf{k}, t) \tag{42}$$

The imaginary part of the susceptibility can now be found from the difference $\chi_{BB} - \chi^*_{BB}$,

$$\chi''_{BB}(\mathbf{k}, \omega) = \frac{1}{2\hbar} \int_{-\infty}^{+\infty} dt\, e^{i\omega t} \langle [B_k(t), B_{-k}]_- \rangle \tag{43}$$

The quantity $\langle [B_k(t); B_{-k}]_- \rangle$ can be expanded in terms of the complete set of energy eigenstates $|n)$,

$$\langle [B_k(t), B_{-k}]_- \rangle = \sum_{nm} (\rho_n - \rho_m)(n|B_k|m)(m|B_{-k}|n) \exp(i\omega_{nm} t)$$

where ρ_n is the Boltzmann factor $Q^{-1} \exp(-\beta E_n)$, $\omega_{nm} = (E_n - E_m)/\hbar$, and E_n is the nth energy eigenvalue. The right-hand side of this equation can be simplified by expressing the difference between the Boltzmann factors as

$$\rho_n - \rho_m = [1 - e^{-\beta\hbar\omega_{mn}}]\rho_n$$

Substitution of the resulting equation into $\chi''_{BB}(\mathbf{k}, \omega)$ and subsequent use of the definition of the delta function yields

$$\chi''_{BB}(\mathbf{k}, \omega) = \frac{\pi}{\hbar} \sum_{nm} [1 - e^{-\beta\hbar\omega_{mn}}]\rho_n (n|B_k|m)(m|B_{-k}|n)\, \delta(\omega + \omega_{nm})$$

Thus from the properties of the delta function it is seen that

$$\chi''_{BB}(\mathbf{k}, \omega) = \frac{1}{\hbar}(1 - e^{-\beta\hbar\omega}) \int_{-\infty}^{\infty} dt\, e^{i\omega t} \langle B_k(t) B_{-k}(0) \rangle \tag{44}$$

The quantity $\langle B_k(t) B_{-k}(0) \rangle$ appearing in the integral is a "one-sided" quantum-mechanical time-correlation function. The quantum-mechanical cross-correlation function $C_{AB}(\mathbf{k}, t)$ of the dynamical variables A_k, B_k is defined as

$$C_{AB}(\mathbf{k}, t) \equiv \langle \tfrac{1}{2}[A_k(t), B_{-k}(0)]_+ \rangle \tag{45}$$

where $[\ ]_+$ denotes the anticommutator, or symmetrized product,

$$[\alpha, \beta]_+ = \alpha\beta + \beta\alpha$$

From the preceding section it is easily shown that

(i) $$C_{AB}(\mathbf{k}, t) = C_{BA}(-\mathbf{k}, -t)$$

(ii) $$C_{AB}(\mathbf{k}, t) = \gamma_A \gamma_B C_{AB}(+\mathbf{k}, -t)$$

(iii) $$C^*_{AB}(\mathbf{k}, t) = C_{AB}(-\mathbf{k}, t) = \gamma_A \gamma_B C_{BA}(\mathbf{k}, t)$$

(iv) $$C_{AB}(\mathbf{k}, t) = \varepsilon_A \varepsilon_B C_{AB}(-\mathbf{k}, t)$$

Combining the results leads to the relations

$$C_{AB}(\mathbf{k}, t) = \lambda_A \lambda_B C_{BA}(\mathbf{k}, t) \tag{46b}$$

The autocorrelation function satisfies the following relations

$$C_{BB}(\mathbf{k}, t) = C_{BB}(-\mathbf{k}, t) = C_{BB}(\mathbf{k}, -t) = C_{BB}(-\mathbf{k}, t)$$

and (46c)

$$C^*_{BB}(\mathbf{k},t) = C_{BB}(\mathbf{k},t)$$

The autocorrelation function is a real even function of $\mathbf{k}$ and t.

The Fourier transform, $G_{AB}(\mathbf{k}, \omega)$ of the time-correlation function $C_{AB}(\mathbf{k}, t)$,

$$G_{AB}(\mathbf{k}, \omega) = \int_{-\infty}^{\infty} dt\, e^{i\omega t} C_{AB}(\mathbf{k}, t) \tag{47}$$

plays a very important role in linear response theory. Expansion of $G_{BB}(\mathbf{k}, \omega)$ in the energy representation and repetition of the same steps that resulted in Eq. (44) leads to the result

$$G_{BB}(\mathbf{k}, \omega) = \tfrac{1}{2}[1 + e^{-\beta\hbar\omega}] \int_{-\infty}^{\infty} dt\, e^{i\omega t} \langle B_k(t) B_{-k}(0) \rangle \tag{48}$$

This equation is now used to eliminate the integral on the right-hand side of Eq. (44) so that

$$\chi''_{BB}(\mathbf{k}, \omega) = \frac{1}{\hbar} \tan\left(\frac{\beta\hbar\omega}{2}\right) G_{BB}(\mathbf{k}, \omega) \tag{49}$$

or

$$\chi''_{BB}(\mathbf{k}, \omega) = \frac{1}{\hbar} \tanh\left(\frac{\beta\hbar\omega}{2}\right) \int_{-\infty}^{\infty} dt\, e^{i\omega t} \langle \tfrac{1}{2}[B_k(t), B_{-k}(0)]_+ \rangle \tag{50}$$

Since $\chi_{BB}(\mathbf{k}, \omega) = \chi_{BB}(-\mathbf{k}, \omega)$, it follows that $C_{BB}(\mathbf{k}, t) = C_{BB}(-\mathbf{k}, t)$. Substitution of Eq. (50) into $Q(\mathbf{k},\omega)$ yields

$$Q(\mathbf{k}, \omega) = \frac{V\omega}{2\hbar} \tanh\left(\frac{\beta\hbar\omega}{2}\right) |F_{k,\omega}|^2 G_{BB}(\mathbf{k}, \omega) \tag{51}$$

The power dissipation is linearly related to $G_{BB}(\mathbf{k}, \omega)$ which is called, for obvious reasons, the *power spectrum* of the random process B_k. It should be noted that the energy dissipated by a system when it is exposed to an external field is related to a time-correlation function $C_{BB}(\mathbf{k}, t)$ which describes the detailed way in which spontaneous fluctuations regress in the equilibrium state. This result, embodied in Eq. (51), is called the *fluctuation*

dissipation theorem.[38] It is a direct consequence of this theorem that weak force fields can be used to probe the dynamics of molecular motion in physical systems. A list of experiments together with the time-correlation functions that they probe is presented in Table I. An experiment which

TABLE I

Time-Correlation Functions and Experiments

Experimental measurement	Dynamical quantity	Time-correlation function
Diffusion coefficient	**V**, C.M. velocity of tagged molecule	$\langle \mathbf{V}(0) \cdot \mathbf{V}(t) \rangle$
Rotational diffusion coefficient	$\boldsymbol{\Omega}$ angular velocity about molecular C.M.	$\langle \Omega_\alpha(0)\Omega_\beta(t) \rangle$
Infrared absorption	**u**, unit vector along molecular transition dipole	$\langle \mathbf{u}(0) \cdot \mathbf{u}(t) \rangle$
Raman scattering; depolarization of fluorescence	**u**	$\langle P_2(\mathbf{u}(0) \cdot \mathbf{u}(t)) \rangle$
Spin-rotation relaxation time	**J**, angular momentum about molecular C.M.	$\langle \mathbf{J}(0) \cdot \mathbf{J}(t) \rangle$
NMR lineshape	M_x, x component of the magnetization of the system	$\langle M_x(0)M_x(t) \rangle$
Mossbauer lineshape	$\mathbf{r}_l$, position of lth nucleus	$\frac{1}{N}\sum_{l=1}^{N} \langle e^{-i\mathbf{k}\cdot\mathbf{r}_l(0)} e^{i\mathbf{k}\cdot\mathbf{r}_l(t)} \rangle$
Neutron scattering	$\mathbf{r}_l$, position of lth nucleus in fluid	$\frac{1}{N}\sum_{l=1}^{N} \langle e^{-i\mathbf{k}\cdot\mathbf{r}_l(0)} e^{i\mathbf{k}\cdot\mathbf{r}_l(t)} \rangle$ $\frac{1}{N}\left\langle \sum_{l=1}^{N} e^{-i\mathbf{k}\cdot\mathbf{r}_l(0)} \sum_{j=1}^{N} e^{i\mathbf{k}\cdot\mathbf{r}_j(t)} \right\rangle$
Brillouin scattering (polarized scattering)	α_l^I; trace of the polarizability tensor of molecule l	$\frac{1}{N}\left\langle \sum_{j,l}^{N} \alpha_l^I(0)\alpha_j^I(t)\, e^{i\mathbf{k}\cdot[\mathbf{r}_j(t)-\mathbf{r}_l(0)]} \right\rangle$
Brillouin scattering: (depolarized scattering)	xyth element of polarizability tensor of molecule l	$\frac{1}{N}\left\langle \sum_{l,j}^{N} \alpha_l^{xy}(0)\alpha_j^{xy}(t)\, e^{i\mathbf{k}[\mathbf{r}_j(t)-\mathbf{r}_l(0)]} \right\rangle$

determines $Q(\mathbf{k}, \omega)$ determines $G_{BB}(\mathbf{k}, \omega)$ and consequently through Fourier inversion $C_{BB}(\mathbf{k}, t)$,

$$C_{BB}(\mathbf{k}, t) = \frac{\hbar}{\pi V} \int_{-\infty}^{+\infty} d\omega \, e^{-i\omega t} \frac{Q(\mathbf{k}, \omega) \coth (\beta\hbar\omega/2)}{\omega |F_{k\omega}|^2} \tag{52}$$

The one-sided correlation function $\langle B_k(t) B_{-k}(0) \rangle$ could have been determined instead of $C_{BB}(\mathbf{k}, t)$. From Eqs. (48) and (51)

$$\langle B_k(t) B_{-k}(0) \rangle = \frac{2\hbar}{\pi V} \int_{-\infty}^{+\infty} dt \, e^{-i\omega t} \frac{Q(\mathbf{k}, \omega)}{\omega[1 - e^{-\beta\hbar\omega}] |F_{k\omega}|^2} \tag{53}$$

This kind of investigation is becoming so common in infrared spectroscopy that investigators are becoming more concerned with the appropriate time-correlation function than with the frequency spectrum itself.

In the classical limit ($\hbar \to 0$) Eq. (49) reduces to

$$\chi''_{BB}(\mathbf{k}, \omega) = \frac{\omega}{KT} G_{BB}{}^{cl}(\mathbf{k}, \omega) \tag{54}$$

where

$$G_{BB}{}^{cl}(\mathbf{k}, \omega) = \lim_{\hbar \to 0} \int_{-\infty}^{+\infty} dt \, e^{i\omega t} C_{BB}(\mathbf{k}, t)$$

is the correspondence rule limit of the power spectrum of the quantum-mechanical time-correlation function. The classical time-correlation function $C_{BB}{}^{cl}(\mathbf{k}, t)$ is defined as

$$C_{BB}{}^{cl}(\mathbf{k}, t) = \int d\Gamma f^{(N)}(\Gamma) B_{-k}(\Gamma) \, e^{iLt} B_k(\Gamma) \tag{55}$$

Where Γ is the initial phase point of the system, L is the Liouville operator, $f^{(N)}(\Gamma)$ is the canonical distribution function, and $B_k(\Gamma)$ and $B_{-k}(\Gamma)$ are the values of the classical properties B_k and B_{-k} when the system is in the classical state Γ. Much work has been done to determine how the quantum-mechanical functions approach the corresponding classical functions.

There is an alternative, and perhaps more intuitive way to derive the results of the preceding section. For simplicity we consider the case when a monochromatic force is applied to the system. The Hamiltonian of Eq. (2) then takes the form

$$H'(t) = -\tfrac{1}{2}[\hat{B}_{-k} F_k \, e^{i\omega t} + \hat{B}_k F^*{}_{k\omega} \, e^{-i\omega t}]$$

when the applied force is monochromatic. The operator $\hat{B}_k$ is as before

$$\hat{B}_k = \sum_{m=1}^{N} \hat{B}_m \, e^{+i\mathbf{k} \cdot \mathbf{r}_m}$$

From the definition of $\hat{B}_k$ it should be noted that $\hat{B}_k$ and $\hat{B}_{-k}$ are Hermitian conjugates. According to the Golden Rule of time-dependent perturbation theory the probability per unit time, $W_{i\to f}(\mathbf{k}, \omega)$, that the field $(\mathbf{k}, \omega)$ induces a transition in the system from the initial state $|i\rangle$ to the final state $|f\rangle$ is given by

$$W_{i\to f}(\mathbf{k}, \omega) = \frac{2\pi}{4\hbar^2} |F_{k,\omega}|^2 |(i| B_{+k} |f)|^2 \delta(\omega - \omega_{fi})$$

where $\hbar\omega_{fi} \equiv E_f - E_i$ and the delta function conserves energy. In a sense the external field transfers momentum, $\hbar\mathbf{k}$ and energy $\hbar\omega$ to the system in the transition. The probability that the system is initially in the state $|i\rangle$ is simply the Boltzmann factor $\rho_i = Q^{-1} e^{-\beta E_i}$. The probability per unit time that the probe will transfer momentum $\hbar\mathbf{k}$ and energy $\hbar\omega$ to the time regardless of the initial and final state is

$$P(\mathbf{k}, \omega) = \frac{2\pi}{4\hbar^2} |F_{k,\omega}|^2 \sum_{if} \rho_i |(i| B_{+k} |f)|^2 \delta(\omega - \omega_{fi}) \tag{56}$$

There is a corresponding inverse process in which the system makes a transition from the state $|f\rangle$ to the state $|i\rangle$ thereby giving momentum $\hbar\mathbf{k}$ and energy $\hbar\omega$ to the probe. In this process the system suffers a momentum change $-\hbar\mathbf{k}$ and an energy change $-\hbar\omega$ with a probability per unit time

$$W_{f\to i}(-\mathbf{k}, -\omega) = \frac{2\pi}{4\hbar^2} |F_{k,\omega}|^2 |(f| \hat{B}_{-k} |i)|^2 \delta(\omega - \omega_{fi}) \tag{57}$$

The probability per unit that the system will transfer momentum, $\hbar\mathbf{k}$, and energy, $\hbar\omega$, to the probe regardless of the initial state is consequently

$$P(-\mathbf{k}, -\omega) = \frac{2\pi}{4\hbar^2} |F_{k,\omega}|^2 \sum_{if} \rho_f |(f| B_{-k} |i)|^2 \delta(\omega - \omega_{fi}) \tag{58}$$

It should be noted that $W_{f\to i}(-\mathbf{k}, -\omega) = W_{f\to i}(\mathbf{k}, \omega)$. This follows directly from the fact that the operator $\hat{B}_k$ is the Hermitian adjoint of $\hat{B}_{-k}$. The transition probabilities $P(\mathbf{k}, \omega)$ and $P(-\mathbf{k}, -\omega)$ are in general unequal as can be seen by a comparison of Eqs. (56) and (58). In fact, since $\rho_f = \rho_i \exp(-\beta\hbar\omega_{fi})$ it is clear from the properties of the delta function that Eq. (58) is

$$P(-\mathbf{k}, -\omega) = \frac{2\pi}{4\hbar^2} |F_{k,\omega}|^2 e^{-\beta\hbar\omega} \sum_{if} \rho_i |(f| B_{-k} |i)|^2 \delta(\omega - \omega_{fi}) \tag{59}$$

B_{-k} and B_k are Hermitian conjugates so that

$$|(f|\hat{B}_{-k}|i)| = {}^2|(i|\hat{B}_{+k}|f)|^2$$

Substitution of this into Eq. (59) and subsequent comparison with Eq. (5) yields

$$P(-\mathbf{k}, -\omega) = \mathrm{e}^{-\beta\hbar\omega} P(\mathbf{k}, \omega) \tag{60}$$

This equation expresses the well-known condition of *detailed balance* according to which every transition out of a microscopic state of a system in equilibrium is balanced on the average by a transition into that state. This condition is sufficient for the maintenance of thermodynamic equilibrium. Equation (60) demonstrates that the system absorbs more energy per unit time than it emits. It can be concluded that there is a net energy dissipation from the external field with a consequent production of heat.

The above transition probabilities can be written in terms of one-sided time-correlation functions. For this purpose we define the dynamic form factor $S_B(\mathbf{k}, \omega)$ as

$$S_B(\mathbf{k}, \omega) = \sum_{if} \rho_i |\langle i| B_{+k} |f\rangle|^2 \, \delta(\omega - \omega_{fi}) \tag{61}$$

It follows from Eqs. (56), (58), and (60) that

$$P(\mathbf{k}, \omega) = \frac{2\pi}{4\pi^2} |F_{k,\omega}|^2 S_B(\mathbf{k}, \omega) \tag{62}$$

$$P(-\mathbf{k}, -\omega) = \frac{2\pi}{4\pi^2} |F_{k,\omega}|^2 S_B(-\mathbf{k}, -\omega) \tag{63}$$

$$S_B(-\mathbf{k}, -\omega) = e^{-\beta\hbar\omega} S_B(\mathbf{k}, \omega) \tag{64}$$

Equation (64) expresses the condition of detailed balance which is at the root of the fluctuation dissipation theorem.

The dynamic form factors can be written in terms of one-sided time-correlation functions. This is accomplished by transformation of Eq. (61) to the Heisenberg representation,

$$S_B(\mathbf{k}, \omega) = \frac{1}{2\pi} \int_{-\infty}^{+\infty} dt \, \mathrm{e}^{i\omega t} \langle B_k(t) B_{-k} \rangle \tag{65}$$

and

$$S_B(-\mathbf{k}, -\omega) = \frac{1}{2\pi} \int_{-\infty}^{+\infty} dt \, \mathrm{e}^{i\omega t} \langle B_{-k} B_k(t) \rangle \tag{66}$$

From the physical interpretation of $P(\mathbf{k}, \omega)$ and $P(-\mathbf{k}, -\omega)$ as absorption and emission rates, it is clear that the power dissipated per unit time and per unit volume, $Q(\mathbf{k}, \omega)$, is

$$Q(\mathbf{k}, \omega) = \hbar\omega [P(\mathbf{k}, \omega) - P(-\mathbf{k}, -\omega)] \tag{67}$$

This becomes, after simple rearrangement,

$$Q(\mathbf{k}, \omega) = \frac{\pi\omega}{\hbar} |F_{k,\omega}|^2 \tanh\left(\frac{\beta\hbar\omega}{2}\right)\left[\frac{S_B(\mathbf{k}, \omega) + S_B(-\mathbf{k}, -\omega)}{2}\right]$$

$$= \frac{\omega}{2\hbar} |F_{k,\omega}|^2 \tanh\left(\frac{\beta\hbar\omega}{2}\right) \int_{-\infty}^{\infty} dt\, e^{i\omega t} \langle \tfrac{1}{2}[B_k(t), B_{-k}(0)]_+ \rangle \quad (68)$$

Comparison of Eq. (68) with Eq. (51) shows that

$$\chi''_{BB}(\mathbf{k}, \omega) = \frac{1}{\hbar} \tanh\left(\frac{\beta\hbar\omega}{2}\right) \int_{-\infty}^{\infty} dt\, e^{i\omega t} C_{BB}(\mathbf{k}, t) \quad (69)$$

where

$$C_{BB}(\mathbf{k}, t) = \langle \tfrac{1}{2}[B_k(t), B_{-k}(0)]_+ \rangle \quad (70)$$

is the quantum-mechanical autocorrelation function.

The transition rates computed in this section provide a simple derivation of the susceptibility. Furthermore, they can be used to determine cross sections in many scattering processes.

E. Doppler Broadened Spectra

To illustrate how the preceding formalism is generally used, we apply it to the solution of a well-known problem. Let us derive an analytic expression for the Doppler broadening in the dipole approximation. The Hamiltonian which describes the interaction between radiation of polarization, ε, and matter in the dipole approximation was discussed in the first section of this review article.

$$H'(t) = -\int d\mathbf{r}[\boldsymbol{\varepsilon} \cdot \mathbf{M}(\mathbf{r})]E(\mathbf{r}, t)$$

with

$$\mathbf{M}(\mathbf{r}) = \sum_j \boldsymbol{\mu}_j \delta(\mathbf{r} - \mathbf{r}_j)$$

where $\boldsymbol{\mu}_j$ is the dipole operator and $\mathbf{r}_j$ the center of mass position of molecule j. From our preceding analysis we see that the crucial quantum-mechanical autocorrelation function is

$$C_{MM}(\mathbf{k}, t) = \boldsymbol{\varepsilon} \cdot \langle \tfrac{1}{2}[\mathbf{M}_k(t), \mathbf{M}_{-k}]_+ \rangle \cdot \boldsymbol{\varepsilon}$$

where

$$\mathbf{M}_k = \sum_j \boldsymbol{\mu}_j \exp(+ik \cdot \mathbf{r}_j)$$

In electronic or vibrational transitions it is often a very good approximation to ignore correlations between dipoles on different molecules, then

$$C_{MM}(\mathbf{k}, t) = \sum_{j=1}^{N} \boldsymbol{\varepsilon} \cdot \langle \tfrac{1}{2}[\boldsymbol{\mu}_j(t)\, e^{+i\mathbf{k} \cdot \mathbf{r}_j(t)}, \boldsymbol{\mu}_j(0)\, e^{-i\mathbf{k} \cdot \mathbf{r}_j(0)}]_+ \rangle \cdot \boldsymbol{\varepsilon}$$

(In microwave spectroscopy the correlations between different molecules cannot be ignored.) The translational motion of the molecules is classical at sufficiently high temperatures. Furthermore, the translational motion of a molecule is, to a very good approximation, independent of the motion of the internal degrees of freedom which determine the motion of the molecular dipole moment. Thus,

$$C_{MM}(\mathbf{k}, t) \cong \sum_{j=1}^{N} \langle \exp\{+i\mathbf{k} \cdot [r_j(t) - r_j(0)]\}\rangle_{cl} [\boldsymbol{\varepsilon} \cdot \langle \tfrac{1}{2}[\boldsymbol{\mu}_j(0), \boldsymbol{\mu}_j(t)]_+\rangle \cdot \boldsymbol{\varepsilon}]$$

If all of the N absorbing molecules are identical and the total system is isotropic, this equation reduces to

$$C_{MM}(\mathbf{k}, t) = \tfrac{1}{3} N F_S(\mathbf{k}, t) U(t)$$

where

$$F_S(\mathbf{k}, t) = \langle \exp\{+i\mathbf{k}[\mathbf{r}(t) - \mathbf{r}(0)]\}\rangle_{cl}$$

describes the translational diffusive motion of a typical molecule and consequently the Doppler effect, and

$$U(t) = \langle \tfrac{1}{2}[\boldsymbol{\mu}(0) \cdot \boldsymbol{\mu}(t) + \boldsymbol{\mu}(t) \cdot \boldsymbol{\mu}(0)]\rangle$$

describes the dipolar motion. $U(t)$ is called the dipolar correlation function[2,15] and $F_S(\mathbf{k}, t)$ is called the diffusion function.[18] The power spectrum of $C_{MM}(\mathbf{k}, t)$ is thus seen to be the convolution product.

$$G_{MM}(\mathbf{k}, \omega) = \frac{1}{3} N \int_{-\infty}^{\infty} d\omega' \, S_S(\mathbf{k}, \omega - \omega') \bar{U}(\omega') \tag{71}$$

where $S_S(\mathbf{k}, \omega)$ is the power spectrum of $F_S(\mathbf{k}, t)$ and $\bar{U}(\omega)$ is the power spectrum of $U(t)$. $S_S(\mathbf{k}, \omega)$ was first introduced by Van Hove.[18*] To describe the spectral lineshape of isolated vibration rotation bands it is sufficient to consider $\bar{U}(\omega)$ for the specific vibrational transition. Suppose for

* It should be noted that if the system consists of a gas of non-interacting molecules then

$$F_S(\mathbf{k}, t) = \langle e^{i\mathbf{k}\cdot\mathbf{v}t}\rangle = \left(\frac{M}{2\pi kT}\right)^{-3/2} \int d^3 v \exp\left(\frac{\beta M v^2}{2}\right) e^{i\mathbf{k}\cdot\mathbf{v}t}$$

$$= \exp\left(\frac{1}{6} k^2 \langle v^2\rangle t^2\right)$$

From this it follows that,

$$S_S(\mathbf{k}, \omega) = \left(\frac{2\pi M\beta}{k^2}\right)^{1/2} \exp\left(\frac{\beta M \omega^2}{2k^2}\right)$$

If $U(\omega)$ is very sharply peaked at ω_0, it follows from Eq. (71) that the spectral lineshape is dominated by $S_S(k, \omega)$

$$G_{MM}(k, \omega) = \frac{1}{3} N \left(\frac{2\pi M\beta}{k^2}\right)^{1/2} \exp\left[\frac{\beta M}{2} \frac{(\omega - \omega_0)^2}{k^2}\right] U(\omega_0)$$

where $\omega_0 = Ck$. This is the usual Doppler lineshape.

convenience that the experiment is done at sufficiently low temperatures that only the ground vibrational state is populated. Then only transitions between the ground and first excited vibrational states need be considered. The structure of the band is determined by the dynamics of the molecular rotational motions. Then

$$U(t) = |\boldsymbol{\mu}_{01}|^2 \langle \tfrac{1}{2}[\mathbf{u}(0) \cdot \mathbf{u}(t) + \mathbf{u}(t) \cdot \mathbf{u}(0)] \rangle$$

where $\boldsymbol{\mu}_{01}$ is the transition dipole moment of the transition and $\mathbf{u}$ is a unit vector pointing in the direction of the transition dipole. As the molecule rotates, the direction of the transition dipole moment reorients. The correlation function in this preceding equation reflects the average effect of these molecular reorientations. In diatomic molecules $\mathbf{u}$ points along the molecular axis and the lineshape of the infrared band reflects the rotational relaxation of the molecules. For most molecules the rotational spacings are small enough that $\mathbf{u}(t)$ behaves classically at room temperature, and the correlation function can be evaluated classically

$$U(t) = |\mathbf{u}_{01}|^2 \langle \mathbf{u}(0) \cdot \boldsymbol{\mu}(t) \rangle_{cl}. \tag{72}$$

Both of the functions $U(t)$ and $F_S(\mathbf{k}, t)$ will be discussed at great length in the text.

Spectral lineshapes were first expressed in terms of autocorrelation functions by Foley[39] and Anderson.[40] Van Kranendonk gave an extensive review of this and attempted to compute the dipolar correlation function for vibration-rotation spectra in the semi-classical approximation.[2] The general formalism in its present form is due to Kubo.[11] Van Hove related the cross section for thermal neutron scattering to a density autocorrelation function.[18] Singwi et al.[41] have applied this kind of formalism to the shape of Mössbauer lines, and recently Gordon[15] has rederived the formula for the infrared bandshapes and has constructed a physical model for rotational diffusion. There also exists an extensive literature in magnetic resonance where time-correlation functions have been used for more than two decades.[8]

F. Relaxation Times

Relaxation times can be expressed in terms of time-correlation functions. Consider, for example, the case of a diatomic molecule relaxing from the vibrationally excited state $|n+1\rangle$ to the vibrational state $|n\rangle$ due to its interactions with a bath of solvent molecules. The Hamiltonian for the system is

$$\hat{H} = \hat{H}_{\text{mol}} + \hat{H}_{\text{fluid}} + H_I$$

where the molecular Hamiltonian is

$$\hat{H}_{\text{mol}} = \frac{P^2}{2m} + \frac{L^2}{2\mu r^2} + \frac{1}{2}[\pi^2 + Q^2]\hbar\omega_0$$

the fluid Hamiltonian is

$$\hat{H}_{\text{fluid}} = \sum_{j=1}^{N} \frac{P_j^2}{2m_j} + V(\mathbf{r}_1, \ldots, \mathbf{r}_N)$$

and the interaction Hamiltonian, characterizing the interaction between the diatomic molecule and the fluid molecules, is

$$\hat{H}_I = U(\mathbf{R}, \mathbf{r}, \mathbf{r}_1, \ldots, \mathbf{r}_N; 0) + \left(\frac{\partial U}{\partial Q}\right)_{Q=0} Q = U - FQ$$

Here $\mathbf{R}, \mathbf{r}_1, \ldots, \mathbf{r}_N$ are respectively the C.M. position of the diatomic molecule and the position vectors of the fluid atoms, $\mathbf{P}, \mathbf{P}_1, \ldots, \mathbf{P}_N$ are the conjugate momenta, π and Q are the momentum and coordinate characterizing the oscillatory degree of freedom, $\mathbf{r}$ is the vector representing the orientation and length of the bond in the diatomic molecule, and $\mathbf{L}$ is the angular momentum of the molecule about the C.M. The interaction Hamiltonian has already been linearized in the oscillatory coordinate Q in the last equation.

The centrifugal energy can also be linearized in Q

$$\frac{L^2}{2\mu r^2} = \frac{L^2}{2\mu r_0^2} - \frac{L^2}{\mu r_0^3} Q = \varepsilon_R - \frac{2\varepsilon_R}{r_0} Q + \cdots$$

Here ε_R is the rotational energy of a rigid rotor and r_0 is the equilibrium ground state bond length of the diatomic molecule. The total Hamiltonian is thus

$$\hat{H} = \hat{H}_0 + \hat{H}_{\text{vib}} - \left[F + \frac{2\varepsilon_R}{r_0}\right] Q + O(Q^2)$$

where $\hat{H}_{\text{vib}}$ is the vibrational Hamiltonian and $\hat{H}_0$ is the combined rotational-translational Hamiltonian describing a rotor in a bath of molecules with which it interacts. Let $|in\rangle$ be the eigenstate of $\hat{H}_0 + \hat{H}_{\text{vib}}$ corresponding to the energy $\varepsilon_{in} = \varepsilon_i + \varepsilon_n$. $|i\rangle$ stands for the combined translational-rotational state of the molecule plus the bath whereas $|n\rangle$ is the vibrational eigenstate of energy,

$$\varepsilon_n = (n + \tfrac{1}{2})\hbar\omega_0$$

Application of the results from the preceding section clearly shows that the probability per unit time for the diatomic molecule to make a vibrational

transition from $|n+1\rangle$ to $|n\rangle$ without regard to the initial or final rotational-translational states is

$$\left(\frac{1}{T}\right)_{n+1,n} = W_{n+1\to n}$$
$$= \frac{2\pi}{\hbar^2}\sum_{i,f}\rho_i\left|\left\langle i\left|\left[F+\frac{2\varepsilon_R}{R_0}\right]\right|f\right\rangle\right|^2 |Q_{n+1,n}|^2\,\delta\left(\frac{\varepsilon_f+\varepsilon_n-\varepsilon_i-\varepsilon_{n+1}}{\hbar}\right)$$

where $Q_{n+1,n} = \langle n+1\,|Q|\,n\rangle$ is a matrix element of the vibrational coordinate

$$|Q_{n+1,n}|^2 = \frac{(n+1)\hbar}{2\mu\omega_0}$$

Casting this formula into the Heisenberg representation yields the relaxation time

$$\left(\frac{1}{T}\right)_{n+1,n} = \left(\frac{n+1}{2\mu\hbar\omega_0}\right)\int_{-\infty}^{+\infty} dt\, e^{-i\omega_0 t}\left\langle\left[F(0)+\frac{2\varepsilon_R(0)}{r_0}\right]\left[F(t)+\frac{2\varepsilon_R(t)}{r_0}\right]\right\rangle.$$

Note that the correlation function involves cross terms

$$\langle F(0)F(t)\rangle + \frac{4}{r_0}\langle\varepsilon_R(0)F(t)\rangle + \frac{4}{r_0^2}\langle\varepsilon_R(0)\varepsilon_R(t)\rangle.$$

If there is no centrifugal distortion then the only contribution is

$$\langle F(0)F(t)\rangle$$

whereas if there is no force acting on the vibrational coordinate the only term that contributes to vibrational relaxation is

$$\langle\varepsilon_R(0)\varepsilon_R(t)\rangle$$

i.e., the rotational kinetic energy autocorrelation function. In this event,

$$\frac{1}{T_{n+1\to n}} = \left[\frac{(n+1)}{2I\hbar\omega_0}\right]\int_{-\infty}^{+\infty} dt\, e^{-i\omega_0 t}\langle\varepsilon_R(0)\varepsilon_R(t)\rangle$$

Identical techniques have been applied to numerous problems in magnetic resonance spectroscopy.

III. TIME CORRELATION FUNCTIONS AND MEMORY FUNCTIONS

A. Projection Operators and the Memory Functions

Time-correlation functions are of central importance in understanding how systems respond to weak probes in the linear approximation. According to the fluctuation dissipation theorem of the preceding section, spectro-

scopic lineshape studies reflect the detailed way in which dynamical variables relax in the equilibrium state. This fact has been exploited first in radio frequency and microwave spectroscopy and more recently in Mössbauer, neutron, and infrared spectroscopy. It is the aim of statistical physics to predict the stationary and dynamical properties of many-body systems in equilibrium. For this purpose it is often necessary to adopt simple models. Solids and gases are well understood because there exist many very successful simple idealized models for these states of matter. On the other hand, liquids still remain something of a mystery. There is no simple model of the liquid state which accounts for the observed properties. Furthermore, no new phenomena have yet been predicted by models of the liquid state as in the solid state. Liquids have been a challenge and embarrassment to generations of outstanding physicists and chemists. In the last decade a great deal of new information on liquids has been acquired, partly because of new techniques and partly because linear response theory provided a theoretical framework in which different measurements and ideas could be unified. This information is usually in the form of time-correlation functions. Thus it is not difficult to see why theorists have attempted to construct models of condensed media which account for the dynamical behavior of time-correlation functions. In this article we describe some recent attempts to compute time correlation functions by using memory functions.[34,35,16,42]

Consider the arbitrary operators α and β. Let us define the scalar products of α and β, $\langle\alpha \mid \beta\rangle$

$$\text{(i)} \qquad \langle\alpha \mid \beta\rangle = \operatorname{tr} \tfrac{1}{2}[\alpha^+, \beta]_+ \hat{\rho} = \langle \tfrac{1}{2}[\alpha^+, \beta]_+ \rangle$$

$$\text{(ii)} \qquad \langle\alpha \mid \beta\rangle = \frac{1}{\beta}\int_0^\beta d\lambda \, \langle e^{\lambda H}\alpha^+ e^{-\lambda H}\beta\rangle \tag{73}$$

$$\text{(iii)} \qquad \langle\alpha \mid \beta\rangle = \int d\Gamma \, \alpha^+(\Gamma)\beta(\Gamma) f_{\text{eq}}^{(N)}(\Gamma)$$

where $\hat{\alpha}^+$ is the Hermitian conjugate of the operator $\hat{\alpha}$. (i) is the ensemble average of the property $\alpha^+\beta$, (ii) is the Kubo transform of $\alpha^+\beta$, and (iii) is the classical ensemble average of $\alpha^+\beta$. The angular brackets denote an average over the canonical distribution function or density matrix. The scalar products (i), (ii), and (iii) defined above each satisfy the conditions

(*a*) $\langle\alpha \mid \beta\rangle^* = \langle\beta \mid \alpha\rangle$.

(*b*) If $\alpha = c_1\alpha_1 + c_2\alpha_2$ where α_1 and α_2 are two arbitrary observables, and c_1 and c_2 are two arbitrary constants,

$$\langle\beta \mid \alpha\rangle = c_1\langle\beta \mid \alpha_1\rangle + c_2\langle\beta \mid \alpha_2\rangle \tag{74}$$

(*c*) $\langle\alpha \mid \alpha\rangle \geq 0$, the equality sign appears only if $\hat{\alpha} \equiv \hat{0}$.

From (*a*) we see that the norm $\langle \alpha \mid \alpha \rangle$, of the property α, is real. $(\langle \alpha \mid \alpha \rangle)^{1/2}$ can consequently be regarded as the "length" of the property α. A property whose norm is unity is said to be normalized. Two observables α and β are said to be orthogonal if $\langle \alpha \mid \beta \rangle = 0$. It should be noted from (*a*) that $\langle \alpha \mid \beta \rangle$ need not be equal to $\langle \beta \mid \alpha \rangle$.

Consider now the dynamical operators $\hat{U}_1, \ldots, \hat{U}_N$. Suppose that these operators are chosen such that they have a norm of unity and are orthognal

$$\langle U_i \mid U_j \rangle = \delta_{ij} \tag{75}$$

It should be noted that the properties must be chosen differently in order to satisfy the orthonormality condition for each definition of the scalar product.

These properties are so chosen that their ensemble averages are zero.

$$\langle U_i \rangle = 0 \tag{76}$$

Then the properties $\hat{U}_i$ can be regarded as vectors in a Hilbert space of dynamical properties. These dynamical variables obey the equations of motion

$$\frac{\partial U_j}{\partial t} = iLU_j \tag{77}$$

where L is the Liouville operator:

$$\begin{aligned} iL\alpha &\equiv \{\alpha, \hat{H}\} \qquad \text{(classical)} \\ iL\alpha &\equiv \frac{1}{i\hbar}[\alpha, \hat{H}] \qquad \text{(quantum)} \end{aligned} \tag{78}$$

If the properties $\hat{U}_1, \ldots, \hat{U}_N$ all have the same symmetry under time reversal then it is easy to show that

$$\langle U_i | iL | U_j \rangle = 0$$

If the symmetry is different, then of course $\langle U_i | iL | U_j \rangle$ can be nonzero. In this article we assume that $\hat{U}_1, \ldots, \hat{U}_N$ have definite albeit different time reversal symmetries. The properties can be represented by vectors $|U_1\rangle \ldots |U_N\rangle \ldots$ in Hilbert space with scalar product defined above. It is a simple matter to demonstrate that L is Hermitian in this Hilbert Space.

Define the time correlation function

$$C_{ij}(t) = \langle U_i | \, e^{iLt} | U_j \rangle \tag{79}$$

This function describes the correlation between $\hat{U}_i(0)$ and $\hat{U}_j(t)$ as a function of the time. Corresponding to each definition of the scalar product (Eq. (73)) there is a different correlation function.

$$\text{(i)} \qquad \langle \tfrac{1}{2}[U^+{}_i(0), U_j(t)]_+ \rangle$$

$$\text{(ii)} \qquad \frac{1}{\beta}\int_0^\beta d\lambda \, \langle e^{\lambda \mathcal{H}} U^+{}_i(0) e^{-\lambda \mathcal{H}} U_j(t) \rangle \tag{80}$$

$$\text{(iii)} \qquad \int d\Gamma \, U^*{}_i(\Gamma) e^{iLt} U_j(\Gamma) f_{eq}{}^{(N)}(\Gamma)$$

Each of these correlation functions appear in linear response theory.

If these properties satisfy the same conditions as $\hat{A}_k$ and $\hat{B}_k$ in the previous sections, then from the Hermitian property of L_{in} function space it immediately follows† that

$$\begin{aligned} C_{ij}(t) &= \gamma_i \gamma_j C_{ij}(-t) \\ C_{ij}(t) &= \lambda_i \lambda_j C_{ji}(t) \end{aligned} \tag{81}$$

where γ_i and γ_j are the signatures of $\hat{U}_i$ and $\hat{U}_j$ under time reversal, and $C_{ij}(t)$ stands for any of the three different correlation functions.

Define the projection operator onto the vector $|U_l\rangle$ in function space as

$$\hat{P}_l \equiv |U_l\rangle\langle U_l| \tag{82}$$

The projection operator $\hat{P}$ onto the subspace $|\hat{U}_1\rangle, \ldots, |U_N\rangle$ is then simply the sum of the projectors $\hat{P}_l$

$$\hat{P} = \sum_{l=1}^{N} P_l = \sum_{l=1}^{N} |U_l\rangle\langle U_l| \tag{83}$$

It is obvious that $\hat{P}$ is idempotent if the properties $\hat{U}_i$ are orthonormal. That $\hat{P}_l$ and $\hat{P}$ are Hermitian is easy to prove. Note that

$$\begin{aligned} \langle \alpha | \hat{P} | \beta \rangle^* &= \Big[\sum_l \langle \alpha | U_l \rangle\langle U_l | \beta \rangle\Big]^* \\ &= \sum_l \langle \beta | U_l \rangle\langle U_l | \alpha \rangle \\ &= \langle \beta | \hat{P} | \alpha \rangle \end{aligned}$$

From the fact that these operators are indempotent and Hermitian it follows that they are projection operators.

Since $\hat{P}_l$, $\hat{P}$, and L are Hermitian, $\hat{P}_l L$ and $L\hat{P}_l$ are Hermitian conjugates. It follows immediately that

$$\langle \alpha | \, e^{i(1-\hat{P}_l)Lt} | \beta \rangle^* = \langle \beta | \, e^{-iL(1-\hat{P}_l)t} | \alpha \rangle \tag{84}$$

and likewise

$$\langle \alpha | \, e^{-i(1-\hat{P})Lt} | \beta \rangle^* = \langle \beta | \, e^{+iL(1-\hat{P}_l)t} | \alpha \rangle \tag{85}$$

† The same reasoning applies here as was applied to $C_{AB}(k, t)$ in the last section.

The operator $(1 - \hat{P}_l)L$ is Hermitian in the subspace of Hilbert space which is orthogonal to $|U_l\rangle$. To see this define the vectors

$$\begin{aligned} |g\rangle &= (1 - \hat{P}_l)|G\rangle \\ |f\rangle &= (1 - \hat{P}_l)|F\rangle \end{aligned} \tag{86}$$

where $|F\rangle$ and $|G\rangle$ are arbitrary vectors. $|g\rangle$ and $|f\rangle$ are by definition orthogonal to $|U_l\rangle$. Now note that

$$\langle g|(1 - \hat{P}_l)L|f\rangle^* = \langle G|(1 - \hat{P}_l)^2 L(1 - \hat{P}_l)|F\rangle^*$$

Since $(1 - \hat{P}_l)^2 = (1 - \hat{P}_l)$, and $(1 - \hat{P}_l)$ and L are Hermitian.

$$\begin{aligned} \langle g|(1 - \hat{P}_l)L|f\rangle^* &= \langle G|(1 - \hat{P}_l)L(1 - \hat{P}_l)|F\rangle^* \\ &= \langle F|(1 - \hat{P}_l)L(1 - \hat{P}_l)|G\rangle \\ &= \langle f|(1 - \hat{P}_l)L|g\rangle \end{aligned} \tag{87}$$

This proves that $(1 - \hat{P}_l)L$ is Hermitian in the orthogonal subspace of $|U_l\rangle$. It follows therefore that

$$\langle g|\, e^{i(1-\hat{P}_l)Lt}\, |f\rangle^* = \langle f|\, e^{-i(1-\hat{P}_l)Lt}|g\rangle \tag{88}$$

Since the vector $iL|U_l\rangle \equiv |iLU_l\rangle$ is orthogonal to $|U_l\rangle$, it follows from Eq. (88) that

$$\langle iLU_l|\, e^{i(1-\hat{P}_l)Lt}|iLU_l\rangle^* = \langle iLU_l|\, e^{-i(1-\hat{P}_l)Lt}|iLU_l\rangle \tag{89}$$

So that this function is an even function of the time if U_l is real. $\hat{P}$ has corresponding properties.

It is possible to derive an equation which describes the time evolution of the time-correlation function $C_{ll}(t)$ where C_{ll} stands for different auto-correlation functions depending on the definition of the scalar product (i), (ii), or (iii) of Eq. (73) adopted.

The equation of motion for the vector $|U_l(t)\rangle$ is according to Eq. (77),

$$\frac{\partial}{\partial t}|U_l(t)\rangle = iL|U_l(t)\rangle \tag{90}$$

Since $(1 - \hat{P}_l) + \hat{P}_l$ is simply the identity operator, it can be substituted between iL and $|U_l(t)\rangle$ so that

$$\frac{\partial}{\partial t}|U_l(t)\rangle = iL\hat{P}_l|U_l(t)\rangle + iL(1 - \hat{P}_l)|U_l(t)\rangle \tag{91}$$

Since

$$C_{ll}(t) = \langle U_l|\hat{P}_l|U_l(t)\rangle \tag{92}$$

it should be noted that an equation for $C_{ll}(t)$ can be derived by first operating on Eq. (91) with $\hat{P}_l$, and then dotting $\langle U_l|$ into the resulting equation. Following this procedure we find

$$\frac{\partial}{\partial t} C_{ll}(t) = \langle U_l| \hat{P}_l iL\hat{P}_l |U_l(t)\rangle + \langle U_l| \hat{P}_l iL(1 - \hat{P}_l) |U_l(t)\rangle$$

Now note that

$$\langle U_l| \hat{P}_l iL\hat{P}_l |U_l(t)\rangle = \langle U_l| iL |U_l\rangle C_{ll}(t) \tag{93}$$

which vanishes since $\langle U_l| iL |U_l\rangle$ vanishes. Then

$$\frac{\partial}{\partial t} C_{ll}(t) = \langle U_l| iL(1 - \hat{P}_l) |U_l(t)\rangle \tag{94}$$

To complete the derivation we must find how $(1 - \hat{P}_l) |U_l(t)\rangle$ varies with time. For this purpose we operate on Eq. (91) with $(1 - \hat{P}_l)$.

$$\frac{\partial}{\partial t}(1 - \hat{P}_l) |U_l(t)\rangle = (1 - \hat{P}_l) iL\hat{P}_l |U_l(t)\rangle + (1 - \hat{P}_l) iL(1 - \hat{P}_l) |U_l(t)\rangle \tag{95}$$

Now note that

$$(1 - \hat{P}_l) iL\hat{P}_l |U_l(t)\rangle = iL |U_l\rangle C_{ll}(t) \tag{96}$$

and

$$(1 - \hat{P}_l) |U_l(0)\rangle = (1 - \hat{P}_l) |U_l\rangle = 0$$

The solution of Eq. (95) subject to Eq. (96) is

$$(1 - \hat{P}_l) |U_l(t)\rangle = \int_0^t d\tau \, e^{i(1 - \hat{P}_l)L\tau} iL |U_l\rangle C_{ll}(t - \tau) \tag{97}$$

Substitution of this into Eq. (94) yields

$$\frac{\partial}{\partial t} C_{ll}(t) = - \int_0^t d\tau \, K_{ll}(\tau) C_{ll}(t - \tau) \tag{98}$$

where

$$K_{ll}(\tau) = \langle iLU_l| \, e^{i(1 - \hat{P}_l)L\tau} |iLU_l\rangle \tag{99}$$

$K_{ll}(\tau)$ is called the "memory function," and the equation for the time-correlation function that we derived is called the memory function equation.[33,34,42] Note that the propagator in this equation contains the projection operator $\hat{P}_l$. Further note that the memory function is an even function of the time,

$$K_{ll}(-t) = K_{ll}(t) \tag{100}$$

This follows from Eq. (89). It should also be noted that the definition of the memory function* depends strongly on which scalar product (i), (ii), or (iii) of Eq. (73) is used. Corresponding to definition (i), (ii), and (iii), $K_{ll}(\tau)$ is

$$\text{(i)} \qquad \left\langle \frac{1}{2}\left[(iLU_l)^+,\, e^{i(1-P_l)L\tau}(iLU_l)\right]_+ \right\rangle$$

$$\text{(ii)} \qquad \frac{1}{\beta}\int_0^\beta d\lambda\, \langle e^{\lambda H} U_l{}^+ e^{-\lambda H}\, e^{i(1-P_l)L\tau} U_l\rangle \tag{101}$$

$$\text{(iii)} \qquad \int d\Gamma f^{(N)}\mathrm{eq}(\Gamma) U^*{}_l(\Gamma)\, e^{i(1-P_l)L\tau} U_l(\Gamma)$$

where the projection operator is so defined in each case that it is consistent with the definition of the scalar product adopted.

B. Memory Function Equation for Multivariate Processes

An analogous set of equations can be derived for the multivariate random process $\hat{U}_1, \ldots, \hat{U}_N$. To proceed, insert the identity operator $(1 - \hat{P}) + \hat{P}$ between iL and $|U_l(t)\rangle$ in Eq. (90), where $\hat{P}$ is the projection operator onto the subspace $|U_1\rangle, \ldots, |U_N\rangle$, then

$$\frac{\partial}{\partial t}\,|U_l(t)\rangle = iL\hat{P}\,|U_l(t)\rangle + iL(1-\hat{P})\,|U_l(t)\rangle \tag{102}$$

Since

$$C_{jl}(t) = \langle U_j|\,\hat{P}\,|U_l(t)\rangle$$

it should be noted that an equation for $C_{jl}(t)$ can be derived by first operating on Eq. (102) with $\hat{P}$ and then doting $\langle U_j|$ into the resulting equation. Following this procedure we find that

$$\frac{\partial}{\partial t} C_{jl}(t) = \langle U_j|\,\hat{P}iL\hat{P}\,|U_l(t)\rangle + \langle U_j|\,\hat{P}iL(1-\hat{P})\,|U_l(t)\rangle \tag{103}$$

* If the dynamical operator U_l is a vector then the scalar product can be defined as

$$\text{(i)} \qquad \langle \alpha|\beta\rangle = \left\langle \frac{1}{2}\left[\alpha^+\cdot\beta + \beta\cdot\alpha^+\right]\right\rangle$$

$$\text{(ii)} \qquad \langle \alpha|\beta\rangle = \frac{1}{\beta}\int_0^\beta d\lambda \langle e^{\lambda\hat{H}}\alpha^+ e^{-\lambda\hat{H}}\cdot\beta\rangle$$

$$\text{(iii)} \qquad \langle \alpha|\beta\rangle = \int d\Gamma\, \alpha(\Gamma)^*\cdot\beta(\Gamma) f^{(N)}(\Gamma)$$

where the dot stands for a dot product. Thus if $U_l = \mathbf{V}/\langle \mathbf{V}^2\rangle^{1/2}$, where $\mathbf{V}$ is the C.M. velocity, the memory function and time-correlation function of U_l is well defined.

Now note that since $\hat{P} = \sum_{k=1}^{N} |U_k\rangle\langle U_k|$

$$\langle U_j|\,\hat{P}iL\hat{P}\,|U_i(t)\rangle = \sum_{m=1}^{N} \langle U_j|\,iL\,|U_m\rangle C_{mi}(t) \tag{104}$$

This can also be expressed as

$$\langle U_j|\,\hat{P}iL\hat{P}\,|U_i(t)\rangle = \sum_{m=1}^{N} \Omega_{jm} C_{mi}(t) \tag{105}$$

where

$$\Omega_{jm} = \langle U_j|\,iL\,|U_m\rangle \tag{106}$$

Furthermore

$$\langle U_j|\,\hat{P}iL(1-\hat{P})\,|U_j(t)\rangle = -\langle iLU_j|\,(1-\hat{P})\,|U_i(t)\rangle \tag{107}$$

Combining Eqs. (103), (105), and (106) yields

$$\frac{\partial}{\partial t} C_{ji}(t) = \sum_{m=1}^{N} \Omega_{jm} C_{mi}(t) - \langle iLU_j|\,(1-\hat{P})\,|U_i(t)\rangle \tag{108}$$

To proceed we must find how $(1-\hat{P})\,|U_i(t)\rangle$ varies with time. For this purpose we operate on Eq. (102) with $(1-\hat{P})$

$$\frac{\partial}{\partial t}(1-\hat{P})\,|U_i(t)\rangle = (1-\hat{P})iL\hat{P}\,|U_i(t)\rangle + (1-\hat{P})iL(1-\hat{P})\,|U_i(t)\rangle \tag{109}$$

Now note that

$$(1-\hat{P})iL\hat{P}\,|U_i(t)\rangle = \sum_{m=1}^{N} (1-\hat{P})iL\,|U_m\rangle C_{mi}(t) \tag{110}$$

and

$$(1-\hat{P})\,|U_i(0)\rangle = (1-\hat{P})\,|U_i\rangle = 0$$

The solution of Eq. (109) subject to Eq. (110) is

$$(1-\hat{P})\,|U_i(t)\rangle = \sum_{m=1}^{N} \int_0^t d\tau\, e^{i(1-\hat{P}L)\tau}(1-\hat{P})|iLU_m\rangle C_{mi}(t-\tau) \tag{111}$$

Substitution of this into Eq. (108) yields

$$\frac{\partial}{\partial t} C_{ji}(t) = \sum_{m=1}^{N} [\Omega_{jm} C_{mi}(t) - \int_0^t d\tau\, K_{jm}(\tau) C_{mi}(t-\tau)] \tag{112}$$

where

$$K_{jm}(\tau) = \langle iLU_j|\,(1-\hat{P})\,e^{i(1-\hat{P})L\tau}(1-\hat{P})\,|iLU_m\rangle \tag{113}$$

Note that the correlations in a multivariate process $U_1, \ldots, U_N$ are described by the $N \times N$ matrix of time-correlation functions $\mathsf{C}(t)$ whose elements are the time-correlation functions $C_{jl}(t)$. The correlation function matrix evolves in time according to the memory function equation[42]

$$\frac{\partial}{\partial t}\mathsf{C}(t) = \Omega\mathsf{C}(t) - \int_0^t d\tau\, \mathsf{K}(\tau)\mathsf{C}(t-\tau) \tag{114}$$

where Ω is the matrix of "resonance frequencies"

$$\Omega_{jl} = \langle U_j | iL | U_l \rangle$$

$K(\tau)$ is the "memory function" matrix, with elements given by Eq. (113).

The time-correlation functions, $C_{jl}(t)$, resonance frequencies, Ω_{jl}, and memory functions, $K_{jl}(t)$, satisfy the reciprocal relations

$$\begin{aligned} C_{jl}(t) &= \lambda_j \lambda_l C_{lj}(t) \\ K_{jl}(t) &= \lambda_j \lambda_l K_{lj}(t) \\ \Omega_{jl} &= -\lambda_j \lambda_l \Omega_{lj} = \varepsilon_j \varepsilon_l \Omega_{lj} = -\gamma_j \gamma_l \Omega_{jl} \end{aligned} \tag{115}$$

These relations* follow from the time reversal symmetries of the multivariate properties $U_1, \ldots, U_N$. λ_j and λ_l are the signatures of U_j and U^l under inversion and time reversal. It also follows from these arguments that

$$\begin{aligned} C_{jl}(t) &= \gamma_j \gamma_l C_{jl}(-t) \\ K_{jl}(t) &= \gamma_j \gamma_l K_{jl}(-t) \end{aligned} \tag{116}$$

From these properties we see that $\Omega_{ll} = 0$, and $C_{ll}(t)$ and $K_{ll}(t)$ are even functions of the time.

Needless to say, corresponding to each choice of the scalar product there is a different form of the memory function as in Eq. (101).

In the next section a physical interpretation of the memory is presented.

C. The Modified Langevin Equation

The Langevin equation,

$$M\dot{V}(t) = -M\beta V(t) + F(t) \tag{117}$$

is of central importance in the theory of Brownian motion. In this equation V is the velocity of the Brownian particle, M the mass, $M\beta$ the friction coefficient (often called ζ), and $F(t)$ the random force. The random force $F(t)$ is usually assumed to have the following properties:

* It is assumed here that the properties are such that $U_l^+ = \gamma_l U_l^*$ (see II.C).

(*a*) The stochastic process $F(t)$ is a stationary, Gaussian process.

(*b*) It has an infinitely short correlation time so that its autocorrelation function is

$$\langle F(0)F(t)\rangle = \gamma\delta(t)$$

where γ is a constant of proportionality.

(*c*) The motion of the Brownian particle is due to equilibrium thermal fluctuations of the bath in which it is moving, and $\langle V(0)F(t)\rangle = 0$.

Assumption (*a*) implies that $V(t)$ is a stationary Gaussian process. The Langevin equation when solved subject to assumption (*b*) yields the velocity autocorrelation function

$$\langle V(0)V(t)\rangle = \langle V^2\rangle \, e^{-\beta|t|} \tag{118}$$

Doob's theorem states that a Gaussian process is Markovian if and only if its time correlation function is exponential. It thus follows that V is a Gaussian-Markov Process. From this it follows that the probability distribution, $P(V, t)$, in velocity space satisfies the Fokker-Planck equation,

$$\frac{\partial}{\partial t}P(V,t) = \frac{\partial}{\partial V}\left[\beta V + D_v \frac{\partial}{\partial V}\right]P(V,t) \tag{119}$$

which is a diffusion equation in velocity space with D_v the diffusion constant in this space. D_v is related to the fluctuating force according to the equation

$$D_v = M^{-2}\int_0^\infty dt\, \langle F(0)F(t)\rangle = M^{-2}\gamma$$

Condition (c) requires that the stationary solution of the Fokker-Planck equation should be the Maxwellian distribution function. Substitution leads to

$$D_v = \frac{KT}{M}\beta = M^{-2}\gamma$$

and

$$\beta = \frac{1}{MKT}\int_0^\infty dt\, \langle F(0)\, F(t)\rangle \tag{120}$$

The friction constant is consequently related to the time dependence of the random force in the equilibrium system.

The question immediately arises: How can we generalize the Langevin model to, say, the motion of an atom or molecule in a liquid?

To describe the more complicated physical systems it is necessary to consider the following points:

(*a*) $F(t)$ may be non-Gaussian.
(*b*) $F(t)$ may have a finite correlation time.
(*c*) The friction constant may be frequency-dependent.

It can be shown by arguments similar to those presented in the preceding sections that the correct generalization of the Langevin equation is[35]

$$M\frac{d}{dt}V(t) = -M\int_0^t dt\, K(t-\tau)V(\tau) + F(t) \tag{121}$$

where $F(t)$ is a stochastic force which satisfies the conditions

$$\text{(i)} \qquad \langle F(t)\rangle = 0$$

$$\text{(ii)} \qquad \langle V(0)F(t)\rangle = 0 \tag{122}$$

and $K(t)$ is a time-dependent friction coefficient. Multiplying the modified Langevin equation by $V(0)$ and averaging over the equilibrium ensemble it is found that,

$$M\frac{d}{dt}\langle V(0)V(t)\rangle = -M\int_0^t d\tau\, K(t-\tau)\langle V(0)V(\tau)\rangle + \underbrace{\langle V(0)F(t)\rangle}_{0} \tag{123}$$

where the last term is zero due to (ii). This is an equation for the velocity autocorrelation function $\phi(t) = \langle V(0)V(t)\rangle$, and can be solved by Laplace transforming with respect to time.

$$\tilde{\phi}(S) = \frac{1}{S + \tilde{K}(S)}\langle V^2\rangle \tag{124}$$

Note that $K(t)$ is a memory function. Here $\tilde{\phi}(S)$ and $\tilde{K}(S)$ are the Laplace transforms of $\phi(t)$ and $K(t)$, respectively. We can now show that the kernel $K(t)$ is related to the autocorrelation function of the random force according to the equation

$$K(t) = [M^2\langle V(0)^2\rangle]^{-1}\langle F(0)F(t)\rangle \tag{125}$$

Kubo calls this relationship the Second Fluctuation Dissipation Theorem. For its proof it should be noted that the modified Langevin equation can be written as

$$F(t) = M\dot{V}(t) + M\int_0^t dt\, K(t-\tau)V(\tau) \tag{126}$$

Consequently,

$$F(0) = M\dot{V}(0)$$

It follows directly that the autocorrelation function of the random force is

$$\langle F(0)F(t)\rangle = M^2[\langle \dot{V}(0)\dot{V}(t)\rangle + \int_0^t dt\, K(t-\tau)\langle \dot{V}(0)V(\tau)\rangle] \tag{127}$$

Note the following properties of the functions that appear in this equation:

$$\text{(i)} \qquad \langle \dot{V}(0)\dot{V}(t)\rangle = \langle (iLV)\, e^{iLt}(iLV)\rangle = -\frac{d^2}{dt^2}\langle V(0)V(t)\rangle$$

$$\text{(ii)} \qquad \langle \dot{V}(0)V(t)\rangle = \langle (iLV)\, e^{iLt}V\rangle = -\frac{d}{dt}\langle V(0)V(t)\rangle \tag{128}$$

Taking the Laplace transform of Eq. (127) and substituting Eq. (128) yields

$$\begin{aligned}\langle F(0)F(S)\rangle' &= M^2\{-[S^2\tilde{\phi}(S) - S\langle V(0)^2\rangle] - \tilde{K}(S)[S\tilde{\phi}(S) - \langle V^2(0)\rangle]\} \\ &= -M^2[S + \tilde{K}(S)][S\tilde{\phi}(S) - \langle V^2(0)\rangle]\end{aligned}$$

where $\langle F(0)F(S)\rangle'$ is the Laplace transform of $\langle F(0)F(t)\rangle$. Substitution for $\tilde{\phi}(S)$ from Eq. (124) yields

$$\langle F(0)F(t)\rangle' = M^2[S + \tilde{K}(S)]\tilde{K}(S)[S + \tilde{K}(S)]^{-1}\langle V^2(0)\rangle$$

so that

$$\tilde{K}(S) = [M^{+2}\langle V^2(0)\rangle]^{-1}\langle F(0)F(S)\rangle' \tag{129}$$

thus proving the second fluctuation dissipation theorem. Since the averages are done over an equilibrium ensemble $\langle V^2(0)\rangle = M^{-1}KT$, and it follows that

$$K(t) = \frac{1}{MKT}\langle F(0)F(t)\rangle \tag{125}$$

In the Langevin theory the memory function is proportional to the time-correlation function for the random force.

If the random force has a delta function correlation function then $K(t)$ is a delta function and the classical Langevin theory results. The next obvious approximation to make is that F is a Gaussian-Markov process. Then $\langle F(0)F(t)\rangle$ is exponential by Doob's theorem and $K(t)$ is an exponential. The velocity autocorrelation function can then be found. This approximation will be discussed at length in a subsequent section. The main thing to note here is that the second fluctuation dissipation theorem provides an intuitive understanding of the memory function.*

* A modified Langevin equation can be derived for any property $\hat{U}_t$. In addition the memory function will be related to the autocorrelation function of the "random force" in this equation. These results can be extended to multivariate processes.

D. Continued Fraction Representation of Time-Correlation Functions

The memory function equation for the time-correlation function of a dynamical operator U_l can be cast into the form of a continued fraction as was first pointed out by Mori.[43] We prove this in a different way than Mori. In order to proceed it is necessary to define the set of memory functions $K_0(t), \ldots, K_n(t) \ldots$, such that

$$K_n(t) = \langle f_n | e^{iL_n t} | f_n \rangle \tag{130}$$

where the quantities f_n and L_n are defined in terms of the Liouville operator $iL \equiv iL_0$ and the dynamical quantity $\hat{\alpha}_0 \equiv \hat{U}_l \equiv f_0$, as

$$\begin{aligned} iL_n &\equiv (1 - \hat{P}_{n-1}) iL_{n-1} \\ |f_n\rangle &\equiv (1 - \hat{P}_{n-1}) iL_{n-1} |\alpha_{n-1}\rangle \\ |\alpha_n\rangle &\equiv \langle f_n | f_n \rangle^{-1/2} |f_n\rangle \\ \hat{P}_n &\equiv |\alpha_n\rangle\langle\alpha_n| \end{aligned} \tag{131}$$

From these definitions note that

(*a*) $|\alpha_0\rangle, \ldots, |\alpha_n\rangle, \ldots$ are orthonormal

$$(b) \quad iL_n = (1 - P_{n-1})(1 - P_{n-2}) \ldots (1 - P_0) iL_0 = \left[1 - \sum_{l=0}^{n-1} \hat{P}_l\right] iL_0 \tag{132}$$

$$(c) \quad |f_n\rangle = (1 - P_{n-1}) iL_{n-1} |\alpha_{n-1}\rangle = \left(1 - \sum_{l=0}^{n-1} \hat{P}_l\right) iL_0 |\alpha_{n-1}\rangle$$

Therefore $|f_n\rangle$ and $|\alpha_n\rangle$ are orthogonal to all vectors of lower index. Furthermore $(1 - \sum_{l=0}^{n-1} \hat{P}_l) L_0$ is Hermitian in the subspace orthogonal to $|\alpha_0\rangle, \ldots, |\alpha_{n-1}\rangle$. With these definitions we can prove the following theorem by mathematical induction.

Theorem: The set of memory functions $K_0(t), \ldots, K_n(t)$ obey the set of coupled Volterra equations such that

$$\frac{\partial}{\partial t} K_{n-1}(t) = -\int_0^t d\tau\, K_n(\tau) K_{n-1}(t - \tau) \qquad n = 1, \ldots, N \tag{133}$$

Proof: That the theorem holds for $n = 1$ is easy to see. Note that $K_0(t)$ is simply the time-correlation function

$$K_0(t) = \langle U_l | \, e^{iLt} | \, U_l \rangle = C_{ll}(t)$$

and consequently satisfies Eq. (133). Thus if the kernel $K_1(t)$ is identical to the kernel $\langle iLU_l | \exp[i(1 - \hat{P}_l)Lt] | iLU_l \rangle$ of Eq. (99), then the theorem holds for $n = 1$. Note that

$$K_1(t) = \langle f_1 | \, e^{iL_1 t} | f_1 \rangle = \langle iLU_l | \, e^{i(1 - P_l)Lt} | iLU_l \rangle$$

The theorem is consequently valid for $n = 1$.

To proceed we assume that the theorem is valid for n and deduce it for $n + 1$,

$$\frac{\partial}{\partial t} K_n(t) = -\int_0^t dt\, K_{n+1}(\tau) K_n(t-\tau) \tag{134}$$

Here

$$\begin{aligned} K_n(t) &= \langle f_n | \, e^{iL_n t} | f_n \rangle = \langle f_n | f_n \rangle \langle \alpha_n | \, e^{iL_n t} | \alpha_n \rangle \\ &= \langle f_n \, | \, f_n \rangle \hat{K}_n(t). \end{aligned} \tag{135}$$

The equation of motion for $e^{iL_n} |\alpha_n\rangle = |\alpha_n(t)\rangle$ is

$$\frac{\partial}{\partial t} |\alpha_n(t)\rangle = iL_n |\alpha_n(t)\rangle \tag{136}$$

This equation is analogous to Eq. (90). Note that

$$\hat{K}_n(t) = \langle \alpha_n | \, e^{iL_n t} | \alpha_n \rangle = \langle \alpha_n | \, \hat{P}_n | \alpha_n(t) \rangle$$

Thus to find the equation of evolution for $L_n(t)$ operate on Eq. (136) with $\hat{P}_n$

$$\frac{\partial}{\partial t} \hat{P}_n |\alpha_n(t)\rangle = \hat{P}_n iL_n \hat{P}_n |\alpha_n(t)\rangle + \hat{P}_n iL_n (1 - \hat{P}_n) |\alpha_n(t)\rangle \tag{137}$$

Following exactly the same reasoning that led to Eq. (98) we find that

$$\frac{\partial}{\partial t} \hat{K}_n(t) = \int_0^t d\tau \langle \alpha_n | \, iL_n \, e^{iL_n \tau} | iL_n \alpha_n \rangle \hat{K}_n(t-\tau) \tag{138}$$

Multiplication by $\langle f_n \, | \, f_n \rangle$ shows that $K_n(t)$ satisfies this equation. To complete our proof we must show that the kernel above is identical to $-K_{n+1}(t)$ where

$$K_{n+1}(\tau) = \langle f_{n+1} | \, e^{iL_n \tau} | f_{n+1} \rangle \tag{139}$$

This is readily proved by noting that L_n is Hermitian in the space orthogonal to $|\alpha_0\rangle, \ldots, |\alpha_{n-1}\rangle, |\alpha_n\rangle$ so that

$$\langle \alpha_n | \, iL_n \, e^{iL_n \tau} | iL_n \alpha_n \rangle = -\langle iL_n \alpha_n | \, e^{iL_n \tau} | iL_n \alpha \rangle$$

Because of parity $(1 - \hat{P}_n)$ can be inserted in such a way that

$$\langle \alpha_n | \, iL_n \, e^{iL_n \tau} | iL_n \alpha \rangle = -\langle iL_n \alpha_n | (1 - \hat{P}_n) \, e^{iL_n \tau} (1 - \hat{P}_n) | iL_n \alpha_n \rangle$$

Since $1 - \hat{P}_n$ is Hermitian it follows from the fact that $|f_{n+1}\rangle = (1 - \hat{P}_n) iL_n |\alpha_n\rangle$ that

$$\langle \alpha_n | \, iL_n \, e^{iL_n \tau} | iL_n \alpha_n \rangle = -\langle f_{n+1} | \, e^{iL_n \tau} | f_{n+1} \rangle = -K_{n+1}(\tau) \tag{140}$$

Thus

$$\frac{\partial K_n}{\partial t}(t) = -\int_0^t d\tau\, K_{n+1}(\tau) K_n(t-\tau)$$

This proves the theorem.

Let $K_n(0) = \langle f_n | f_n \rangle = \Delta_n{}^2$. Taking the Laplace transform of $K_n(t)$ yields

$$\tilde{K}_n(S) = \frac{\Delta_n{}^2}{S + \tilde{K}_{n+1}(S)}$$

where $\sim K_n(S)$ is the Laplace transform of $K_n(t)$. Iteration leads to

$$\tilde{C}_{ll}(S) = \cfrac{C_{ll}(0)}{S + \cfrac{\Delta_1{}^2}{S + \cfrac{\Delta_2{}^2}{S + \cfrac{\Delta_3{}^2}{S + \cdots \cfrac{\Delta_{n-1}^2}{S + K_n(S)}}}}}$$

with $\Delta_n{}^2 = \langle f_n | f_n \rangle$. In particular $\Delta_1{}^2 = \langle \dot{U}_l | \dot{U}_l \rangle$ and

$$\Delta_2{}^2 = \left[\frac{\langle \dot{U}_l | \dot{U}_l \rangle}{\langle \dot{U}_l | U_l \rangle} - \langle \dot{U}_l | U_l \rangle \right]$$

Continuation of this procedure leads to an infinite continued fraction. It is obvious that the precise definition of the quantities which appear in these formulas depends on the precise definition of the scalar product used. Moreover, this approach is easily extended to the multivariate processes.

E. Dispersion Relations and Sum Rules for the Memory Function

Time-correlation functions $C_{ll}(t)$ obey the memory function equation

$$\frac{\partial}{\partial t} C_{ll}(t) = -\int_0^t d\tau\, K_{ll}(\tau) C_{ll}(t-\tau) \tag{142}$$

According to this equation $C_{ll}(t)$ depends only on the values of the memory function $K_{ll}(\tau)$ for all times τ prior to t. Since the autocorrelation function $C_{ll}(\tau)$ is real the memory function must also be real. This can also be deduced directly from the definition of the memory function, Eq. (99).

The power spectrum $G_{ll}(\omega)$ of the time-correlation function $C_{ll}(t)$ is, according to Eq. (47),

$$G_{ll}(\omega) = \frac{1}{2\pi} \int_{-\infty}^{+\infty} dt\, e^{+i\omega t} C_{ll}(t)$$

The time-correlation function $C_{ll}(t)$ is an even function of the time (see Eq. (81)). Consequently,

$$G_{ll}(\omega) = \frac{1}{\pi}\int_0^\infty dt \cos \omega t \, C_{ll}(t) \tag{143}$$

or

$$G_{ll}(\omega) = \frac{1}{\pi} \operatorname{Re} \int_0^\infty dt \, e^{-i\omega t} C_{ll}(t) \tag{144}$$

The integral in this expression is the Laplace transform, $\tilde{C}_{ll}(i\omega)$ of the time-correlation function, so that

$$G_{ll}(\omega) = \frac{1}{\pi} \operatorname{Re} \tilde{C}_{ll}(i\omega) \tag{145}$$

The Laplace transform of the memory function, $K_{ll}(t)$.

$$\tilde{K}_{ll}(i\omega) = \int_0^\infty dt \, e^{-i\omega t} K_{ll}(t) \tag{146}$$

Since both $C_{ll}(t)$ and $K_{ll}(t)$ are real functions of the time, $\tilde{K}_{ll}(i\omega)$ can be expressed as

$$\tilde{K}_{ll}(i\omega) = K'_{ll}(\omega) + iK''_{ll}(\omega) \tag{147}$$

where $K'_{ll}(\omega)$ and $K''_{ll}(\omega)$ are the real and imaginary parts of $\tilde{K}_{ll}(i\omega)$ or

$$\begin{aligned} K'_{ll}(\omega) &= \int_0^\infty dt \cos \omega t \, K_{ll}(t) \\ K''_{ll}(\omega)' &= -\int_0^\infty dt \sin \omega t \, K_{ll}(t) \end{aligned} \tag{148}$$

From the memory function equation it follows that

$$\begin{aligned} \tilde{C}_{ll}(i\omega) &= \frac{1}{i\omega + \tilde{K}_{ll}(i\omega)} C_{ll}(0) \\ &= \left[\frac{C_{ll}(0)}{i[\omega + K''_{ll}(\omega)] + K'_{ll}(\omega)}\right] \end{aligned} \tag{149}$$

So that the power spectrum is

$$G_{ll}(\omega) = \frac{1}{\pi} \frac{K'_{ll}(\omega)}{[\omega + K''_{ll}(\omega)]^2 + [K'_{ll}(\omega)]^2} C_{ll}(0) \tag{150}$$

The imaginary and real parts of $\tilde{K}_{ll}(i\omega)$ determine the shift and breadth of the power spectrum and consequently the lineshape. $K'_{ll}(\omega)$ and $K''_{ll}(\omega)$

are, respectively, even and odd functions of the frequency. This follows from Eq. (148) and the symmetry of the sin and cos. Thus $G_{ll}(\omega)$ is a symmetric function of the frequency as is expected.

Consider now the complex Fourier transform of the memory function, $\tilde{K}_{ll}(z)$,

$$\tilde{K}_{ll}(z) = \int_0^\infty dt\, e^{izt} K_{ll}(t) \tag{151}$$

with $z = x + iy$. Because of the properties of $K(t)$ it follows that $\tilde{K}_{ll}(z)$ is analytic in the entire lower plane and uniformly goes to zero as $|z| \to \infty$.

That $\tilde{K}_{ll}(z)$ is analytic in the lower half plane can be demonstrated by showing that $\tilde{K}_{ll}(z)$ obeys the Cauchy-Riemann conditions according to which: if

$$\tilde{K}_{ll}(z) \equiv u + iv \tag{152}$$

where u and v are real functions of (x, y) then $\tilde{K}_{ll}(z)$ is analytic in a given region if and only if the Cauchy-Riemann conditions,

$$\frac{\partial u}{\partial x} = \frac{\partial v}{\partial y}; \qquad \frac{\partial v}{\partial x} = -\frac{\partial u}{\partial y} \tag{153}$$

are satisfied in that region.

From Eq. (151) we have

$$\begin{aligned} u(z) &= \int_0^\infty d\tau\, K_{ll}(\tau) \cos x\tau\, e^{y\tau} \\ v(z) &= -\int_0^\infty d\tau\, K_{ll}(\tau) \sin x\tau\, e^{y\tau} \end{aligned} \tag{154}$$

It follows that

$$\begin{aligned} \frac{\partial u}{\partial x} &= -\int_0^\infty d\tau\, K_{ll}(\tau)\tau \sin x\tau\, e^{y\tau} = \frac{\partial v}{\partial y} \\ \frac{\partial u}{\partial y} &= \int_0^\infty d\tau\, K_{ll}(\tau)\tau \cos x\tau\, e^{y\tau} = -\frac{\partial v}{\partial x} \end{aligned} \tag{155}$$

and consequently $\tilde{K}_{ll}(z)$ is analytic only in a region where these operations are valid—that is, in a region where the integrals converge. These integrals will be convergent in the region $y \leq 0$—that is, in the lower half plane. Thus $\tilde{K}_{ll}(z)$ is analytic on the real axis and in the lower half plane. Moreover, we note that

$$|\tilde{K}_{ll}(z)| \to 0 \qquad \text{as } y \to -\infty$$

It is also intuitively obvious that

$$|\tilde{K}_{ll}(z)| \to 0 \qquad \text{as } x \to \pm\infty$$

since the rapidly oscillating cos x and sin x wash out the integrals u and v. It thus follows that

$$|\tilde{K}_{ll}(z)| \to 0 \qquad \text{as } |z| \to \infty \quad \text{for} \quad y \leq 0$$

$\tilde{K}_{ll}(z)$ vanishes on an infinite semicircle in the lower half of the complex z plane.

The real and imaginary parts of $\tilde{K}_{ll}(z)$ are therefore Hilbert transforms of each other,

$$\begin{aligned} K'_{ll}(\omega) &= \frac{1}{\pi} P \int_{-\infty}^{+\infty} d\omega' \frac{\tilde{K}''_{ll}(\omega')}{\omega' - \omega} \\ K''_{ll}(\omega) &= -\frac{1}{\pi} P \int_{-\infty}^{+\infty} d\omega' \frac{K'_{ll}(\omega')}{\omega' - \omega} \end{aligned} \tag{156}$$

or since $K'_{ll}(\omega)$ and $K''_{ll}(\omega)$ are, respectively, even and odd functions of ω,

$$\begin{aligned} K'_{ll}(\omega) &= P \int_{-\infty}^{+\infty} \frac{d\omega'}{\pi} \frac{\omega' K''_{ll}(\omega')}{(\omega')^2 - \omega^2} \\ K''_{ll}(\omega) &= -\omega P \int_{-\infty}^{+\infty} \frac{d\omega'}{\pi} \frac{K'_{ll}(\omega')}{(\omega')^2 - \omega^2} \end{aligned} \tag{157}$$

From these relations we see that the width and shift of the power spectrum and consequently the spectroscopic lines are related through the Kronig-Kramers dispersion relations. Exactly the same arguments apply to the Laplace transform of the time-correlation function, $\tilde{C}_{ll}(i\omega)$. The real and imaginary parts, $C'_{ll}(\omega)$ and $C''_{ll}(i_\omega)$, are related by Kramers-Kronig dispersion relation.

From the definition of $K'_{ll}(\omega)$, Eq. (148), the following general sum rules can be deduced

$$\mu_{(2n)} = \int_{-\infty}^{+\infty} \frac{d\omega}{\pi} \omega^{2n} K'_{ll}(\omega) = (-1)^n \left[\frac{d^{2n}}{dt^{2n}} K_{ll}(t)\right]_{t=0} \tag{158}$$

All odd moments vanish due to the evenness of $K_{ll}(t)$.

It is a simple but lengthy matter to determine the explicit form of all these frequency moments. From Eqs. (99) and (158) it follows that

$$\mu_{(2n)} = (-1)^n \langle iLU_l | [i(1 - P_l)L]^{2n} | iLU_l \rangle \tag{159}$$

In the previous section we saw that $(1 - P_l)L$ is Hermitian in the subspace orthogonal to $|U_l\rangle$. Consequently

$$\mu_{(2n)} = \langle A_n | A_n \rangle \tag{160}$$

where

$$|A_n\rangle = [i(1 - P_l)L]^n |iLU.\rangle \tag{161}$$

From the definition of the projection operator we see that

$$\begin{aligned} \mu_0 &= \langle iLU_l | iLU_l \rangle \equiv \langle \dot{U}_l | \dot{U}_l \rangle \\ \mu_2 &= +\langle \dot{U}_l | \dot{U}_l \rangle - \langle \dot{U}_l | \dot{U}_l \rangle^2 \\ \mu_4 &= \langle U_l^{(3)} | U_l^{(3)} \rangle - 2\langle \dot{U}_l | \dot{U}_l \rangle \langle \dot{U}_l | \dot{U}_l \rangle + \langle \dot{U}_l | \dot{U}_l \rangle^3 \end{aligned} \tag{162}$$

where $U_l^{(n)}$ is the nth time derivative of U_l or $(iL)^n U_l$.

Likewise from the definition of $C'_{ll}(\omega)$, as

$$C'_{ll}(\omega) = \int_0^\infty dt \cos \omega t \, C_{ll}(t) \tag{163}$$

The following general sum rules can be deduced

$$\gamma_{(2n)} = \int_{-\infty}^{+\infty} \frac{d\omega}{\pi} \omega^{2n} C'_{ll}(\omega) = (-1)\left[\frac{d^{2n}}{dt^{2n}} C_{ll}(t)\right]_{t=0} \tag{164}$$

All odd moments vanish due to the evenness of $C_{ll}(t)$.

From Eqs. (164) and (79) it follows that

$$\gamma_{(2n)} = (-1)^n \langle U_l | [iL]^{2n} | U_l \rangle \tag{165}$$

Since L is Hermitian it follows that

$$\gamma_{(2n)} = \langle [iL]^n U_l | [iL]^n U_l \rangle$$

or

$$\gamma_{(2n)} = \langle U_l^{(n)} | U_l^{(n)} \rangle \tag{166}$$

Comparison of Eqs. (166) and (162) allows the moments $\{\mu_{2n}\}$ of the memory function and the moments $\{\gamma_{2n}\}$ of the autocorrelation function to be related

$$\begin{aligned} \mu_0 &= \gamma_2 \\ \mu_2 &= \gamma_4 - \gamma_2^2 \\ \mu_4 &= \gamma_6 - 2\gamma_4\gamma_2 + \gamma_2^2 \end{aligned} \tag{167}$$

Note that μ_{2n} depends on γ_{2n+2} and γ's of lower index.

The memory function $K_{ii}(t)$ and the time-correlation function $C_{ii}(t)$ are easily expanded in an even power series in time. It follows from Eqs. (158), (159), (164), and (165) that

$$C_{ii}(t) = \sum_{n=0}^{\infty} \frac{(-1)^n}{(2n)!} \gamma_{2n} t^{2n} \tag{168}$$

$$K_{ii}(t) = \sum_{n=0}^{\infty} \frac{(-1)^n}{(2n)!} \mu_{2n} t^{2n} \tag{169}$$

F. Properties of Time-Correlation Functions and Memory Functions

Consider the vectors $|\alpha\rangle$ and $|\beta\rangle$. According to the Schwartz inequality,

$$0 \leq |\langle \alpha \mid \beta \rangle| \leq [\langle \alpha | \alpha \rangle \langle \beta | \beta \rangle]^{1/2}$$

First let

$$|\alpha\rangle = |U_i\rangle$$
$$|\beta\rangle = e^{iLt} |U_i\rangle$$

Then according to the Schwartz's inequality,

$$0 \leq |\langle U_i| e^{iLt} |U_i\rangle| \leq \langle U_i | U_i \rangle = 1$$

so that the time-correlation function, $C_{ii}(t)$, which is real, is bounded below by -1 and above by $+1$

$$-1 \leq C_{ii}(t) \leq 1 \tag{170}$$

Now let

$$|\alpha\rangle = |U_i\rangle$$
$$|\beta\rangle = e^{iLt} |U_j\rangle$$

Then

$$0 \leq |C_{ij}(t)| \leq 1 \tag{170a}$$

and the cross-correlation functions are bounded. The same kind of argument can be applied to the corresponding memory function. Let

$$|\alpha\rangle = (1 - \hat{P}_i) |\dot{U}_i\rangle$$
$$|\beta\rangle = e^{i(1-\hat{P}_i)Lt} (1 - \hat{P}_i) |\dot{U}_i\rangle$$

where $\hat{P}_i$ is the projector onto $|U_i\rangle$. Then

$$0 \leq |K_{ii}(t)| \leq \langle \dot{U}_i | \dot{U}_i \rangle \neq 1 \tag{170b}$$

Likewise let

$$|\alpha\rangle = (1 - \hat{P}) |\dot{U}_i\rangle$$
$$|\beta\rangle = e^{i(1-\hat{P})Lt} (1 - \hat{P}) |\dot{U}_j\rangle$$

where $\hat{P}$ is the projector onto the subspace $|U_1\rangle, \ldots, |U_N\rangle, \ldots,$

$$0 \leq |K_{ij}(t)| \leq [\langle \dot{U}_i|\dot{U}_i\rangle\langle \dot{U}_j|\dot{U}_j\rangle]^{1/2} \tag{170c}$$

A complex function of the time $C(t)$ is called positive definite if and only if,

$$\sum_{j,k=1}^{n} Z_j C(t_j - t_k) Z^*_k \geq 0$$

holds for every choice of the finitely many real numbers $t_1, \ldots, t_n$ and complex numbers $Z_1, \ldots, Z_n$.

According to Bochner's theorem, a continuous function $C(t)$ is the characteristic function of a probability distribution, $R(\omega)$, if and only if $C(t)$ is positive definite and $C(0) = 1$. Thus, if $C(0) = 1$, and $C(t)$ is positive definite,

$$C(t) = \int_{-\infty}^{+\infty} d\omega \, e^{i\omega t} R(\omega)$$

$R(\omega)$ is a probability distribution function and consequently satisfies

$$0 \leq R(\omega) = \frac{1}{2\pi} \int_{-\infty}^{+\infty} dt \, e^{-i\omega t} C(t)$$

(A rigorous statement of Bochner's theorem should be in terms of a Fourier-Steltjes representation of the integral.)

Bochner's theorem plays an important part in the theory of time correlation functions. Consider the time correlation functions corresponding to definitions (i), (ii), or (iii).

$$C(\tau) = \langle U(t) \,|\, U(t + \tau)\rangle$$

These correlation functions are stationary; that is, they are independent of the time t. Furthermore, since the "vector" $|U\rangle$ is normalized,

$$C(0) = 1$$

Now define a vector $|\alpha_n\rangle$ such that

$$|\alpha_n\rangle = \sum_{k=1}^{n} |U(t_k)\rangle Z_k$$

for every choice of the finitely real numbers $t_1, \ldots, t_n$, and complex numbers $Z_1, \ldots, Z_n$. It follows from the fact that the norm of the vector $|\alpha\rangle$ is positive, that

$$\langle \alpha_n \,|\, \alpha_n\rangle = \sum_{j,k=1}^{n} Z^*_k \langle U(t_k) \,|\, U(t_j)\rangle Z_j \geq 0$$

From stationarity, $\langle U(t_k)|U(t_j)\rangle = C(t_j - t_k)$ so that,

$$\sum_{j,k=1}^{n} Z_j\, C(t_j - t_k) Z^*{}_k \geq 0$$

It follows from Bochner's theorem that the normalized time autocorrelation function $C(t)$ is the characteristic function of a probability distribution $G(\omega)$ so that

$$C(t) = \int_{-\infty}^{+\infty} d\omega\, e^{i\omega t} G(\omega) \tag{170d}$$

Furthermore, the probability distribution $G(\omega)$ satisfies the condition

$$0 \leq G(\omega) \tag{170e}$$

The interesting thing to note is that $G(\omega)$ is none other than the power spectrum of the time-correlation function (see (Eq. 144)). Bochner's theorem gives us reason to regard the power spectrum as a probability distribution function. The same conclusion applies to the memory functions corresponding to $C(t)$.

Consider the vector,

$$|\dot{U}(t)\rangle_p = e^{i(1-\hat{P})Lt}|\dot{U}\rangle$$

where $\hat{P}$ is the projection operator $|U\rangle\langle U|$.

A p is fixed to the ket to denote the fact that this vector is not found with the ordinary propagator e^{iLt}. Let us now define a function

$$\tilde{K}(\tau) = \frac{p\langle\dot{U}(t)|\dot{U}(t+\tau)\rangle p}{\langle\dot{U}|\dot{U}\rangle}$$

Now note that since $(1 - \hat{P})L$ is Hermitian in the orthogonal subspace to $|U\rangle$, the vector $|\dot{U}\rangle$ lies in this orthogonal subspace so that $\hat{K}$ is stationary, or

$$\hat{K}(\tau) = \frac{\langle\dot{U}|\, e^{(1-\hat{P})L\tau}|\dot{U}\rangle}{\langle\dot{U}|\dot{U}\rangle}$$

Thus $\hat{K}(\tau)$ is related to the memory function $K(t)$ corresponding to $C(t)$.

$$\langle\dot{U}|\dot{U}\rangle\hat{K}(t) = K(t)$$

$\hat{K}(t)$ is called the normalized memory function since

$$\hat{K}(0) = 1$$

Furthermore, $\hat{K}(t)$ is positive definite as we now show. Define the vector

$$|\gamma_n\rangle_p = \sum_{k=1}^{n} |\dot{U}(t_k)\rangle_p Z_k$$

for every choice of the n real numbers $\{t_k\}$ and n complex numbers $\{Z_k\}$. It follows that

$$ {}_p\langle \gamma_n \mid \gamma_n \rangle_p = \sum_{j,k=1}^{n} Z^*{}_{kp} \langle \dot{U}(t_k) \mid \dot{U}(t_j) \rangle_p Z_j \geq 0 $$

From stationarity,

$$ {}_p\langle \dot{U}(t_k) \mid \dot{U}(t_j) \rangle_p = \langle \dot{U} \mid \dot{U} \rangle \hat{K}(t_j - t_k) $$

It follows that

$$ \sum_{j,k=1}^{n} Z_j \hat{K}(t_j - t_k) Z^*{}_k \geq 0 $$

Consequently $\hat{K}(t)$ is positive definite. It follows from Bochner's theorem that the normalized memory function can be regarded as the characteristic function of the probability distribution, $P(\omega)$, such that

$$ \hat{K}(t) = \int_{-\infty}^{+\infty} d\omega \, P(\omega) \, e^{i\omega t} \tag{170f} $$

From Eq. (148) we see that

$$ 0 \leq P(\omega) = K'(\omega)/\pi \langle \dot{U} \mid \dot{U} \rangle \tag{170g} $$

We will return to this interpretation later.

Consider the one-sided quantum mechanical correlation function

$$ \Phi(\tau) = \text{tr } \rho \hat{U}^+(t) \hat{U}(t + \tau) $$

$\Phi(\tau)$ is a stationary function of the time. Moreover, the property $\hat{U}$ is so defined that

$$ \Phi(0) = 1 $$

Define the property,

$$ \alpha_n = \sum_{k=1}^{n} U(t_k) Z_k $$

Then

$$ \text{tr } \rho \alpha^+{}_n \alpha_n = \sum_{jk=1}^{n} Z^*{}_k \, \text{tr } \rho U^+(t_k) U(t_j) Z_j \geq 0 $$

Thus $\Phi(\tau)$ satisfies the condition of Bochner's theorem so that there exists a probability density or spectral density $R(\omega)$ such that

$$ \Phi(\tau) = \int_{-\infty}^{+\infty} d\omega \, R(\omega) \, e^{i\omega t} \tag{170h} $$

where $0 \leq R(\omega) \leq 1$.

From Bochner's theorem it is seen that power spectra are everywhere positive and bounded, and furthermore, time-correlation functions have power spectra that can be regarded as probability distribution functions.

The Wiener-Khinchin theorem is a special case of Bochner theorem applicable to time averages of stationary stochastic variables. Bochner's theorem enables the Wiener-Khinchin theorem to be applied to ensemble averaged time-correlation functions in quantum mechanics where it is difficult to think of properties as stochastic processes.

The power spectrum $G(\omega)$ of the normalized time-correlation function, $C(t)$, like any distribution function, can be decomposed into a continuous and a discrete part, $G_c(\omega)$ and $G_d(\omega)$, respectively:

$$G(\omega) = G_d(\omega) + G_c(\omega) \tag{170i}$$

The discrete part is of the form

$$G_d(\omega) = \sum_k P_k \delta(\omega - \omega_k), \qquad k = 1, \ldots \tag{170j}$$

Here $\{\omega_k\}$ is a denumerable set of frequencies and $\{P_k\}$ is the set of corresponding probabilities ($0 \leq P_k \leq 1$ and $0 \leq \sum_k P_k \leq 1$). It is assumed here that the continuous part of the spectrum, $G_c(\omega)$, is a continuous well-behaved function of the frequency, although it is quite possible to find physical $G_c(\omega)$ which have singular points. From previous chapters it follows that $G(\omega)$ is even in ω.

The normalized time-correlation function can thus be decomposed in a corresponding way,

$$C(t) = \int_{-\infty}^{+\infty} d\omega \, G_d(\omega) \, e^{i\omega t} + \sum_k P_k \cos \omega_k t \tag{170k}$$

In this case $C(t)$ does not have any long-time limit. If the spectrum is entirely continuous, then it follows from the lemma of Riemann-Lebesque that $C(t)$ vanishes as $t \to \infty$. A system is irreversible if and only if all time correlation functions of properties $\hat{U}$ (with zero mean) vanish as $t \to \infty$. Consequently, irreversible systems must have continuous spectra. In finite isolated systems, the spectrum is discrete and

$$C(t) = \sum_k P_k \cos \omega_k t \tag{170l}$$

is almost periodic. This is a consequence of Poincaré's theorem. In specialized cases it can be shown that in the thermodynamic limit, $N \to \infty$, $V \to \infty$ such that $N/V = \text{const}$, the discrete spectrum becomes continuous. Irreversibility enters in an asymptotic manner. This is a very important point.

Computer experiments on condensed media simulate finite systems and moreover use periodic boundary conditions. The effect of these boundary conditions on the spectrum of different correlation functions is difficult to assess. Before the long-time behavior of covariance functions can be studied on a computer, there are a number of fundamental questions of this kind that must be answered.

$\tilde{K}(t)$ is the characteristic function of the probability distribution

$$P(\omega) = \frac{K'(\omega)}{\langle \dot{U}|\dot{U}\rangle \pi} \tag{170m}$$

The moments of $P(\omega)$ are consequently

$$\langle \omega^n \rangle = \int_{-\infty}^{+\infty} d\omega^n \, P(\omega) = [\langle \dot{U}|\dot{U}\rangle \pi]^{-1} \int_{-\infty}^{+\infty} d\omega \, \omega^n K'(\omega)$$

From Eqs. (158), (160), and (162) it should be noted that these moments can be related to the sum rules on $K'(\omega)$, and that furthermore

$$(a) \qquad \langle \omega^{2n+1} \rangle = 0$$

$$(b) \qquad \langle \omega^0 \rangle = 1$$

$$(c) \qquad \langle \omega^2 \rangle = \frac{\mu_2}{\mu_0} \tag{170n}$$

$$(d) \qquad \langle \omega^4 \rangle = \frac{\mu_4}{\mu_0}$$

where μ_0, μ_2, and μ_4 are the first few sum rules on $K'(\omega)$. The first condition follows from the fact that $K'(\omega)$ is an even function of ω.

It is often a very complicated problem to compute $K'(\omega)$ for a given many-body system. We have devised an approximate method for finding $P(\omega)$. For this purpose we define the information measure of a distribution as

$$S[P(\omega)] = -\int_{-\infty}^{+\infty} d\omega \, P(\omega) \ln P(\omega) \tag{170o}$$

The measure $S[P(\omega)]$ is called the entropy corresponding to the distribution $P(\omega)$. According to information theory, if a certain set of moments of $P(\omega)$ are known, that $P(\omega)$ is optimum which maximizes $S[P(\omega)]$ subject to the moment constraints. Suppose we know only

$$\langle \omega^0 \rangle = 1$$

$$\langle \omega^2 \rangle = \frac{\mu_2}{\mu_0} \tag{170p}$$

Then we must find that $P(\omega)$ for which

$$\delta S[(\omega)] = -\delta \int_{-\infty}^{+\infty} d\omega\, P(\omega) \ln P(\omega) = 0 \tag{170q}$$

and

$$\delta \int_{-\infty}^{+\infty} d\omega\, P(\omega) = 0$$

$$\delta \int_{-\infty}^{+\infty} d\omega\, \omega^2 P(\omega) = 0$$

are satisfied. This problem can be solved using Lagrange multipliers. The optimum $P(\omega)$ turns out to be

$$P(\omega) = \left[\frac{\mu_0}{2\pi\mu_2}\right]^{1/2} \exp\left(-\frac{\mu_0\,\omega^2}{2\mu_2}\right) \tag{170r}$$

Since $K(t)$ is the characteristic function of the distribution it follows that

$$\hat{K}(t) = \int_{-\infty}^{+\infty} d\omega\, P(\omega)\, e^{i\omega t}$$

Information theory consequently leads to the normalized memory function which is a Gaussian function of the time

$$\hat{K}(t) = \exp\left(-\frac{\mu_2}{2\mu_0}\, t^2\right) \tag{170s}$$

From which it follows that the memory function $K(t)$ is

$$K(t) = \langle \dot{U}|\dot{U}\rangle \exp -\frac{1}{2}\left[\frac{\langle \ddot{U}|\ddot{U}\rangle}{\langle \dot{U}|\dot{U}\rangle} - \langle \dot{U}|\dot{U}\rangle\right] t^2 \tag{170t}$$

This approximation will be very useful in the following sections. It should be noted that higher-order moments could have been used to generate higher-order approximations.

This approach is not entirely satisfactory. From Eqs. (148) and (149) it is seen that rigorously

$$K'(0) = \int_0^\infty dt\, K(t) = \left[\int_0^\infty dt\, C(t)\right]^{-1}$$

Yet from information theory

$$K'(0) = \mu_0 \left[\frac{\mu_0}{2\pi\mu_2}\right]^{1/2}$$

In general, this interpolative result is not identical with the rigorous result. Nevertheless, as we shall see in later sections, the information theory result often is in good agreement. Needless to say it would be better to use an optimization procedure which would simultaneously satisfy the moment theorems and give the correct $K'(0)$, but we have not been able to devise such a procedure.

Given an approximate $K(t)$, the Volterra equation can be solved for $C(t)$. Our $P(\omega)$ satisfies the sum rules on $K'(\omega)$ for μ_0 and μ_2 and is therefore satisfactory to this order. It will fail to satisfy the higher-order sum rules. Nevertheless, as we pointed out, these sum rules can be built into the theory.

IV. COMPUTER EXPERIMENTS

A. Introductory Remarks

At the present time the complete time dependence of only a few correlation functions have been determined experimentally because:

(1) Some experiments only measure the power spectrum of correlation functions over very restricted frequency ranges. Hence, the correlation functions themselves cannot be reconstructed from the experimental data. This is the case in static transport coefficient measurements where only the power spectra of specific correlation functions at zero frequency are measured.[12]

(2) Some experiments are difficult to perform and analyze. This is the case in slow neutron-scattering experiments.[5]

Hence, despite these theoretical advances, we still have very little quantitative experimental information on the detailed motion of fluid molecules.

The present state in the theory of time-dependent processes in liquids is the following. We know which correlation functions determine the results of certain physical measurements. We also know certain general properties of these correlation functions. However, because of the mathematical complexities of the N-body problem, the direct calculation of the full-time dependence of these functions is, in general, an extremely difficult affair. This is analogous to the theory of equilibrium properties of liquids. That is, in equilibrium statistical mechanics the equilibrium properties of a system can be found if certain multidimensional integrals involving the system's partition function are evaluated. However, the exact evaluation of these integrals is usually extremely difficult, especially for liquids.

In the case of monatomic fluids, digital computers have recently been employed to cope with the mathematical difficulties encountered above. Two methods have been used and both have been reviewed by Nelson.[30]

The first evaluates the multidimensional integrals for equilibrium properties by Monte Carlo techniques. However, this method does not provide any dynamical information. The second method, molecular dynamics, is essentially a brute force solution of the N-body problem. Alder and Wainwright[31] have used this latter method to study fluids of hard sphere molecules and square well molecules. These authors originally pointed out the potential applications and limitations of this method. In 1964, Rahman[32] demonstrated that it is feasible to do dynamics studies using much more realistic potentials. In particular he simulated liquid argon assuming a Lennard-Jones potential of interaction. He was primarily interested in time-dependent correlation functions which enter into the theory of neutron scattering. Among other things, his correlation functions show that the motion of argon atoms in the fluid is much more complicated than that assumed earlier in simplified model calculations. According to Zwanzig,[12] "Rahman's calculations provide what is probably the most detailed 'experimental' information currently available about dynamical processes in liquids." Verlet[44] then did a series of dynamics studies on liquid argon at various temperatures and densities. He again used the Lennard-Jones potential and found that these studies represent, to a good approximation, the equilibrium properties of real liquid argon.

Until now there have been no simulations done on liquids whose constituent molecules possess internal degrees of freedom. We have therefore undertaken a series of computer studies of the simplest liquids of this type: liquids made up of the diatomic molecules carbon monoxide and nitrogen. There were several compelling reasons for making these studies:

(1) To obtain a realistic and detailed picture of how individual molecules rotate and translate in classical fluids.

(2) To examine in detail some of the time-correlation functions that enter into the theories of transport, light absorption, light scattering, and neutron scattering.

(3) To see how well simulations based on various proposed potentials reflect physical reality.

(4) To test various stochastic assumptions for molecular motion that would simplify the N-body problem if they were valid. Molecular dynamics is far superior to experiment for this purpose since it provides much more detailed information on molecular motion than is provided by any experiment or group of experiments.

These computer experiments have provided insight into the microscopic dynamical behavior of real diatomic liquids for both the experimentalist

and theoretician alike. Further it is hoped that these studies will motivate more realistic approximate theories of the liquid state and provide "experimental" data to test these theories against.

B. Method Employed

The molecular dynamics calculations were carried out in a manner similar to that used by Rahman in his original study of liquid argon.[32] A finite number of molecules, N, were assumed to interact pairwise through a given truncated intermolecular pair potential. In addition, the atoms on the same molecule were assumed to interact through a harmonic potential, $\frac{1}{2}K_v(r_i - \bar{r})^2$, where K_v is the ground state vibrational force constant for the molecule, r_i is the internuclear separation for the ith molecule, and $\bar{r}$ is the ground state equilibrium internuclear separation. For carbon monoxide, $K_v = 1.9020 \times 10^6$ dynes/cm and $\bar{r} = 1.1281$ Å. For nitrogen, $K_v = 2.2962 \times 10^6$ dynes/cm and $\bar{r} = 1.094$ Å.[45] The harmonic potential was added because the calculations were done in the cartesian coordinates of the atoms forming the molecules. These atoms were originally separated by the equilibrium internuclear distance. They remained separated by this distance to within $\sim 10^{-4}$ Å throughout the course of the calculations. Therefore the results of these computations are essentially those for systems of rigid rotors.

The center of mass of each molecule was initially placed in a cubic lattice system within a large cube. The length, L, of a side of the cube was $(NM/\rho)^{1/3}$ where M was the mass of a molecule and ρ was the density of the fluid. L was typically ~ 30 Å in these calculations. The molecular orientation angles were chosen randomly on a unit sphere. That is, if θ and ϕ were the usual molecular axis, polar orientation angles, then ϕ was assumed to be uniformly distributed between 0 and 2π and $\cos\theta$ was assumed to be uniformly distributed between -1 and 1. The relative and center of mass velocity components were chosen by the Von Neuman[46] rejection method from Gaussian distributions appropriate to a gas of rigid rotors at some preselected temperature, T. That is, if V_x, V_y, and V_z were the center of mass velocity components and $\dot{\theta}$ and $\dot{\phi}$ were angular velocities, then the probability of selecting these velocities was given by

$$P(V_x, V_y, V_z, \dot{\theta}, \dot{\phi}) = \left(\frac{M}{2\pi KT}\right)^{3/2}\left(\frac{I\sin\theta}{2\pi KT}\right)\exp\left(\frac{-M[V_x^2 + V_y^2 + V_z^2]}{2KT}\right)$$
$$\times \exp\left(\frac{-I[\sin^2\theta\dot{\phi}^2 + \dot{\theta}^2]}{2KT}\right)$$

The selected relative and center of mass positions and velocities for each molecule were then transformed to cartesian coordinates to give an initial set of velocities and positions to each of the two atoms making up the molecule. Periodic boundary conditions were imposed.[31,32] That is, if (x, y, z) were the coordinates of a particle in the original cube, then there were assumed to be 26 images of this particle with coordinates gotten by adding and subtracting L from each cartesian coordinate of the original particle. A given particle i then interacted not only with every particle j within the original cube but also with all of particle j's images. Further, if during the course of the calculation a particle passed outside the original cube, then it was replaced by a particle entering the opposite side of the cube and having the same velocity as the particle that left. In other words, the number of molecules in the cube was constant. Hamilton's equations of motion for the N molecules were then solved numerically using the Runga-Kutta-Gill method with a stepsize in time, Δt, of 5×10^{-15} s. See Appendix A for a general discussion of the reasons why this numerical method[47] and time step were used.

During the course of the calculations the translational and rotational temperatures, T_T and T_R, respectively, were monitored at each step. These temperatures were defined by the equipartition theorem:

$$T_T = \frac{M}{3KN} \sum_{i=1}^{N} \mathbf{V}_i \cdot \mathbf{V}_i \tag{171}$$

$$T_R = \frac{1}{2KN} \left[\sum_{i=1}^{N} m_1 \mathbf{V}_i^1 \cdot \mathbf{V}_i^1 + m_2 \mathbf{V}_i^2 \cdot \mathbf{V}_i^2 \right] - \frac{3}{2} T_T \tag{172}$$

where $\mathbf{V}_i$ is the center of mass velocity of the ith molecule, $\mathbf{V}_i^j$ is the velocity of the jth atom on the ith molecule, and M_1 and M_2 are the masses of the two atoms making up the molecule. The formula for T_R assumes explicitly that we were dealing with systems of rigid rotors. This was actually a very good assumption since the vibrational coordinates only contributed ~ 0.02°K to T_R and the variance of T_R due to statistical fluctuations was typically 1000 times larger than this contribution. The total kinetic temperature, T_K, was then defined by

$$T_K = \frac{3}{2} T_T + T_R \tag{173}$$

The initial distribution of positions and velocities was not that of an equilibrium fluid at the preselected temperature T. Therefore, during the initial or equilibration phase of these calculations the monitored temperatures fluctuated wildly. This behavior is illustrated in Figure 1 where T_T

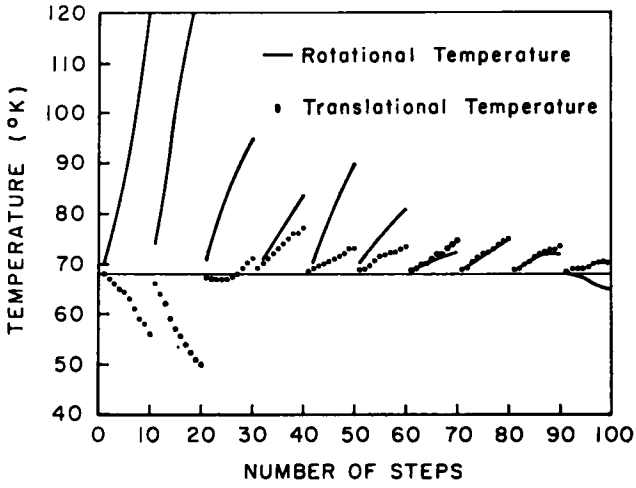

Fig. 1. Rotational and translational temperatures during the first 100 steps in the equilibribration phase of the modified Stockmayer simulation of CO. One step is equal to 5×10^{-15}s. The discontinuities correspond to points where velocities were changed.

and T_R for the first 100 steps in the equilibration phase of a typical calculation are presented. The preselected temperature was 68°K in this particular instance. Note that during the first 100 steps of this calculation the rotational temperature climbed from ~68 to ~130°K while the translational temperature dropped from ~68 to ~55°K. In order to force the system to equilibrate at the preselected temperature, T_T and T_R were examined after every 10 steps, and if these temperatures fell outside the range $T \pm \Delta T$ then:

(1) The cartesian velocities of all the molecules were transformed to relative and center of mass velocities.

(2) The center of mass velocities were multiplied by $(T/T_T)^{1/2}$ and the relative velocities were multiplied by $(T/T_R)^{1/2}$.

(3) The new relative and center of mass velocities were transformed back to the cartesian frame to give a new set of starting velocities.

(4) The equilibration phase was allowed to proceed.

ΔT usually varied from 0.5°K during the first 100 steps to 2.5 or 5°K for the last 100 steps. The maximum value of ΔT depended on the number of molecules being followed and the expected temperature or kinetic energy fluctuations at equilibrium for this number of molecules. The effect on temperature fluctuations of applying the above method in the first 100 steps of the equilibration phase is again illustrated in Figure 1. Note that

in the first 10 steps the fluctuations are as large as 50°K but in the last 10 steps they are only ~3°K. A given system usually took 300 steps to equilibrate.

After a system had equilibrated it was followed for an additional 600 steps or for 3×10^{-12} s. During this production phase of the calculations the velocities were not changed but the temperatures were continually monitored. The random translational and rotational temperature fluctuations that occurred during this phase are illustrated by Figure 2. In this particular instance, the rotational and translational temperature fluctuations are out of phase with one an other. This behavior is typical of a system with a strong angular dependent potential. The distribution of the x

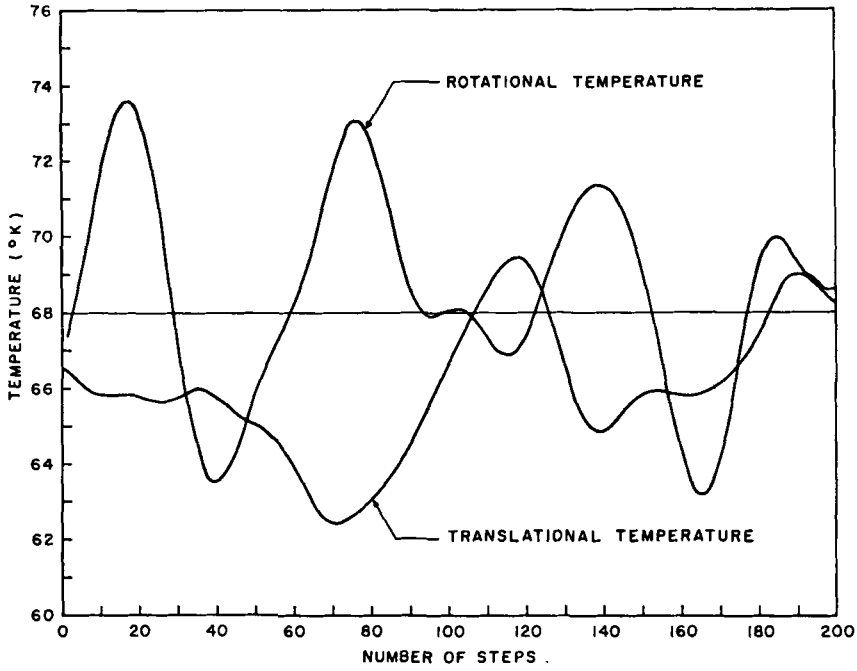

Fig. 2. Rotational and translational temperatures during the first 200 steps in the production phase of the modified Stockmayer simulation CO.

component of the center of mass velocity for this same simulation is presented in Figure 3. This is a Gaussian distribution with a mean of 0 and a variance of 1. 404×10^4 cm/s, i.e., that characteristic of a system of carbon monoxide molecules in equilibrium at a temperature of 66.4°K.

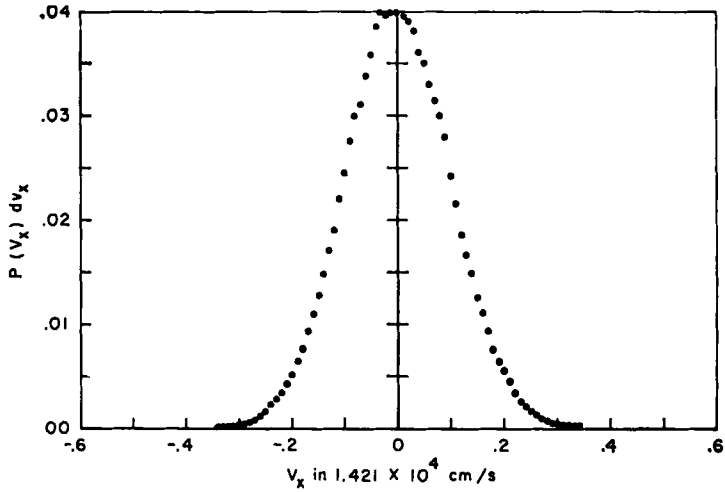

Fig. 3. Distribution of the x component of the C.M. velocity for CO from the modified Stockmayer simulation of CO. $\langle V_x \rangle = 0$ and $\langle V_x^2 \rangle^{1/2} = 1.404 \times 10^4$ cm/s.

C. Data Reduction

During the production phase, the positions, velocities, and accelerations created at each step in time were put on magnetic tapes. These tapes were later analyzed for the time-dependent and independent properties of the system. From a statistical mechanical standpoint, the data on these tapes may be viewed in one of two ways:

(1) The 600 blocks of positions and velocities represent an ensemble of 600 points in the phase space Γ_N, of the entire system being studied or an ensemble of $600N$ points in the reduced phase or μ space of a single molecule. This approach was taken in calculating time-independent properties. For example, the mean square force on a molecule, $\langle F^2 \rangle$, was given by

$$\langle F^2 \rangle = \frac{1}{600N} \sum_{i=1}^{N} \sum_{j=1}^{600} \mathbf{F}_i(j) \cdot \mathbf{F}_i(j) \tag{174}$$

where $\mathbf{F}_i(j)$ is the total force on the ith molecule in the jth block. Since N was either 216 or 512, averages of this type utilized either 129,600 or 3,072,000 points in μ space.

(2) The first 100 blocks of data may be viewed as 100 initial phase points in Γ_N, in which case the data represents 100 trajectories in Γ_N or $100N$ trajectories in μ space over a time interval $\sim 2{\cdot}5 \times 10^{-12}$ s. This

approach was taken in calculating autocorrelation functions. For example, the dipolar correlation function was given by:

$$\langle \boldsymbol{\mu}(0) \cdot \boldsymbol{\mu}(t_i) \rangle = \frac{1}{100N} \sum_{j=1}^{100} \sum_{k=1}^{N} \boldsymbol{\mu}_k(j) \cdot \boldsymbol{\mu}_k(j+i) \tag{175}$$

where $t_i = (i-1)\Delta t$, $i = 1, \ldots, 500$, and $\boldsymbol{\mu}_k(l)$ is a unit vector pointing along the internuclear axis of the kth molecule in the lth block. Autocorrelation functions were averaged over from 21,600 to 51,200 trajectories in μ space.

D. Potentials Used

One source of information on intermolecular potentials is gas phase virial coefficient and viscosity data. The usual procedure is to postulate some two-body potential involving 2 or 3 parameters and then to determine these parameters by fitting the experimental data. Unfortunately, this data for carbon monoxide and nitrogen can be adequately represented by spherically symmetric potentials such as the Lennard-Jones (6–12) potential.[48] That is, this data is not very sensitive to the orientational-dependent forces between two carbon monoxide or nitrogen molecules. These forces actually exist, however, and are responsible for the behavior of the correlation functions $\langle \boldsymbol{\mu}(0) \cdot \boldsymbol{\mu}(t) \rangle$ and $\langle P_2(\boldsymbol{\mu}(0) \cdot \boldsymbol{\mu}(t)) \rangle$. In the gas phase, where orientational forces are relatively unimportant, these functions resemble those in Figure 6. On the other hand, in the liquid these functions behave quite differently and resemble those in Figures 7 and 8.

One of the simplest orientational-dependent potentials that has been used for polar molecules is the Stockmayer potential.[48] It consists of a spherically symmetric Lennard-Jones potential plus a term representing the interaction between two point dipoles. This latter term contains the orientational dependence. Carbon monoxide and nitrogen both have permanent quadrupole moments. Therefore, an obvious generalization of Stockmayer potential is a Lennard-Jones potential plus terms involving quadrupole-quadrupole, dipole-dipole interactions. That is, the orientational part of the potential is derived from a multipole expansion of the electrostatic interaction between the charge distributions on two different molecules and only permanent (not induced) multipoles are considered. Further, the expansion is truncated at the quadrupole-quadrupole term. In all of the simulations discussed here, we have used potentials of this type. The components of the intermolecular potentials we considered are given by:

1. Lennard-Jones

$$V_{\text{L-J}}(R) = 4\varepsilon\left[\left(\frac{\sigma}{R}\right)^{12} - \left(\frac{\sigma}{R}\right)^{6}\right] \tag{176}$$

where R is the distance between the center of masses of two molecules. For nitrogen we used $\varepsilon/K = 87.5°\text{K}$ and $\sigma = 3.702$ Å.[49] For carbon monoxide we used $\varepsilon/K = 109.9°\text{K}$ and $\sigma = 3.585$ Å.[48]

2. Dipole-Dipole

$$V_{\text{D-D}}(R, \theta_1, \theta_2, \phi) = -\frac{\mu^2}{R^3}[2\cos\theta_1\cos\theta_2 - \sin\theta_1\sin\theta_2\cos\phi] \tag{177}$$

where θ_1, θ_2, and ϕ are the orientational angles of two molecules with respect to a line joining their center of masses. For CO, we used $\mu = 0.1172$ Debyes.[48]

3. Quadruple-Dipole

$$V_{\text{Q-D}}(R, \theta_1, \theta_2, \phi) = \frac{3\mu Q}{4R^4}[\cos\theta_1(3\cos^2\theta_2 - 1) + \cos\theta_2(3\cos^2\theta_1 - 1) - 2\sin\theta_1\sin\theta_2\cos\phi(\cos\theta_2 + \cos\theta_1)] \tag{178}$$

The quadrupole-dipole interaction differs by a factor of 2 from the usual definition of this term.[48] However, the effect of this difference on the overall results of the simulation that it was used in is thought to be small. The sign of Q was taken as positive and the dipole moment direction was from the oxygen atom to the carbon atom.[50]

4. Quadrupole-Quadrupole

$$V_{\text{Q-Q}}(R, \theta_1, \theta_2, \phi) = \frac{3Q^2}{4R^5}[1 - 5\cos^2\theta_1 - 5\cos^2\theta_2 - 15\cos^2\theta_1\cos^2\theta_2 + 2(\sin\theta_1\sin\theta_2\cos\phi - 4\cos\theta_1\cos\theta_2)^2] \tag{179}$$

For carbon monoxide we used $Q = 2.43 \times 10^{-26}$ esu and for nitrogen we used $Q = 2.05 \times 10^{-26}$ esu.[49] Q is defined here as $\frac{1}{2}$ the zz component of the quadrupole tensor in a coordinate system whose z axis lies along the internuclear axis.

The four simulations of carbon monoxide and nitrogen discussed here were done at a preselected temperature of 68°K and usually equilibrated within 2 or 3°K of this value. The densities of carbon monoxide and nitrogen liquids used were 0.8558 and 0.8537 g/cc, respectively. The range of all potentials used was 2.25σ: the same range that Rahman[32] used in his

studies of liquid argon. At any instant there were ~40 molecules within a particular molecule's range of interaction. The four simulations and their intermolecular potentials are:

1. The Stockmayer Simulation of Carbon Monoxide with $\mu = 0.1172$ *Debye*

The intermolecular potential consists of the sum of Eqs. (176) and (177). This simulation was done for 216 and 512 molecules. However, only the autocorrelation functions from the 512 molecules case are discussed here. The small dipole moment of carbon monoxide makes the orientational part of this potential so weak that molecules rotate essentially freely, despite the fact that this calculation was done at a liquid density. The results for the Stockmayer simulation serve the purpose of providing a framework for contrasting results from more realistic, stronger angular-dependent potentials.

2. The Stockmayer Simulation of Carbon Monoxide with $\mu = 1.172$ *Debye*

The potential form is the same as that in *1* except for the dipole moment used. This simulation was run for 216 molecules. We were primarily interested in seeing the effect on rotational motion of increasing the dipole moment. Although this particular dipole moment is ten times larger than carbon monoxide's, it is a reasonable one for a more polar substance such as HCl. Note: Henceforth a reference to the Stockmayer simulation will refer to the first one discussed. Any specific reference to this calculation will mention the dipole moment used.

3. The Modified Stockmayer Simulation of Carbon Monoxide

The intermolecular potential consists of the sum of Eqs. (176), (177), (178), and (179). This simulation was done for 216 and 512 molecules but again only the autocorrelation functions for 512 molecules are discussed here. This potential is the strongest angular dependent potential we considered. The results from this potential indicate that it is slightly stronger than that in real liquid carbon monoxide. For example the mean square torque, $\langle N^2 \rangle$, for this simulation is $\sim 36 \times 10^{-28}$ (dyne-cm)^2 [51] and the experimental value is $\sim 21 \times 10^{-28}$ (dyne-cm)^2. If this potential is taken seriously, then it should be pointed out that this small discrepancy in torques could be easily removed by using a smaller quadrupole moment. This would be a well justified step since experimental quadrupole moments for carbon monoxide range from $\sim 0.5 \times 10^{-26}$ to 2.43×10^{-26} esu.[49]

4. The Lennard-Jones plus Quadrupole-Quadrupole Simulation of Nitrogen

The intermolecular potential consists of the sum of Eqs. (176) and (179) and was done for 216 molecules.

E. Summary and Discussion of Errors

Our original goal was to study liquids of carbon monoxide and nitrogen. Ideally this would involve solving the equations of motion for a macroscopic number of molecules ($\sim 10^{23}$). However, in practice we only considered ~ 512 molecules in an infinite periodic environment. Even this number strained both the storage capacity and computing ability of our IBM 7094. For example, the 6144 first-order differential equations for the modified Stockmayer simulation for 512 carbon monoxide molecules took 5.1 min of 7094 time/step or a total of 76.5 hr of 7094 time for the 900 steps of the equilibration and production phase of this calculation. The data reduction for this calculation took approximately another 75 hr of 7094 time.

We have tried to assess the effects of the finite number of molecules, or, equivalently, the periodic boundary effects by comparing the results of simulations done with 216 and 512 molecules. For equilibrium properties such $\langle N^2 \rangle$ and $\langle F^2 \rangle$, the primary effect of increasing the number of molecules is to reduce the measured variances of these quantities (see Tables II and III). We therefore feel that these quantities are within a few percent of

TABLE II

Equilibrium Properties from Modified Stockmayer Simulation of CO

N	512	216
T_K	(67.43 ± 1.26)°K	$(69.45 \pm .43)$°K
T_T	(66.35 ± 1.72)°K	(68.87 ± 3.38)°K
T_R	(69.06 ± 2.47)°K	(70.31 ± 3.91)°K
$\langle F^2 \rangle$	$(9.460 \pm .657) \times 10^{-11}$ (dyne)^2	$(10.07 \pm 1.05) \times 10^{-11}$ (dyne)^2
$\langle N^2 \rangle$	$(35.74 \pm 1.46) \times 10^{-28}$ (dyne-cm)^2	$(35.32 \pm 3.00) \times 10^{-28}$ (dyne-cm)^2
$\langle J^2 \rangle$	$(27.63 \pm .991) \times 10^{-54}$ (g cm^2/s)^2	$(28.14 \pm 1.60) \times 10^{-54}$ (g cm^2/s)^2
$D_\#$	1.88×10^{-5} cm^2/s	1.82×10^{-5} cm^2/s
$\frac{\langle V_C \rangle}{N}$	$(-8.21 \pm .05) \times 10^{-14}$ erg	$\sim -8.2 \times 10^{-14}$ erg
$\frac{\langle V_T \rangle}{N}$	$(-11.34 \pm .04) \times 10^{-14}$ erg	$\sim -11 \times 10^{-14}$ erg

those measured for an infinite number of molecules. For the correlation functions discussed here, the primary effect of increasing the number of molecules is to reduce fluctuations in these functions that occur for $t \lesssim 4 \times 10^{-13}$ s. This effect on the velocity autocorrelation function, $\psi(t)$, for the Stockmayer simulation is illustrated in Figure 4. $\psi(t)$ is defined by

$$\psi(t) = \frac{\langle \mathbf{V}(0) \cdot \mathbf{V}(t) \rangle}{\langle V^2 \rangle} \tag{180}$$

TABLE III

Equilibrium Properties from Stockmayer Simulation of CO

N	512	216
T_K	$(69.18 \pm .97)$°K	(67.86 ± 1.55)°K
T_T	(70.03 ± 1.60)°K	(67.89 ± 2.54)°K
T_R	$(67.91 \pm .12)$°K	$(67.80 \pm .29)$°K
$\langle F^2 \rangle$	$(8.722 \pm .541) \times 10^{-11}$ (dyne)^2	$(8.696 \pm .878) \pm 10^{-11}$ (dyne)^2
$\langle N^2 \rangle$	$(6.716 \pm .144) \times 10^{-31}$ (dyne-cm)^2	$(6.635 \pm .434) \times 10^{-31}$ (dyne-cm)^2
$\langle J^2 \rangle$	$(27.17 \pm .04) \times 10^{-54}$ (g cm^2/s)^2	$(27.13 \pm .12) \times 10^{-54}$ (g cm^2/s)^2
D_*	2.39×10^{-5} cm^2/s	2.48×10^{-5} cm^2/s
$\frac{\langle V_C \rangle}{N}$	$(-8.49 \pm .03) \times 10^{-14}$ erg	$\sim -8.4 \times 10^{-14}$ erg
$\frac{\langle V_T \rangle}{N}$	$(-8.49 \pm .03) \times 10^{-14}$ erg	$\sim -8.4 \times 10^{-14}$ erg

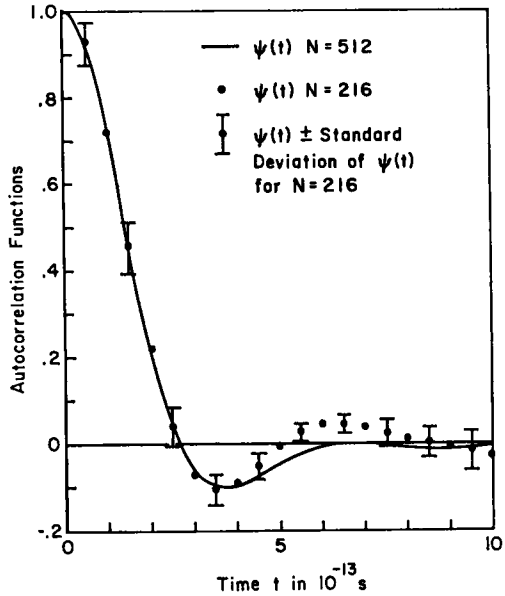

Fig. 4. The velocity autocorrelation functions from the Stockmayer simulation of CO using 216 and 512 molecules.

where V is the center of mass velocity of a molecule. This function will be discussed in greater detail shortly. Because of the boundary effect, we feel that the fine details of the correlation functions from simulations involving

216 molecules and for times $\lesssim 4 \times 10^{-13}$ s should not be taken too seriously.

We have also tried to assess the effects of integrating Hamilton's equations numerically. This is a rather difficult task since the exact solutions to these equations are not known. However, we can use the observed conservation of total energy and linear momentum as an indication that the equations are being integrated properly. For the Stockmayer and modified Stockmayer simulations the total energy and linear momentum were conserved to ~ 0.05 and $\sim 0.0006\%$, respectively, over the 600 integration steps of the production phase of these calculations.

In comparing our systems to real liquids of carbon monoxide and nitrogen, we are assuming implicitly that these real liquids behave like classical systems of rigid rotors. That is, quantum effects are relatively small. The usual criteria that have to be satisfied for this to be true are:

(1) The De Broglie wavelength of a molecule must be small compared to the average distance between molecules, i.e., $(h^2/3MKT)^{1/2}/(\rho/M)^{1/3} < 1$.

(2) Many rotational states must be occupied or, equivalently, the rotational energy spacing must be small with respect to KT, i.e., $\hbar^2/2IKT < 1$.

(3) The molecules must be predominantly in their ground state vibrational level, i.e., $h\omega_e c/KT \gtrsim 1$, where c is the velocity of light and ω_e is the energy separation of successive levels in wave numbers. For carbon monoxide at 68°K with $\rho = 0.8558$ g/cc and $\omega_e = 2.170 \times 10^3$ cm^{-1},[45] the above factors are $\sim 2 \times 10^{-1}$, $\sim 5 \times 10^{-2}$, and $\sim 5 \times 10^{1}$, respectively. Therefore, to a first approximation real liquid carbon monoxide at this temperature and density behaves classically, and our comparisons will be justified.

F. Liquid or Solid

All of these simulations were done at temperatures at or near the melting point of carbon monoxide and nitrogen. Therefore we must show that these simulations represent liquids, not solids. The following characteristics of our results all indicate that we are dealing with liquids.

The coefficients of self diffusion for each of these simulations (see Tables II, III, IV, and V), are all very close to those measured experimentally for liquid CO.[52] If we were dealing with solids these coefficients would be an order of magnitude or more smaller.

Following Verlet,[44] consider the function $\rho_{K,\mathbf{R}}(t)$ defined by

$$\rho_{K,\mathbf{R}}(t) = \frac{1}{3}\sum_{i=1}\{\cos KX_i(t) + \cos KY_i(t) + \cos KZ_i(t)\} \qquad (181)$$

where $K = 4\pi N^{1/3}/L$, L is the length of a side of the cube enclosing the N molecules, and $X_i(t)$, $Y_i(t)$, and $Z_i(t)$ are the center of mass coordinates of

TABLE IV

Equilibrium Properties from Stockmayer Simulation of CO with $\mu = 1.172$ Debyes and from Lennard-Jones Plus Quadrupole-Quadrupole Simulation of N_2

Liquid	CO	N_2
N	216	216
T_K	(71.84 ± 2.99)°K	(66.29 ± 2.09)°K
T_T	(69.94 ± 3.59)°K	(68.86 ± 2.69)°K
T_R	$(74.67) \pm 6.95)$°K	(62.43 ± 3.29)°K
$\langle F^2 \rangle$	$(10.54 \pm 1.18) \times 10^{-11}$ (dyne)^2	$(10.22 \pm .96) \times 10^{-11}$ (dyne)^2
$\langle N^2 \rangle$	$(19.99 \pm 1.50) \times 10^{-28}$ (dyne-cm)^2	$(18.29 \pm 1.29 \times 10^{-28}$ (dyne-cm)^2
$\langle J^2 \rangle$	$(29.88 \pm 2.78) \times 10^{-54}$ (g cm^2/s)^2	$(23.99 \pm 1.27) \times 10^{-54}$ (g cm^2/s)
D_*	1.86×10^{-5} cm^2/s	1.15×10^{-5} cm^2/s
$\frac{\langle V_C \rangle}{N}$	$\sim -8.1 \times 10^{-14}$ erg	$\sim -6.6 \times 10^{-14}$ erg
$\frac{\langle V_T \rangle}{N}$	$\sim -13 \times 10^{-14}$ erg	$\sim -8.4 \times 10^{-14}$ erg

TABLE V

Data for Approximate Memory Functions

Simulation	Stockmayer	Modified Stockmayer
$\int_0^\infty \psi(t)\, dt$	1.1503×10^{-13}/s	0.9564×10^{-13}/s
$\int_0^\infty A_J(t)\, dt$		0.5710×10^{-13}/s
$\frac{\langle a^2 \rangle}{\langle V^2 \rangle}$	0.6469×10^{26}/s^2	0.7406×10^{26}/s^2
$\frac{\langle \dot{a}^2 \rangle}{\langle V^2 \rangle}$	$(1.050 \pm .20) \times 10^{52}$/s^4	$(1.4067 \pm .12) \times 10^{52}$/s^4
$\frac{\langle N^2 \rangle}{\langle J^2 \rangle}$		1.2932×10^{26}/s^2
$\frac{\langle \dot{N}^2 \rangle}{\langle J^2 \rangle}$		$(3.3249 \pm .20) \times 10^{52}$/s^4

the ith molecule at time t. For a cubic lattice, which was our initial starting configuration in each of the simulations, the distribution of X_i is given by

$$P(x_i)\,dx_i = \delta\left(x_i - \frac{m}{2}\frac{L}{N^{\frac{1}{3}}}\right) \qquad m = 1, \ldots, N^{1/3} \tag{182}$$

Using this distribution, the mean and variance of $\rho_{K,\mathbf{R}}$ are N and 0, respectively. Therefore $\rho_{K,\mathbf{R}}(t)$ should be N for all times in a solid. On the other hand, for a gas or liquid the X_i are uniformly distributed between 0 and L:

$$P(x_i)\,dx_i = \frac{dx_i}{L} \qquad 0 \leq x_i \leq L \tag{183}$$

The mean and variance of $\rho_{K,\mathbf{R}}$ for the uniform distribution are 0 and $(N/2)^{1/2}$, respectively. This implies that for a liquid, $\rho_{K,\mathbf{R}}(t)$ should oscillate around 0 with an amplitude of oscillation of $\sim(N)^{1/2}$. Plots of $\rho_{K,\mathbf{R}}(t)$ for the Stockmayer and the modified Stockmayer simulation of carbon monoxide using 512 molecules are shown in Figure 5. The behavior of $\rho_{K,\mathbf{R}}(t)$ in each of these simulations is that of a liquid.

Finally, consider the behavior of the mean square displacement of the center of mass of a molecule, $\langle(\Delta\mathbf{R}(t))^2\rangle$. $\mathbf{R}(t)$ is the center of mass of the molecule at time t and $\Delta\mathbf{R}(t) = \mathbf{R}(t) - \mathbf{R}(0)$. Rahman has just completed a dynamics study of liquid and solid argon[53] in the neighborhood of 84°K—the melting point of argon. He finds that for short times, $0 \leq t \leq 2.5 \times 10^{-13}$ s, the mean square displacement of an atom in the solid is identical with that of an atom in the liquid at the same temperature. That is, for short times the atoms in both states behave like free gas particles and their displacements are given by $(3KT/M)t^2$. However, the long time behavior of these functions is quite different. In the liquid $\langle(\Delta\mathbf{R}(t))^2\rangle$ increases monotonically with time. On the other hand, in the solid $\langle(\Delta\mathbf{R}(t))^2\rangle$ reaches a maximum value of $\sim 0.5\,\text{Å}^2$ at $t = \sim 6 \times 10^{-13}$ s and then decreases slightly in an oscillatory fashion to a value of $\sim 0.4\,\text{Å}^2$ at $t = 25 \times 10^{-13}$ s. The main point of interest here is that the mean square displacement in the solid is bounded, whereas in the liquid it is not. Our mean square displacements behave like Rahman's: they increase monotonically in the real time interval $0 \leq t \leq 25 \times 10^{-13}$ s. (See Figures 35 and 39.) However, we can not yet conclude from this that we are dealing with liquids because it is possible that for $t > 25 \times 10^{-13}$ s these functions will approach some asymptotic value characteristic of a solid. The following arguments suggest that this is not the case: If we were dealing with solids, then these functions would have approached their asymptotic values long before 25×10^{-13} s. Consider a cubic harmonic Debye solid which is a fair

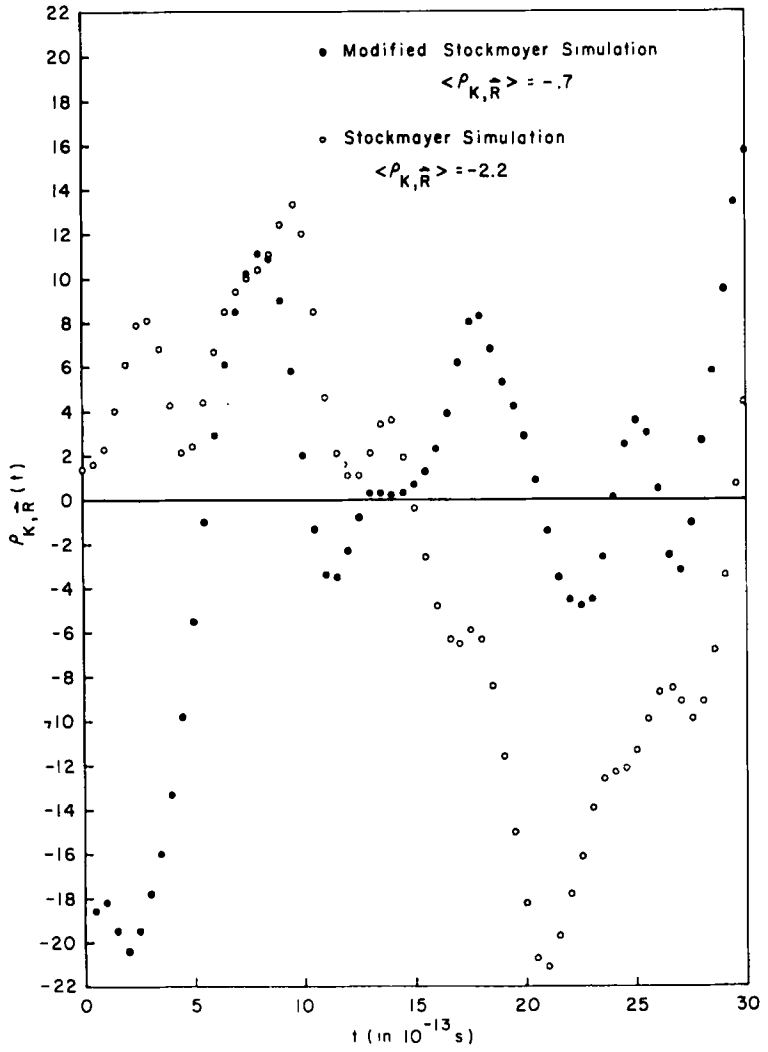

Fig. 5. The functions $\rho_{K,\hat{R}}(t)$ from the Stockmayer and modified Stockmayer simulation of CO.

approximation to solid nitrogen, carbon monoxide, and argon. Vineyard[54] has shown that if θ_D is the characteristic temperature of a solid of this type, then the mean square displacement of an atom in the lattice is given by:

$$\langle(\Delta \mathbf{R}(t))^2\rangle_D = \frac{18KT}{M\omega_D{}^2}\left[1 - \frac{\sin\omega_D t}{\omega_D t}\right] \tag{184}$$

where $\omega_D = K\theta_D/\hbar$. This function goes as $(3KT/M)t^2$ for short times and approaches the asymptotic value of $18KT/M\omega_D{}^2$ in a damped oscillatory fashion. It reaches its maximum value of $22KT/M\omega_D{}^2$ at $t \sim 4.4/\omega_D$. Therefore, $\langle(\Delta\mathbf{R}(t))^2\rangle_D$ behaves at least qualitatively like Rahman's function for solid argon. The characteristic temperatures for solid argon and nitrogen are 85 and 68°K,[55] respectively. It follows that $\langle(\Delta\mathbf{R}(t))^2\rangle_D$ in solid argon at 84°K should reach its maximum value of ~ 0.3 Å^2 in $\sim 4 \times 10^{-13}$ s. These values are approximately a factor of 1.5 smaller than what Rahman actually observed. For solid nitrogen at 68°K, $\langle(\Delta\mathbf{R}(t))^2\rangle_D$ should reach its maximum value of ~ 0.6 Å^2 in $\sim 5 \times 10^{-13}$ s. Since we have not seen the mean square center of mass displacements approach any asymptotic values over a time range five times larger than this value, we conclude again that we are dealing with liquids.

G. Equilibrium Properties

Tables II, III, and VI contain a few equilibrium properties for the 4

TABLE VI[a]

Equilibrium Properties

Memory function	Corresponding friction coefficient	Numerical value of friction coefficients ($\times 10^{-12}$ s^{-1}) γ	γ_J
Gaussian	$\left(\frac{\pi}{2}\right)^{1/2}\mu$	5.98	14.34
Delta function	$\left(\frac{\pi}{2}\right)^{1/2}\mu$	5.98	14.34
Lorentzian	$\left(\frac{\pi}{\sqrt{2}}\right)\mu$	10.60	25.41
Exponential (*a*)	$\left[\frac{2}{\ln 2}\right]\mu$	8.10	19.43
Exponential (*b*)	$\left[\frac{\sqrt{2}}{\ln 2}\right]^{1/2}\mu$	9.73	16.38
Experimental[b]		9.38	17.54

[a] μ is calculated from moments given in Nijboer and Rahman to be 4.77×10^{12} s^{-1}, μ_J from moments given in Table V.

[b] The experimental friction coefficient comes from Nijboer and Rahman.[95]

systems we studied. The data is presented in the form of the mean value of a given property averaged over 600 blocks plus or minus the variance of that property within the 600 blocks. For example, the mean square force is given by (see Eq. 5):

$$\langle F^2 \rangle = \frac{1}{600} \sum_{j=1}^{600} \langle F_j^2 \rangle \tag{185}$$

$$\langle F_j^2 \rangle = \frac{1}{N} \sum_{i=1}^{N} \mathbf{F}_i(j) \cdot \mathbf{F}_i(j) \tag{186}$$

and the variance of the mean square force, σ_F, is then given by:

$$\sigma_F = \left[\sum_{j=1}^{600} \frac{[\langle F_j^2 \rangle - \langle F^2 \rangle]^2}{599} \right]^{1/2} \tag{187}$$

The kinetic temperatures, T_K, T_R, and T_T, are mainly given for completeness. The fact that these three temperatures are not equal indicates that our heuristic method for forcing each system to equilibrate at a preselected temperature was not 100% effective. The largest differences between these temperatures occur in the Stockmayer simulation of CO with $\mu = 1.172$ Debyes and in the Lennard-Jones etc., simulation of N_2.

The mean square force is one test of the validity of the pair potentials used in the dynamics calculations. The calculated mean square forces for the four simulations are not very different: they only vary between $\sim 9 \times 10^{-11}$ and $\sim 10 \times 10^{-11}$ (dynes)^2. The experimental values[51] of the mean square force in solid CO at 68°K and in liquid CO at 77.5°K are $\sim 15 \times 10^{-11}$ and $\sim 14 \times 10^{-11}$ (dynes)^2, respectively. Therefore, our mean square forces are $\sim 30\%$ too small.

The mean square torque is another test of the pair potentials used. The calculated mean square torques are very potential dependent: they range from $\sim 7 \times 10^{-31}$ to $\sim 36 \times 10^{-28}$ (dyne-cm)^2. The experimental values[51] of the mean square torque in solid CO at 68°K and in liquid CO at 77.5°K are $\sim 19 \times 10^{-28}$ and $\sim 21 \times 10^{-28}$ (dyne-cm)^2, respectively. Therefore, the Stockmayer potential clearly does not represent the noncentral forces in liquid CO, i.e., this potential is much too weak. On the other hand, the noncentral part of the modified Stockmayer potential is too strong. However, as pointed out previously, this problem can easily be solved by using a smaller quadrupole moment. The mean square torques from the other two potentials agree quite favorably with the experimental values. We conclude from the above that the quadrupole-quadrupole interaction can easily account for observed mean square torques in liquid CO.

A further test of the pair potentials used is the translational diffusion coefficients, D. The coefficients in Tables II, III, and IV were all evaluated using the Einstein-Kubo relation:

$$D = \frac{\langle V^2 \rangle}{3} \int_0^\infty \psi(t)\, dt \tag{188}$$

The experimental value[52] of D in liquid CO at 69°K is $(2.25 \pm .1) \times 10^{-5}$ cm^2/s. The calculated values of D for the Stockmayer and modified Stockmayer simulations of CO are 2.39×10^{-5} and 1.88×10^{-5} cm^2/s, respectively. Therefore, the diffusion coefficients from these two simulations agree fairly well with the experiment.

The average central or Lennard-Jones potential energy per molecule, $\langle V_C \rangle / N$, and the average total potential energy per molecule, $\langle V_T \rangle / N$, are also given in Tables I, II, and III. The noncentral part of the Stockmayer potential contributes nothing to this system's total potential energy. On the other hand, the noncentral parts of the other three potentials contribute from 22 to 38% to their system's total potential energies.

H. The Classical Limit

In the previous section it was shown how classical many-body systems can be studied by computer experiments. Actual laboratory experiments probe real systems which are, strictly speaking, entirely quantum-mechanical in nature. What, then, is the relationship between the classical and quantum-mechanical time-correlation function of the dynamical variable $\hat{U}_l$? To expedite this discussion consider the one sided function $\langle U^+{}_l(0) U_l(t) \rangle$. This correlation function is in general complex with real part $\phi'_l(t)$ and imaginary part $\phi''_l(t)$ so that

$$\phi_{ll}(t) \equiv \langle U^+{}_l(0) U_l(t) \rangle = \phi'_l(t) + i\phi''_l(t) \tag{189}$$

Expansion of $\langle U^+{}_l(0) U_l(t) \rangle$ in the exact energy eigenstates of $\hat{H}$ yields

$$\begin{aligned} \phi_{ll}(t) &= \sum_{nm} \rho_n \, |(n|\, U^+{}_l \,|m)|^2 \exp(i\omega_{mn} t) \\ \phi'_{ll}(t) &= \sum_{nm} \rho_n \, |(n|\, U^+{}_l \,|m)|^2 \cos(\omega_{mn} t) \\ \phi''_{ll}(t) &= \sum_{nm} \rho_n \, |(n|\, U^+{}_l \,|m)|^2 \sin(\omega_{mn} t) \end{aligned} \tag{190}$$

from which it follows that $\phi'_{ll}(t)$ and $\phi''_{ll}(t)$ are odd and even functions of the time, respectively.

The complex conjugate of $\langle U^+{}_l(0) U_l(t) \rangle$ is thus,

$$\langle U^+{}_l(0) U_l(t) \rangle^* = \langle U_l(t) U^+{}_l(0) \rangle = \phi'_{ll}(t) - i\phi''_{ll}(t) = \langle U^+{}_l(0) U_l(-t) \rangle \tag{191}$$

It follows from Eqs. (189) and (191) that

$$\begin{aligned} \phi'_{ll}(t) &= \langle \tfrac{1}{2}[U_l(t), U^+{}_l(0)]_+ \rangle \\ \phi''_{ll}(t) &= \langle \tfrac{1}{2}[U_l(t), U^+{}_l(0)]_- \rangle \end{aligned} \tag{192}$$

The Fourier transform, $\phi_{ll}(\omega)$, of $\phi_{ll}(t)$ is simply

$$\phi_{ll}(\omega) = \int_{-\infty}^{\infty} dt\, e^{i\omega t}\, \phi_{ll}(t) = 2\pi \sum_{nm} \rho_n\, |(n|\, U^+{}_l\, |m)|^2\, \delta(\omega + \omega_{mn})$$

Since $\rho_n = \rho_m \exp(\beta\hbar\omega_{mn})$ it follows that

$$\begin{aligned} \phi_{ll}(\omega) &= 2\pi\, e^{-\beta\hbar\omega} \sum_{nm} \rho_n\, |(n|\, U^+{}_l\, |m)|^2\, \delta(\omega + \omega_{mn}) \\ &= e^{-\beta\hbar\omega} \int_{-\infty}^{+\infty} dt\, e^{i\omega t}\, \phi^*{}_{ll}(t) \end{aligned} \tag{193}$$

Now $\phi^*{}_{ll}(t) = \phi_{ll}(-t)$, and consequently

$$\int_{\infty}^{\infty} dt\, e^{i\omega t}\, \phi^*{}_{ll}(t) = \int_{-\infty}^{+\infty} dt\, e^{-i\omega t}\, \phi_{ll}(t) = \phi_{ll}(-\omega) \tag{194}$$

So that

$$\phi_{ll}(\omega) = e^{-\beta\hbar\omega}\, \phi_{ll}(-\omega) \tag{195}$$

This equation expresses the well-known condition of detailed balance.

Substitution of Eqs. (189) and 191) into Eq. (193) leads to

$$\int_0^{\infty} dt\, \phi'_{ll}(t) \cos \omega t = \coth\left(\frac{\beta\hbar\omega}{2}\right) \int_0^{\infty} dt\, \phi''_{ll}(t) \sin \omega t \tag{196}$$

after exploiting the fact that $\phi'_{ll}(t)$ is even and $\phi''_{ll}(t)$ is odd in the time. This gives the fluctuation dissipation theorem.

The classical time-correlation function, $\langle U^+{}_l(0) U_l(t) \rangle$, does not obey the condition of detailed balance. Computer experiments provide detailed information about classical time-correlation functions. Is there any way to use the classical functions to predict quantum-mechanical time-correlation functions? The answer to this question is affirmative. There exist approximations which enable the quantum-time-correlation functions to be predicted from the corresponding classical functions. Let us denote by $\psi_{ll}(t)$ the classical time-correlation function and by $\phi_{ll}(t)$ the one-sided quantum-mechanical correlation function:

$$\begin{aligned} \phi_{ll}(t) &= \langle U^+{}_l(0) U_l(t) \rangle \\ \psi_{ll}(t) &= \langle U^*{}_l(0) U_l(t) \rangle_{Cl} \end{aligned} \tag{197}$$

Theorem: If $F'(t) \equiv \phi_{II}(t + i\hbar\beta/2)$, then the Fourier transform, $F'(\omega)$, of $F'(t)$ is related to the Fourier transform, $\phi_{II}(\omega)$, of $\phi_{II}(t)$, according to the equation,

$$F'(\omega) = e^{-\beta\hbar\omega/2}\, \phi_{II}(\omega) \tag{198}$$

Proof: Expansion of $\phi_{II}(t)$ in the energy eigenstates of the Hamiltonian leads to the equation

$$\phi_{II}(t) = \sum_{nm} \rho_n\, |(n|U^+{}_I|m)|^2 \exp(i\omega_{nm}t)$$

From this it follows that

$$F'(t) = \sum_{nm} \rho_n |(n|U^+{}_I|m)|^2\, e^{i\omega_{nm}t}\, e^{-\beta\hbar\omega_{nm}/2}$$

Fourier transformation of $F'(t)$ is then,

$$\begin{aligned} F'(\omega) &= \int_{-\infty}^{+\infty} dt\, e^{i\omega t} F'(t) \\ &= 2\pi\, e^{\beta\hbar\omega/2} \sum_{nm} \rho_n\, |(n|U^+{}_I|m)|^2\, \delta(\omega + \omega_{nm}) \end{aligned}$$

The term

$$2\pi \sum_{nm} \rho_n\, |(n|U^+{}_I|m)|^2\, \delta(\omega + \omega_{nm})$$

is the Fourier transform of $\phi_{II}(t)$, so that

$$F'(\omega) = e^{\beta\hbar\omega/2}\, \phi_{II}(\omega)$$

This proves the theorem.

That $F'(\omega)$ is an even function of the frequency and consequently $F'(t)$ is an even function of the time follows from the detailed balance condition and the previous theorem. Combining the condition of detailed balance

$$\phi_{II}(\omega) = e^{-\beta\hbar\omega}\, \phi_{II}(-\omega)$$

with Eq. (198) yields

$$F'(\omega) = e^{-\beta\hbar\omega/2}\, \phi_{II}(-\omega)$$

From this it follows that

$$F'(-\omega) = e^{\beta\hbar\omega/2}\, \phi_{II}(\omega) = F'(\omega) \tag{199}$$

This last step follows from Eq. (198) and demonstrates that $F'(\omega)$ and $F'(t)$ are even functions of their arguments.

Schofield[56] suggested that the quantum-mechanical time-correlation

function, $\phi_{ll}(t)$, can be approximated from the classical correlation function, $\psi_{ll}(t)$, by taking $F'(t)$ equal to $\psi_{ll}(t)$ since both of these functions are even functions of the time. Then

$$F'(t) = \phi_{ll}\left(t + \frac{i\hbar\beta}{2}\right) = \psi_{ll}(t) \tag{200}$$

and the quantum-mechanical function is

$$\phi_{ll}(t) = \psi_{ll}\left(t - \frac{i\hbar\beta}{2}\right) \tag{201}$$

The Schofield approximation is useful insofar as it gives an approximate quantum-mechanical time-correlation function which satisfies the condition of detailed balance as it must. Needless to say if $\phi_{ll}(t)$ is equated to $\psi_{ll}(t)$ the condition of detailed balance will not hold. It should be noted that the Schofield approximation does not satisfy the moment sum rules on $\phi'_l(t)$. It was for this reason that Egelstaff proposed his y time approximation. Egelstaff showed that if $y^2 = t^2 - i\hbar\beta t$, then taking

$$\phi_{ll}(t) = \psi_{ll}(y) \tag{202}$$

would give an approximate $\phi_{ll}(t)$ which satisfies both the condition of detailed balance and the first few sum rules on $\phi_{ll}(t)$. In addition to these approximations there have been some recent attempts to relate classical time-correlation functions to their quantum analogues. The approximate quantum-mechanical time-correlation functions so obtained deviate significantly from their classical counterparts only for short times.

V. EXPERIMENTAL CORRELATION AND MEMORY FUNCTIONS

In this section we shall first investigate the following auto-correlation and memory functions obtained from these simulations:

(1) The linear momentum or velocity autocorrelation function $\psi(t)$, defined by

$$\psi(t) = \frac{\langle \mathbf{v}(0) \cdot \mathbf{v}(t) \rangle}{\langle v^2 \rangle} \tag{203}$$

$$= \frac{\langle \mathbf{P}(0) \cdot \mathbf{P}(t) \rangle}{\langle \mathbf{P}^2 \rangle} \tag{204}$$

where $\mathbf{P}$ is the center of mass, C.M., linear momentum of a molecule, i.e.,

$$\mathbf{P} = m_1 \mathbf{v}_1 + m_2 \mathbf{v}_2 \tag{205}$$

It has already been pointed out that the power spectrum of this function at zero frequency determines the translational diffusion coefficient, D. The full-time dependence of this function can be obtained indirectly from inelastic slow neutron experiments.[57] Unfortunately, these experiments are not yet precise enough to say anything quantitatively about this function. $\psi(t)$'s memory function, $K_\psi(t)$, is defined by

$$-\frac{d\psi}{dt} = \int_0^t K_\psi(t')\,\psi(t-t')\,dt' \tag{206}$$

(2) The angular momentum autocorrelation function, $A_J(t)$, defined by

$$A_J(t) = \frac{\langle \mathbf{J}(0)\cdot\mathbf{J}(t)\rangle}{\langle \mathbf{J}^2\rangle} \tag{207}$$

where $\mathbf{J}$ is the angular momentum of a molecule about its C.M., i.e.,

$$\mathbf{J} = m_1[\mathbf{r}_1 - \mathbf{R}]\times[\mathbf{v}_1 - \mathbf{V}] + m_2[\mathbf{r}_2 - \mathbf{R}]\times[\mathbf{v}_2 - \mathbf{V}] \tag{208}$$

where m_i, $\mathbf{r}_i$, and $\mathbf{v}_i$ are the mass, position, and velocity of the ith atom, respectively, and $\mathbf{R}$ and $\mathbf{V}$ are the position and velocity of a molecule's C.M., respectively. The power spectrum of this function at the Larmour precession frequency determines the contribution of the nuclear spin-rotation coupling to nuclear spin relaxation in NMR experiments.[8,15] Unfortunately, there has been very little if anything reported on the full-time dependence of this function. $A_J(t)$'s memory function, $K_J(t)$, is defined by

$$-\frac{dA_J}{dt} = \int_0^t K_J(t')A_J(t-t')\,dt' \tag{209}$$

(3) The dipole autocorrelation function, $\langle\boldsymbol{\mu}(0)\cdot\boldsymbol{\mu}(t)\rangle$, defined previously. The full-time dependence of this function for liquid carbon monoxide has been successfully determined experimentally from Fourier inversion of infrared band shapes.[2,15] In fact, this was one of the reasons this system was studied. This function has also been successfully evaluated in terms of models of the molecular reorientation process.[58] $\langle\boldsymbol{\mu}(0)\cdot\boldsymbol{\mu}(t)\rangle$'s memory function, $K_D(t)$, is defined by

$$-\frac{d\langle\boldsymbol{\mu}(0)\cdot\boldsymbol{\mu}(t)\rangle}{dt} = \int_0^t K_D(t')\langle\boldsymbol{\mu}(0)\cdot\boldsymbol{\mu}(t-t')\rangle dt' \tag{210}$$

Note: $K_\psi(t)$, $K_D(t)$, and $K_J(t)$ are defined formally in terms of projection operators by appropriate modifications of Eq. (99).

These three autocorrelation and memory functions have one thing in common: They all depend on the average interaction of a molecule with its

surroundings. This dependence can easily be seen in the moment expansions of each of these functions. For short times we have (see Eqs. 168 and 169):

$$\psi(t) = 1 - \frac{t^2}{2}\frac{\langle F^2\rangle}{\langle P^2\rangle} + \frac{t^4}{4!}\frac{\langle \dot{F}^2\rangle}{\langle P^2\rangle} + \cdots \tag{211}$$

$$K_\psi(t) = \frac{\langle F^2\rangle}{\langle P^2\rangle} + \frac{t^2}{2}\left[\left[\frac{\langle F^2\rangle}{\langle P^2\rangle}\right]^2 - \frac{\langle \dot{F}^2\rangle}{\langle P^2\rangle}\right] + \cdots \tag{212}$$

$$A_J(t) = 1 - \frac{t^2}{2}\frac{\langle N^2\rangle}{\langle J^2\rangle} + \frac{t^4}{4!}\frac{\langle \dot{N}^2\rangle}{\langle J^2\rangle} + \cdots \tag{213}$$

$$K_J(t) = \frac{\langle N^2\rangle}{J^2} + \frac{t^2}{2}\left[\left[\frac{\langle N^2\rangle}{\langle J^2\rangle}\right]^2 - \frac{\langle \dot{N}^2\rangle}{\langle J^2\rangle}\right] + \cdots \tag{214}$$

$$\langle \mu(0)\cdot\mu(t)\rangle = 1 - \frac{t^2\langle J^2\rangle}{2I^2} + \frac{t^4}{4!}\left[\frac{\langle J^4\rangle}{I^4} + \frac{\langle N^2\rangle}{I^2}\right] + \cdots \tag{215}$$

$$K_D(t) = \frac{\langle J^2\rangle}{\langle I^2\rangle} - \frac{t^2}{2}\left[\frac{\langle J^2\rangle^2}{I^4} + \frac{\langle N^2\rangle}{I^2}\right] + \cdots \tag{216}$$

where $\langle F^2\rangle$ and $\langle N^2\rangle$ are the mean square force and torque on a molecule. $\langle \dot{F}^2\rangle$ and $\langle \dot{N}^2\rangle$ are the mean square first time derivatives of the force and torque. $\langle P^2\rangle$, $\langle J^2\rangle$, and $\langle J^4\rangle$ are quantities that are independent of any molecular interactions. In particular for a linear molecule.

$$\langle P^2\rangle = 3MKT \tag{217}$$

$$\langle J^2\rangle = 2IKT \tag{218}$$

$$\langle J^4\rangle = 8(IKT)^2 \tag{219}$$

$$= 2\langle J^2\rangle^2 \tag{220}$$

This latter expression has been used to simplify $K_D(t)$. Note that the time dependences of the linear and angular momentum autocorrelation functions depend only on interactions between a molecule and its surroundings. In the absence of torques and forces these functions are unity for all time and their memories are zero. There is some justification then for viewing these particular memory functions as representing a molecule's temporal memory of its interactions. However, in the case of the dipolar correlation function, this interpretation is not so readily apparent. That is, both the dipolar autocorrelation function and its memory will decay in the absence of external torques. This decay is only due to the fact that there is a distribution of rotational frequencies, ω, for each molecule in the gas phase. In

particular we have for a gas of rigid rotors

$$\omega^2 = \left[\frac{J}{I}\right]^2 \tag{221}$$

$$P(J)\,dJ = \frac{1}{IKT} e^{(-J^2/2IKT)}\, J\,dJ \tag{222}$$

where $P(J)\,dJ$ is the probability distribution for the magnitude of the angular momentum. Therefore for a gas of non-interacting rigid rotors the dipolar autocorrelation function is given by

$$\langle \boldsymbol{\mu}(0) \cdot \boldsymbol{\mu}(t) \rangle_G = \int_0^\infty \cos\left(\frac{J}{I} t\right) P(J)\,dJ \tag{223}$$

The decay of this function as well as the results of the Stockmayer simulation of carbon monoxide are presented in Figure 6. Note that the gas phase

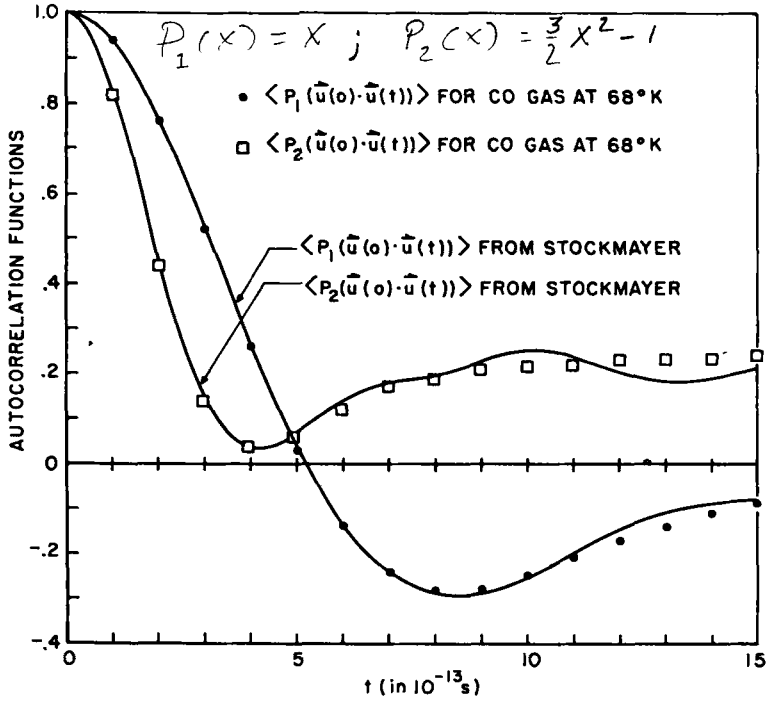

Fig. 6. The autocorrelation functions $\langle P_1(\mu(0)\cdot\mu(t))\rangle$ and $\langle P_2(\mu(0)\cdot\mu(t))\rangle$ for CO in the gas phase and in the liquid using the Stockmayer potential.

and Stockmayer results are practically identical—which again indicates that this potential with the small dipole moment of CO is of little importance in rotational relaxation. Note further that for the dipolar correlation function:

(*a*) The coefficient of the t^2 term, KT/I, depends only on the temperature and a molecule's moment of inertia. Therefore the dipolar correlation functions from each of the four simulations should have the same initial curvature.

(*b*) Molecular interactions enter in the t^4 term which is positive. Therefore, interactions will delay the decay of the gas phase function.

These points are all illustrated in Figures 6, 7, and 8. That is, the dipolar correlation functions all have the same initial curvature, and the functions from simulations using strongly angular dependent potentials decay more slowly than the gas phase function. The memory functions for the Stockmayer and modified Stockmayer simulations are presented in Figure 19; the angular momentum autocorrelation function from this latter simulation is also shown. The memory for the gas phase or Stockmayer dipolar function decays monotonically and is positive for $0 \leq t \leq 10^{-12}$ s. On the other hand, the modified Stockmayer memory decays in an entirely different fashion. It goes negative in $\sim 2 \times 10^{-13}$ s and is approximately equal to the angular momentum autocorrelation function for this simulation. This is a very important observation because it presents the possibility of obtaining approximate angular momentum correlation functions from infrared bandshape studies. Looking closer at Eq. (211) we see that

$$K_D(t)/K_D(0) = 1 - \frac{t^2}{2}\left(\frac{\langle J^2\rangle}{\langle I^2\rangle} + \frac{\langle N^2\rangle}{\langle J^2\rangle}\right) + \cdots \tag{224}$$

This function's decay will be dominated initially at least by molecular interactions provided $(\langle N^2\rangle I^2/\langle J^2\rangle^2) < 1$. This is actually not a difficult condition to satisfy. In the modified Stockmayer simulation this ratio is ~ 9.8 and experimentally this ratio is ~ 4.5 for liquid carbon monoxide at 78°K.[59] There are probably other physical systems for which this ratio is much larger. In the event that this criteria is satisfied $K_D(t)/K_D(0) \sim A_J(t)$ to terms in t^2 at least. In the case of the modified Stockmayer simulation we have just seen that this approximation is actually valid throughout the interesting negative region of $A_J(t)$. Hopefully, this approximation will also be valid in real systems, and the interesting negative region of $A_J(t)$ can be verified experimentally from infrared bandshape studies.

For completeness consider also the correlation function $\langle P_2(\boldsymbol{\mu}(0) \cdot \boldsymbol{\mu}(t))\rangle$

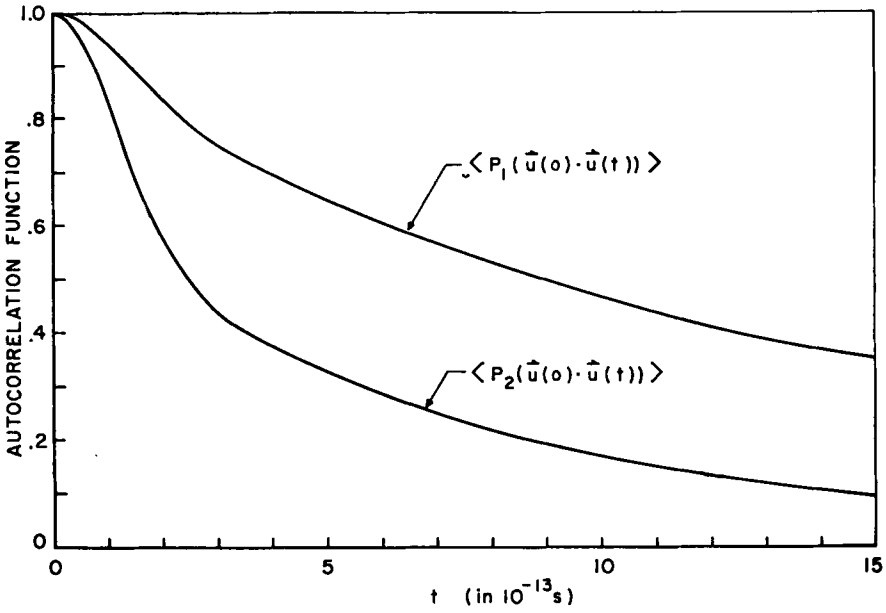

Fig. 7. The autocorrelation function $\langle P_1(\mu(0)\cdot\mu(t))\rangle$ and $\langle P_2(\mu(0)\cdot\mu(t))\rangle$ for CO from the modified Stockmayer simulation.

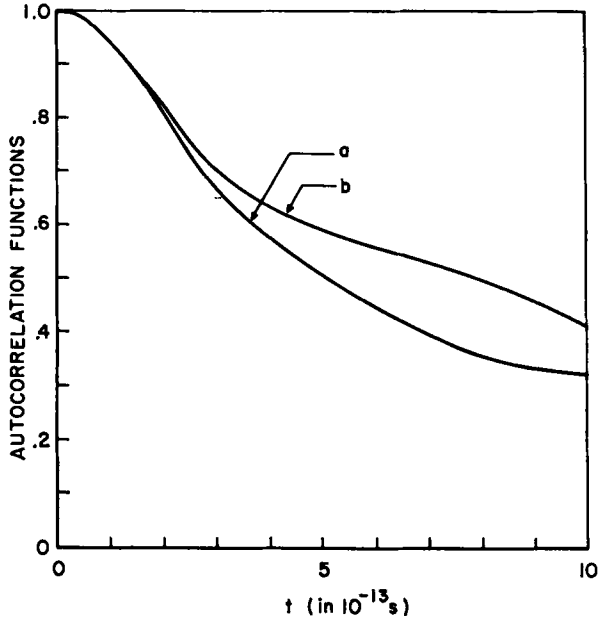

Fig. 8. The autocorrelation function $\langle P_1(\mu(0)\cdot\mu(t))\rangle$ from (*a*) the Stockmayer simulation of CO with a dipole moment of 1.172 Debye, and (*b*) the Lennard-Jones plus quadrupole-quadrupole simulation of N_2.

which can also be obtained from the Fourier inversion of rotation-vibration Raman bandshapes.[15] The short-time expansion of this function is[60]

$$\langle P_2(\boldsymbol{\mu}(0)\cdot\boldsymbol{\mu}(t))\rangle = 1 - \frac{3t^2}{2}\frac{\langle J^2\rangle}{I^2} + \left(\frac{\langle J^4\rangle}{2I^4} + \frac{\langle N^2\rangle}{8I^2}\right)t^4 + \cdots \quad (225)$$

From Eq. (225) it is seen that this function will: (*a*) have a time dependence in the absence of interactions, (*b*) initially decay faster than $\langle \boldsymbol{\mu}(0)\cdot\boldsymbol{\mu}(t)\rangle$, and (*c*) decay slower in the presence of interactions than in their absence. The behavior of this function in the gas phase is given by

$$\langle P_2(\boldsymbol{\mu}(0)\cdot\boldsymbol{\mu}(t))\rangle_G = \frac{3}{4}\int_0^\infty \cos\left(\frac{2Jt}{I}\right)P(J)\,dJ + \frac{1}{4} \quad (226)$$

In the limit $t \to \infty$ this equation goes to 1/4 whereas in a system with interactions $\langle P_2(\boldsymbol{\mu}(0)\cdot\boldsymbol{\mu}(t))\rangle$ goes to zero in this limit. These characteristics are all illustrated in Figures 6 and 7 where the results from the Stockmayer and modified Stockmayer simulations and from a system of gas phase molecules (Eq. 226) are presented.

Before discussing other results it is informative to first consider some correlation and memory functions obtained from a few simple models of rotational and translational motion in liquids. One might expect a fluid molecule to behave in some respects like a Brownian particle. That is, its actual motion is very erratic due to the rapidly varying forces and torques that other molecules exert on it. To a first approximation its motion might then be governed by the Langevin equations for a Brownian particle:[61]

$$M\frac{d\mathbf{v}}{dt} + \zeta_T\mathbf{v} = \mathbf{F}(t) \quad (227)$$

$$\frac{d\mathbf{J}}{dt} + \zeta_R\mathbf{J} = \mathbf{N}(t) \quad (228)$$

where $\mathbf{F}(t)$ and $\mathbf{N}(t)$ are small stochastic forces and torques whose time averages are zero, and ζ_T and ζ_R are translational and rotational friction coefficients. This is an oversimplification of the actual motion of a molecule surrounded by other molecules of similar mass but nevertheless is an interesting situation to consider. The linear and angular momentum autocorrelation and memory functions obtained from the solutions to the Langevin are simply:

$$\psi(t) = e^{-\zeta_T t/M} \quad (229)$$

$$K_\psi(t) = \frac{\zeta_T}{M}\delta(t) \quad (230)$$

$$A_J(t) = e^{(-\zeta_R t)} \quad (231)$$

$$K_J(t) = \zeta_R\delta(t) \quad (232)$$

Debye[62] showed that for a Brownian particle whose molecular orientation changes through small erratic angular displacements, $\langle \boldsymbol{\mu}(0) \cdot \boldsymbol{\mu}(t) \rangle$ and $\langle P_2(\boldsymbol{\mu}(0) \cdot \boldsymbol{\mu}(t)) \rangle$ are also exponentials. In particular under these conditions these functions are given by

$$\langle \boldsymbol{\mu}(0) \cdot \boldsymbol{\mu}(t) \rangle = e^{-2D_R t} \tag{233}$$

$$K_D(t) = 2D_R \delta(t) \tag{234}$$

$$\langle P_2(\boldsymbol{\mu}(0) \cdot \boldsymbol{\mu}(t)) \rangle = e^{-6D_R t} \tag{235}$$

where D_R is the rotational diffusion coefficient. There are two points of interest here:

(1) All of the autocorrelation functions are exponentials and, as such, are always ≥ 0

(2) All of the memory functions are Dirac delta functions which implies that at any given time t a Brownian particle has no memory of interactions that occurred before t. That is, the decay of each of these autocorrelation functions proceeds through a series of uncorrelated events.

We have already seen that even in the case of strong intermolecular interactions neither $\langle \boldsymbol{\mu}(0) \cdot \boldsymbol{\mu}(t) \rangle$ nor $\langle P_2(\boldsymbol{\mu}(0) \cdot \boldsymbol{\mu}(t)) \rangle$ decay initially as exponentials. Gordon has been able to reproduce the decay of these latter functions in liquid CO and N_2 by allowing for large angular displacements between interactions.[58] However, Gordon's model incorrectly predicts the angular momentum autocorrelation function.

The phenomenological Langevin Eqs. (227) and (228) are only applicable to a very restricted class of physical processes. In particular, they are only valid when the stochastic forces and torques have infinitely short correlation times, i.e., their autocorrelation functions are proportional to Dirac delta functions. As was shown in the previous section, these restrictions can be removed by a suitable generalization of these Langevin equations. As we saw in the particular case of the velocity, the modified Langevin equation is

$$M \frac{d\mathbf{v}}{dt} = -M \int_0^t d\tau\, \gamma(\tau)\mathbf{V}(t-\tau)\tau + \mathbf{F}(t) \tag{236}$$

where $\gamma(t)$ is a time-dependent friction coefficient. Equation (125) shows that the friction coefficient is related to the random force by

$$\gamma(t) = \frac{\langle \mathbf{F}(0) \cdot \mathbf{F}(t) \rangle}{M^2 \langle v^2 \rangle} \tag{237}$$

This is the second fluctuation-dissipation theorem. It was shown that if $\gamma(t)$ is equal to $\zeta_T \delta(t)/M$, one recovers the original Langevin equation for v.

It was also shown that the generalized Langevin equation is an exact equation of motion for v provided $\gamma(t)$ is the exact memory function, $K_\psi(t)$.[35,42]

Mori[43] pointed out that the random force, $\mathbf{F}(t)$, is not the actual force that acts on a molecule except at $t = 0$. That is, the evolution of the random force is governed by a different equation of motion than that which determines the evolution of the actual force on a molecule. The major point of interest here is that the approximations for the velocity and angular momentum autocorrelation functions which are based on postulating various memory functions are equivalent to assuming generalized Langevin equations of motion for the velocity and angular momentum. Therefore, from that viewpoint the memory functions $K_\psi(t)$ and $K_J(t)$ might be interpreted as being proportional to the autocorrelation functions of the random forces and torques acting on a molecule.

At the other extreme we might expect a fluid to have some characteristic of a simple Einstein solid, i.e., a collection of independent oscillators each oscillating at the same frequency ω_1. The linear momentum correlation function and its memory would then simply be

$$\psi(t) = \cos \omega_1 t \tag{238}$$

$$K_\psi(t) = \omega_1^2 \tag{239}$$

In this particular instance the memory is a constant, that is, the molecule "remembers" all of its past interactions. We might expect that the actual motion of a fluid particle will have both a diffusive or Brownian character and a solid or vibratory nature. If this were true, then the linear momentum autocorrelation function should decay in damped oscillatory fashion. This is indeed the case. All of these studies show clearly that there is an interval of time for which the velocity or linear momentum autocorrelation function is negative. See for example Figures 9 and 10. This negative region indicates that, on the average, a displacement of a molecule toward its nearest neighbors is followed by a displacement back toward its initial position. This behavior is also displayed in Rahman's results for liquid argon[32] and in Alder's results for systems of hard spheres at high density.[63] This similar behavior is interesting since neither Rahman's nor Alder's systems have internal degrees while these systems do.

All of these studies likewise show clearly that in liquids with potentials that have a strong noncentral character there is an interval of time for which the angular momentum correlation function is negative (see Figures 12 and 13) whereas in liquids for which the pair potential has a small noncentral character this function remains positive and changes very little over the

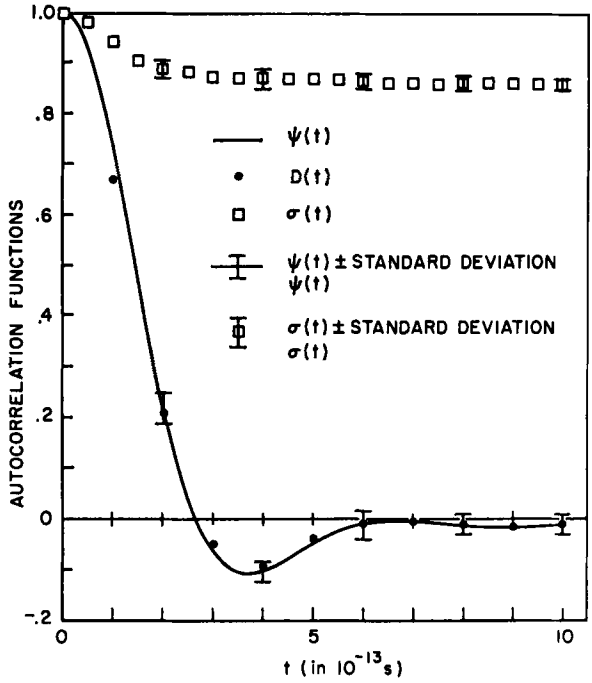

Fig. 9. Velocity autocorrelation functions from the Stockmayer simulation of CO.

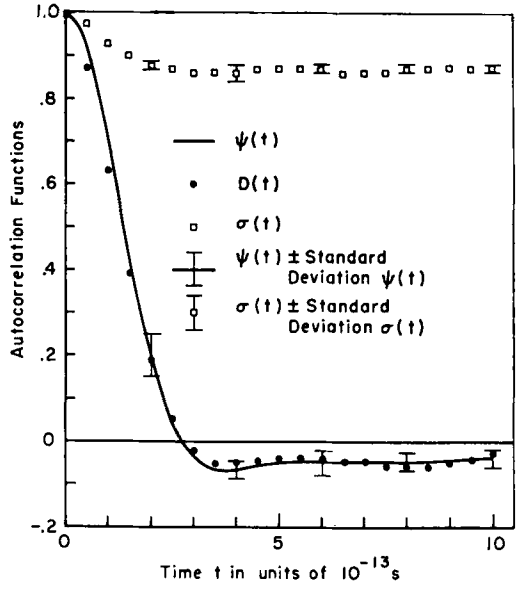

Fig. 10. Velocity autocorrelation functions from the modified Stockmayer simulation of CO.

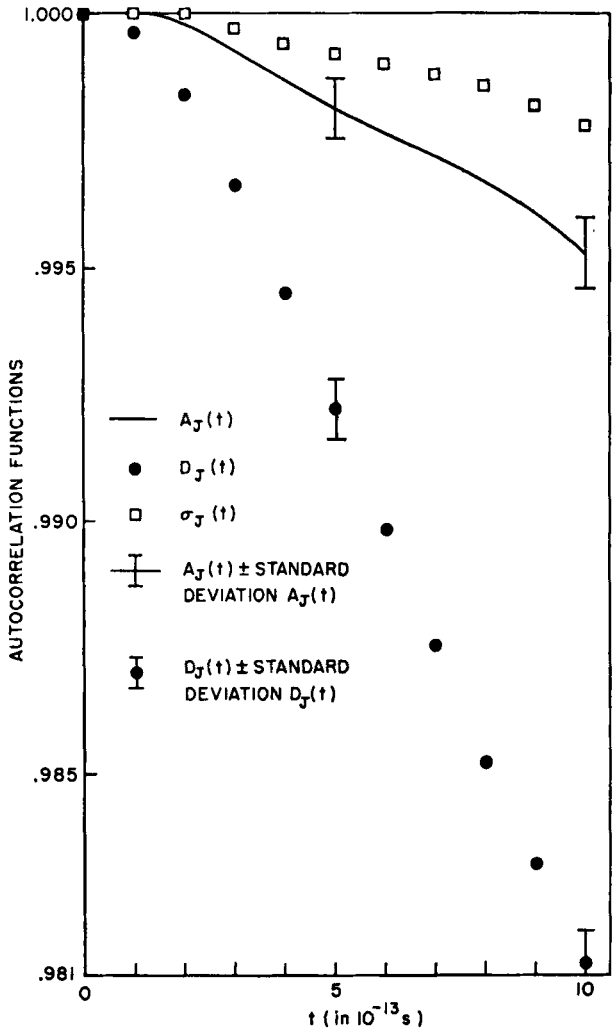

Fig. 11. Angular momentum autocorrelation functions from the Stockmayer simulation of CO.

observed time interval (see Figure 11). The negative region indicates that on the average a molecule suffers a sufficiently strong collision with the cage of its nearest neighbors that the torque acting on it is large enough to reverse the direction of its angular momentum.

Because these autocorrelation functions go negative, the events leading to the decay of these functions are not uncorrelated. In other words, a

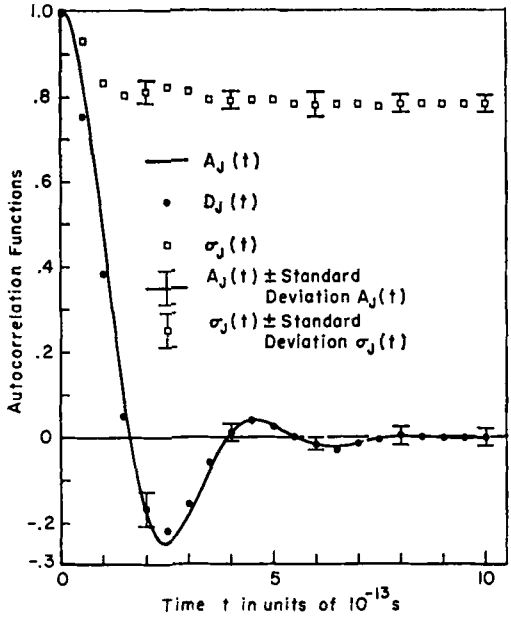

Fig. 12. Angular momentum autocorrelation functions from the modified Stockmayer simulation of CO.

molecule must retain some memory of its interactions for a finite time period. This behavior is illustrated in the memory functions for the linear and angular momentum autocorrelation functions for the modified Stockmayer simulation, Figures 27 and 32, and for the linear momentum autocorrelation function for the Stockmayer simulation, Figure 9. Note that each of the memories discussed here was calculated using the numerical method outlined in Appendix B. All of these memories quickly decay (in an approximately Gaussian fashion) almost to zero in the time interval $0 \leq t \leq 3 \times 10^{-13}$ s and they all have small positive tails for $t \gtrsim 3 \times 10^{-13}$ s which display much slower time dependences. 3×10^{-13} s is approximately the average time that it would take a molecule to travel from the center of its cage of nearest neighbors to the "cage wall."

Both $\psi(t)$ and $A_J(t)$ depend on changes in both the direction and magnitude of the linear and angular moments. Therefore, it is important to determine which of these changes contributes the most to the overall time dependence of $\psi(t)$ and $A_J(t)$. In order to investigate this problem we have also computed the normalized linear and angular speed autocorrelation functions, $\sigma(t)$ and $\sigma_J(t)$:

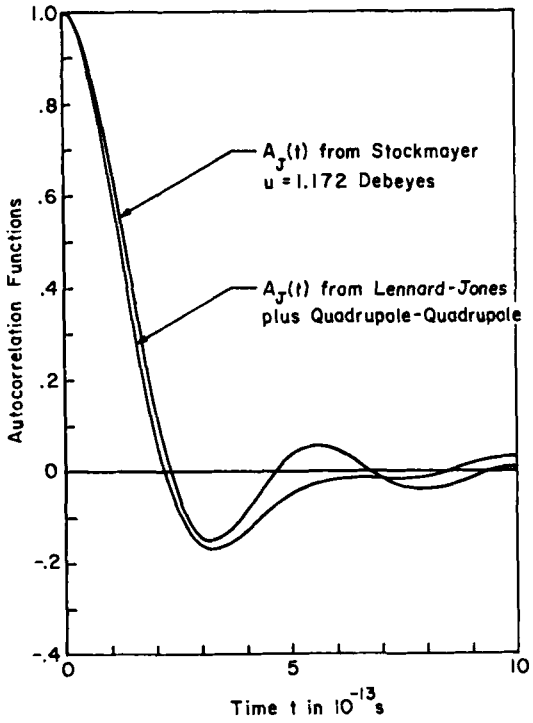

Fig. 13. Angular momentum autocorrelation functions from (*a*) the Stockmayer simulation of CO with a dipole moment of 1.172 Debye, and (*b*) the Lennard-Jones plus quadrupole-quadrupole simulation of N_2.

$$\sigma(t) = \frac{\langle |\mathbf{P}(0)|\,|\mathbf{P}(t)| \rangle}{\langle P^2 \rangle} \tag{240}$$

$$\sigma_J(t) = \frac{\langle |\mathbf{J}(0)|\,|\mathbf{J}(t)| \rangle}{\langle J^2 \rangle} \tag{241}$$

together with the corresponding directional correlation functions, $D(t)$ and $D_J(t)$:

$$D(t) = \langle \mathbf{e}(0) \cdot \mathbf{e}(t) \rangle \tag{242}$$

$$D_J(t) = \langle \mathbf{e}_J(0) \cdot \mathbf{e}_J(t) \rangle \tag{243}$$

where $|\mathbf{P}(t)|$, $|\mathbf{J}(t)|$, $\mathbf{e}(t)$, and $\mathbf{e}_J(t)$ are respectively the magnitude of the linear and angular moments and unit vectors in the direction of the linear and angular momenta.

These functions are all normalized such that they are initially unity. Their long-time limits are

$$\lim_{t\to\infty} \psi(t) = \frac{\langle \mathbf{P}\rangle \cdot \langle \mathbf{P}\rangle}{\langle P^2\rangle} = 0 \tag{244}$$

$$\lim_{t\to\infty} \sigma(t) = \frac{\langle |\mathbf{P}|\rangle^2}{\langle P^2\rangle} = \frac{8}{3\pi} \tag{245}$$

$$\lim_{t\to\infty} D(t) = \langle \mathbf{e}\rangle \cdot \langle \mathbf{e}\rangle = 0 \tag{246}$$

$$\lim_{t\to\infty} A_J(t) = \frac{\langle \mathbf{J}\rangle \cdot \langle \mathbf{J}\rangle}{\langle J^2\rangle} = 0 \tag{247}$$

$$\lim_{t\to\infty} \sigma_J(t) = \frac{\langle |\mathbf{J}|\rangle^2}{\langle J^2\rangle} = \frac{\pi}{4} \tag{248}$$

$$\lim_{t\to\infty} D_J(t) = \langle e_J\rangle \cdot \langle e_J\rangle = 0 \tag{249}$$

As mentioned previously the above relations follow from the fact that at long times the value of the random variable in each correlation function becomes statistically independent of its initial value—provided of course interactions are present.

Figures 9 and 10 correspond to $\psi(t)$, $\sigma(t)$, and $D(t)$ determined from the Stockmayer and modified Stockmayer simulation of carbon monoxide. Figures 11 and 12 represent $A_J(t)$, $\sigma_J(t)$, and $D_J(t)$ for the same two potentials. The behavior of $A_J(t)$, $\sigma_J(t)$, $D_J(t)$, $\psi(t)$, $\sigma(t)$, and $D(t)$ for the other two simulations considered are similar to the results from the modified Stockmayer simulation. Therefore, only the $A_J(t)$'s for these latter two simulations are presented in Figure 13.

Note that for the weak noncentral Stockmayer potential $A_J(t)$ changes very little and is positive during the time it is observed, while for the stronger noncentral potentials there are regions in which $A_J(t)$ is negative.

Note further in the Stockmayer and modified Stockmayer simulations how closely $D(t)$ resembles $\psi(t)$. $\sigma(t)$ varies between its initial value of unity and its long-time value of $8/3\pi$, and therefore, because of only a 13% change over the whole time axis, contributes very little to the overall time dependence of $\psi(t)$. Note also in the modified Stockmayer simulation how closely $D_J(t)$ resembles $A_J(t)$. $\sigma_J(t)$ varies between 1 and its long-time value of $\pi/4$ and therefore, because of only a 21% change over the whole time axis, contributes very little to the overall time dependence of $A_J(t)$. $D(t)$ is an excellent approximation to $\psi(t)$ in each of these simulations. In a sense,

these results can be construed as an argument for a constant linear and angular speed approximation in calculating linear and angular momentum autocorrelation functions.

A. Approximate Distribution Functions

It would be very convenient to know whether or not the linear and angular momenta can be accurately represented by stationary Gaussian random variables. If they are, then the probability of finding a molecule at time t with a velocity $\mathbf{V}$, given that it was moving with a velocity $\mathbf{V}_0$ at the initial $t = 0$, is the Gaussian transition probability

$$P_v(\mathbf{v}, t \mid \mathbf{v}_0, 0) = \left[\frac{M}{2\pi KT(1 - \psi^2(t))}\right]^{3/2} \exp - \left[\frac{M(\mathbf{v} - \mathbf{v}_0 \psi(t))^2}{2KT(1 - \psi^2(t))}\right] \quad (250)$$

The corresponding transition probability for the angular momentum is similarly given by

$$P_J(\mathbf{J}, t \mid \mathbf{J}_0, 0) = \frac{1}{2\pi IKT(1 - A_J^2(t))} \exp - \left[\frac{(\mathbf{J} - \mathbf{J}_0 A_J(t))^2}{2IKT(1 - A_J^2(t))}\right] \quad (251)$$

If these relations were true, then one could compute any autocorrelation function involving a higher power of $\mathbf{V}$ or $\mathbf{J}$ by just knowing $\psi(t)$ or $A_J(t)$. For example, the normalized translation kinetic energy autocorrelation function $\varepsilon_2(t)$, where

$$\varepsilon_2(t) = \frac{\langle v^2(0)v^2(t)\rangle}{\langle v^4\rangle} \quad (252)$$

can be determined in terms of $\psi(t)$ from the Gaussian transition probability to be

$$\varepsilon_{2G}(t) = \left(\frac{M}{2\pi KT}\right)^{3/2} \int d^3v \int d^3v_0 \mathbf{v} \cdot \mathbf{v}\mathbf{v}_0 \cdot \mathbf{v}_0 P_v(\mathbf{v}, t \mid \mathbf{v}_0, 0)\, e^{-Mv_0^2/2KT} \quad (253)$$

$$= \tfrac{3}{5}[1 + \tfrac{2}{3}\psi^2(t)] \quad (254)$$

The subscript G indicates that this is an approximate and an as yet unverified result based on the Gaussian approximation. Similarly, the normalized rotational kinetic energy autocorrelation function $\varepsilon_2{}^J(t)$, where

$$\varepsilon_2{}^J(t) = \frac{\langle J^2(0)J^2(t)\rangle}{\langle J^4\rangle} \quad (255)$$

can be determined in terms of $A_J(t)$ from the Gaussian transition probability to be

$$\varepsilon_{2G}{}^{J}(t) = \frac{1}{2\pi IKT} \int dJ^2 \int dJ_0{}^2 \mathbf{J} \cdot \mathbf{J}\mathbf{J}_0 \cdot \mathbf{J}_0 P_J(\mathbf{J}, t \mid \mathbf{J}_0, 0)\, e^{-J_0{}^2/2IKT} \tag{256}$$

$$= \tfrac{1}{2}[1 + A_J{}^2(t)] \tag{257}$$

In like manner, the fourth-order correlation functions $\varepsilon_4(t)$ and $\varepsilon_4{}^J(t)$ and the eighth-order correlation function $\varepsilon_8(t)$, which are defined as

$$\varepsilon_4(t) = \frac{\langle V^4(0)V^4(t)\rangle}{\langle V^8\rangle} \tag{258}$$

$$\varepsilon_4{}^J(t) = \frac{\langle J^4(0)J^4(t)\rangle}{\langle J^8\rangle} \tag{259}$$

$$\varepsilon_8(t) = \frac{\langle V^8(0)V^8(t)\rangle}{\langle V^{16}\rangle} \tag{260}$$

can be determined in terms of $\psi(t)$ and $A_J(t)$, from the Gaussian transition probabilities to be

$$\varepsilon_{4G}(t) = \left[\frac{225}{945} + \frac{600\psi^2(t)}{945} + \frac{120\psi^4(t)}{945}\right] \tag{261}$$

$$\varepsilon_J{}^{4G}(t) = \left[\frac{64}{384} + \frac{256A_J{}^2(t)}{384} + \frac{64A_J{}^4(t)}{384}\right] \tag{262}$$

$$\varepsilon_{8G} = \frac{[945 + 10{,}080\psi^2(t) + 18{,}144\psi^4(t) + 6{,}912\psi^6(t) + 384\psi^8(t)]}{36{,}465} \tag{263}$$

These higher-order correlation functions play a large role in determining many physical properties of polyatomic systems. For example, the vibrational relaxation can, in some cases, be expressed in terms of the rotational kinetic energy autocorrelation function.[28]

At this time the only "experimental" method available for determining to what extent the Gaussian approximation is realistic is molecular dynamics studies of polyatomic liquids such as the ones we have been discussing. We have therefore tested this approximation by

(1) Computing $\varepsilon_2(t)$, $\varepsilon_4(t)$, $\varepsilon_8(t)$, $\varepsilon_2{}^J(t)$, and $\varepsilon_4{}^J(t)$ from the modified Stockmayer simulation.

(2) Evaluating $\varepsilon_{2G}(t)$, $\varepsilon_{4G}(t)$, $\varepsilon_{8G}(t)$, $\varepsilon_{2J}(t)$, and $\varepsilon_{4J}(t)$ using the previous formulas and $\psi(t)$ and $A_J(t)$ from this simulation.

The results of these computations are presented in Figures 14, 15, 16, 17, and 18. These first few calculated moments indicate that the Gaussian transition probabilities for the linear and angular momentum may represent the dynamics fairly well, However, it may not yet be concluded that the Gaussian approximation is actually correct, since this same test must

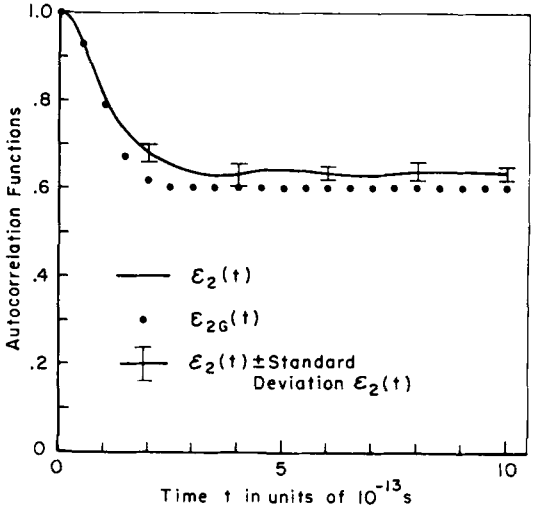

Fig. 14. The autocorrelation function $\varepsilon_2(t)$ from the modified Stockmayer simulation of CO and the autocorrelation function $\varepsilon_{2G}(t)$ from the Gaussian approximation.

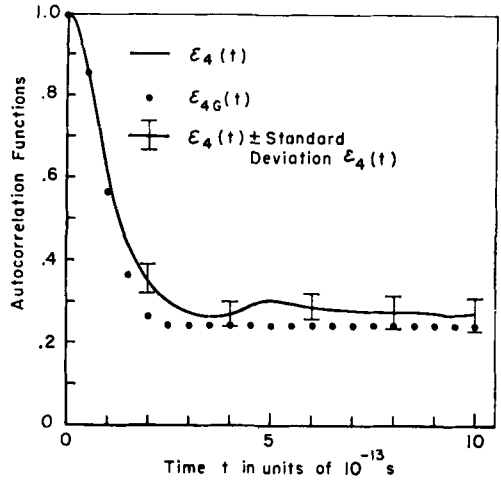

Fig. 15. The autocorrelation function $\varepsilon_4(t)$ from the modified Stockmayer simulation of CO and the autocorrelation function $\varepsilon_{4G}(t)$ from the Gaussian approximation.

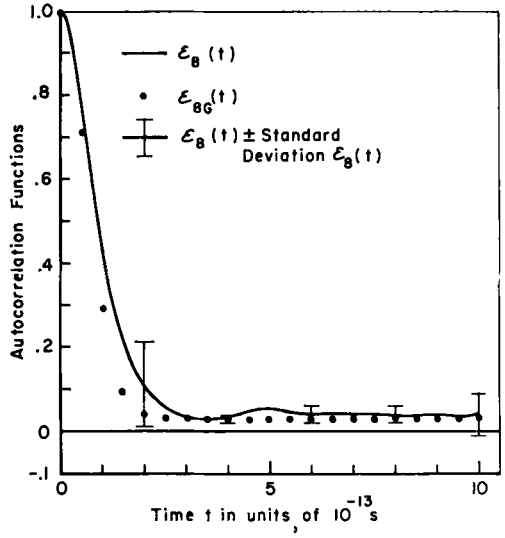

Fig. 16. The autocorrelation function $\varepsilon_8(t)$ from the modified Stockmayer simulation of CO and the autocorrelation $\varepsilon_{8G}(t)$ from the Gaussian approximation.

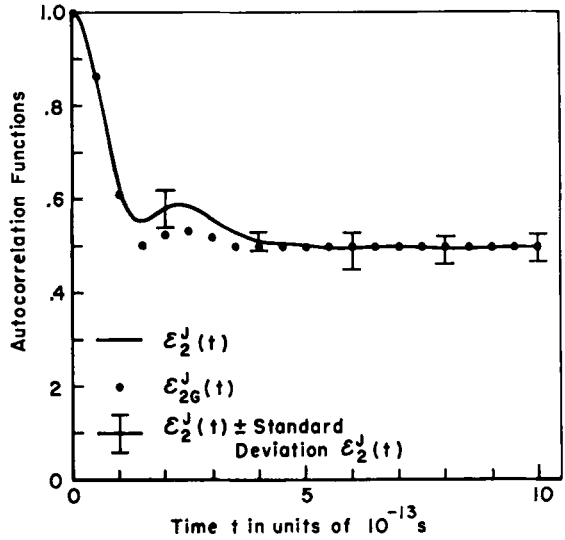

Fig. 17. The autocorrelation function $\varepsilon_2{}^J(t)$ from the modified Stockmayer simulation of CO and the autocorrelation function $\varepsilon_{2G}{}^J(t)$ from the Gaussian approximation.

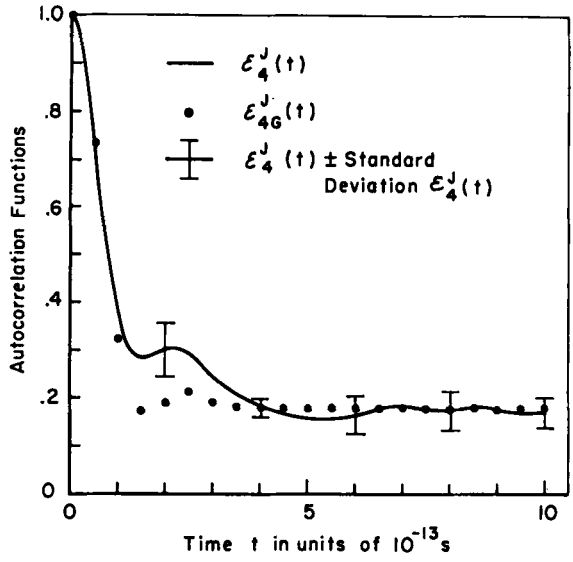

Fig. 18. The autocorrelation function $\varepsilon_4{}^J(t)$ from the modified Stockmayer simulation of CO and the autocorrelation function $\varepsilon_{4G}{}^J(t)$ from the Gaussian approximation.

be made on the corresponding higher moments, i.e., $\varepsilon_{12}(t)$, $\varepsilon_{12}{}^J(t)$, ..., etc. If the linear and angular momentum were truly Gaussian random processes, then they are not Markovian. This follows from the facts that $\psi(t)$ and $A_J(t)$ are not exponential with time—Figures 10 and 12—and from Doob's theorem[64] (according to which a stationary Gaussian process is Markovian if and only if the autocorrelation function for the process is exponential in time).

In the preceding we were very successful in predicting autocorrelation functions of powers of V and J from $\psi(t)$, $A_J(t)$, and the assumptions of Gaussian transition probabilities for V and J. It would be very convenient if we could similarly predict $\langle P_2(\boldsymbol{\mu}(0) \cdot \boldsymbol{\mu}(t))\rangle$, ..., $\langle P_N(\boldsymbol{\mu}(0) \cdot \boldsymbol{\mu}(t))\rangle$ from $\langle \boldsymbol{\mu}(0) \cdot \boldsymbol{\mu}(t)\rangle$. If we could, then we would be able to at least predict Raman band shapes from infrared band shapes. In order to make these predictions, we have to guess the distribution of $\boldsymbol{\mu}(0) \cdot \boldsymbol{\mu}(t)$ from one or more of its known moments. In the following we shall make this guess by maximizing the information entropy[65] of this distribution subject to the constraint that it yields the correct value of $\langle \boldsymbol{\mu}(0) \cdot \boldsymbol{\mu}(t)\rangle$.

First suppose that a spherical surface of unit radius is drawn and the center of this sphere is taken as the origin of a spherical polar coordinate system. Suppose further that $\boldsymbol{\mu}(0)$, the initial orientation of a diatomic molecule, is represented by the unit vector, $\mathbf{k}$, along the positive Z axis of

this system. As time progresses μ will move about on the surface of this sphere and at any particular instant of time t its orientation will be uniquely specified by its polar and azimuthal angles θ and ϕ. The actual path that μ traces out on the surface will, in general, be very complicated due to the continual interaction of the diatomic molecule with its neighbors. Let $P(\theta, \phi, t)\, d\Omega$ be the probability at time t that μ is oriented in the direction of the solid angle $d\Omega$. After a time t which is long compared to the orientational relaxation time, $P(\theta, \phi, t)$ will be independent of its initial value and will tend toward the uniform distribution, i.e.,

$$\lim_{t \to \infty} P(\theta, \phi, t)\, d\Omega = \frac{d\Omega}{4\pi} \tag{264}$$

$\langle \mu(0) \cdot \mu(t) \rangle$ and $\langle P_2(\mu(0) \cdot \mu(t)) \rangle$ can be computed provided $P(\theta, \phi, t)$ is known since

$$\langle \mu(0) \cdot \mu(t) \rangle = \int_0^{2\pi} d\phi \int_0^{\pi} d\theta \sin\theta \cos\theta\, P(\theta, \phi, t) \tag{265}$$

$$\langle P_2(\mu(0) \cdot \mu(t)) \rangle = \frac{1}{2} \int_0^{2\pi} d\phi \int_0^{\pi} d\theta \sin\theta\, [3\cos^2\theta - 1] P(\theta, \phi, t) \tag{266}$$

Likewise all higher-order correlation functions, $\langle P_N(\mu(0) \cdot (t)) \rangle$ can also be computed.

We now assume that $\langle \mu(0) \cdot \mu(t) \rangle$ is known and we want to guess the probability distribution P. We do this by maximizing the information entropy,[65] S_I, of this distribution

$$S_I(P(\theta, \phi, t)) = -\int d\Omega P(\theta, \phi, t) \ln P(\theta, \phi, t) \tag{267}$$

subject to the constraints

$$P(\theta, \phi, t) \geqslant 0 \tag{268}$$

$$\int d\Omega P(\theta, \phi, t) = 1 \tag{269}$$

$$\int d\Omega P(\theta, \phi, t) \cos\theta = \langle \mu(0) \cdot \mu(t) \rangle \tag{270}$$

where Eqs. (268) and (269) are the conditions that P be a probability distribution and Eq. (270) the condition that P gives the right dipolar correlation function, $\langle \mu(0) \cdot \mu(t) \rangle$.

Introducing Eqs. (269) and (270) into the problem via Lagrange multipliers α and β gives

$$\delta[\int d\Omega [P \ln P - (\alpha + 1)P - \beta \cos\theta\, P]] = 0 \tag{271}$$

$$\int d\Omega [\ln P - \alpha - \beta \cos\theta] \delta P = 0 \tag{272}$$

or

$$P(\theta, \phi, t) = e^{\alpha + \beta \cos \theta} \tag{273}$$

This distribution automatically satisfies the positivity condition, Eq. (268). The Lagrange multipliers α and β are determined from the constraints shown by Eqs. (269) and (270). From Eq. (269) we see that

$$\int d\Omega e^{\alpha + \beta \cos \theta} = 2\pi e^{\alpha} \left[\frac{e^{\beta} - e^{-\beta}}{\beta}\right] = 1 \tag{274}$$

or

$$2\pi e^{\alpha} = \frac{\beta}{e^{\beta} - e^{-\beta}} \tag{275}$$

From Eq. (270) we see that

$$\langle \boldsymbol{\mu}(0) \cdot \boldsymbol{\mu}(t) \rangle = \int d\Omega e^{\alpha + \beta \cos \theta} \cos \theta = 2\pi e^{\alpha} \left[- \frac{(e^{\beta} - e^{-\beta})}{\beta^2} + \frac{(e^{\beta} + e^{-\beta})}{\beta} \right] \tag{276}$$

or

$$\langle \boldsymbol{\mu}(0) \cdot \boldsymbol{\mu}(t) \rangle = \left[- \frac{1}{\beta} + \coth \beta \right] \tag{277}$$

$\beta(t)$ can be determined from $\langle \boldsymbol{\mu}(0) \cdot \boldsymbol{\mu}(t) \rangle$ by inverting Eq. (277) either graphically or numerically.

The higher correlation functions such as $\langle P_2(\boldsymbol{\mu}(0) \cdot \boldsymbol{\mu}(t)) \rangle$ can now be found in terms of $\beta(t)$ and thereby in terms of $\langle \boldsymbol{\mu}(0) \cdot \boldsymbol{\mu}(t) \rangle$. For example

$$\langle P_2(\boldsymbol{\mu}(0) \cdot \boldsymbol{\mu}(t)) \rangle = \tfrac{1}{2} \int d\Omega e^{\alpha + \beta \cos \theta} [3 \cos^2 \theta - 1] \tag{278}$$

$$= 1 + \frac{3}{\beta(t)} \left[\frac{1}{\beta(t)} - \coth [\beta(t)] \right] \tag{279}$$

Maximizing the information entropy of a distribution gives in some sense the "smoothest" distribution consistent with our available information[65] on this distribution. We have tested the information theory prediction of $\langle P_2(\boldsymbol{\mu}(0) \cdot \boldsymbol{\mu}(t)) \rangle$ from $\langle \boldsymbol{\mu}(0) \cdot \boldsymbol{\mu}(t) \rangle$ for two different systems: the Stockmayer and modified Stockmayer simulations of CO. We have already seen that these two systems represent two extreme forms of molecular rotational motion. In the Stockmayer simulation the molecules rotate essentially freely whereas in the modified Stockmayer simulation there is evidence for strongly hindered rotational motion. $\langle \boldsymbol{\mu}(0) \cdot \boldsymbol{\mu}(t) \rangle$ from the

Stockmayer simulation is presented in Figure 6 and the experimental $\langle P_2(\boldsymbol{\mu}(0) \cdot \boldsymbol{\mu}(t))\rangle$ and its information theory prediction are presented in Figure 45. In this particular instance the information theory prediction agrees with experiment only for short times, i.e., $t \lesssim 4.5 \times 10^{-13}$ s. $\langle \boldsymbol{\mu}(0) \cdot \boldsymbol{\mu}(t)\rangle$ from the modified Stockmayer simulation is presented in Figure 7 and the experimental $\langle P_2(\boldsymbol{\mu}(0) \cdot \boldsymbol{\mu}(t))\rangle$ and its information theory prediction are presented in Figure 46. Note that in this example the information theory prediction is in excellent agreement with experiment for $t \leq 10^{-12}$ s. This is a significant result since in this particular instance the decay of $\langle P_2(\boldsymbol{\mu}(0) \cdot \boldsymbol{\mu}(t))\rangle$ is predominantly governed by intermolecular interactions and, hence, would be very difficult to calculate theoretically from first principles.

The information theory approach to calculating approximate probabilities is quite general and, as we have just shown, is quite straight forward to use. One might then ask why we did not use this approach in the previous section to predict $\varepsilon_2(t)$, $\varepsilon_4(t)$, ..., $\varepsilon_2{}^J(t)$, and $\varepsilon_4{}^J(t)$ from $\psi(t)$ and $A_J(t)$? The answer to this question is that we did. That is, information theory predicts Gaussian transition probabilities for V and J and these were the transition probabilities that we assumed. We shall now elaborate on this remark. Let $P(\mathbf{V}, t; \mathbf{V}_0, 0)$ be the joint probability that a molecule has a velocity $\mathbf{V}$ at time t and a velocity $\mathbf{V}_0$ at $t = 0$. then P is related to the transition probability P_V by

$$P(\mathbf{V}, t; \mathbf{V}_0, 0) = P_V(\mathbf{V}, t \mid \mathbf{V}_0, 0) f(\mathbf{V}_0) \tag{280}$$

where $f(\mathbf{V}_0)$ is the Maxwell distribution function, i.e., the probability distribution that a molecule has a velocity $\mathbf{V}_0$ at $t = 0$. The information entropy of P is defined by

$$S_I[P] = -\int dV^3 \int dV_0{}^3 P(\mathbf{V}, t; \mathbf{V}_0, 0) \ln P(\mathbf{V}, t; \mathbf{V}_0, 0) \tag{281}$$

$S_I[P]$ is to be maximized subject to the constraints.

$$\int dV^3 \int dV_0{}^3 P(\mathbf{V}, t; \mathbf{V}_0, 0) = 1 \tag{282}$$

$$\int dV^3 \int dV_0{}^3 \mathbf{V}_0 \cdot \mathbf{V}_0 P(\mathbf{V}, t; \mathbf{V}_0, 0) = \langle V^2 \rangle \tag{283}$$

$$\int dV^3 \int dV_0{}^3 \mathbf{V} \cdot \mathbf{V} P(\mathbf{V}, t; V_0, 0) = \langle V^2 \rangle \tag{284}$$

$$\int dV^3 \int dV_0{}^3 \mathbf{V} \cdot \mathbf{V}_0 P(\mathbf{V}, t; \mathbf{V}_0, 0) = \langle V^2 \rangle \psi(t) \tag{285}$$

Introducing the Lagrange multipliers α_1, α_2, α_3, and α_4 into the problem and proceeding as before, we find

$$P(\mathbf{V}, t; \mathbf{V}_0, 0) = \exp\left(-[\alpha_1 + \alpha_2 V_0{}^2 + \alpha_3 \mathbf{V} \cdot \mathbf{V}_0 + \alpha_4 V^2]\right) \tag{286}$$

Evaluating α_1, α_2, α_3, and α_4 from Eqs. (282), (283), (283), and (285), we find that the information theory approach to calculating P is equivalent to assuming a Gaussian transition probability for $\mathbf{V}$. Note that the approximate distribution functions we derived from information theory for $\boldsymbol{\mu}$, $\mathbf{V}$, and $\mathbf{J}$ were only required to give the correct autocorrelation functions $\langle \boldsymbol{\mu}(0) \cdot \boldsymbol{\mu}(t) \rangle$, $\psi(t)$, and $A_J(t)$, respectively. Hence, improved approximate distribution functions could be derived by requiring these new distributions to give the correct higher moments of $\boldsymbol{\mu}(0) \cdot \boldsymbol{\mu}(t)$, $\mathbf{V}$, and $\mathbf{J}$ as well as the fundamental autocorrelation functions.

VI. APPROXIMATIONS TO TIME-CORRELATION FUNCTIONS

A. A Simple Model for Linear and Angular Momentum Correlations

In the preceding sections it was shown that the normalized linear and angular momentum autocorrelation functions, $\Psi(t)$ and $A_J(t)$, are identical within experimental error with the corresponding directional autocorrelation functions,

$$D(t) = \langle \mathbf{e}(0) \cdot \mathbf{e}(t) \rangle$$

$$D_J(t) = \langle \mathbf{e}'(0) \cdot \mathbf{e}'(t) \rangle$$

where $\mathbf{e}(t) = \mathbf{v}(t)/|\mathbf{v}(t)|$ and $\mathbf{e}'(t) = \mathbf{J}(t)/|\mathbf{J}(t)|$ are unit vectors pointing in the direction of $\mathbf{v}(t)$ and $\mathbf{J}(t)$, respectively. It will be our purpose in this section to give a simple theory for these two correlation functions.

The time evolution and geometrical aspects of the directional autocorrelation function are given by the following considerations. Consider the time variation of $\mathbf{e}(t)$ (or $\mathbf{e}'(t)$) and of its projection $\mathbf{e}(0) \cdot \mathbf{e}(t)$ (or $\mathbf{e}'(0) \cdot \mathbf{e}'(t)$) on its original direction. In order to describe this motion we adopt the Rice-Allnatt model of simple liquids according to which a fluid molecule moves in the long-range weak-fluctuating force field of its many neighbors between strong repulsive binary collisions. The soft-fluctuating force field destroys correlations between successive binary collisions. It is this particular aspect of the model which makes it particularly amenable to mathematical analysis.

During the first diffusional step in which the molecule executes a kind of translational and rotational Brownian motion in the soft-fluctuating force field of its neighbors, its direction cosines are represented as

$$\mathbf{e}(0) \cdot \mathbf{e}(t)\big|_1 = F_1{}^T(t)$$

$$\mathbf{e}'(0) \cdot \mathbf{e}'(t)\big|_1 = F_1{}^R(t)$$

These functions must be unity at $t = 0$.

The first diffusional step is interrupted by a strongly repulsive collision which in general is of finite but very short duration. For simplicity it will be assumed that the collision is hard core and consequently of zero duration. The direction of the velocity and the angular momentum will suffer a discontinuous change. If the collision occurs at t_1, then immediately after the collision at t_1^+ the direction cosines will be given by spherical geometry as

$$\mathbf{e}(0) \cdot \mathbf{e}(t^+_1)\big|_{\text{coll}_1} = \cos \chi_1{}^T F_1{}^T(t_1) + \sin \alpha_1{}^T \sin \chi_1{}^T \sin\ [\text{arc } F_1{}^T(t_1)]$$

$$\mathbf{e}'(0) \cdot \mathbf{e}'(t^+_1)\big|_{\text{coll}_1} = \cos \chi_1{}^R F_1{}^R(t_1) + \sin \alpha_1{}^R \sin \chi_1{}^R[\sin \text{arc } F_1{}^R(t_1)]$$

where $\alpha_1{}^{T,R}$ is the dihedral angle between the two planes formed by the two pairs of unit vectors $[\mathbf{e}(0), \mathbf{e}(t^-_1)]$ and $[\mathbf{e}(t^-_1), \mathbf{e}(t^+_1)]$, where t^-_1 and t^+_1 are times immediately before and after the hard core collision. Cos χ^T gives the change in the direction of the unit vector $\mathbf{e}$ at the time t^+_1 caused by a strong collision which began at time t^-_1. $\alpha_1{}^R$ and $\chi_1{}^R$ have exactly the same meaning for the changes in the angular momentum.

In this model we assume that the set of all diffusional steps randomizes the angle α, so that $\langle \sin \alpha_1{}^R \rangle = \langle \sin \alpha_1{}^T \rangle = 0$, and

$$\mathbf{e}(0) \cdot \mathbf{e}(t_1)\big|_{\text{coll}_1} = \cos \chi_1{}^T F_1{}^T(t_1)$$

and

$$\mathbf{e}'(0) \cdot \mathbf{e}'(t_1)\big|_{\text{coll}_1} = \cos \chi_1{}^R F_1{}^R(t_1)$$

So far we have derived an expression for the direction cosines corresponding to a molecule which has followed one diffusional step for a time t_1 when it undergoes a hard-core collision. Suppose now that up to the time t the molecule does not suffer another collision. The direction cosine for a molecule in its second diffusional step is then, according to spherical geometry,

$$\mathbf{e}(0) \cdot \mathbf{e}(t)\big|_{(2)} = F_2{}^T(t - t_1) \cos \chi_1{}^T F_1{}^T(t_1)$$

$$\mathbf{e}'(0) \cdot \mathbf{e}'(t)\big|_{(2)} = F_2{}^R(t - t_1) \cos \chi_1{}^R F_1{}^R(t_1)$$

where again we use the fact that the dihedral angles are randomized. $F_2(t)$ represents the diffusional change of the direction cosines during the 2nd diffusional step.

The collision ending the first diffusional step could have occurred with equal probability at any time between 0 and t. Averaging $\mathbf{e}(0) \cdot \mathbf{e}(t)\big|_{(2)}$ and $\mathbf{e}'(0) \cdot \mathbf{e}'(t)\big|_{(2)}$ over the time of the first collision yields

$$(\mathbf{e}(0) \cdot \mathbf{e}(t))_{(2)} = t^{-1} \int_0^t dt_1\, F_2{}^T(t - t_1) F_1{}^T(t_1) \cos \chi_1{}^T$$

$$(\mathbf{e}'(0) \cdot \mathbf{e}'(t))_{(2)} = t^{-1} \int_0^t dt_1\, F_2{}^R(t - t_1) F_1{}^R(t_1) \cos \chi_1{}^R$$

where ( ) indicates an average over all collision times. Carrying through this procedure for a molecule which is in its $(n+1)$th diffusional step at time t, it is found that

$$(\mathbf{e}(0)\cdot\mathbf{e}(t))_{n+1}=\frac{n!}{t^n}\int_0^t dt_n F_{n+1}^T(t-t_n)\cos\chi_{n+1}^T\int_0^t dt_{n-1}$$
$$\times F_n(t_n-t_{n-1})\cos\chi_n{}^T\cdots\int_0^{t_2}dt_1\,F_2{}^T(t_2-t_1)\cos\chi_1{}^TF_1{}^T(t_1)$$

with an identical expression for $(\mathbf{e}'(0)\cdot\mathbf{e}'(t))_{n+1}$.

We see therefore, that the contribution of the diffusional motion in the soft force field is determined by the rate ω_0 at which collisions terminate the diffusional steps. In terms of this collisional rate, the probability of finding a molecule in its $(n+1)$th diffusional step at time t is given by the Poisson distribution $(1/n!)(\omega t)^n\exp(-\omega_0 t)$. In order to determine $D(t)$ and $D_J(t)$, $(\mathbf{e}(0)\cdot e(t))_{n+1}$ and $(\mathbf{e}'(0)\cdot\mathbf{e}'(t))_{n+1}$ must be averaged over the Poisson distribution

$$\langle\mathbf{e}(0)\cdot\mathbf{e}(t)\rangle_p=\exp(-\omega_0 t)\sum_{n=0}^{\infty}\frac{(\omega_0 t)^n}{n!}(\mathbf{e}(0)\cdot\mathbf{e}(t))_{n+1}$$
$$=\mathrm{e}^{-\omega_0 t}\sum_{n=0}^{\infty}\omega_0{}^n\int_0^t dt_n F_{n+1}^T(t-t_n)\cos\chi_n{}^T\cdots$$
$$\times\int_0^{t_2}dt_1F_2{}^T(t_2-t_1)\cos\chi_1{}^TF^T(t_1)$$

$\langle\mathbf{e}'(0)\cdot\mathbf{e}'(t)\rangle_p$ is given by an analogous formula.

The subscript p refers to the specific set of diffusional paths $(F_1\ldots F_{n+1})$ and deflection angles $(\chi_1\ldots\chi_n)$. The nth term in this series represents the contribution to $D(t)$ or $D_J(t)$ from a molecule in its $(n+1)$th diffusional step at time t.

The total directional-correlation function is determined by averaging the above formula over all possible diffusional paths between collisions and all sets of deflection angles. The specific F's and χ's may be quite different for each path. According to the model that we are studying, successive binary collisions are uncorrelated. Each diffusional step starts out with knowledge of the preceding diffusional steps, and each deflection angle χ_j is uncorrelated with successive or preceding deflection angles χ_{j-1} or χ_{j+1}. This assumed lack of correlation leads to the statistical independence of successive paths and deflection angles, and the resulting directional correlation are

$$D(t)=\mathrm{e}^{-\omega_0 t}\sum_{n=0}^{\infty}[\omega_0\langle\cos\chi^T\rangle]^n\int_0^t dt_n\,F^T(t-t_n)\cdots\int_0^{t_2}dt_1\,F^T(t_2-t_1)F^T(t_1)$$

$$D_J(t)=\mathrm{e}^{-\omega_0 t}\sum_{n=0}^{\infty}[\omega_0\langle\cos\chi^R\rangle]^n\int_0^t dt_n\,F^R(t-t_n)\cdots\int_0^{t_2}dt_1\,F^R(t_2-t_1)F^R(t_1)$$

where $F^T(t)$ and $F^R(t)$ represent the path averaged translational and rotational diffusional motions, and $\langle \cos \chi^T \rangle$ and $\langle \cos \chi^R \rangle$ are the averages of $\cos \chi^T$ and $\cos \chi^R$ over all collisions. The above formulas for $D(t)$ and $D_J(t)$ can be reduced to the integral equation.

$$D(t) = e^{-\omega_0 t} F^T(t) + \omega_0 \langle \cos \chi^T \rangle \int_0^t dt_1 \, e^{-\omega_0 (t - t_1)} F^T(t - t_1) D(t_1)$$

$D_J(t)$ satisfies a completely analogous equation. This equation can be solved in terms of Laplace transforms,

$$\tilde{D}(s) = \tilde{F}^T(s + \omega_0) + \omega_0 \langle \cos \chi^T \rangle F^T(s + \omega_0) \tilde{D}(s)$$

or

$$\tilde{D}(s) = \frac{\tilde{F}^T(s + \omega_0)}{1 - \omega_0 \langle \cos \chi^T \rangle \tilde{F}^T(s + \omega_0)}$$

Likewise

$$\tilde{D}_J(s) = \frac{\tilde{F}^R(s + \omega_0)}{1 - \omega_0 \langle \cos \chi^R \rangle \tilde{F}^R(s + \omega_0)}$$

Consistent with our model is the assumption that $F^T(t)$ and $F^R(t)$ are the ordinary weakly coupled or Brownian motion exponentials.

$$F^T(t) = e^{-\beta^s |t|}$$

$$F^R(t) = e^{-\beta_R{}^s |t|}$$

where β^s and $\beta_R{}^s$ are the translational and rotational friction coefficients due to the soft forces, Then $\tilde{F}^T(s) = (s + \beta)^{-1}$, $\tilde{F}^R(s) = (s + \beta_R)^{-1}$. It follows directly that

$$D(t) = \exp\left(-\{\beta + \omega_0[1 - \langle \cos \chi^T \rangle]\}|t|\right)$$

$$D_J(t) = \exp\left(-\{\beta_J + \omega_0[1 - \langle \cos \chi^R \rangle]\}|t|\right)$$

The Rice-Allnat model predicts an exponential directional correlation functions with time constants which are additive in the weak soft force and the hard force. When no soft forces are present $D(t)$ reduces to

$$D(t) = \exp\left(-\omega_0[1 - \langle \cos \chi^T \rangle]t\right)$$

which is precisely the form of the velocity correlation function discussed by Longuett-Higgins and Pople. These authors evaluated $\langle \cos \chi^T \rangle$ from the Boltzmann equation. Similarly $D_J(t)$ turns out to be in the absence of soft forces,

$$D_J(t) = \exp\left(-\omega_0[1 - \langle \cos \chi^R \rangle]t\right)$$

It is a trivial matter to evaluate $\langle \cos \chi^R \rangle$ from the Boltzmann equation. This gives the rotational diffusion coefficient in gases as a function of pressure and temperature.

Thus our stochastic model predicts a monotonic decay of $D(t)$ and $D_J(t)$. This may be valid for gases, but it is incorrect for liquids. From our computer experiments we saw that there are negative regions in both $D(t)$ and $D_J(t)$ in liquids. Thus we must search for better models of the liquid state.

B. Memory Function Theory of Linear and Angular Momentum Correlations

The first attempt to account for the structure of the empirically determined velocity autocorrelation function using the memory function $K_\psi(t)$,

$$K_\psi(t) = \frac{\langle iL\mathbf{V}| \, e^{i(1-P)Lt} \, |iL\mathbf{V}\rangle}{\langle V^2 \rangle} = \frac{\langle \mathbf{a}| \, e^{i(1-P)Lt} \, |\mathbf{a}\rangle}{\langle v^2 \rangle} \tag{287}$$

$$K_\psi(0) = \frac{\langle \mathbf{a}|\mathbf{a}\rangle}{\langle v^2 \rangle} = \frac{\langle a^2 \rangle}{\langle v^2 \rangle} \tag{288}$$

was based on the simple ansatz that the memory function depends on a single relaxation time[34]; that is

$$K_\psi(t) = \frac{\langle a^2 \rangle}{\langle v^2 \rangle} e^{-\alpha|t|} \tag{289}$$

where α is the reciprocal of the relaxation time, $\langle a^2 \rangle$ is the mean square acceleration, and $\langle v^2 \rangle$ is the mean square velocity of a labeled molecule. In this discussion computer-generated values of $\langle a^2 \rangle$ are used. Alternatively it is quite possible to determine $\langle a^2 \rangle$ over a narrow range of temperatures and densities using isotope separation data.

The single relaxation time approximation corresponds to a stochastic model in which the fluctuating force on a molecule has a Lorentzian spectrum. Thus if the fluctuating force is a Gaussian-Markov process, it follows that the memory function must have this simple form.[64] Of course it would be naïve to assume that this exponential memory will accurately account for the dynamical behavior on liquids. It should be regarded as a simple model which has certain qualitative features that we expect real memory functions to have. It decays to zero and, moreover, is of a sufficiently simple mathematical form that the velocity autocorrelation function,

$$\psi(t) = \frac{\langle \mathbf{v}(0) \cdot \mathbf{v}(t) \rangle}{\langle v^2 \rangle}$$

can be determined analytically from the memory function equation. That the exponential form of the memory function can never be the exact memory function follows from the fact that it has odd derivatives at the initial instant and, furthermore, it has moments, μ_{2n}, which do not exist for $n \geq 1$. The corresponding power spectrum of the velocity will be non-Lorentzian with finite moments, v_{2n}, for $n \leq 1$, and infinite moments for $n > 1$. It should be noted that this non-Lorentzian power spectrum is a considerable improvement over more traditional theories according to which the power spectrum of the velocity is Lorentzian (*vida* Brownian motion). A Lorentzian power spectrum has finite moments only for $n = 0$ whereas the exponential memory function leads to a velocity power spectrum which has finite moments for $n \leq 1$. It is therefore quite profitable to study the properties of the exponential memory.

To proceed it is necessary to evaluate the single relaxation time, α^{-1}, which appears in Eq. (288). For this purpose it is important to note the relationship between the normalized velocity autocorrelation function and the self-diffusion coefficient, D,

$$D = \tfrac{1}{3}\langle v^2 \rangle \int_0^\infty dt\, \psi(t) = \tfrac{1}{3}\langle v^2 \rangle \tilde{\psi}(t) \tag{290}$$

where $\tilde{\psi}(0)$ is the Laplace transform, $\tilde{\psi}(S)$, of $\psi(t)$ evaluated at $S = 0$. Eq. (290) is the Kubo relation for the diffusion coefficient. It can be derived from the Einstein relation,

$$D = \lim_{t \to \infty} \frac{\langle \Delta R^2(t) \rangle}{6t} \tag{291}$$

in which $\Delta \mathbf{R}(t)$ is the displacement of the tagged particle during the time t,

$$\Delta \mathbf{R}(t) = \int_0^t dt_1\, \mathbf{V}(t_1)$$

Substitution of this into the Einstein relation yields

$$D = \frac{1}{3} \lim_{t \to \infty} \frac{1}{t} \int_0^t dt_2 \int_0^{t_2} dt_1\, \langle \mathbf{v}(t_1) \cdot \mathbf{v}(t_2) \rangle$$

The velocity is a stationary stochastic process so that

$$\langle \mathbf{v}(t_1) \cdot \mathbf{v}(t_2) \rangle = \langle \mathbf{v}(0) \cdot \mathbf{v}(t_2 - t_1) \rangle = \langle v^2 \rangle \psi(t_2 - t_1)$$

Substitution of this into Eq. (291), followed by an integration by parts, yields

$$D = \frac{\langle v^2 \rangle}{3} \lim_{t \to \infty} \int_0^t dt_1 \left(1 - \frac{t_1}{t}\right) \psi(t_1) \tag{292}$$

If the integral $\int_0^\infty dt_1\, t_1\psi(t_1)$ exists, the limit can be taken so that

$$D = \frac{1}{3}\langle v^2\rangle\,\tilde{\psi}(0) = \frac{KT}{M}\,\tilde{\psi}(0) \tag{293}$$

The friction coefficient, γ, is so defined that

$$D = \frac{KT}{M\gamma} \tag{294}$$

from which it follows that,

$$\gamma^{-1} = \tilde{\psi}(0) \tag{295}$$

The Laplace transform of the memory function equation

$$-\frac{\partial\psi}{\partial t} = \int_0^t d\tau\, K_\psi(\tau)\psi(t-\tau)$$

subject to the conditions $\psi(0) = 1$, $\tilde{\psi}(0) = 0$ leads to

$$\tilde{\psi}(S) = [S + \tilde{K}_\psi(S)]^{-1} \tag{296}$$

where $\tilde{K}_\psi(S)$ is the Laplace transform of the memory function. It follows directly that $\psi(0) = [\tilde{K}_\psi(0)]^{-1}$, and consequently from Eq. (296) that

$$\gamma = \tilde{K}_\psi(0) \tag{297}$$

The exponential memory function has the property that

$$\tilde{K}_\psi(S) = \left(\frac{\langle a^2\rangle}{\langle v^2\rangle}\right)\frac{1}{S+\alpha} \tag{298}$$

from which it follows that

$$\alpha = \frac{1}{\gamma}\left(\frac{\langle a^2\rangle}{\langle v^2\rangle}\right) \tag{299}$$

Consequently if $\langle a^2\rangle$ and γ are known, the single relaxation time, α^{-1}, can be determined. In terms of the velocity autocorrelation function, α is

$$\alpha = \frac{\langle a^2\rangle}{\langle v^2\rangle}\,\tilde{\psi}(0) = \frac{\langle a^2\rangle}{\langle v^2\rangle}\int_0^\infty dt\,\psi(t) \tag{300}$$

Thus the single relaxation time approximation to the memory function is

$$K_\psi(t) = \frac{\langle a^2\rangle}{\langle v^2\rangle}\exp -\left[\frac{\langle a^2\rangle}{\langle v^2\rangle}\int_0^\infty dt'\,\psi(t')\right]t \tag{301}$$

To find the velocity-correlation function corresponding to this memory substitute Eq. (298) into Eq. (296) and then find the inverse Laplace transform

$$\tilde{\psi}(S) = \frac{(S+\alpha)}{S(S+\alpha)+\langle a^2\rangle/\langle v^2\rangle} \tag{302}$$

Laplace inversion then yields

$$\psi(t) = \frac{1}{S_+ - S_-}\left[S_+ e^{s^- t} - S_- e^{s^+ t}\right] \tag{303}$$

where $S_\pm$ are the roots of the equation $[S^2 + \alpha S + \langle a^2\rangle/\langle v\rangle^2 = 0]$,

$$S_\pm = -\frac{\alpha}{2} \pm \frac{\alpha}{2}\left(1 - 4\frac{\langle a^2\rangle}{\langle v^2\rangle}\alpha^{-1}\right)^{1/2} \tag{304}$$

Depending on the value of $\langle a^2\rangle$, $\langle v^2\rangle$, and γ, these roots can be real or complex. Explicitly, if

$$D < 2\left(\frac{KT}{m}\right)[\langle a^2\rangle/\langle v^2\rangle]^{1/2}$$

the roots are complex and $\psi(t)$ will oscillate. In this case

$$S_\pm = -\frac{\alpha}{2}[1 \mp i\lambda] \tag{305}$$

where $\lambda = [-1 + 4(\langle\alpha^2\rangle/\langle v^2\rangle)\alpha^{-1}]^{1/2}$. Then

$$\psi(t) = \exp^{-\alpha/2t}\left[\cos\left(\frac{\lambda\alpha}{2}t\right) + \frac{1}{\lambda}\sin\left(\frac{\lambda\alpha}{2}t\right)\right] \tag{306}$$

The power spectrum of the velocity-correlation function is consequently

$$G(\omega) = \frac{4S_+S_-(S_+ + S_-)}{(S_+{}^2 + \omega^2)(S_-{}^2 + \omega^2)} \tag{307}$$

and goes asymptotically as $1/\omega^4$. This is why v_{2n} does not exist for $n \geq 2$. The exponential approximation will be discussed later in this section.

This initial attempt to compute the time-correlation function was followed by a study of the Gaussian memory function with no significantly new results.[67] The Gaussian memory, adjusted to give the correct diffusion coefficient, is found in exactly the same way as the exponential memory. It turns out to be

$$K_\psi(t) = \frac{\langle a^2\rangle}{\langle v^2\rangle}\exp -\left\{\frac{\pi}{4}t^2\left[\frac{\langle a^2\rangle}{\langle v^2\rangle}\int_0^\infty dt'\,\psi(t')\right]^2\right\} \tag{308}$$

The major advantage of this memory function is that all of its moments are finite. The corresponding velocity correlation function cannot be determined analytically, but must be studied numerically. More will be said about this approximation later.

Prior to our computer experiments little, if indeed anything, had been reported about the full-time evolution of the angular momentum autocorrelation function of diatomic molecules in gases and liquids. The relaxation of nuclear spins is determined by the coupling of the spins to the rotational and translational motions of the molecules in the system. For nuclei with spin 1/2, the spin-rotation interaction of a linear molecule leads to an interaction Hamiltonian of the form $(-c\mathbf{I}\cdot\mathbf{J})$ where $\mathbf{I}$ is the spin angular momentum of the nucleus, $\mathbf{J}$ is the angular momentum of the molecule, and c is the spin rotation coupling constant. When this is the only part of the Hamiltonian leading to nuclear spin relaxation, the spin relaxation time, T_1, is

$$\frac{1}{T_1}=\frac{c^2}{3\hbar^2}\int_{-\infty}^{\infty} dt\, e^{-i\omega_0 t}\langle \mathbf{J}(0)\cdot\mathbf{J}(t)\rangle \tag{309}$$

where ω_0 is the Larmour precession frequency.[8] In liquids the angular momentum autocorrelation function decays on a time scale of the order of 10^{-12} which is many orders of magnitude shorter than typical precessional periods ($1/\omega_0 \sim 10^{-6}$ s). Thus the integral above is to an excellent approximation $\int_{-\infty}^{\infty} dt\,\langle \mathbf{J}(0)\cdot\mathbf{J}(t)\rangle$.

As we saw in the previous sections, the normalized angular momentum autocorrelation function, $A_J(t)$,

$$A_J(t)=\frac{\langle \mathbf{J}(0)\cdot\mathbf{J}(t)\rangle}{\langle \mathbf{J}^2\rangle} \tag{310}$$

satisfies the memory function equation with memory

$$K_J(t)=\frac{\langle \mathbf{N}|\, e^{i(1-P)Lt}\,|\mathbf{N}\rangle}{\langle J^2\rangle}$$

$$K_J(0)=\frac{\langle N^2\rangle}{\langle J^2\rangle} \tag{311}$$

where $\mathbf{N}$ is the torque acting on the molecule.

Consider the unit vector $\mathbf{u}(t)$ pointing in the direction of the molecular axis of a diatomic molecule at time t. The angle that this vector makes with $\mathbf{u}(0)$ is denoted by $\theta(t)$. According to Debye[63] the rotational diffusion coefficient, D_R, is

$$D_R=\lim_{t\to\infty}\frac{\langle\theta^2(t)\rangle}{4t} \tag{312}$$

The mean square angular deviation $\langle\theta^2(t)\rangle$ can be found in the following way. Note that the following integral of the C.M. angular velocity, $\Omega(t)$.

$$\int_0^t dt_1\, \Omega(t_1)$$

is a vector whose magnitude is the angular displacement, $\theta(t)$. The mean square angular displacement can consequently be written in terms of this integral as

$$\langle\theta^2(t)\rangle = \frac{1}{I^2}\int_0^t dt_1 \int_0^t dt_2\, \langle \mathbf{J}(t_1)\cdot\mathbf{J}(t_2)\rangle$$

where I is the moment of inertia of the molecule. The correlation function $\langle \mathbf{J}(t_1)\cdot\mathbf{J}(t_2)\rangle$ is a stationary even function of the time—a result which follows from the fact that an equilibrium average is being taken,

$$\langle \mathbf{J}(t_1)\cdot\mathbf{J}(t_2)\rangle = \langle \mathbf{J}(0)\cdot\mathbf{J}(t_2 - t_1)\rangle$$

then

$$\langle\theta^2(t)\rangle = \frac{2}{I^2}\int_0^t dt_1 \int_0^{t_1} dt_2\, \langle \mathbf{J}(0)\cdot\mathbf{J}(t_2 - t_1)\rangle \tag{313}$$

Introduction of the normalized angular momentum correlation functions, $A_J(t)$, into this integral, followed by an integration by parts yields

$$D_R = \frac{\langle J^2\rangle}{2I^2}\lim_{t\to\infty}\int_0^t dt'\left(1 - \frac{t'}{t}\right)A_J(t')$$

If the integral $\int_0^\infty dt\, t\, A_J(t)$ exists then the limit above is

$$D_R = \frac{KT}{I}\int_0^\infty dt\, A_J(t) = \frac{KT}{I}\,\tilde{A}_J(0) \tag{314}$$

where the equilibrium mean square angular momentum, $2IKT$, has been used and $\tilde{A}_J(0)$ is the Laplace transform, $\tilde{A}_J(S)$, of $A_J(t)$ at $S = 0$. The rotational friction coefficient, γ_J, is so defined that

$$D_R = \frac{KT}{I\gamma_J} \tag{315}$$

from which it follows that

$$\gamma_J{}^{-1} = \tilde{A}_J(0) \tag{316}$$

or in terms of the memory function, $K_J(t)$

$$\gamma_J = \tilde{K}_J(0) \tag{317}$$

The single relaxation time approximation can be applied to the angular momentum memory function in a completely analogous way.[68] $K_J(t)$ can be interpreted as the time-correlation function of the random torque acting on the molecule. If this random torque has a Lorentzian spectrum or, more restrictively, is a Gaussian-Markov process, $K_J(t)$ is exponential.

$$K_J(t) = \frac{\langle N^2 \rangle}{\langle J^2 \rangle} \exp -t\left[\frac{\langle N^2 \rangle}{\langle J^2 \rangle} \int_0^\infty dt' \, A_J(t')\right] \tag{318}$$

The mean square torque is taken from computer experiments. Nevertheless, it could have been found from the infrared bandshapes. Likewise the integral in this expression can be found from the experimental spin rotation relaxation time, or it can be found directly from the computer experiment as it is here. The memory function equation can be solved for this memory. The corresponding angular momentum correlation function has the same form as $\psi(t)$ in Eq. (302) with

$$S_\pm = -\frac{\alpha_J}{2} \pm \frac{\alpha_J}{2}\left[1 - 4\frac{\langle N^2 \rangle}{\langle J^2 \rangle}\alpha_J{}^{-1}\right]^{1/2} \tag{319}$$

where

$$\alpha_J = \frac{\langle N^2 \rangle}{\langle J^2 \rangle} \tilde{A}_J(0) = \frac{\langle N^2 \rangle}{\langle J^2 \rangle} \int_0^t dt' \, A_J(t') \tag{320}$$

The solution is oscillatory if

$$\int_0^\infty dt' \, A_J(t') < 4$$

These solutions are described later.

The Gaussian approximation to $K_J(t)$ is in like manner

$$K_J(t) = \frac{\langle N^2 \rangle}{\langle J^2 \rangle} \exp -\left\{\frac{\pi}{4} t^2 \left[\frac{\langle N^2 \rangle}{\langle J^2 \rangle} \int_0^\infty dt' \, A_J(t')\right]^2\right\} \tag{321}$$

There are alternative forms of the Gaussian memories* corresponding to both $\psi(t)$ and $A_J(t)$. From Eq. (169) we see that the formal power series expansions of $K_\psi(t)$ and $K_J(t)$ are

$$\begin{aligned} K_\psi(t) &= \frac{\langle a^2 \rangle}{\langle v^2 \rangle} - \frac{1}{2}\left[\frac{\langle \dot{a}^2 \rangle}{\langle v^2 \rangle} - \frac{\langle a^2 \rangle^2}{\langle v^2 \rangle^2}\right] t^2 + \cdots \\ K_J(t) &= \frac{\langle N^2 \rangle}{\langle J^2 \rangle} - \frac{1}{2}\left[\frac{\langle \dot{N}^2 \rangle}{\langle J^2 \rangle} - \frac{\langle N^2 \rangle^2}{\langle J^2 \rangle^2}\right] t^2 + \cdots \end{aligned} \tag{322}$$

* This form follows from Eq. (188a).

If $K_\psi(t)$ is assumed to have a Gaussian form, as suggested by the information theory interpolative model presented in Section III.F.

$$K_\psi(t) = B\, e^{-\alpha^2 t^2} \tag{323}$$

Then

$$K_\psi(t) = B[1 - \alpha^2 t^2 + \cdots] \tag{324}$$

Comparison of this expansion with Eq. (322) shows that

$$\begin{aligned} B &= \frac{\langle a^2 \rangle}{\langle v^2 \rangle} \\ \alpha^2 &= \frac{1}{2}\left[\frac{\langle \dot{a}^2 \rangle}{\langle a^2 \rangle} - \frac{\langle a^2 \rangle}{\langle v^2 \rangle}\right] \end{aligned} \tag{325}$$

The Laplace transform of $K_\psi(t)$ is

$$\tilde{K}_\psi(S) = \frac{(\pi)^{1/2}}{2\alpha} B\, e^{(S^2/4\alpha^2)} \operatorname{erfc}(S/2\alpha) \tag{326}$$

from which it follows that the friction coefficient γ is

$$\gamma = \tilde{K}_\psi(0) = \frac{(\pi)^{1/2}}{2}\frac{B}{\alpha} = \frac{(\pi)^{1/2}}{2}\frac{\langle a^2 \rangle}{\langle v^2 \rangle}\left(\frac{\langle \dot{a}^2 \rangle}{\langle a^2 \rangle} - \frac{\langle a^2 \rangle}{\langle v^2 \rangle}\right)^{-1/2} \tag{327}$$

Let the factor multiplying $\pi^{1/2}/2$ be called μ. Thus we see that if we assume a functional form for the memory function, then it is possible to determine the parameters in the functional form by using the moment theorems of Eq. (162) and to determine, thereby, the transport coefficients, such as the friction coefficient. Moreover, the time correlation function, $\psi(t)$, can also be determined.

Here we see that

$$K_\psi(t) = \frac{\langle a^2 \rangle}{\langle v^2 \rangle} \exp -\left[\frac{t^2}{2}\left(\frac{\langle \dot{a}^2 \rangle}{\langle a^2 \rangle} - \frac{\langle a^2 \rangle}{\langle v^2 \rangle}\right)\right] \tag{328}$$

Exactly the same procedure can be carried through for the angular momentum memory function.[68] Then the rotational friction coefficient is

$$\gamma_J = \frac{(\pi)^{1/2}}{2}\mu_J \tag{329}$$

$$\mu_J = \frac{\langle N^2 \rangle}{\langle J^2 \rangle}\left[\frac{\langle \dot{N}^2 \rangle}{\langle N^2 \rangle} - \frac{\langle N^2 \rangle}{\langle J^2 \rangle}\right]^{-1/2} \tag{330}$$

$$K_J(t) = \frac{\langle N^2 \rangle}{\langle J^2 \rangle} \exp -\left[\frac{t^2}{2}\left[\frac{\langle \dot{N}^2 \rangle}{\langle N^2 \rangle} - \frac{\langle N^2 \rangle}{\langle J^2 \rangle}\right]\right] \tag{331}$$

Corresponding to the following memory functions are the indicated friction coefficients.

Delta function memory: $K(t) = B\delta(t)$

$$\gamma = \frac{(\pi)^{1/2}}{2}\mu \qquad (332)$$

$$\gamma_J = \frac{(\pi)^{1/2}}{2}\mu_J$$

Lorentzian memory: $K(t) = B/(1 + \alpha^2 t^2)$

$$\gamma = \frac{\pi}{\sqrt{2}}\mu \qquad (333)$$

$$\gamma_J = \frac{\pi}{\sqrt{2}}\mu_J$$

Gaussian memory: $K(t) = B\,e^{-\alpha^2 t^2}$

$$\gamma = \frac{(\pi)^{1/2}}{2}\mu$$

$$\gamma_J = \frac{(\pi)^{1/2}}{2}\mu_J \qquad (334)$$

Exponential memory: $K(t) = Be^{-\alpha|t|}$, (*a*) adjusted so that the half-life for the exponential memory is identical to the Gaussian memory

$$\gamma = \left[\frac{2}{\ln 2}\right]^{1/2}\mu$$

$$\gamma_J = \left[\frac{2}{\ln 2}\right]^{1/2}\mu_J \qquad (335)$$

(*b*) is adjusted so that the half-life for the exponential is identical with the Lorentzian memory:

$$\gamma = \frac{\sqrt{2}}{\ln 2}\mu$$

$$\gamma_J = \frac{\sqrt{2}}{\ln 2}\mu_J \qquad (336)$$

This very last procedure is not really justified since the exponential memory starts out with nonvanishing odd time derivatives.

Values of $\langle a^2 \rangle$ and $\langle \dot{a}^2 \rangle$ are required to compute μ. For this purpose we use the moments determined by Nijboer and Rahman from Rahman computer studies on liquid argon. The results are presented in Table VI.

C. The Martin Formalism

There is an alternative approach to the theory of time-correlation functions. According to Eqs. (148), (156), and (157) the real and imaginary parts of the frequency dependent memory function

$$\tilde{K}_{ll}(i\omega) = \int_0^\infty dt\, e^{-i\omega t} K_{ll}(t)$$

are related by Kramer's-Kronig relations. The real part, $K'_{ll}(\omega)$, is an even function of ω and the imaginary part, $K''_{ll}(\omega)$, is an odd function of ω. The real part $K'_{ll}(\omega)$ satisfies the sum rules of Eqs. (158)

$$\mu_{2n} = \int_{-\infty}^{\infty} \frac{d\omega}{\pi} \omega^{2n} K'_{ll}(\omega)$$

with

$$\mu_0 = \langle \dot{U}_l | \dot{U}_l \rangle$$
$$\mu_2 = \langle \ddot{U}_l | \dot{U}_l \rangle - \langle \dot{U}_l | \dot{U}_l \rangle^2 \text{ etc.}$$

Thus if a functional form is chosen for $K'_{ll}(\omega)$, $K''_{ll}(\omega)$ and $K_{ll}(t)$ can be determined from the Kramers-Kronig relations. Moreover, the parameters in the functional form, $K'_{ll}(\omega)$, can be related to the moments μ_{2n}, in addition to the friction constant $\tilde{K}_{ll}(0)$, so that these parameters can thereby be determined.

This approach was recently proposed by Martin and was exploited in a number of papers.[16] It should be noted that this method is entirely equivalent to the memory function approach of Berne, Boon, and Rice.[34]

The previous remarks are demonstrated by the following simple example: Choose

$$K'_{ll}(\omega) = \frac{B\alpha}{\omega^2 + \alpha^2} \tag{337}$$

Of course this Lorentzian form has finite moments, μ_{2n}, only for $n = 0$, in which case

$$\mu_0 = \int_{-\infty}^{+\infty} \frac{d\omega}{\pi} \frac{B\alpha}{\omega^2 + \alpha^2} = B = \langle \dot{U}_l^2 \rangle \tag{338}$$

For the memory function corresponding to the velocity correlation function this yields $B = \langle a^2 \rangle / \langle v^2 \rangle$, Kramers-Kronig inversion of Eq. (337) leads to

$$K_{II}(t) = Be^{-\alpha|t|}. \tag{339}$$

so that

$$\tilde{K}_{II}(S) = \frac{B}{S + \alpha} \tag{340}$$

From this last formula we see that the friction coefficient, γ, is

$$\gamma = \frac{B}{\alpha} = \frac{\langle a^2 \rangle}{\langle v^2 \rangle} \alpha^{-1} \tag{341}$$

Thus the choice of Eq. (337) is entirely equivalent to the exponential memory of Berne, Boon, and Rice. If the assumed form of $K'_{II}(\omega)$ is Gaussian, and the two parameters characterizing this Gaussian are found from μ_0 and μ_2, it is found that $K(t)$ is identical to the Gaussian memory of Eq. (328). We conclude therefore that the Martin formalism is completely equivalent to the work presented previously. It is merely a matter of intuition and taste which dictates which method to use.

D. The Continued Fraction Approximations

Time-correlation functions can also be computed from their continued fraction representations (see section III.D) by exploiting a hierarchy of approximations of the following kind. Suppose that the nth order "random force" has a white spectrum.[34] It then follows that

$$\begin{aligned} K_n(t) &= \lambda_n \, \delta(t) \\ \tilde{K}_n(S) &= \lambda_n \end{aligned} \tag{342}$$

It is obvious from Eq. (141) that this assumption allows the continued fraction approximation to be truncated at the nth iterate so that

$$\tilde{C}_{II}(S) = C_{II}(0) \cfrac{1}{S + \cfrac{\Delta_1^2}{S + \cfrac{\Delta_2^2}{S + \cfrac{\Delta_3^2}{\ddots \; + \cfrac{}{S + \lambda_n}}}}} \tag{343}$$

The terms Δ_j^2 are well-defined equilibrium averages. λ_n on the other hand depends on the integral

$$\lambda_n = \int_0^\infty dt\, K_n(t) \tag{344}$$

To proceed it is necessary to evaluate this coefficient. One possible procedure is to use a measured value of the transport coefficient which is related to $\tilde{C}_{ll}(0)$ through a Kubo relation. Another possibility is to relate λ_n to the moments of $C_{ll}(\omega)$.

This method of approximation is illustrated on the velocity correlation function, although it can be applied to the other time-correlation functions that have been discussed. For the purpose of this illustrative example let us assume that the second-order random force has a white spectrum. Then the continued fraction representation of $\tilde{\psi}(S)$ is

$$\tilde{\psi}(S) = \cfrac{1}{S + \cfrac{\Delta_1^2}{S + \lambda_2}} \tag{345}$$

Comparison with Eq. (296) shows that

$$\tilde{K}(S) = \frac{\Delta_1^2}{S + \lambda_2} \tag{346}$$

so that the memory function corresponding to the velocity correlation function is

$$K_1(t) = \Delta_1^2\, e^{-\lambda_2 t} \tag{347}$$

This is just the single relaxation time memory with

$$\Delta_1^2 = \frac{\langle a^2 \rangle}{\langle v^2 \rangle} \tag{348}$$

and

$$\frac{\Delta_1^2}{\lambda_2} = \gamma \tag{349}$$

where γ is the friction coefficient. Consequently the truncation of the continued fraction expansion, K_2, leads to the simple exponential memory function that we described earlier and thereby to the corresponding time-correlation function. This approximation can be carried through for higher-order truncations. For example the truncation at $\tilde{K}_3(S)$ yields

$$\tilde{\psi}(S) = \cfrac{1}{S + \cfrac{\Delta_1^2}{S + \cfrac{\Delta_2^2}{S + \lambda_3}}} \tag{350}$$

Δ_1^2 and Δ_2^2 are the well-defined equilibrium moments

$$\Delta_1^2 = \langle f_1 | f_1 \rangle = \frac{\langle a^2 \rangle}{\langle v^2 \rangle}$$

and (351)

$$\Delta_2^2 = \langle f_2 | f_2 \rangle = \left(\frac{\langle \dot{a}^2 \rangle}{\langle a^2 \rangle} - \frac{\langle a^2 \rangle}{\langle v^2 \rangle} \right)$$

which have already been evaluated. The Laplace transform of the memory function is

$$\tilde{K}(S) = \tilde{K}_1(S) = \frac{\Delta_1^2}{S + \dfrac{\Delta_2^2}{S + \lambda_3}} \tag{352}$$

The friction coefficient γ is consequently

$$\gamma = \tilde{K}(0) = \frac{\Delta_1^2 \lambda_3}{\Delta_2^2} \tag{353}$$

The parameter λ_3 is therefore

$$\lambda_3 = \frac{\langle v^2 \rangle}{\langle a^2 \rangle} \left(\frac{\langle \dot{a}^2 \rangle}{\langle v^2 \rangle} - \frac{\langle a^2 \rangle}{\langle v^2 \rangle} \right) \gamma \tag{354}$$

and can consequently be determined from the experimental value of the friction coefficient. It follows from Eq. (350) that

$$\tilde{\psi}(S) = \frac{(S^2 + \Delta_2^2) + S\lambda_3}{S[\Delta_1^2 + \Delta_2^2 + S^2] + \lambda_3[\Delta_1^2 + S^2]} \tag{355}$$

This expression can be analytically inverted to yield the velocity autocorrelation function. The power spectrum, $G(\omega)$, corresponding to this correlation function is

$$G(\omega) = \text{Re}\, \tilde{\psi}(i\omega) = \frac{\lambda_3 \Delta_1^2 \Delta_2^2}{\omega^2(\Delta_1^2 + \Delta_2^2 - \omega^2)^2 + \lambda_3^2(\Delta_1^2 - \omega^2)^2} \tag{356}$$

This power spectrum falls off asymptotically as $1/\omega^6$ and has finite moments, μ_{2n}, for $n \leq 2$. A comparison of this approximation with experiment is presented in Figure 29.*

Other approximations have been used to truncate the continued fraction representation. Newman and Rice have recently shown that the velocity

* It should be noted that any comparison based purely on the computer generated power spectrum is inaccurate. A better comparison would be between the actual $\psi(t)$'s.

correlation function for a Brownian particle in a simple cubic lattice can be determined by truncating the continued fraction in a certain way. Their results coincide with those of Rubin.[70]

E. Approximate Correlation Functions from Memory Functions

In the following we focus our attention on approximate velocity and angular momentum autocorrelation functions generated from postulated memory functions. The theory behind these approximations has been outlined previously in this section. Each of the proposed memory functions that we shall consider has already been discussed in the previous sections. Here we examine how well the time-correlation functions generated from these postulated memories reproduce our experimental correlation functions and spectra. It is also informative to see the relationships between the postulated and "experimental" memories for our systems.

The specific memories and their exact functional form for $K_\psi(t)$ and $K_J(t)$ that we shall consider are[34]:

(1) Berne et al.'s exponential memory:

$$K^*_\psi(t) = \frac{\langle a^2 \rangle}{\langle v^2 \rangle} \exp -t\left[\frac{\langle a^2 \rangle}{\langle v^2 \rangle} \int_0^\infty \psi(t')\, dt'\right] \tag{357}$$

$$K^*_J(t) = \frac{\langle N^2 \rangle}{\langle J^2 \rangle} \exp -t\left[\frac{\langle N^2 \rangle}{\langle J^2 \rangle} \int_0^\infty A_J(t')dt'\right] \tag{358}$$

where a is the magnitude of the total acceleration on a molecule and the asterisks imply that these are postulated memory functions.

(2) Singwi and Tosi's Gaussian memory [67] which is referred to hereafter as Gaussian memory I:

$$K^*_\psi(t) = \frac{\langle a^2 \rangle}{\langle v^2 \rangle} \exp -\left\{\frac{\pi}{4} t^2 \left[\frac{\langle a^2 \rangle}{\langle v^2 \rangle} \int_0^\infty \psi(t')\, dt'\right]^2\right\} \tag{359}$$

$$K^*_J(t) = \frac{\langle N^2 \rangle}{\langle J^2 \rangle} \exp -\left\{\frac{\pi}{4} t^2 \left[\frac{\langle N^2 \rangle}{\langle J^2 \rangle} \int_0^\infty dt'\, A_J(t')\, dt'\right]^2\right\} \tag{360}$$

(3) Berne and Martin, and Yip's Gaussian memory[71] which is referred to hereafter as Gaussian memory II:

$$K^*_\psi(t) = \frac{\langle a^2 \rangle}{\langle v^2 \rangle} \exp -\left[\frac{t^2}{2}\left[\frac{\langle \dot{a}^2 \rangle}{\langle a^2 \rangle} - \frac{\langle a^2 \rangle}{\langle v^2 \rangle}\right]\right] \tag{361}$$

$$K^*_J(t) = \frac{\langle N^2 \rangle}{\langle J^2 \rangle} \exp -\left[\frac{t^2}{2}\left(\frac{\langle \dot{N}^2 \rangle}{\langle N^2 \rangle} - \frac{\langle N^2 \rangle}{\langle J^2 \rangle}\right)\right] \tag{362}$$

These two memories satisfy the first two moments of the exact memories, $K_\psi(t)$ and $K_J(t)$ (see Eqs. 324 and 325), but they do not necessarily satisfy the relations (see Eq. 296):

$$\int_0^\infty \psi(t)\,dt = \left[\int_0^\infty K^*_\psi(t)\,dt\right]^{-1} \tag{363}$$

$$\int_0^\infty A_J(t)\,dt = \left[\int_0^\infty K^*_J(t)\,dt\right]^{-1} \tag{364}$$

Each of these postulated memories was used to solve the appropriate Volterra equation numerically for the approximate autocorrelation functions $\psi^*(t)$ and $A^*_J(t)$ (see Appendix B). Three different experimental autocorrelation functions were tested: the velocity autocorrelation function from both the Stockmayer and modified Stockmayer simulations and the angular momentum autocorrelation function from the modified Stockmayer simulation. The parameters needed by the postulated memory functions for each of these three autocorrelation functions are tabulated in Table IV.

Consider first the postulated and experimental memories which are displayed in Figures 20, 22, 25, 27, 30, and 32. The exponential memories are the poorest approximations to the "experimental" memories: for short times they decay too rapidly and for long times too slowly. The differences between the short-time behavior of the Gaussian I and the experimental memories are quite dependent on the magnitude of the positive tails present in these latter memories: if the tails are large, then the differences are large. The Gaussian II memories are excellent approximations to the short-time behavior of the experimental memories. Note that none of the approximate memories takes into account the presence of the tails in the experimental memories.

Consider next the experimental and approximate autocorrelation functions displayed in Figures 21, 23, 26, 28, 31, and 33. All of the autocorrelation functions based on the above memories are better than the truncated moment expansions in representing the experimental correlation functions (see Figures 23, 28, and 33). The Gaussian II autocorrelation functions approximate both the long- and short-time dependences of the experimental autocorrelations better than the functions from either of the other two memories. By comparing the Gaussian II autocorrelation functions to the experimental ones, we can get some idea of how the tails or long-time behavior of the experimental memories affect their autocorrelation functions. $K_\psi(t)$ from the modified Stockmayer simulation has the largest tail. From Figure 28 we see that this tail primarily delays $\psi(t)$'s

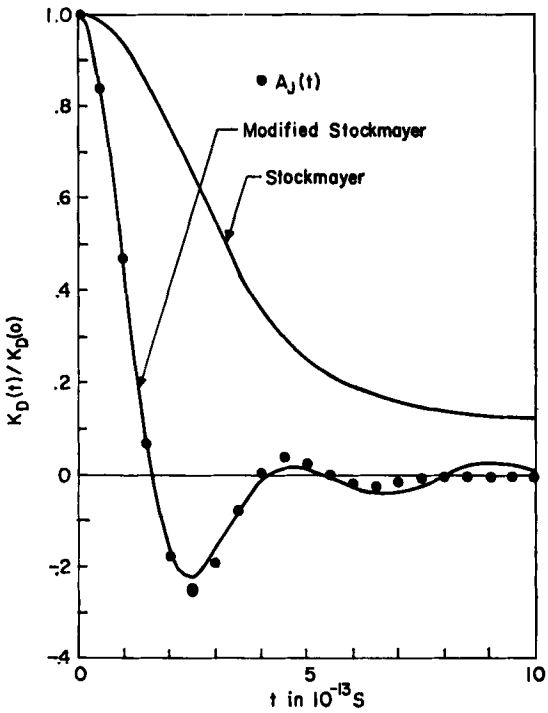

Fig. 19. Memory functions for $\langle P_1(\mu(0) \cdot \mu(t))\rangle$ from the Stockmayer and modified Stockmayer simulation of CO. $A_J(t)$ from the modified Stockmayer simulation of CO is also plotted.

approach to zero. On the other hand, the tails from the other two experimental memories seem to have very little effect on their correlation functions. This is not quite true when one compares $\int_0^\infty A^*_J(t)\,dt$ and $\int_0^\infty \psi^*(t)\,dt$ for the correlation functions generated form the Gaussian II memories to the appropriate experimental values which are presented in Table IV:

(1) For the Stockmayer simulation

$$\int_0^\infty \psi^*(t)\,dt \sim 1.22 \times 10^{-13}\text{ s} \quad \text{while} \quad \int_0^\infty \psi(t)\,dt \sim 1.15 \times 10^{-13}\text{ s}$$

(2) For the modified Stockmayer simulation

$$\int_0^\infty \psi^*(t)\,dt \sim 1.16 \times 10^{-13}\text{ s} \quad \text{while} \quad \int_0^\infty \psi(t)\,dt \sim 0.96 \times 10^{-13}\text{ s}$$

$$\int_0^\infty A^*_J(t)\,dt \sim 0.70 \times 10^{-13}\text{ s} \quad \text{while} \quad \int_0^\infty A_J(t)\,dt \sim 0.57 \times 10^{-13}\text{ s}$$

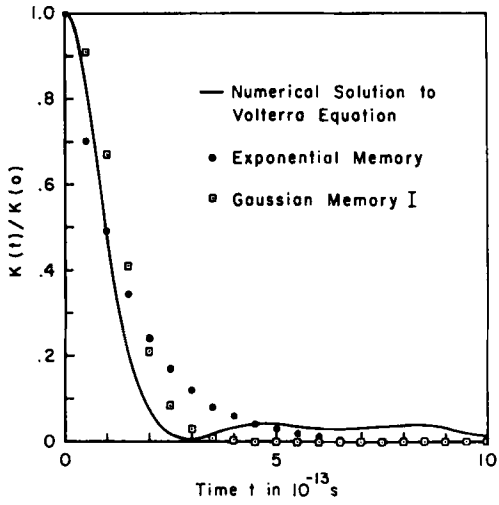

Fig. 20. Memory functions for $\psi(t)$ from the Stockmayer simulation of CO. The approximate memories are based on $\langle a^2 \rangle / \langle v^2 \rangle$ and $\int_0^\infty \psi(t)\, dt$.

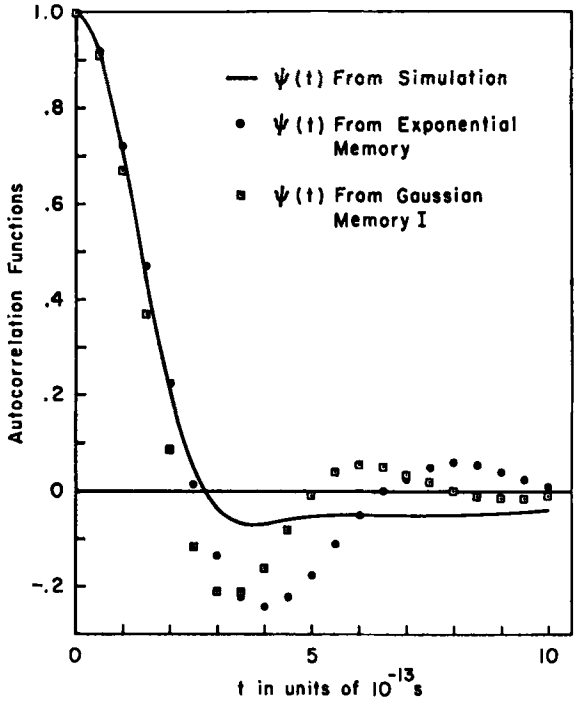

Fig. 21. Velocity autocorrelation functions from the Stockmayer simulation of CO, the exponential memory, and the Gaussian memory I.

In each case the integral of the approximate correlation function is larger than the integral of the experimental function. Also the difference between the integral of an approximate and the integral of an experimental function is proportional to the magnitude of the long-time behavior of the corresponding experimental memory. In these three examples the neglect of the tail in the experimental memory functions leads to a maximum error of $\sim 23\%$ in the integral of the resulting, approximate autocorrelation function.

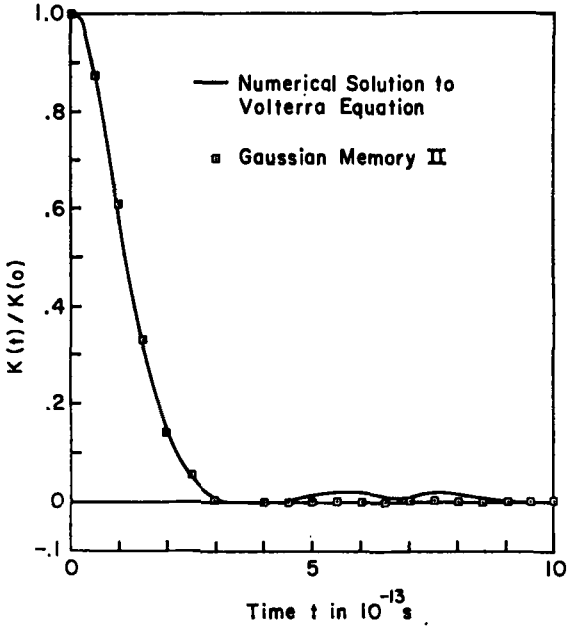

Fig. 22. Memory functions for $\psi(t)$ from the Stockmayer simulation of CO. The approximate memory is based on $\langle a^2 \rangle / \langle v^2 \rangle$ and $\langle \dot{a}^2 \rangle / \langle v^2 \rangle$.

Finally, consider the power spectra of the experimental approximate correlation functions which are displayed in Figures 24, 29, and 34. Note that each of these spectra has been normalized to unity at $\omega = 0$. Note also that the experimental spectrum from the angular momentum correlation function is much broader than the experimental velocity autocorrelation power spectra. The power spectra of the Gaussian II autocorrelation functions are in much better agreement with the experimental spectra at all frequencies than the power spectra of the other approximate autocorrelation functions.

We conclude the following from the above discussion:

(1) The experimental memories for our velocity and angular momentum autocorrelation functions decay initially to approximately zero in a Gaussian fashion.

(2) This initial decay can be adequately approximated by knowing the 2nd and 4th moments of the corresponding autocorrelation function.

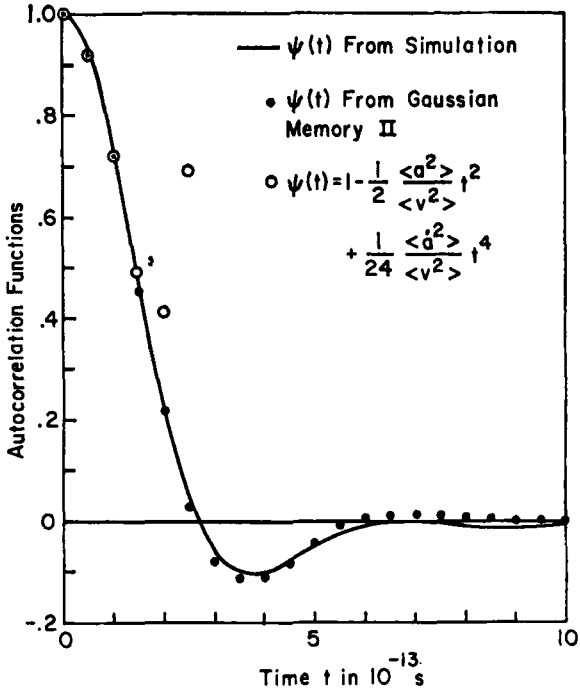

Fig. 23. Velocity autocorrelation functions from the Stockmayer simulation of CO, the Gaussian memory based on $\langle a^2\rangle/\langle v^2\rangle$ and $\langle \dot{a}^2\rangle/\langle v^2\rangle$, and the short time expansion of $\psi(t)$.

(3) The correlation function generated from this approximate memory gives a good approximation to the exact correlation function at least through this latter function's first minimum.

(4) The power spectrum of this approximate correlation function is in fair to excellent agreement with the experimental spectrum at high frequencies ($\omega \lesssim 10^{13}$/s).

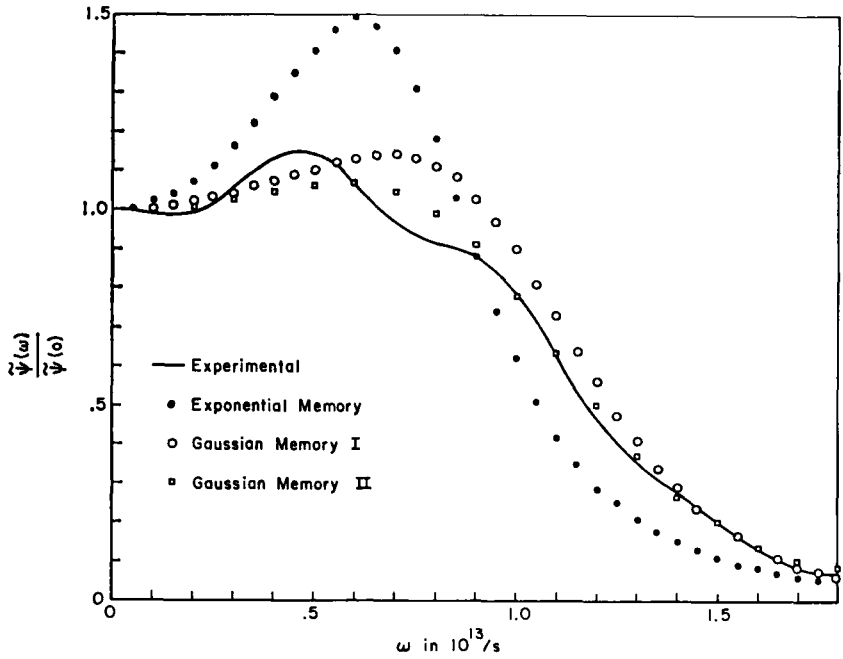

Fig. 24. Normalized power spectra of $\psi(t)$ from the Stockmayer simulation of CO, the exponential memory, and Gaussian memories I and II.

F. Elementary Excitations in Liquids

Many important properties of liquids, solids, and gases can be probed by scattering neutrons off the system in question. The differential scattering crossection in monatomic systems is related to the time Fourier transforms of the intermediate scattering functions[3–5,8]

$$F(\mathbf{k}, t) = \frac{1}{N}\left\langle \sum_l e^{-i\mathbf{k}\cdot\mathbf{r}_l(0)} \sum_m e^{i\mathbf{k}\cdot\mathbf{r}_m(t)} \right\rangle \tag{365}$$

and

$$F_S(\mathbf{k}, t) = \frac{1}{N}\left\langle \sum_l e^{-i\mathbf{k}\cdot\mathbf{r}_l(0)} e^{i\mathbf{k}\cdot\mathbf{r}_l(t)} \right\rangle$$

$F(\mathbf{k}, t)$ and $F_s(\mathbf{k}, t)$, it should be noted, are one-sided quantum-mechanical time-correlation functions. We shall be interested in the classical behavior

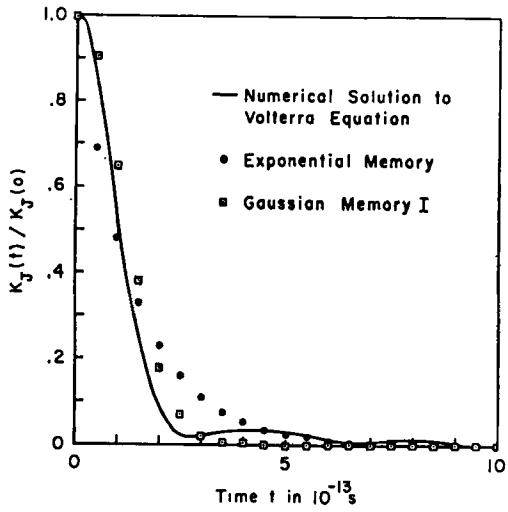

Fig. 25. Memory functions for $\psi(t)$ from the modified Stockmayer simulation of CO. The approximate memories based on $\langle a^2 \rangle / \langle v^2 \rangle$ and $\int_0^\infty \psi(t)$.

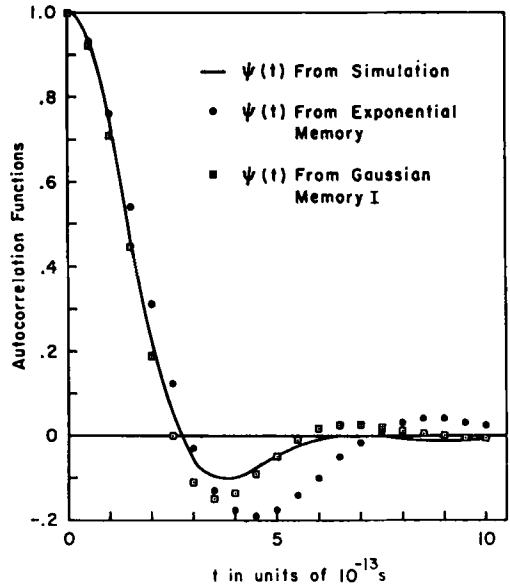

Fig. 26. Velocity autocorrelation functions from the modified Stockmayer simulation of CO, the exponential memory and the Gaussian memory I.

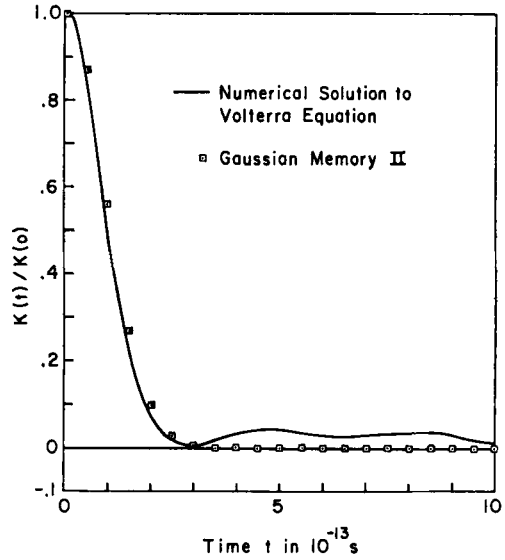

Fig. 27. Memory functions for $\psi(t)$ from the modified Stockmayer simulation of CO. The approximate memory function is based on $\langle \dot{o}^2 \rangle / \langle v^2 \rangle$ and $\langle \dot{a}^2 \rangle / \langle v^2 \rangle$.

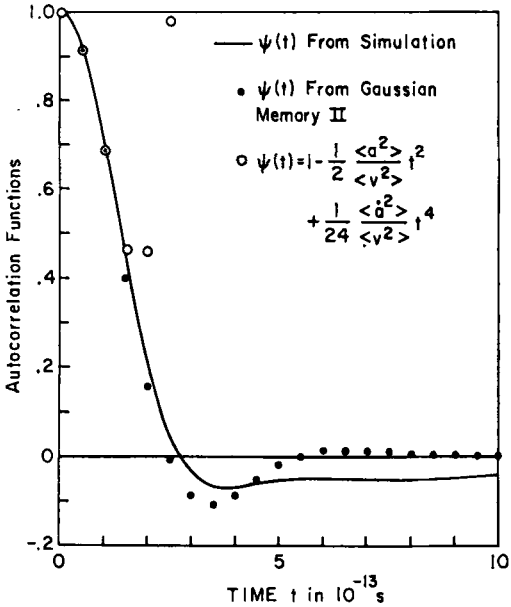

Fig. 28. Velocity autocorrelation functions from the modified Stockmayer simulation of CO, the Gaussian memory based on $\langle a^2 \rangle / \langle v^2 \rangle$ and $\langle \dot{a}^2 \rangle / \langle v^2 \rangle$, and the short time expansion of $\psi(t)$.

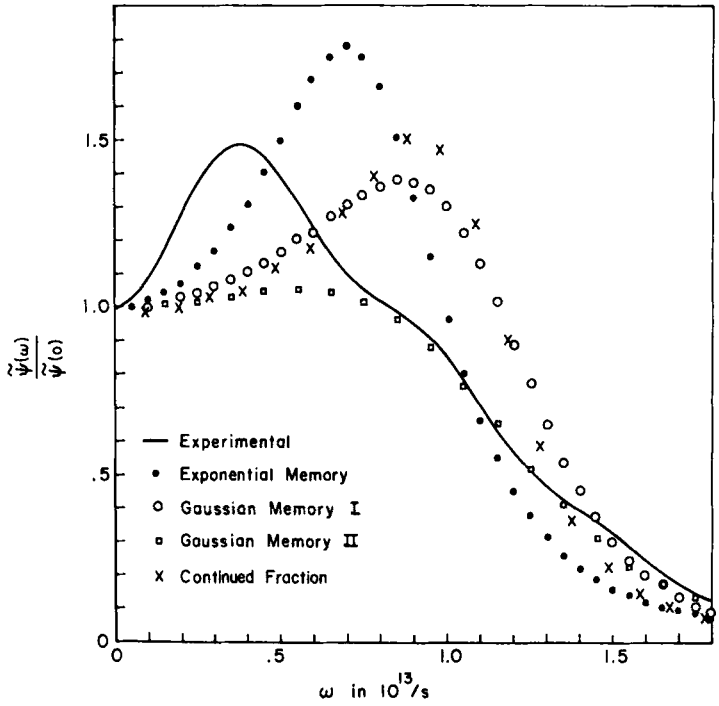

Fig. 29. Normalized power spectra of $\psi(t)$ from the modified Stockmayer simulation of CO, the exponential memory, and the Gaussian memories I and II, and the continued fraction approximation of Eq. (356)

of these functions. The differential scattering cross section for neutrons turns out to be a linear combination of the two spectral density functions

$$S(\mathbf{k}, \omega) = \frac{1}{2\pi} \int_{-\infty}^{+\infty} dt\, e^{i\omega t} F(\mathbf{k}, t)$$
$$S_S(\mathbf{k}, \omega) = \frac{1}{2\pi} \int_{-\infty}^{+\infty} dt\, e^{i\omega t} F_S(\mathbf{k}, t) \tag{366}$$

The first function, $S(\mathbf{k}, \omega)$ contributes to the coherent scattering, and the second function, $S_S(\mathbf{k}, \omega)$, contributes to the incoherent scattering of the neutrons. Neutrons consequently probe the spontaneous fluctuations of the property

$$\rho_k(t) = \frac{1}{(N)^{1/2}} \sum_{l=1}^{N} e^{i\mathbf{k} \cdot \mathbf{r}_l(t)} \tag{367}$$

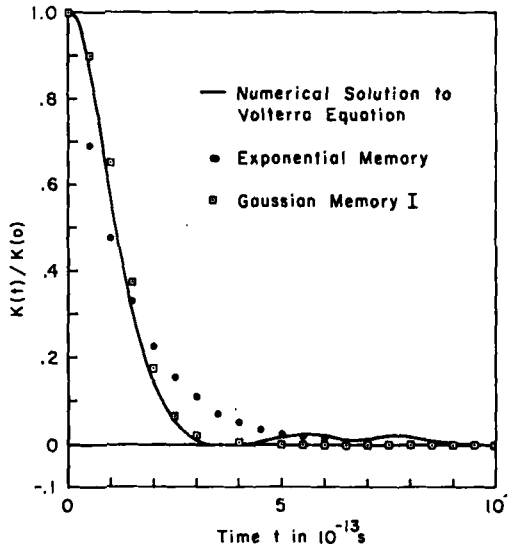

Fig. 30. Memory functions for $A_J(t)$ from the modified Stockmayer simulation of CO. The approximate memories are based on $\langle N^2\rangle/\langle J^2\rangle$ and $\int_0^\infty A_J(t)\,dt$.

which is proportional to the spatial Fourier transform of the number density,

$$\rho(\mathbf{r}, t) = \sum_{l=1}^{N} \delta(\mathbf{r} - \mathbf{r}_l(t))$$

Thus neutrons probe the dynamics of density fluctuations. The properties $\rho_k(t)$ can be regarded as collective coordinates.

From the definition of $F(\mathbf{k}, t)$ it is obvious that

$$F(\mathbf{k}, t) = F_S(\mathbf{k}, t) + F_d(\mathbf{k}, t)$$

where $F_d(\mathbf{k}, t)$ is called the distinct intermediate scattering function because it involves correlations between different or distinct nuclei,

$$F_d(\mathbf{k}, t) = \frac{1}{N}\left\langle \sum_{l\neq m=1} e^{-i\mathbf{k}\cdot\mathbf{r}_l(0)}\, e^{i\mathbf{k}\cdot\mathbf{r}_m(t)} \right\rangle \tag{368}$$

Let $G_S(\mathbf{r}, t)$ and $G_d(\mathbf{r}, t)$ denote the Fourier transform with respect to the vector $\mathbf{k}$ of $F_S(\mathbf{k}, t)$ and $F_d(\mathbf{k}, t)$. Then

$$\begin{aligned} G_S(\mathbf{r}, t) &= \frac{1}{N}\left\langle \sum_{l=1}^{N} \delta(\mathbf{r} - [\mathbf{r}_l(t) - \mathbf{r}_l(0)]) \right\rangle \\ G_d(\mathbf{r}, t) &= \frac{1}{N}\left\langle \sum_{l\neq m=1}^{N} \delta(\mathbf{r} - [\mathbf{r}_m(t) - \mathbf{r}_l(0)]) \right\rangle \end{aligned} \tag{369}$$

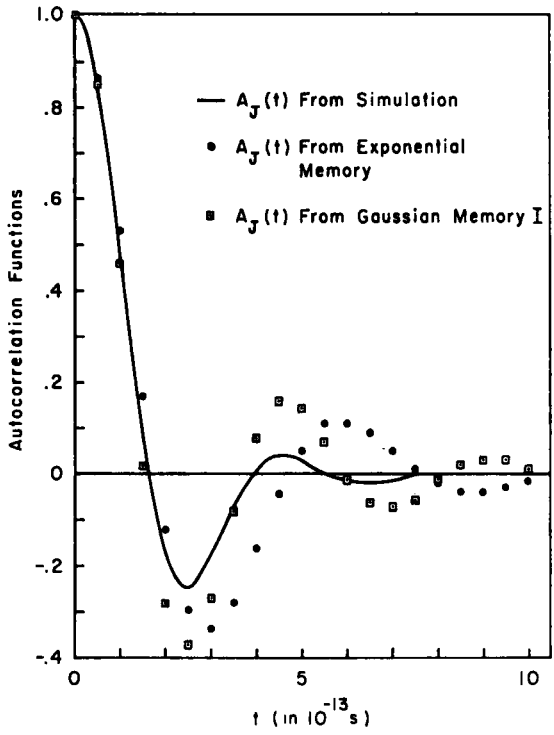

Fig. 31. Angular momentum autocorrelation functions from the modified Stockmayer simulation of CO, the exponential memory, and the Gaussian memory I.

$G_S(\mathbf{r}, t)$ and $G_d(\mathbf{r}, t)$ are called the Van Hove self and distinct space-time correlation functions.[18] It clearly follows that $G_S(\mathbf{r}, t)$ is a probability distribution describing the event that a molecule is at the origin at $t = 0$ and at the point $\mathbf{r}$ at the time t. $G_S(\mathbf{r}, t)$ is consequently the probability distribution characterizing the net displacement or diffusion of a particle in the time t. $G_d(\mathbf{r}, t)$ on the other hand is a probability distribution describing the event that a molecule is at the origin at $t = 0$ and a different molecule is at the point $\mathbf{r}$ at the time t. $G_d(\mathbf{r}, t)$ describes the correlated motion of two molecules. It should be noted that the initial value of $G_S(\mathbf{r}, t)$ is

$$G_S(\mathbf{r}, 0) = \delta(\mathbf{r}) \tag{370}$$

and the initial value of $G_d(\mathbf{r}, t)$ is related to the pair correlation function, $g^{(2)}(r)$

$$G_d(\mathbf{r}, 0) = ng^{(2)}(r) \tag{371}$$

where n is the number density of fluid molecules.

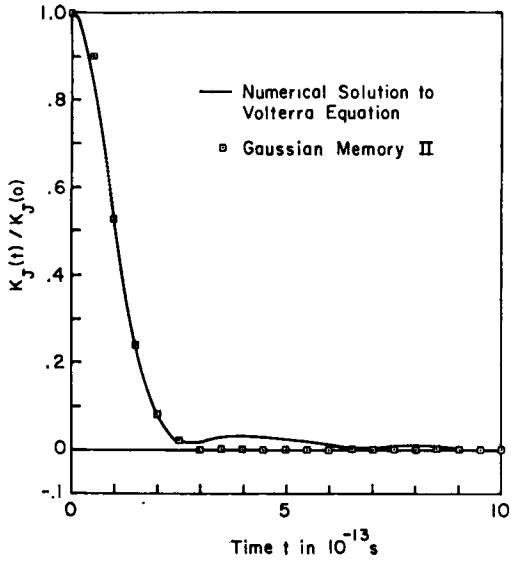

Fig. 32. Memory functions for $A_J(t)$ from the modified Stockmayer simulation of CO. The approximate memory is based on $\langle N^2\rangle/\langle J^2\rangle$ and $\langle \dot{N}^2\rangle/\langle J^2\rangle$.

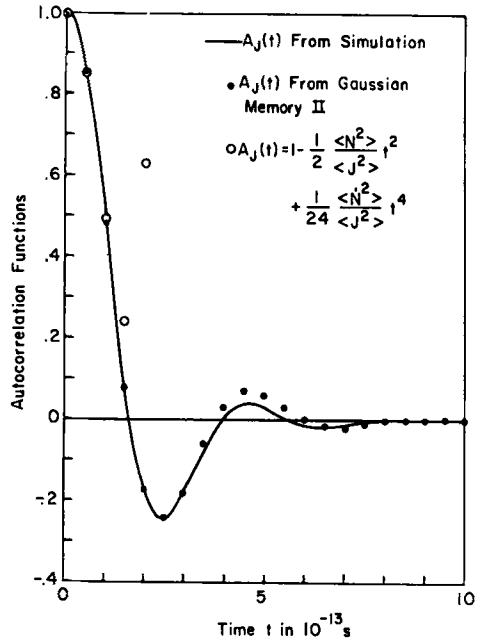

Fig. 33. Angular momentum autocorrelation functions from the modified Stockmayer simulation of CO, the Gaussian memory based $\langle N^2\rangle/\langle J^2\rangle$ and $\langle \dot{N}^2\rangle/\langle J^2\rangle$, and the short time expansion of $A_J(t)$.

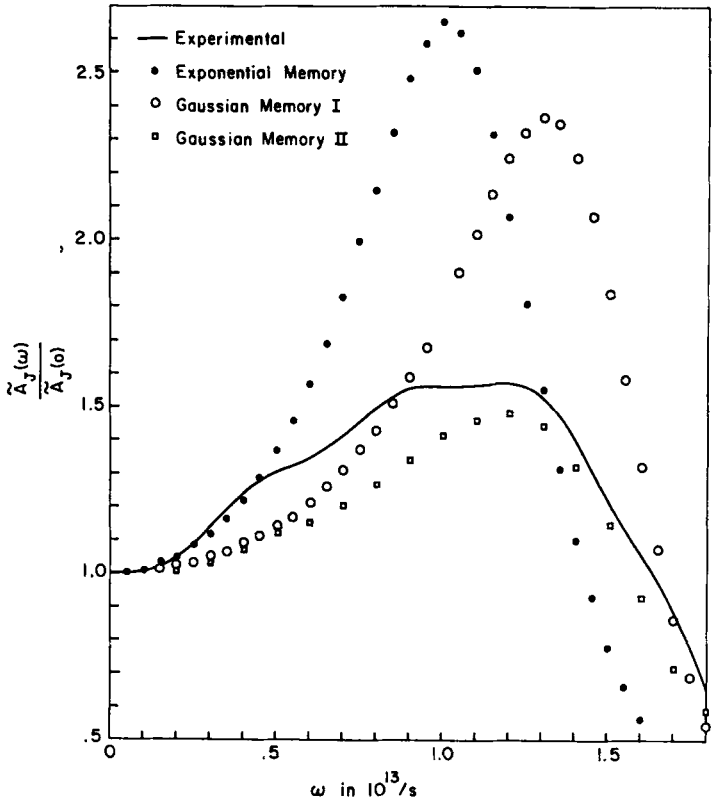

Fig. 34. Normalized power spectra of $A_J(t)$ from the modified Stockmayer simulation of CO, the exponential memory, and the Gaussian memories I and II.

Consider first the theoretical calculation of $F_S(\mathbf{k}, t)$. $G_S(\mathbf{r}, t)$ is normalized,

$$\int d^3r\, G_S(\mathbf{r}, t) = 4\pi \int_0^\infty dr\, r^2 G_S(r, t) = 1 \tag{372}$$

The second moment of $G_S(\mathbf{r}, t)$ is the mean square displacement $\langle \Delta R^2(t) \rangle$, of a particle in the fluid,

$$4\pi \int_0^\infty dr\, r^4\, G_S(r, t) = \langle \Delta R^2(t) \rangle \tag{373}$$

$G_S(\mathbf{r}, t)$ would be known completely if all of its moments $\langle \Delta R^n(t) \rangle$ were known. This, however, is not the case at all. Suppose that the mean square displacement $\langle \Delta R^2(t) \rangle$ is known. Information theory [65] can then be used to

find the optimum $G_S(\mathbf{r}, t)$ consistent with the known $\langle \Delta R^2(t) \rangle$ and normalization. For this purpose define the information entropy,

$$S[G_S(\mathbf{r}, t)] = -4\pi \int_0^\infty dr\, r^2 G_S(\mathbf{r}, t) \ln G_S(\mathbf{r}, t) \tag{374}$$

This information measure is maximized subject to the constraints of Eqs. (372) and (373). The optimum function turns out to be

$$G_S(\mathbf{r}, t) = [2\pi w(t)]^{-3/2} e^{-r^2/2w(t)} \tag{375}$$

where

$$w(t) = \frac{1}{3} \langle \Delta R^2(t) \rangle$$

This is the well-known Gaussian approximation for $G_S(r, t)$. Vineyard[82] motivated the Gaussian approximation for monatomic systems when he pointed out that $G_S(r, t)$ is a Gaussian for a particle which is moving in a gas, or diffusing according to the simple diffusion equation, or vibrating in an harmonic lattice. Dasannacharya and Rao[73] have determined $G_S(r, t)$ experimentally for liquid argon by Fourier inversion of their incoherent differential scattering cross sections for slow neutrons. They found that, within experimental error, $G_S(r, t)$ is also a Gaussian in liquid argon. Janik and Kowalska[5] have suggested that the Gaussian approximation might also be extended to systems with internal degrees of freedom. However, Rahman's molecular dynamics studies of liquid argon[32,74] indicate that $G_S(r, t)$ is not a Gaussian except for short and long times. We also find non-Gaussian corrections to our Van Hove functions, but before we discuss these corrections it is informative to examine models which can account for the non-Gaussian behavior. The Gaussian approximation leads to the intermediate scattering function

$$F_S(\mathbf{k}, t) = e^{-(k^2/6)\langle \Delta R^2(t) \rangle} \tag{376}$$

The long-time behavior of $F_S(\mathbf{k}, t)$ can be extracted from the memory function equation by using a technique originally due to Zwanzig.[75] If $\tilde{F}_S(\mathbf{k}, S)$ and $\tilde{\Phi}_{2k}(S)$ denote the Laplace transforms of $F_S(\mathbf{k}, t)$ and $\Phi_{2k}(t)$, then Laplace transformation of the memory function equation yields

$$\tilde{F}_S(\mathbf{k}, S) = \frac{1}{S + \Phi_{2k}(S)} \tag{377}$$

Inversion symmetry shows that $\Phi_{-2k}(t) = \tilde{\Phi}_{2k}(t)$ so that the memory function can be expressed as

$$\Phi_{2k}(t) = \frac{k^2}{3} \Lambda_k(t)$$

where

$$\Lambda_k(t) = \langle \mathbf{V}\, e^{i\mathbf{k}\cdot\mathbf{r}} | \, e^{i(1-P)Lt} \, | \mathbf{V}\, e^{i\mathbf{k}\cdot\mathbf{r}} \rangle \tag{378}$$

It consequently follows that

$$\tilde{F}_S(\mathbf{k}, t) = \frac{1}{S + \frac{1}{3}k^2\tilde{\Lambda}_k(S)} \tag{379}$$

The function $F_S(\mathbf{k}, t)$ is the inverse Laplace transform of the preceding equation

$$F_S(k, t) = \frac{1}{2\pi i}\oint dS\, e^{st}\frac{1}{S + \frac{1}{3}k^2\tilde{\Lambda}_k(S)} \tag{380}$$

The Zwanzig technique[75] proceeds as follows: the variables τ and x are so defined that

$$\begin{aligned} S &= k^2 x \\ t &= \frac{1}{k^2}\tau \end{aligned} \tag{381}$$

Introducing the reduced variables x and τ into Eq. (380) leads to

$$F_S(k, t) = \frac{1}{2\pi i}\oint dx\, e^{x\tau}\frac{1}{x + \frac{1}{3}\tilde{\Lambda}_k(k^2 x)} \tag{382}$$

The long-time behavior of $F_S(k, t)$ is simply

$$F_S(\mathbf{k}, t) = \frac{1}{2\pi i}\lim_{\substack{k^2\to 0 \\ x,\tau\ \text{const}}}\oint dx\, e^{x\tau}\frac{1}{x + \frac{1}{3}\tilde{\Lambda}_k(k^2 x)} \tag{383}$$

where the limit is taken such that $k \to 0$ whereas $t \to \infty$ and $S \to 0$ in such a way that x and τ remain constant. k^2 acts like a parameter of smallness. It follows that the long time behavior of $F_S(\mathbf{k}, t)$ is

$$F_S(\mathbf{k}, t) = \frac{1}{2\pi i}\oint dx\, e^{x\tau}\frac{1}{x + \frac{1}{3}\tilde{\Lambda}_0(0)}$$

or

$$F_S(\mathbf{k}, t) = e^{-1/3\Lambda_0(0)\tau} = e^{-1/3\Lambda_0(0)k^2 t}$$

with

$$\tilde{\Lambda}_0(0) = \lim_{S\to 0}\lim_{k^2\to 0}\int_0^\infty dt\, e^{-St}\langle \mathbf{V}\, e^{i\mathbf{k}\cdot R} | \, e^{i(1-P_2)Lt} \, | \mathbf{V}\, e^{i\mathbf{k}\cdot R}\rangle$$

From the definition of the projection operator it is easy to evaluate the $k^2 \to 0$ limit. Then

$$\tilde{\Lambda}_0(0) = \int_0^\infty dt \, \langle \mathbf{V}(0) \cdot \mathbf{V}(t) \rangle \tag{384}$$

Call

$$D = \frac{1}{3} \int_0^\infty dt \, \langle \mathbf{V}(0) \cdot \mathbf{V}(t) \rangle \tag{385}$$

Then

$$F_S(\mathbf{k}, t) = \mathrm{e}^{-k^2 D t} \tag{386}$$

Thus from the memory function equation we have succeeded in showing that $F_S(\mathbf{k}, t)$ satisfies the diffusion equation

$$\frac{\partial}{\partial t} F_S(\mathbf{k}, t) = -k^2 D F_S(\mathbf{k}, t) \tag{387}$$

at long times with a diffusion coefficient D. Moreover, we have succeeded in showing that the diffusion coefficient is determined by the velocity autocorrelation function according to Eq. (385). This is a simple example of a Kubo relation.[11]

In order to apply the memory function formalism to the collective coordinates of Eq. (367), it is necessary to define the dimensionless normalized collective coordinates,

$$\begin{aligned} |U_{1k}\rangle &\equiv \langle \rho_k | \rho_k \rangle^{-1/2} |\rho_k\rangle \\ |U_{2k}\rangle &\equiv |\mathrm{e}^{i\mathbf{k}\cdot\mathbf{r}}\rangle \end{aligned} \tag{388}$$

where the classical scalar product is intended. The structure factor $S(\mathbf{k})$ is defined as $F(\mathbf{k}, 0)$, or

$$S(\mathbf{k}) = \langle \rho_k | \rho_k \rangle = \frac{1}{N} \left\langle \sum_{l,m=1}^{N} \mathrm{e}^{i\mathbf{k}\cdot[r_l - r_m]} \right\rangle \tag{389}$$

From the preceding formulas we see that the structure factor is related to the pair correlation function

$$S(k) = 1 + \frac{4\pi n}{k} \int_0^\infty dr \, g^{(2)}(r) r \sin kr \tag{390}$$

The intermediate scattering functions can be expressed in terms of the normalized properties $|U_{1k}\rangle$ and $|U_{2k}\rangle$

$$F(\mathbf{k}, t) = S(k) \langle U_{1k} | \mathrm{e}^{iLt} | U_{1k} \rangle \tag{391}$$

and

$$F_S(\mathbf{k}, t) = \langle U_{2k} | \, e^{iLt} \, | U_{2k} \rangle \tag{392}$$

$F(\mathbf{k}, t)$ and $F_S(\mathbf{k}, t)$ consequently satisfy memory function equations with corresponding memories

$$\begin{aligned} \Phi_{1k}(t) &= \langle \dot{U}_{1k} | \, e^{i(1-\hat{P}_1)Lt} \, | \dot{U}_{1k} \rangle \\ \Phi_{2k}(t) &= \langle \dot{U}_{2k} | \, e^{i(1-\hat{P}_2)Lt} \, | \dot{U}_{2k} \rangle \end{aligned} \tag{393}$$

where $|\dot{U}_{1k}\rangle = iL|U_{1k}\rangle$, $|\dot{U}_{2k}\rangle = iL|U_{2k}\rangle$, and the projection operators are $\hat{P}_{1k} \equiv |U_{1k}\rangle\langle U_{1k}|$ and $\hat{P}_{2k} = |U_{2k}\rangle\langle U_{2k}|$.

Consider first the memory function equation for $F_S(\mathbf{k}, t)$. From Eqs. (167) and (168) it is seen that the short-time behavior of the memory function $\Phi_{2k}(t)$ is

$$\Phi_{2k}(t) = \frac{1}{3} k^2 \langle v^2 \rangle - \frac{t^2}{2} \left[\frac{2}{9} \langle v^2 \rangle^2 k^4 + \frac{1}{3} \langle a^2 \rangle k^2 \right] + \cdots \tag{394}$$

To second order in the momentum transfer it can be shown that

$$\Phi_{2k}(t) = \frac{1}{3} \langle v^2 \rangle k^2 \psi(t) + 0(k^4) \tag{395}$$

where $\psi(t)$ is the normalized velocity autocorrelation function. Thus for sufficiently small values of k,

$$\Phi_{2k}(t) \cong \frac{1}{3} \langle v^2 \rangle k^2 \psi(t) \tag{396}$$

To get some idea of the values of k for which this approximation may be valid, let us look at the second term in the short-time behavior of $\Phi_{2k}(t)$. Note that the term of order k^4 can be neglected if k is such that

$$k^2 \langle v^2 \rangle \ll \frac{3}{2} \frac{\langle a^2 \rangle}{\langle v^2 \rangle}$$

or for our conditions $k \ll 4A^{0-1}$. The interesting feature of the approximate memory function in Eq. (396) is that it will lead to a non-Gaussian $G_S(\mathbf{r}, t)$, and may thus provide an approximate method for determining the self Van Hove correlation function, $G_S(\mathbf{r}, t)$, for intermediate values of k when it is known that this function deviates from Gaussian behavior. It should be noted that this approximation correctly gives the initial time dependence of $\langle \Delta R_{\text{C.M.}}{}^{2n}(t) \rangle$ only for $n = 1$, whereas the Gaussian approximation correctly accounts for all of these moments at short times, and the diffusion approximation fails completely at short times.

$F_S(k, t)$ for different values of k is presented in Figure 43; these functions were evaluated using the series expansion for $F_S(k, t)$ discussed in Appendix C and the coefficients $\alpha_N(t)$ from the modified Stockmayer simulation. The memory functions for these intermediate scattering functions are presented in Figure 44. Both of these memories were computed using the numerical method outlined in Appendix B. The absolute error in recovering $F_S(k, t)$ from $\Phi_{2k}(t)$ was $\lesssim 0.005$ for all times $t \lesssim 10^{-12}$ s. Note that although the two scattering functions are quite different, their normalized memories are very similar. Note further that these normalized memories resemble the velocity autocorrelation function for this simulation (see Figure 10). In addition the approximate memory function, Eq. (396), is used to compute approximate intermediate scattering functions, $F_S(k, t)$. The results of this approximate theory are presented along with the corresponding experimental functions in Figure 47. Note that this approximate theory is better than the Gaussian $G_S(\mathbf{r}, t)$ for intermediate values of k.

There is another approach to the problem of determining $F_S(\mathbf{k}, t)$. Note that,

$$\begin{aligned} &\frac{d^2}{dt^2} F_S(\mathbf{k}, t) = -C_S(\mathbf{k}, t) \\ &C_S(\mathbf{k}, t) \equiv \langle \mathbf{k} \cdot \mathbf{v}\, e^{i\mathbf{k}\cdot\mathbf{r}} | e^{iLt} | \mathbf{k} \cdot \mathbf{v}\, e^{i\mathbf{k}\cdot\mathbf{r}} \rangle \\ &C_S(\mathbf{k}, 0) = \langle \mathbf{k} \cdot \mathbf{v} | \mathbf{k} \cdot \mathbf{v} \rangle = \tfrac{1}{3} k^2 \langle v^2 \rangle \end{aligned} \tag{397}$$

$F_S(\mathbf{k}, t)$ can be determined from $C_S(\mathbf{k}, t)$, which in turn satisfies the memory function equation

$$\frac{\partial}{\partial t} C_S(\mathbf{k}, t) = -\int_0^t d\tau\, L_4(\mathbf{k}, \tau) C_S(\mathbf{k}, t - \tau) \tag{398}$$

where

$$\begin{aligned} &L_4(\mathbf{k}, t) = \langle \dot{A}_k | e^{i(1 - \hat{P}_4)Lt} | \dot{A}_k \rangle \\ &|A_k\rangle \equiv \langle \mathbf{k} \cdot \mathbf{v} | \mathbf{k} \cdot \mathbf{v} \rangle^{-1/2} | (\mathbf{k} \cdot \mathbf{v})\, e^{i\mathbf{k}\cdot\mathbf{r}} \rangle \end{aligned} \tag{399}$$

and

$$\hat{P}_4 \equiv |A_k\rangle\langle A_k|$$

It follows from these formulae that

$$\lim_{k \to 0} \hat{C}_S(\mathbf{k}, t) = \psi(t) \tag{400}$$

where

$$\hat{C}_S(\mathbf{k}, t) = C_S(\mathbf{k}, t)/C_S(\mathbf{k}, 0)$$

Since $\hat{C}_S(k, t)$ is equal to the normalized velocity autocorrelation function, it follows from Eq. (399) that the memory function $L_4(\mathbf{k}, t)$ has the $k \to 0$ limit

$$\lim_{k\to 0} L_4(\mathbf{k}, t) = L_4(0, t) = K_\psi(t) \tag{401}$$

where $K_\psi(t)$ is the memory function corresponding to the velocity.

Let

$$L_4(\mathbf{k}, t) = K_\psi(t) + G(\mathbf{k}, t) \tag{402}$$

where $G(\mathbf{k}, t)$ has the limit,

$$\lim_{k\to 0} G(\mathbf{k}, t) = 0 \tag{403}$$

as required by Eq. (401).

Suppose now that $G(\mathbf{k}, t)$ decays with a single k-dependent relaxation time, $\tau(k)$, so that

$$G(\mathbf{k}, t) = g(k)\mathrm{e}^{-t/\tau(k)} \tag{404}$$

where $g(k) \to 0$ as $k \to 0$. Note that in this case

$$L(k, 0) = K_\psi(0) + g(k) = \frac{\langle a^2\rangle}{\langle v^2\rangle} + g(k) \tag{405}$$

This last result follows from Eq. (417).

In order to identify the function $g(k)$ it is necessary to know that the exact short-time behavior of $L(k, t)$ is

$$L(k, t) = \langle \dot{U}_{4k}|\dot{U}_{4k}\rangle - \frac{t^2}{2}[\langle \ddot{U}_{4k}|\ddot{U}_{4k}\rangle - (\langle \dot{U}_{4k}|\dot{U}_{4k}\rangle)^2] \tag{406}$$

which is explicitly

$$L(\mathbf{k},t) = \left(\frac{\langle a^2\rangle}{\langle v^2\rangle} + k^2\langle v^2\rangle\right) - \frac{t^2}{2}\left[\left(\frac{\langle \dot{a}^2\rangle}{\langle v^2\rangle} - \frac{\langle a^2\rangle^2}{\langle v^2\rangle^2}\right) + \left(3k^2\langle a^2\rangle + \frac{2}{3}k^4\langle v^2\rangle^2\right)\right] + \cdots \tag{407}$$

Consequently the function $g(k)$ in the single relaxation time equation turns out to be

$$g(k) = k^2\langle v^2\rangle$$

and

$$L_4(t) = K_\psi(t) + k^2\langle v^2\rangle \mathrm{e}^{-t/\tau(k)} \tag{408}$$

It is our intention to use either approximate or exact forms of $K_\psi(t)$ in the approximate memory function $L_4(t)$. The relaxation time $\tau(k)$ can be found in the following way. Since

$$\tilde{L}_4(s) = \tilde{K}_\psi(S) + \frac{k^2\langle v^2\rangle}{S + \frac{1}{\tau}(k)} \tag{409}$$

it follows that

$$\tilde{L}_4(0) \equiv \gamma(k) = \gamma + k^2\langle v^2\rangle\tau(k) \tag{410}$$

According to this formula the k-dependent friction coefficient,

$$\gamma(k) = \tilde{L}_4(0) = \left[\int_0^\infty dt\, \tilde{C}_S(\mathbf{k}, \tau)\right]^{-1} \tag{411}$$

is equal to the sum of the friction coefficient $\gamma = KT/MD$ and the term $k^2\langle v^2\rangle\tau(k)$. If $\gamma(k)$ is determined from the computer experiments, $\tau(k)$ can be determined, and $\hat{C}_S(k, t)$ and the corresponding $F_S(\mathbf{k}, t)$ can be determined. The trouble with this approximation is that it does not predict the correct moments $\langle \Delta R^n(t)\rangle$ for short times.

An alternative procedure is to assume the form,

$$G(k, t) = g(k)\, e^{-\alpha^2(k)t^2} \tag{412}$$

and then to evaluate the functions $g(k)$ and $\alpha(k)$ from the equilibrium moments in Eq. (407). By carrying out this precedure it is found that

$$\begin{aligned} g(k) &= k^2\langle v^2\rangle \\ \alpha^2(k) &= \frac{1}{2}\left[3\frac{\langle \alpha^2\rangle}{\langle v^2\rangle} + \frac{2}{3}k^2\langle v^2\rangle\right] \end{aligned} \tag{413}$$

Consequently the Gaussian approximation is

$$\tilde{L}_4(t) = K_\psi(t) + k^2\langle v^2\rangle \exp\left(-\frac{t^2}{2}\left[3\frac{\langle a^2\rangle}{\langle v^2\rangle} + \frac{2}{3}k^2\langle v^2\rangle\right]\right) \tag{414}$$

The Laplace transform of this is

$$\tilde{L}_4(S) = K_\psi(S) + \frac{k^2\langle v^2\rangle(\pi)^{1/2}}{2\alpha(k)}\, e^{S^2/4\alpha^2(k)}\, \mathrm{erfc}\left(\frac{S}{2\alpha(k)}\right) \tag{415}$$

so that

$$\gamma(k) = \gamma + \frac{(\pi)^{1/2}}{2}k^2\langle v^2\rangle\alpha^{-1}(k) \tag{416}$$

Note that

$$\lim_{k\to\infty}\frac{1}{\gamma(k)}=0\left[\left(\frac{3\pi}{4}k^2\langle v^2\rangle\right)^{1/2}\right] \tag{417}$$

which is roughly the time it takes an average particle to traverse a distance of the order of a wavelength $\lambda/2\pi$.

Similar methods[76–80] have been applied to the study of $F(\mathbf{k}, t)$. In two entirely independent studies $F(\mathbf{k}, t)$ was computed from "generalized hydrodynamics." In this theory memory function equations were derived for the normal hydrodynamic variables—mass, momentum, and energy density. The derivation follows a development that is similar to the treatment of multivariate processes presented in this review (the major difference being the definition of the projection operator). The memory functions are then chosen so that these equations reduce in the hydrodynamic limit ($k\to 0$, $t\to\infty$, such that $k^2t=$ const.) to the known hydrodynamic equations. Moreover, these memory functions are also chosen to give the correct short time behavior (i.e., moments). Given these constraints functional forms are chosen for the memories with parameters fixed in terms of equilibrium moments and transport coefficients. The generalized hydrodynamic equations (memory function equations) are solved and $F(\mathbf{k}, t)$ is determined. These calculations are very much in the spirit of the earlier papers[34,67] on the memory function approach to the calculation of the velocity autocorrelation function and $F_S(\mathbf{k}, t)$.

G. Van Hove Self-Correlation Functions from Computer Experiments

We shall now discuss three Van Hove correlation functions [18,72] obtained from our CO simulations. These functions are defined as follows:

(1) $G_S(r, t)$ is the probability that the C.M. of a molecule moves a distance r in time t given that it was at the origin at $t=0$.

(2) $G_S^C(r, t)$ is the probability that the carbon atom on a given molecule moves a distance r in time t given that it was at the origin at $t=0$.

(3) $G_S^O(r, t)$ is the probability that the oxygen atom on a given molecule moves a distance r in time t given it was at the origin at $t=0$.

$G_S^O(r, t)$ and $G_S^C(r, t)$ determine the incoherent differential scattering cross section for slow neutrons from CO through a weighted sum of their space-time Fourier transforms. Each of these functions is normalized to unity when integrated over all space.

If one wanted to predict slow neutron incoherent scattering from CO then, in the Gaussian approximation, all one would need would be the

mean square displacements of the carbon and oxygen atoms, i.e., $\langle(\Delta\mathbf{R}_C(t))^2\rangle$ and $\langle(\Delta\mathbf{R}_O(t))^2\rangle$, respectively. These two functions depend in general on both the average translational and rotational behavior of a molecule as well as translational-rotational coupling. For example, if we express $\mathbf{R}_C$ and $\mathbf{R}_O$ in relative and C.M. coordinates, then it is easy to show

$$\langle(\Delta\mathbf{R}_C(t))^2\rangle = \langle(\Delta\mathbf{R}_{C.M.}(t))^2\rangle + \frac{2M_O r_0}{M}\langle\Delta\mathbf{R}_{C.M.}(t)\cdot\Delta\boldsymbol{\mu}(t)\rangle + 2\left(\frac{M_O r_0}{M}\right)^2[1-\langle\boldsymbol{\mu}(0)\cdot\boldsymbol{\mu}(t)\rangle]$$

$$\langle(\Delta\mathbf{R}_O(t))^2\rangle = \langle(\Delta\mathbf{R}_{C.M.}(t))\rangle^2 - \frac{2M_C r_0}{M}\langle\Delta\mathbf{R}_{C.M.}(t)\cdot\Delta\boldsymbol{\mu}(t)\rangle + 2\left(\frac{M_C r_0}{M}\right)^2[1-\langle\boldsymbol{\mu}(0)\cdot\boldsymbol{\mu}(t)\rangle]$$

where $\boldsymbol{\mu}$ is a unit vector pointing along the internuclear axis from the oxygen atom to the carbon atom, r_0 is the equilibrium internuclear separation, $\Delta\boldsymbol{\mu} = \boldsymbol{\mu}(t) - \boldsymbol{\mu}(0)$, and $\Delta\mathbf{R}_{C.M.}(t) = \mathbf{R}_{C.M.}(t) - \mathbf{R}_{C.M.}(0)$. Note that the atomic displacement functions depend on the dipolar correlation function. Hence this portion of these functions could be determined from infrared bandshape studies. One can prove that

$$\langle(\Delta\mathbf{R}_{C.M.}(t))^2\rangle = 2\langle v^2\rangle\int_0^t (t-t')\psi(t')dt' \tag{418}$$

Therefore the approximate velocity autocorrelation functions we considered previously could be used to generate $\langle(\Delta\mathbf{R}_{C.M.}(t))^2\rangle$. In fact Berne[81] and Desai and Yip[82] have used the exponential memory to generate the approximate mean square displacement of an argon atom in the liquid. Desai and Yip then used this Gaussian approximation to predict neutron scattering from liquid argon.[82]

The translational-rotational term, $\langle(\Delta\mathbf{R}_{C.M.}(t)\cdot\Delta\boldsymbol{\mu}\rangle(t))$, is much more difficult to treat. However, for homonuclear diatomic molecules this term vanishes,* and for the two systems we studied this term contributed less to the mean square displacements than either the translational or the rotational terms. If we ignore the coupling term then for short times we have

$$\langle(\Delta\mathbf{R}_{C.M.}(t))^2\rangle = \frac{3KT}{M}t^2 + 0(t^4) \tag{419}$$

* This follows from the invariance of the Hamiltonian to the interchange of the two atoms in a homonuclear diatomic molecule.

$$\langle(\Delta\mathbf{R}_C(t))^2\rangle = \frac{KT}{M}\left[3 + 2\frac{M_O}{M_C}\right]t^2 + 0(t^4) \tag{420}$$

$$\langle(\Delta\mathbf{R}_O(t))^2\rangle = \frac{KT}{M}\left[3 + 2\frac{M_C}{M_O}\right]t^2 + 0(t^4) \tag{421}$$

Since M_O is greater than M_C, the displacement of the carbon atom should be initially greater than the displacement of the oxygen atom which in turn should be greater than the displacement of the C.M. Since $1 - \langle\boldsymbol{\mu}(0)\cdot\boldsymbol{\mu}(t)\rangle$ is positive for $t > 0$, the above order of displacements should persist for all time. That is, provided the translational-rotational term can be neglected. In the diffusion limit, or equivalently, for long times we have

$$\langle(\Delta\mathbf{R}_{C.M.}(t))^2\rangle = 6Dt + C \tag{422}$$

$$\langle(\Delta\mathbf{R}_C(t))^2\rangle = 6Dt + C + 2\left(\frac{M_O r_0}{M}\right)^2 \tag{423}$$

$$\langle(\Delta\mathbf{R}_O(t))^2\rangle = 6Dt + C + 2\left(\frac{M_C r_0}{M}\right)^2 \tag{424}$$

where C is a constant that allows for the fact that a molecule in a fluid is moving coherently initially. Note that for long times the net atomic displacements should be parallel to the C.M. displacement provided again that the translational-rotational terms can be neglected. These characteristics are all illustrated in Figures 35 and 39 where the atomic and C.M. displacement functions from the Stockmayer and modified Stockmayer simulations are presented. The translational-rotational coupling function, $2r_0\langle\Delta\mathbf{R}_{C.M.}(t)\cdot\Delta\boldsymbol{\mu}(t)\rangle$, is also presented in these figures. This coupling term is largest for long times in the modified Stockmayer simulation. The translational, rotational, and translational-rotational coupling contributions to the mean square displacement of a carbon atom in the Stockmayer and modified Stockmayer simulations are presented in Figures 36 and 40, respectively. The maximum contribution from the coupling term is $\sim 3\%$ in the Stockmayer simulation and $\sim 8\%$ in the modified Stockmayer simulation. Initially the translational and rotational motions contribute approximately equally to the carbon atom displacement. In the modified Stockmayer simulation which represents hindered rotational motion, the translational contribution is larger than the rotational contribution for all times. In fact for $t \gtrsim 10^{-12}$ s the translational contribution is ~ 4 times the rotational one. On the other hand, in the Stockmayer simulation which represents free rotational motion there is a region near $t = 5 \times 10^{-13}$ s where the rotational contribution is larger than the translational one.

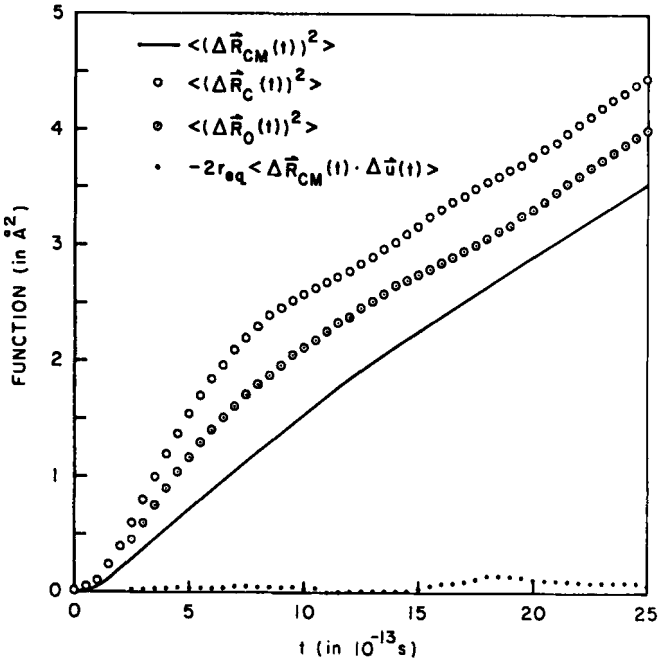

Fig. 35. The atomic displacement functions from the Stockmayer simulation of CO.

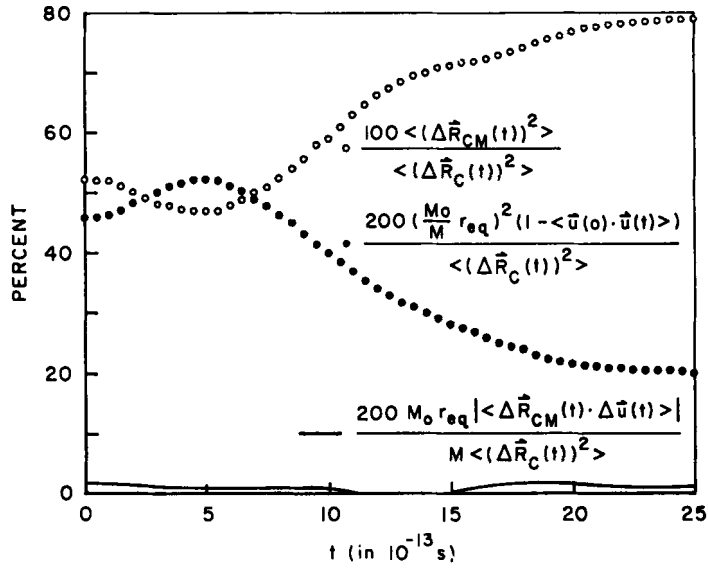

Fig. 36. Contributions to the mean square displacement of the C atom in Stockmayer simulation of CO.

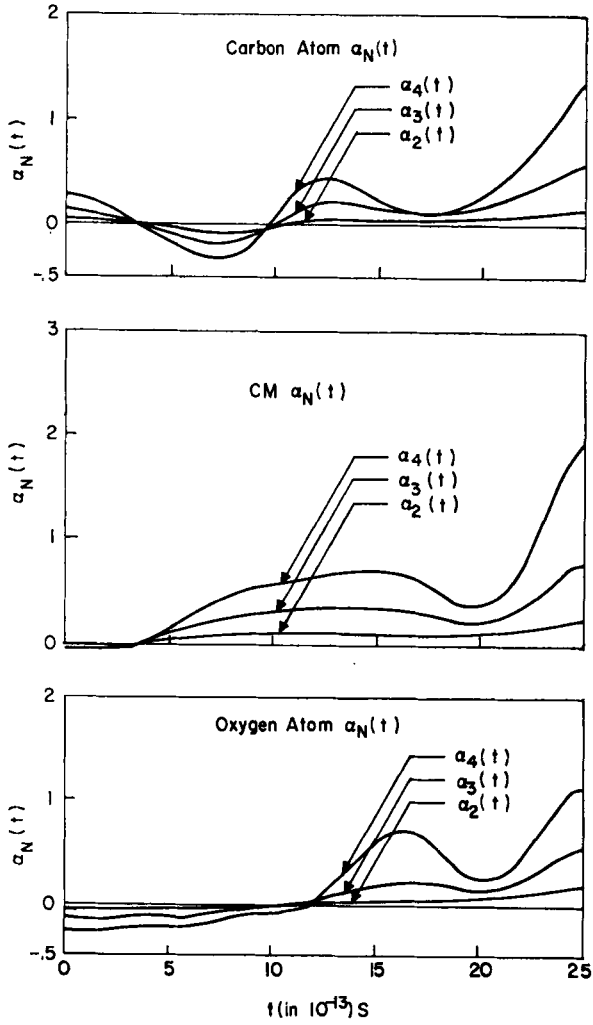

Fig. 37. Non-Gaussian behavior of $G_s^{(v)}(r, t)$ in the Stockmayer simulation of CO using 216 molecules.

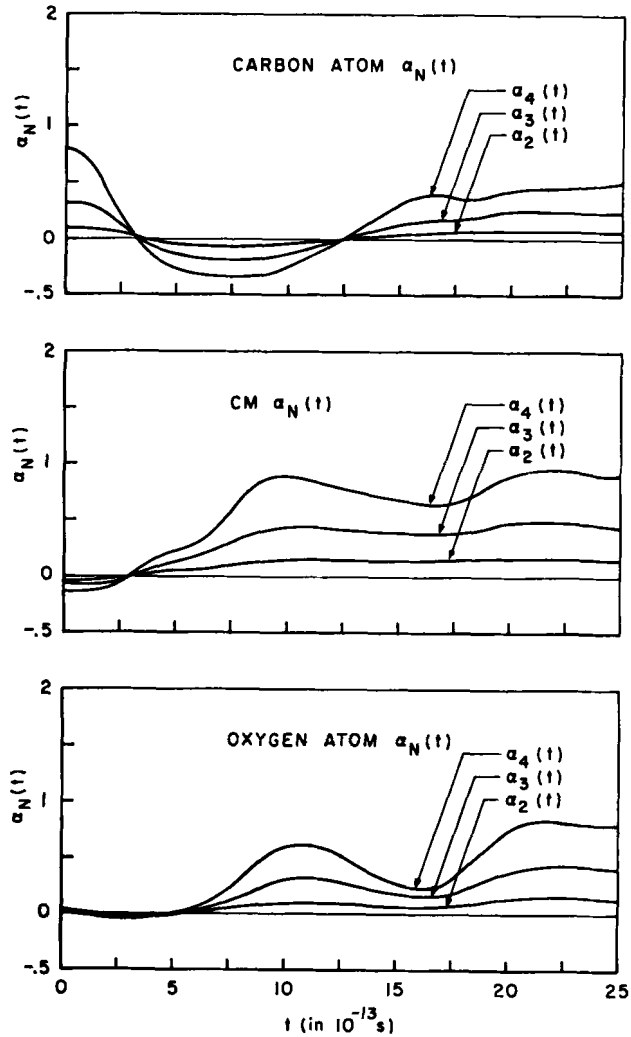

Fig. 38. Non-Gaussian behavior of $G_s^{(v)}(r, t)$ in the Stockmayer simulation of CO using 512 molecules.

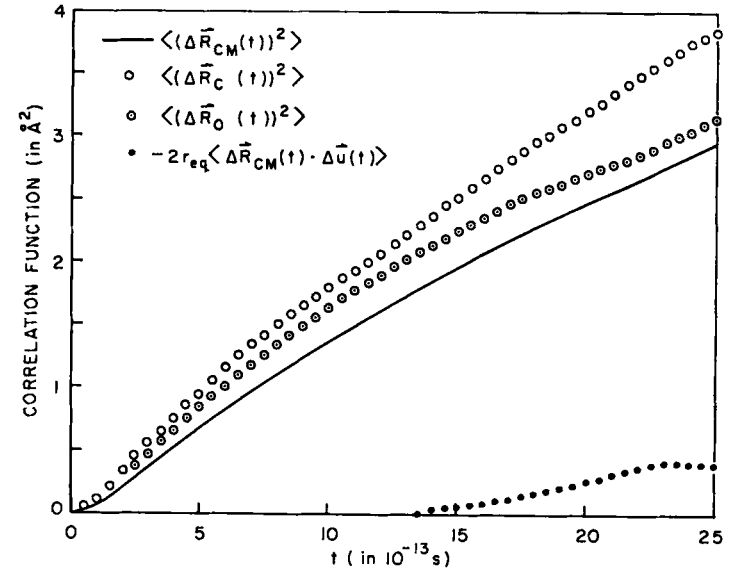

Fig. 39. The atomic displacement functions from the modified Stockmayer simulation of CO.

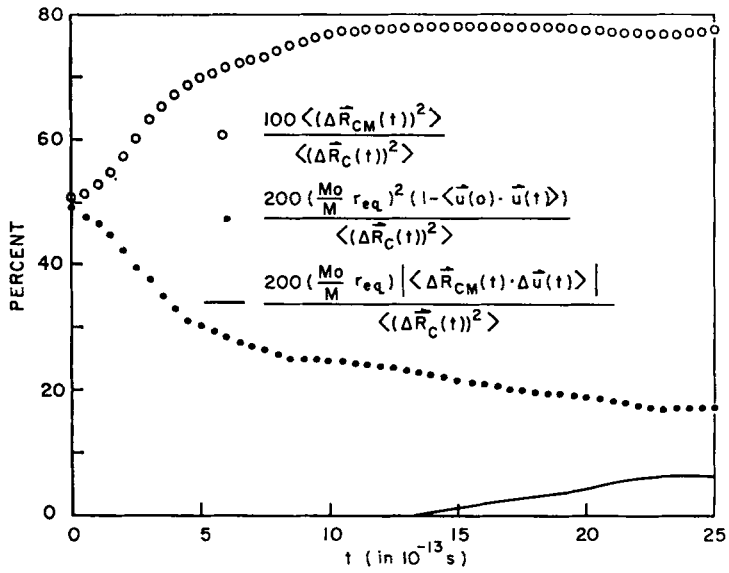

Fig. 40. Contributions to the mean square displacement of the C atom in the modified Stockmayer simulation of CO.

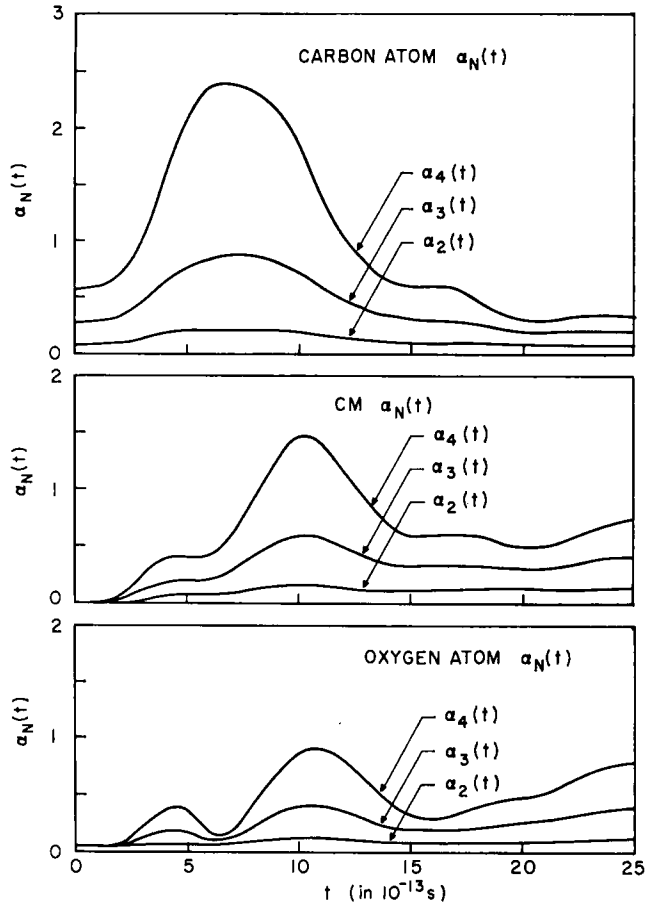

Fig. 41. Non-Gaussian behavior of $G_S^{(v)}(r, t)$ in the Stockmayer simulation of CO.

However, for long times the translational contribution is again larger than the rotational contribution in this simulation.

We shall now discuss the non-Gaussian behavior of our self-correlation functions. Rahman[32] pointed out that it is convenient to do this by introducing the coefficients $\alpha_N(t)$ which for $G_S(r, t)$ are defined as

$$\alpha_N(t) = \frac{\langle(\Delta \mathbf{R}_{\text{C.M.}}(t))^{2N}\rangle}{C_N\langle(\Delta \mathbf{R}_{\text{C.M.}}(t))^2\rangle^N} - 1 \qquad N = 2, 3, 4$$

where C_N is given by

$$C_N = \frac{1 \times 3 \times \cdots \times (2N+1)}{3^N}$$

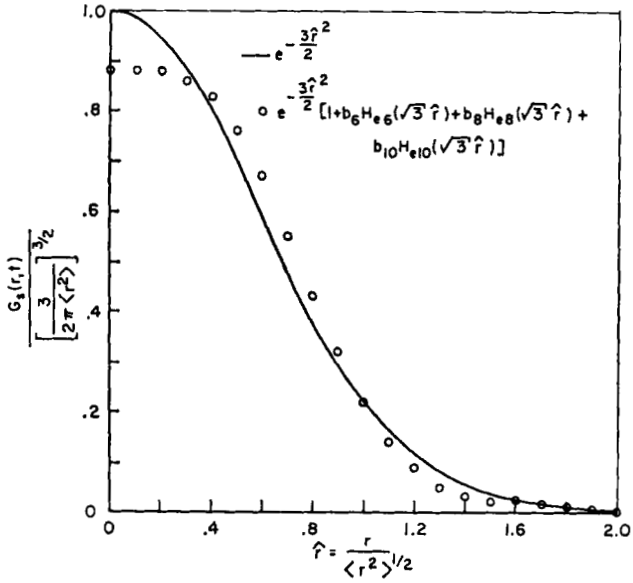

Fig. 42. $G_S(r, t)[3/2\pi\langle r^2\rangle]^{-3/2}$ for the C atom in the modified Stockmayer simulation of CO at $t = 7.75 \times 10^{1-3}$ s. $G_S(r, t)$ shows its maximum departure from a Gaussian at this time.

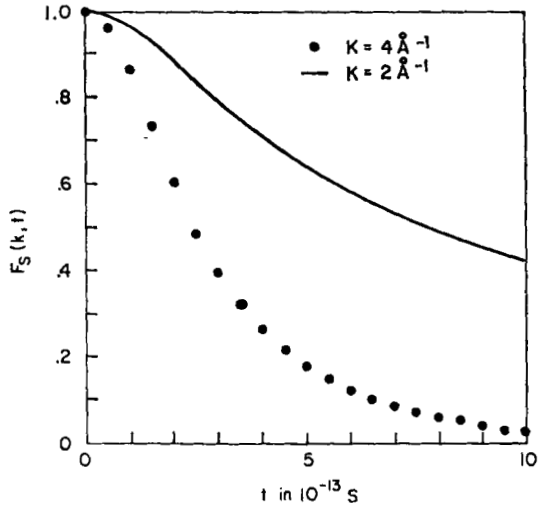

Fig. 43. Intermediate scattering functions for the C.M. motion of a CO molecule from the modified Stockmayer simulation.

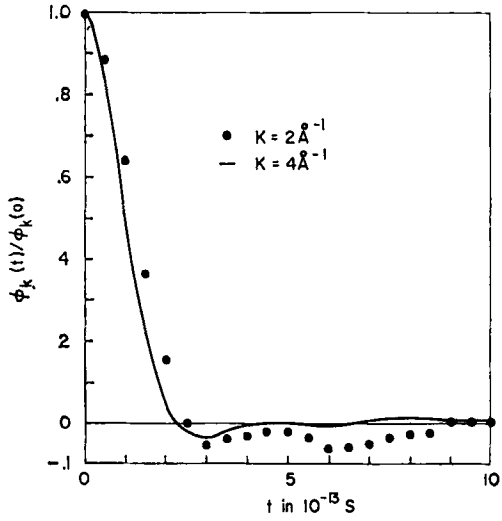

Fig. 44. Intermediate scattering memory functions for the C.M. motion of a CO molecule from the modified Stockmayer simulation.

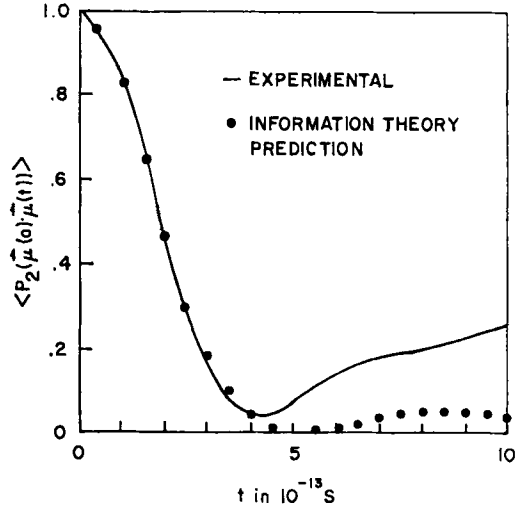

Fig. 45. $\langle P_2(\mu(0)\cdot\mu(t))\rangle$ from the Stockmayer simulation of CO and $\langle P_2(\mu(0)\cdot\mu(t))\rangle$ as predicted from information theory.

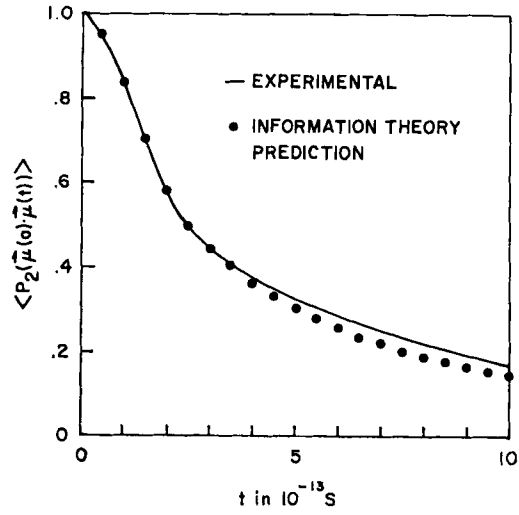

Fig. 46. $\langle P_2(\mu(0)\cdot\mu(t))\rangle$ from the modified Stockmayer simulation of CO and $\langle P_2(\mu(0)\cdot\mu(t))\rangle$ as predicted from information theory.

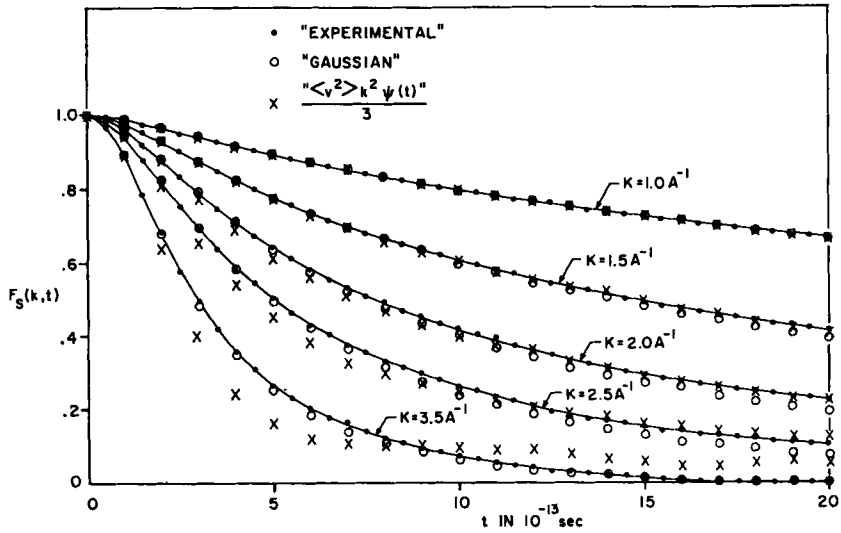

Fig. 47. Intermediate scattering functions for the C.M. motion of a CO molecule from the modified Stockmayer potential and from Eqs. (376) and (396).

The coefficients for $G_S^O(r, t)$ and $G_S^C(t, r)$ are defined in a similar manner. If a self-correlation function is a Gaussian, then the corresponding coefficients $\alpha_N(t)$ will vanish, For example, for short times $\langle(\Delta \mathbf{R}_{C.M.}(t))^{2N}\rangle = \langle V^{2N}\rangle t^{2N}$ and $\langle V^{2N}\rangle = C_N\langle \mathbf{V}^2\rangle^N$. Therefore, for short times the coefficients for $G_S(r,t)$ should vanish.

These coefficients are strongly dependent on the number of molecules used in the simulations. For example, Figures 37 and 38 present the coefficients from the Stockmayer simulation using 216 and 512 molecules, respectively. The corresponding coefficients from the 216 and 512 molecule systems differ substantially from each other. Therefore, we feel that these coefficients from our simulations are only qualitative indications of the non-Gaussian behavior of our self-correlation functions. Figure 41 presents the coefficients from the modified Stockmayer simulation. Comparing the results for the two simulations we see:

(1) None of the self-correlation functions is a Gaussian for all time.

(2) The self-correlation functions from the Stockmayer simulation are closer to Gaussians than those from the modified Stockmayer simulation.

(3) The modified Stockmayer coefficients are always nonnegative in contrast to the Stockmayer coefficients.

(4) The Stockmayer coefficients for $G_S(r, t)$ do not vanish for short times.

Rahman has shown that the Van Hove functions may be expanded in the Hermite polynomials,[32] $He_{2N}(x)$, where the coefficients in this expansion depend on the coefficients $\alpha_N(t)$. This expansion and its derivation are discussed in Appendix C. It is informative to compare the Gaussian approximation for $G_S^C(r, t)$ to this series expansion. The largest difference between $G_S^C(r, t)$ and the Gaussian approximation should occur at 7.75×10^{-13} s in the modified Stockmayer simulation. That is, at this time $G_S^C(r, t)$ shows its largest departure from a Gaussian. $G_S^C(\mathbf{r}, t)$ and its Gaussian approximation at 7.75×10^{-13} s are presented in Figure 42. For convenience $G_S^C(r, t)$ is plotted against $\hat{r} = r/[\langle(\Delta \mathbf{R}_C(t))^2\rangle 1/2]$. The largest difference between two curves is for small distances. That is, the Gaussian approximation favors small displacements of the C atoms more than $G_S^C(r, t)$ does.

VII. CONCLUSION

In this article the memory function formalism has been used to compute time-correlation functions. It has been shown that a number of seemingly disparate attempts to account for the dynamical behavior of time correlation functions, such as those of Zwanzig,[33,34] Mori,[42,43] and Martin,[16] are

completely equivalent. The memory function formalism yields time-correlation functions which are in qualitative and in some cases quantitative agreement with computer experiments. In all cases time-correlation functions are obtained which are consistent with physical intuition. For example, the velocity autocorrelation functions in liquids has a negative region which reflects the fact that the velocity of a fluid particle is on the average reversed by collision with the cage of nearest neighbors. Likewise, when the noncentral potential is large, the angular momentum correlation function has a negative region which reflects the fact that a fluid molecule's angular momentum is on the average reversed by a collision with the cage of nearest neighbors. When the noncentral potential is weak the torques are small and there is no such negative region in the angular momentum correlation function. This is as it should be. It is encouraging to note that the memory function approximations predict this behavior.

No attempt was made in this article to describe the few exact analytical calculations of time-correlation functions that exist. It is appropriate in closing, nevertheless, to mention some of the interesting papers that have appeared. Lebowitz and co-workers[83] have computed the velocity autocorrelation function, and the Van Hove space time correlation functions for a one dimensional system of hard rods. Nossal[84] has computed the classical velocity autocorrelation function of a particle in a one-dimensional box. Recently Kinsey, Deutch, and Silbey have determined the quantum-mechanical velocity autocorrelation function of a particle in a one-dimensional box and have analyzed recurrence times and the semiclassical limit.[85] Fixman and Rider[86] have determined classical orientational time-correlation functions, and Steele[87] has analyzed their quantum-mechanical counterparts. Lastly, Zwanzig[88] has presented an analysis of the velocity correlation function based on a generalization of the Navier-Stokes equation with frequency-dependent viscosity coefficients.

APPENDIX A. Numerical Integration of Differential Equations

This appendix contains a few remarks on the numerical integration of the large systems of differential equations dealt with in the dynamics calculations. There have been a number of general numerical methods or algorithms developed for integrating such systems.[89] Therefore one problem in solving these equations is finding the particular algorithm which is best suited to them. We used the following criteria in making our selection of such an algorithm:

(1) It must use a minimum amount of computer storage to integrate a given number of differential equations. This was a major consideration

because such a method would also maximize the number of molecules that could be followed in the dynamics calculations. This would in turn minimize the periodic boundary effects on calculated properties such as autocorrelation functions, etc.

(2) It must minimize the computer time needed to get the solutions to a given point in real time. This was purely an economic consideration.

(3) It must be stable. That is, the numerical solutions must not diverge exponentially with time from the true solutions.

(4) It must minimize the error in the solutions in getting to a given point in real time.

For convenience, consider the equations of motion for a single particle of mass M moving in one dimension and acted on by a force $g(x, t)$:

$$\frac{dx}{dt} = V \qquad X(t_0) = X_0 \tag{A.1}$$

$$\frac{dV}{dt} = \frac{1}{M} g(x, t) = f(x, t) \qquad V(t_0) = V_0 \tag{A.2}$$

Let $x(t)$ and $V(t)$ be the actual solutions to these differential equations. In general a given algorithm will replace these differential equations by a particular set of difference equations. These difference equations will then give approximate values of $x(t)$ and $V(t)$ at discrete, equally spaced points in time: $t_1, t_2, \ldots, t_n$ where $t_{j+1} = t_j + \Delta t$. The differences between the solutions to the difference equations at t_N and the solutions to the differential equations at t_N depend critically on the time step Δt. If Δt is too large, the system of difference equations may be unstable or be in error due to truncation effects. On the other hand, if Δt is too small, the solutions to the difference equations may be in error due to the accumulation of machine rounding of intermediate results.

In our search for a suitable algorithm, we tested four different integration procedures. The general analysis leading to each of these procedures is discussed by Ralston and Wilf.[47] The first we tried was used by Verlet in his study of liquid argon.[44] It replaces Eq. (A.1) and (A.2) by

$$X_{N+1} = -X_{N-1} + 2X_N + \Delta t^2 f(X_N, t_N) + \theta(\Delta t^4) \tag{A.3}$$

$$V_N = (X_{N+1} - X_{N-1})/2\Delta t + \theta(\Delta t^2) \tag{A.4}$$

$\theta(\Delta t^N)$ implies the truncation error in this formula is proportional to Δt^N. This method only requires storage for X_N, X_{N-1}, and $f(X_N, t_N)$. However, Eq. (A.4) can contribute machine-rounding errors to V_N if Δt and the floating point word length of X_N and X_{N-1} are small. Verlet used a CDC

6600 for his work which has a word length of 60 bits in contrast to our machine, an IBM 7094, which has a word length of 36 bits. Therefore our velocities would suffer more from this problem than his. This method is not self-starting, i.e., one needs both X_0 and X_1 to start. A non self-starting algorithm such as this requires a second algorithm to get its auxiliary initial values. In this case, a Taylor's series expansion of X around X_0 would probably suffice to get X_1. A non self-starting method used to obtain velocities presents extra difficulties in the equilibration phase of dynamics calculations. During this phase, the velocities are changed frequently. This implies that after every velocity change the second algorithm must be used to obtain new auxiliary values before equilibration can proceed. Verlet's method requires only one derivative evaluation per step. This latter property is a decided advantage since most of the computer time used in these calculations is for derivative evaluations.

The second method we tried was used by Rahman[32] in his original study of argon. It replaces Eqs. (A.1) and (A.2) by

$$\bar{X}_{N+1} = X_{N-1} + 2\Delta t V_N + \theta(\Delta t^3) \tag{A.5}$$

$$\bar{V}_{N+1} = V_{N-1} + 2\Delta t f(X_N, t_N) + \theta(\Delta t^3) \tag{A.6}$$

$$X_{N+1} = X_N + \tfrac{1}{2}\Delta t[V_N + \bar{V}_{N+1}] + \theta(\Delta t^3) \tag{A.7}$$

$$V_{N+1} = V_N + \tfrac{1}{2}\Delta t[f(X_N, t_N) + f(\bar{X}_{N+1}, t_{N+1})] + \theta(\Delta t^3) \tag{A.8}$$

This method is not self-starting and requires two derivative evaluations per step. It also requires storage for X_{N-1}, X_N, V_{N-1}, V_N, $f(X_N, t_N)$, and $f(X_{N+1}, t_{N+1})$.

The third method we tried replaces Eqs. (A.1) and (A.2) by[47]

$$X_{N+1} = X_{N-3} + \tfrac{4}{3}\Delta t[2V_N - V_{N-1} + 2V_{N-2}] + \theta(\Delta t^5) \tag{A.9}$$

$$V_{N+1} = V_{N-3} + \tfrac{4}{3}\Delta t[2f(X_N, t_N) - f(X_{N-1}, t_{N-1}) + 2f(X_{N-2}, t_{N-2})] + \theta(\Delta t^5) \tag{A.10}$$

This method at first looked very attractive because it has a very small truncation error and requires only one derivative evaluation per step. However, it requires much more storage than any of the other methods and is not self-starting.

The final method we tried is the Runga-Kutta-Gill algorithm[47] which replaces Eq. (A.2) by

$$V_{N+1} = V_N + \tfrac{1}{6}K_1 + \tfrac{1}{3}(1 - \sqrt{1/2})K_2 + \tfrac{1}{3}(1 + \sqrt{1/2})K_3 + \tfrac{1}{6}K_4 + \theta(\Delta t^5) \tag{A.11}$$

where

$$K_1 = \Delta t f(X_N, t_N) \tag{A.12}$$

$$K_2 = \Delta t f\left(X_N + \tfrac{1}{2}K_1, t_N + \frac{\Delta t}{2}\right) \tag{A.13}$$

$$K_3 = \Delta t f(X_N + (-\tfrac{1}{2} + \sqrt{\tfrac{1}{2}})K_1 + \left(1 - \sqrt{\tfrac{1}{2}}\right)K_2, t_N + \frac{\Delta t}{2}\Big) \tag{A.14}$$

$$K_4 = \Delta t f(X_N - \sqrt{\tfrac{1}{2}}k_2 + (1 + \sqrt{\tfrac{1}{2}})K_2, t_{N+1}) \tag{A.15}$$

It replaces Eq. (A.1) by a similar formula for X_{N+1}. The Runga-Kutta-Gill method can be programmed to minimize storage and rounding error accumulation.[47] When this is done, it requires storage equivalent to X_N, X_{N-1}, V_N, V_{N-1}, and $f(X_N, t_N)$. It has a very small truncation error and is self-starting. However, it requires 4 derivative evaluations per step.

Each of these algorithms has a different range of time steps Δt which yields stable solutions to the differential equations. We tried to find each algorithm's stability region by using its set of difference equations to integrate the equations of motion for two CO molecules. These molecules were assumed to interact via the Stockmayer potential described previously. We integrated these equations in double precision using a variety of initial conditions and times steps. It was found that an unstable solution to these differential equations quickly lead to an exponential elongation of the CO bond length. This suggested that we could get an estimate of an algorithm's stability region by considering the solutions to

$$\frac{d^2q}{dt^2} = -\frac{Kq}{\mu} \tag{A.16}$$

where K is the CO molecule's vibrational force constant, μ is its reduced mass, and q is the deviation in the internuclear separation from its equilibrium value. This does indeed give a fairly good estimate. For example, consider Verlet's method applied to Eq. (A.16)

$$q_{N+1} + q_{N-1} + \left[\frac{K}{\mu}\Delta t^2 - 2\right]q_N = 0 \tag{A.17}$$

The solution to this difference equation is

$$q_N = A[b_+]^N + B[b_-]^N \tag{A.18}$$

where A and B depend on the initial boundary conditions and the accumulated error up to the Nth step. $b_\pm$ is given by

$$b_\pm = \frac{2\mu - K\Delta t^2 \pm \Delta t(K^2\Delta t^2 - 4K\mu)^{1/2}}{2\mu} \tag{A.19}$$

Since A and B are not necessarily zero, this difference equation will be stable only if $|b_{\pm}| \leq 1$ or equivalently only if $\Delta t \leq 2(\mu/K)^{1/2}$. For CO this implies Δt has to be less than or equal 4.89×10^{-15} s. Verlet's method gave stable solutions to the equations of motion for $\Delta t = 2.5 \times 10^{-15}$ s but unstable solutions for $\Delta t = 5 \times 10^{-15}$ s. This is in remarkable agreement with the above results.

The "experimentally" determined stability regions for Rahman's method, the Runga-Kutta-Gill method, and the third method were $\Delta t \gtrsim 2.5 \times 10^{-15}$ s, $\Delta t \gtrsim 5 \times 10^{-15}$ s, and $\Delta t \gtrsim 1 \times 10^{-15}$ s, respectively The Runga-Kutta-Gill method with $\Delta t = 5 \times 10^{-15}$ s was chosen to be used in the dynamics calculations because:

(1) It took less machine time and used fewer storage locations than the 3rd method.

(2) It took less storage than Rahman's and was self-starting.

(3) It was more accurate than Verlet's method in terms of energy conservation. For example, in one experiment in which the equations of motion were integrated from $t = 0$ to $t = 3.75 \times 10^{-12}$ s, the Runga-Kutta-Gill method with $\Delta t = 5 \times 10^{-15}$ s conserved energy to $7.31 \times 10^{-6}\%$ while Verlet's method with $\Delta t = 2.5 \times 10^{-15}$ s conserved energy to $3.96 \times 10^{-3}\%$. In all of these experiments, both of these methods conserved the total momenta to all 8 figures printed.

APPENDIX B. The Numerical Solution of the Volterra Equation

The general problem is to solve the Volterra equation

$$-\frac{dy}{dt} = \int_0^t K_y(t')y(t - t')\,dt' \tag{B.1}$$

for either $y(t)$ given $K_y(t)$ or $K_y(t)$ given $y(t)$.

$$y(t) = \frac{\langle \alpha(0)\alpha(t) \rangle}{\langle \alpha^2 \rangle} \tag{B.2}$$

is the normalized autocorrelation function for the dynamical property $\alpha(t)$ and $K_y(t)$ is the memory function for that property. Specifically we are considering $y(t)$ to be either the velocity or the angular momentum or the dipolar autocorrelation function. However, the general numerical method outlined here is applicable to the solution of the Volterra equation for any autocorrelation function.

The following properties of $y(t)$ and $K_y(t)$ are exploited in solving the general problem:

(1) $y(t)$ is an even function in time and may be expanded for short times as

$$y(t) = 1 - \frac{1}{2}\frac{\langle(\dot{\alpha})^2\rangle}{\langle\alpha^2\rangle}t^2 + \frac{1}{4!}\frac{\langle(\ddot{\alpha})^2\rangle}{\langle\alpha^2\rangle}t^4 \tag{B.3}$$

(2) $K_y(t)$ is also an even function and may be expanded for short times as

$$K_y(t) = \frac{\langle(\dot{\alpha})^2\rangle}{\langle\alpha^2\rangle} + \frac{1}{2}\left\{\left[\frac{\langle(\dot{\alpha}^2)\rangle}{\langle\alpha^2\rangle}\right]^2 - \frac{\langle(\ddot{\alpha})^2\rangle}{\langle\alpha^2\rangle}\right\}t^2 \tag{B.4}$$

The important point to note here is that the 2nd moment of $K_y(t)$ depends on the 2nd and 4th moments of $y(t)$. The 2nd moments of each of the three previously mentioned autocorrelation functions may be calculated from ensemble averages of appropriate functions of the positions, velocities, and accelerations created in the dynamics calculations. Likewise, the 4th moment of the dipolar autocorrelation function may also be calculated in this manner. However the 4th moments of the velocity and angular momentum correlation functions depend on the derivative with respect to time of the force and torque acting on a molecule and, hence, cannot be evaluated directly from the primary dynamics information. Therefore, these moments must be calculated in another manner before Eq. (B.3) may be used.

K_y *from* $y(t)$

Consider first the problem of developing $K_y(t)$ from $y(t)$. $y(t)$ from the molecular dynamics calculations is tabulated for the equally spaced times

$$t_i = i\Delta t \qquad i = 0, \ldots, 499 \tag{B.5}$$

where $t = 0.05$ with time in units of 10^{-13} s. Therefore, it is necessary to determine $K_y(t_i)$ $i = 0, \ldots, 499$ from $y(t_i)$ $i = 0, \ldots, 499$. It is more advantageous in terms of stability to do this by considering the first derivative of Eq. (B.1) rather than Eq. (B.1) itself:

$$K_y(t_i) = -\left.\frac{d^2y}{dt^2}\right|_{t_i} - \int_0^{t_i} K_y(t')\frac{dy}{dt'}(t_i - t')\,dt' \qquad i = 0, \ldots, 499 \tag{B.6}$$

Approximating the integral on the right-hand side of Eq. (B.6) by a closed quadrature formula[89] such as the trapezoidal rule, one obtains.

$$K_y(t_i) = -\left.\frac{d^2y}{dt^2}\right|_{t_i} - \Delta t\sum_{j=0}^{i}\omega_j K_y(t_j)\frac{dy}{dt}(t_i - t_j) \tag{B.7}$$

$$i = 0, \ldots, 499$$

where ω_j is the weight assigned to the jth point of the integrand. ω_j will depend on the particular formula used to perform the integration. In this form the right-hand side of Eq. (B.7) depends only on values of $K_y(t_j)$ for $t_j \leq t_{i-1}$ because

$$\omega_i K_y(t_i) \frac{dy}{dt}(t_0) = 0 \tag{B.8}$$

However, in order to actually use Eq. (B.7) one needs:

(1) $dy/dt|_{t_i}$ and $d^2y/dt^2|_{t_i}$ for $t_i \quad i = 1, \ldots, 499$

(2) Accurate starting values of $K_y(t)$, i.e.,

$$K_y(t_0),\ K_y(t_1),\ K_y(t_2),\ K_y(t_3)$$

(3) A convenient and accurate quadrature formula.

The derivatives of $y(t)$ were obtained by two different methods: one used for short times and the other used for long times. For short times, $0 \leq t_i \leq t_M$, $y(t)$ was approximated by Eq. (B.3). If the 4th moment of $y(t)$ was not known, then $y(t)$ was first fit via least squares to Eq. (B.3) to obtain $\langle(\ddot{\alpha}^2)\rangle/\langle\alpha^2\rangle$. 4th moments of the velocity and angular momentum autocorrelation functions determined this way are tabulated in Table IV. The error quoted for each of these values of $\langle(\ddot{\alpha})^2\rangle/\langle\alpha^2\rangle$ is the statistical error from the least square fit which amounts to $\sim 10\%$. The number of points used in the least squares process in general depends on how fast the autocorrelation function changes around t_0. For the velocity and angular momentum autocorrelation functions, 8 points were used to determine $\langle(\ddot{\alpha})^2\rangle/\langle\alpha^2\rangle$. $dy/dt|t_i$ and $d^2y/dt^2|t_i$ for $t_0, \ldots, t_4$ were then calculated by evaluating Eq. (B.3) at the points $t_0, \ldots, t_4$. For long times, $t_5 \leq t_i \leq t_{499}$, $y(t)$ was assumed to be represented by the interpolating polynomial for $y(t)$:[89]

$$y^*_i(t) = \sum_{N=0}^{6} a_N{}^i t^N \tag{B.9}$$

At each point t_i, $t_5 \leq t_i \leq t_{497}$, the coefficients $a_N{}^i$ were determined such that

$$y^*_i(t_j) = y(t_j) \qquad j = i-3, i-2, \ldots, i+3 \tag{B.10}$$

In other words, the exact form of the interpolating polynomials varied from point to point. $dy/dt|t_i$ and $d^2y/dt^2|t_i$ for $t_5 \leq t_i \leq t_{499}$ were then calculated by evaluating the first and second derivatives of the appropriate interpolating polynomial, $y^*_i(t)$.

$K_y(t_0)$ or $\langle(\ddot{\alpha})^2\rangle/\langle\alpha^2\rangle$ was calculated directly from appropriate ensemble averages of the molecular dynamics information (see Tables II, III, and V). $K_y(t_1)$, $K_y(t_2)$, and $K_y(t_3)$ were determined by using Day's[90] starting method applied to Eq. (B.3). After applying Day's method and exploiting the odd property of dy/dt, one obtains three linear equations involving $K_y(t_1)$, $K_y(t_2)$, and $K_y(t_3)$ which can easily be solved:

$$K_y(t_1) = -\left.\frac{d^2y}{dt^2}\right|_{t_1} - \frac{\Delta t}{24}\left[\left.\frac{dy}{dt}\right|_{t_1}[9K_y(t_0) + 5K_y(t_2)] - K_y(t_3)\left.\frac{dy}{dt}\right|_{t_2}\right] \tag{B.11}$$

$$K_y(t_2) = -\left.\frac{d^2y}{dt^2}\right|_{t_2} - \frac{\Delta t}{3}\left[K_y(t_0)\left.\frac{dy}{dt}\right|_{t_2} + 4K_y(t_1)\left.\frac{dy}{dt}\right|_{t_1}\right] \tag{B.12}$$

$$K_y(t_3) = -\left.\frac{d^2y}{dt^2}\right|_{t_3} - \frac{3\,\Delta t}{8}\left[K_y(t_0)\left.\frac{dy}{dt}\right|_{t_3} + 3\left[K_y(t_1)\left.\frac{dy}{dt}\right|_{t_2} + K_y(t_2)\left.\frac{dy}{dt}\right|_{t_1}\right]\right] \tag{B.13}$$

Day's method essentially replaces the integral in Eq. (B.6) by a different quadrature formula at each of the times t_1, t_2, and t_3. Each of these quadrature formulas approximates its appropriate integral with an error which is $\theta(\Delta t^5)$. Therefore, this method gives very accurate starting values for $K_y(t_1)$, $K_y(t_2)$, and $K_y(t_3)$.

For $K_y(t_i)$, $t_4 \leq t_i \leq t_{499}$, the integral in Eq. (B.6) was approximated by the Gregory formula.[90,91]

$$\begin{aligned}\frac{1}{\Delta t}\int_0^{t_i} K_y(t')\frac{dy}{dt'}(t_i - t')\,dt' &= \tfrac{1}{2}K_y(t_0)\left.\frac{dy}{dt}\right|_{t_i} + \sum_{N=1}^{i-1} K_y(t_N)\left.\frac{dy}{dt}\right|_{t_i-N} \\ &+ \frac{1}{12}\left[K_y(t_1)\left.\frac{dy}{dt}\right|_{t_{i-1}} - K_y(t_0)\left.\frac{dy}{dt}\right|_{t_i} + K_y(t_{i-1})\left.\frac{dy}{dt}\right|_{t_1}\right] \\ &- \frac{1}{24}\left[K_y(t_2)\left.\frac{dy}{dt}\right|_{t_{i-2}} - 2K_y(t_1)\left.\frac{dy}{dt}\right|_{t_{i-1}} + K_y(t_0)\left.\frac{dy}{dt}\right|_{t_i}\right. \\ &\left. - 2K_y(t_{i-1})\left.\frac{dy}{dt}\right|_{t_i} + K_y(t_{i-2})\left.\frac{dy}{dt}\right|_{t_2}\right]\end{aligned} \tag{B.14}$$

The Gregory formula used here has the advantage that it requires no special considerations as to whether or not the integral involves an odd or even number of points, in contrast to other integration formulas such as the composite Simpson's rule.

The computational scheme outlined above was tested with the testing set

$$K_y^T(t_i) = e^{-t_i/2} \tag{B.15}$$

$$y_T(t_i) = e^{-t_i/2}\left[\cos\left[\frac{\sqrt{3}}{2}t_i\right] + \frac{\sqrt{3}}{3}\sin\left[\frac{\sqrt{3}}{2}t_i\right]\right] \qquad i = 0, \ldots, 499 \tag{B.16}$$

which behaves approximately like the autocorrelation functions obtained from the dynamics calculations. However, this particular testing function does not satisfy Eq. (B.3). Therefore, in order to get $dy/dt|_{t_i}^T$ and $d^2y/dt^2|_{t_i}^T$ for short times, $y(t)$ was approximately by the interpolating polynomial

$$y^*_T(t) = a_0 + \sum_{M=2}^{7} a_M t^M \tag{B.17}$$

where the coefficients a_M were determined such that

$$y^*_T(t_i) = y_T(t_i) \qquad i = 0, \ldots, 6 \tag{B.18}$$

$K_y^T(t_i)$ for $t_i \leq 10^{-12}$ was recovered to within a maximum absolute error $\lesssim 0.0009$.

$y(t)$ from $K_y(t)$

The problem of developing $y(t)$ numerically from $K_y(t)$ is much simpler than the reverse problem. One reason for this is that $K_y(t)$ is usually a two- or three-parameter, analytic approximation to the true $K_y(t)$ for the system under consideration. Therefore, one need not worry about statistical errors in $K_y(t)$. The following scheme was used in developing $y(t)$ from $K_y(t)$ which depend on properties of $y(t)$ and $K_y(t)$ given in Eqs. (B.1), (B.3), and (B.4).

$$y(t_0) = 1 \tag{B.19}$$

$$y(t_1) = 1 - \tfrac{1}{2}K_y(t_0)t_1^2 \tag{B.20}$$

$$y(t_2) = 1 - (\Delta t)^2[K_y(t_1) + K_y(t_0)y(t_1)] \tag{B.21}$$

$$y(t_{i+1}) = y(t_{i-1}) - (\Delta t)^2[K_y(t) + K_y(t_0)y(t_i)] - 2(\Delta t)^2 \sum_{j=2}^{i-1} K_y(t_j)y(t_i - t_j) \qquad 2 \leq i \tag{B.22}$$

Equations (B.21) and (B.22) involve approximating $dy/dt|_{t_i}$ by

$$\frac{y(t_{i+1}) - y(t_{i-1})}{2\Delta t}$$

and by approximating the integral in Eq. (B.1) by the trapezoidal rule.

The above scheme was tested by using the testing set given in Eq. (B.15) and (B.16). $y(t_i)$ for $t_i \leq 10^{-12}$ s was recovered to within a maximum absolute error of $\lesssim 0.0003$. All computations for both schemes were done in double precision on an IBM 360.

The error in $K_y(t)$ generated in the first scheme from the experimental autocorrelation function was also examined by taking the generated $K_y(t)$ and using it as input to the 2nd scheme to try to recover the original autocorrelation function. The original autocorrelation functions were all recovered in this manner within a maximum absolute error $\lesssim 0.002$ for all times. $t \leq 10^{-12}$ s.

APPENDIX C. Properties of the Polynomials $\mathrm{He}_N(x)$

This appendix gives some of the properties of the Hermite polynomials, $\mathrm{He}_N(x)$. These polynomials form a basis set for Rahman's[32] expansion of $G_S^{(v)}(r, t)$ and play a fundamental role in the discussion of the non-Gaussian behavior of this latter function. Brief sketches of this expansion and of the calculation of $F_S^{(v)}(K, t)$ are also given.

The polynomials $\mathrm{He}_N(x)$ are defined by[92]

$$\mathrm{He}_N(x) = (-1)\, e^{(x^2/2)} \frac{d^N}{dx^N} [e^{(-x^2/2)}] \tag{C.1}$$

They are related to the Hermite polynomials $\mathrm{H}_N(x)$, which are the solutions to the Schrodingen equation for a harmonic oscilator by

$$\mathrm{He}_N(x) = 2^{-N/2}\, \mathrm{H}_N\left(\frac{x}{\sqrt{2}}\right) \tag{C.2}$$

$$\mathrm{H}_N(x) = 2^{N/2} \mathrm{He}_N(x\sqrt{2}) \tag{C.3}$$

$\mathrm{H}_N(x)$ for $N = 0, \ldots, 10$ are given in Pauling and Wilson.[94] $\mathrm{He}_N(x)$ satisfy the recursion relations

$$\mathrm{He}_0(x) = 1 \tag{C.4}$$

$$\mathrm{He}_1(x) = x \tag{C.5}$$

$$\mathrm{He}_{N+1}(x) = x\mathrm{He}_N(x) - N\mathrm{He}_{N-1}(x) \qquad N \geq 1 \tag{C.6}$$

They also satisfy the orthogonality relation[92]

$$\int_{-\infty}^{\infty} \mathrm{He}_N(x)\, e^{(-x^2/2)}\, \mathrm{He}_M(x)\, dx = (2\pi)^{1/2} N! \delta_{M,N} \tag{C.7}$$

Finally the first six even polynomials used in the expansion of $G_S^{(v)}(r, t)$ are

$$\mathrm{He}_0(x) = 1 \tag{C.8}$$

$$\mathrm{He}_2(x) = x^2 - 1 \tag{C.9}$$

$$\mathrm{He}_4(x) = x^4 - 6x^2 + 3 \tag{C.10}$$

$$\mathrm{He}_6(x) = x^6 - 15x^4 + 45x^2 - 15 \tag{C.11}$$

$$\mathrm{He}_8(x) = x^8 - 28x^6 + 210x^4 - 420x^2 + 105 \tag{C.12}$$

$$\mathrm{He}_{10}(x) = x^{10} - 45x^8 + 630x^6 - 3150x^4 + 4725x^2 - 945 \tag{C.13}$$

The expansion of $G_S^{(v)}(r, t)$ in the polynomials $\mathrm{He}_N(x)$ proceeds by determining the coefficients $b_{2N}^{(v)}(t)$ in the expression[32]

$$G_S^{(v)}(r, t) = \sum_{N=0}^{5} b_{2N}^{(v)}(t)\, \mathrm{e}^{(-x^2/2)}\, \mathrm{He}_N(x) \tag{C.14}$$

where $x^2 = 3r^2/\langle(\Delta \mathbf{r}^{(v)}(t))^2\rangle$ and $\Delta \mathbf{r}^{(v)}(t) = \mathbf{r}^{(v)}(t) - \mathbf{r}^{(v)}(0)$.

These coefficients are determined such that the following five moment relations on $G_S^{(v)}(r, t)$ are satisfied:

$$4\pi \int_0^\infty r^2\, G_S(r, t)\, dr = 1 \tag{C.15}$$

$$4\pi \int_0^\infty r^{2M+2}\, G_S(r, t) = \langle(\Delta \mathbf{r}^{(v)}(t))^{2M}\rangle \qquad M = 1, 2, 3, 4 \tag{C.16}$$

Using the properties of $\mathrm{He}_N(x)$ given above and a great deal of algebra, one obtains Rahman's[32] expressions for $b_{2N}^{(v)}(t)$:

$$b_0^{(v)}(t) = 1 \tag{C.17}$$

$$b_2^{(v)}(t) = b_4^{(v)}(t) = 0 \tag{C.18}$$

$$b_6^{(v)}(t) = \frac{1}{48}\, \alpha_2^{(v)}(t) \tag{C.19}$$

$$b_8^{(v)}(t) = \frac{1}{384}\, [\alpha_3^{(v)}(t) - 4\alpha_2^{(v)}(t)] \tag{C.20}$$

$$b_{10}^{(v)}(t) = \frac{1}{3840}\, [\alpha_4^{(v)}(t) - 5\alpha_3^{(v)}(t) + 10\alpha_2^{(v)}(t)] \tag{C.21}$$

where

$$\alpha_N^{(v)}(t) = \frac{\langle(\Delta \mathbf{r}^{(v)}(t))^{2N}\rangle}{C_N \langle(\Delta \mathbf{r}^{(v)}(t))^2\rangle^N} - 1 \tag{C.22}$$

and $C_N = 1 \times 3 \times 5 \times \cdots (2N + 1)/3^N$.

The intermediate scattering function for an isotropic system is given by

$$F_S^{(v)}(k, t) = \frac{4\pi}{k} \int_0^\infty r \sin [kr] G_S^{(v)}(r, t)\, dr \tag{C.23}$$

Using Eq. (C.14) for $G^{(v)}(r, t)$ and the relation[32]

$$\int_0^\infty x e^{(-x_2/2)} \mathrm{He}_{2N}(x) \sin Bx\, dx = (-1)^{N+1} B[2NB^{2N-2} - B^{2N}] e^{(-B^2/2)} \tag{C.24}$$

One obtains Rahman and Nijboer's[95] expression for $F_S^{(v)}(k, t)$:

$$F_S^{(v)}(k, t) = e^{(-y^2)} \sum_{N=0}^{5} a_{2N}^{(v)}(t) y^{2N} \tag{C.25}$$

where

$$y^2 = \frac{k^2 \langle (\Delta \mathbf{r}^{(v)}(t))^2 \rangle}{6} \tag{C.26}$$

$$a_0^{(v)}(t) = 1 \tag{C.27}$$

$$a_2^{(v)}(t) = 0 \tag{C.28}$$

$$a_4^{(v)}(t) = 24 b_6^{(v)}(t) = \frac{\alpha_2^{(v)}(t)}{2!} \tag{C.29}$$

$$a_6^{(v)}(t) = -[8 b_6^{(v)}(t) + 64 b_8^{(v)}(t)] = \frac{-1}{3!} [\alpha_3^{(v)}(t) - 3\alpha_2^{(v)}(t)] \tag{C.30}$$

$$a_8^{(v)}(t) = 16[b_8^{(v)}(t) + 10 b_{10}^{(v)}(t)] = \frac{1}{4!} [\alpha_4^{(v)}(t) - 4\alpha_3^{(v)}(t) + 6\alpha_2^{(v)}(t)] \tag{C.31}$$

$$a_{10}^{(v)}(t) = -32 b_{10}^{(v)}(t) = -\frac{1}{5!} [\alpha_4^{(v)}(t) - 5\alpha_3^{(v)}(t) + 10\alpha_2^{(v)}(t)] \tag{C.32}$$

Acknowledgments

The work reported here was supported by grants from The Petroleum Research Fund of the American Chemical Society and the National Science Foundation. Without the cooperation of the Staff and the free use of the facilities of the Columbia University Computer Center, this work could never have been undertaken.

References

1. Y. Toyazawa, *Prog. Theoret. Phys. (Kyoto)*, **20**, 53 (1958).
2. J. Van Kranendonk, *On the Theory of Pressure-Broadening and Pressure-Induced Absorption*, Thesis, University of Amsterdam, Amsterdam, Holland, December 17, 1952.

3. A. Sjolander, in *Phonons and Phonon Interactions*, T. A. Bak, Ed., Benjamin, New York, 1964.
4. D. Pines and P. Nozieres, *The Theory of Quantum Liquids*, Benjamin, New York, 1966.
5. P. A. Egelstaff, *Thermal Neutron Scattering*, Academic Press, New York, 1965.
6. M. Blume, *Symposium of Inelastic Scattering of Neutrons by Condensed Systems*, Brookhaven National Laboratory, September 1965.
7. T. A. Litivitz and D. Settle, *J. Chem. Phys.*, **21**, 17 (1953).
8. A. Abragam, *The Principles of Nuclear Magnetism*, Oxford Univ. Press, London, 1961.
9. K. F. Herzfeld and T. A. Litivitz, *Absorption and Dispersion of Ultrasonic Waves*, Academic Press, New York, 1959.
10. S. R. De Groot and P. Mazur, *Non-Equilibrium Thermodynamics*, North-Holland, Amsterdam, 1962.
11. R. Kubo, *Lectures in Theoretical Physics*, Vol. I, Interscience, New York, 1961, pp. 120–203.
12. R. Zwanzig, *Ann. Rev. Phys. Chem.*, **16**, 67 (1965).
13. P. Mazur, *Cargese Lectures in Theoretical Physics*, Gordon and Breach, New York, 1966.
14. P. C. Martin, in *Statistical Mechanics of Equilibrium and Non-Equilibrium*, J. Merxner, Ed., North-Holland Amsterdam, 1965, p. 100.
15. R. G. Gordon, in *Advances in Magnetic Resonance*, Vol. 3, J. S. Waugh, Ed., Academic Press, New York, 1968, p. 1.
16. P. C. Martin, in 1967 *Les Houches Lectures*, Gordon and Breach, New York, 1968, p. 39; L. P. Kadanoff and P. C. Martin, *Ann. Phys. (N.Y.)*, **24**, 419 (1963).
17. E. Helfand, *Phys. Rev.*, **119**, 1 (1960).
18. Van Hove, L., *Phys. Rev.*, **95**, 249 (1954).
19. I. L. Fabelinsky, *Molecular Scattering of Light*, Plenum Press, New York, 1968.
20. R. Pecora, *J. Chem. Phys.*, **40**, 1604 (1964).
21. S. B. Dubin, J. H. Lunacek, and G. B. Benedek, *Proc. Natl. Acad. Sci., U.S.*, **57**, 1164 (1967).
22. R. D. Mountain, *J. Res. Natl. Bur. Std. A.*, **70**, 207 (1966).
23. B. J. Berne and H. L. Frisch, *J. Chem. Phys.*, **47**, 3675 (1967), B. J. Berne, J. M. Deutch, J. T. Hynes, and H. L. Frisch, *J. Chem. Phys.*, **49**, 2864 (1968).
24. B. J. Berne and R. Pecora, *J. Chem. Phys.*, **50**, 783 (1968).
25. L. Blum and Z. W. Salzburg, *J. Chem. Phys.*, **48**, 2292 (1968).
26. F. Perrin, *J. Phys. Radium*, **7**, 390 (1926).
27. T. Tao, *Biopolymers*, in press.
28. B. J. Berne, J. Jortner, and R. G. Gordon, *J. Chem. Phys.*, **47**, 1600 (1967).
29. B. J. Berne, R. G. Gordon and V. F. Sears, *J. Chem. Phys.*, **49**, 475 (1968).
30. P. Nelson, Ph.D. Thesis, Princeton Univ., 1966.
31. B. J. Alder and T. E. Wainwright, *J. Chem. Phys.*, **31**, 459 (1959).
32. A. Rahman, *Phys. Rev.*, **136**, A405 (1964).
33. R. Zwanzig, *Lectures in Theoretical Physics*, Vol. 3, Interscience, New York, 1961, pp. 135–141.
34. B. J. Berne, J. P. Boon, and S. A. Rice, *J. Chem. Phys.*, **45**, 1086 (1966).
35. R. Kubo, in *Reports on Progress in Physics*, Vol. 29, A. C. Stickland, Ed., Inst. of Phys., London, 1966, p. 255.
36. A. Moscowitz, *Advan. Chem. Phys.*, **4**, 67 (1962).

37. F. A. Kaempffer, *Concepts in Quantum Mechanics*, Academic Press, New York, 1965.
38. H. B. Callen and T. A. Welton, *Phys., Rev.*, **83**, 34 (1951).
39. H. M. Foley, *Phys. Rev.*, **69**, 616 (1946).
40. P. W. Anderson, *Phys. Rev.*, **76**, 647 (1949).
41. K. S. Singwi and A. Sjolander, *Phys. Rev.*, **120**, 1093 (1960).
42. H. Mori, *Prog. Theoret. Phys. (Kyoto)*, **33**, 423 (1965).
43. H. Mori, *Prog. Theoret. Phys. (Kyoto)*, **34**, 399 (1965).
44. L. Verlet, *Phys. Rev.*, **159**, 98 (1967).
45. G. Herzberg, *Molecular Spectra and Molecular Structure*, Vol. 1, Van Nostrand, New York, 1961.
46. H. Kahn, Atomic Energy Commission Report AECU-3259.
47. A. Ralston and H. Wilf, *Mathematical Methods for Digital Computers*, Wiley, New York, 1966.
48. J. Hirschfelder, C. Curtiss, and R. Bird, *Molecular Theory of Gases and Liquids*, Wiley, New York, 1954
49. T. Spurling and E. Mason, *J. Chem. Phys.*, **46**, 322 (1967).
50. B. Rosenblum, A. Nethercot, and C. Townes, *Phys. Rev.*, **109**, 400. (1958).
51. R. Gordon, *J. Chem. Phys.*, **44**, 576 (1966).
52. G. Castagnoli, *Physica*, **30**, 937 (1964).
53. A. Rahman, "A Comparative Study of Atomic Motions in Liquid and Solid Argon," unpublished.
54. G. Vineyard, *Phys. Rev.*, **110**, 999 (1958).
55. *International Tables for X-ray Crystallography*, Vol. 3, Kynoch Press, Birmingham, England, 1965.
56. P. Schofield, *Phys. Rev. Letters*, **4**, 39 (1960); *Inelastic Scattering of Neutrons in Solids and Liquids*, IAEA, Vienna, 1961; P. A. Egelstaff and P. Schofield, *Nucl. Sci. Eng.*, **12**, 260 (1962); P. A. Egelstaff. *Advan. Phys.*, **11**, 203 (1962).
57. P. Egelstaff, *An Introduction to the Liquid State*, Academic Press, New York, 1967.
58. R. G. Gordon, J_t *Chem. Phys.*, **44**, 1830 (1966).
59. R. G. Gordon, *J. Chem. Phys.*, **44**, 576 (1966).
60. R. G. Gordon, *J. Chem. Phys.*, **43**, 1307 (1965).
61. S. Chandrasekhar, *Rev. Mod. Phys.*, **15**, 1 (1945).
62. P. Debye, *Polar Molecules*, Dover Publications, New York.
63. B. J. Alder and T. E. Wainwright, in *Transport Processes in Statistical Mechanics*, I. Prigogine, Ed., Interscience, New York, 1958.
64. J. L. Doob, *Ann. Math.*, **43**, 351 (1942).
65. E. T. Jaynes, in *Information Theory and Statistical Mechanics, Statistical Physics, 1962 Brandeis Lectures*, K. W. Ford, Ed., Benjamin, New York, 1963; B. J. Berne, P. Pechukas, and G. D. Harp, *J. Chem. Phys.*, **40**, 2419 (1964).
66. G. Boato, G. Casanova, and A. Levi, *J. Chem. Phys.*, **40**, 2419, (1964).
67. K. Singwi and S. Tosi, *Phys. Rev.*, **157**, 153 (1967).
68. B. J. Berne, "Linear and Angular Momentum Correlations in Liquids and the Memory Function," unpublished.
69. S. Newman and S. A. Rice, Technical Report.
70. R. J. Rubin, *J. Math. Phys.*, **2**, 373 (1961).
71. P. Martin and S. Yip, *Phys. Rev.*, **170**, 151 (1968).
72. G. Vineyard, *Phys. Rev.*, **110**, 999 (1958).
73. B. Dasannacharya and K. Rao, *Phys. Rev.*, **137**, A417 (1965).

74. R. C. Desai and M. Nelkin, *Nucl. Sci. Eng.*, **24**, 142 (1966).
75. R. Zwanzig, *J. Chem. Phys.*, **40**, 2527 (1964), B. U. Felderhoff and I. Oppenheim, *Physica*, **31**, 1441 (1965).
76. R. Zwanzig, *Phys. Rev.*, **156**, 190 (1967).
77. R. Nossal and R. Zwanzig, *Phys. Rev.*, **157**, 120 (1967).
78. N. K. Ailawadi and R. Zwanzig, *Phys. Rev.*, to appear.
79. A. Rahman, *Phys. Rev. Letters*, **19**, 420 (1967).
80. C. Chung and S. Yip, *Phys. Rev.*, to appear.
81. B. J. Berne, Ph.D. Thesis, University of Chicago, 1964.
82. R. Desai and S. Yip, *Phys. Rev.*, **166**, 129 (1968).
83. J. Lebowitz and J. Percus, "Kinetic Equations and Density Expansions; Exactly Solvable One Dimensional Systems," *Phys. Rev.*, to appear.
84. R. Nossal, *J. Math. Phys.*, **6**, 193 (1965).
85. J. Kinsey, J. Deutch, and R. Silbey, Technical Report, Department of Chemistry, M.I.T., 1968.
86. M. Fixmann and K. Rider. To appear in *J. Chem. Phys.*
87. A. G. St. Pierre and W. A. Steele, *J. Chem. Phys.*, to appear.
88. R. Zwanzig, *Phys. Rev.*, to appear.
89. R. Hamming, *Numerical Methods for Scientists and Engineers*, McGraw-Hill, New York, 1962.
90. J. T. Day, *Bit*, **7**, 71 (1967).
91. J. Todd, *Survey of Numerical Analysis*, McGraw-Hill, New York, 1962.
92. *Tables of Integral Transforms*, Bateman Manuscript Project, H. Erdelyi, Ed., McGraw-Hill, New York, 1954.
93. I. Gradshteyn and I. Ryzhik, *Tables of Integrals, Series, and Products*, Academic Press, New York, 1965.
94. L. Pauling and E. Wilson, *Introduction to Quantum Mechanics*, McGraw-Hill, New York, 1935.
95. B. Nijboer and A. Rahman, *Physica*, **32**, 415 (1966).

Advance in Chemical Physics, Volume XVII
Edited by I. Prigogine, Stuart A. Rice

ON THE THEORY OF OPTICAL ABSORPTION PROFILES IN CONDENSED SYSTEMS

WILLIAM L. GREER and STUART A. RICE

The James Franck Institute and The Department of Chemistry
The University of Chicago, Chicago, Illinois

CONTENTS

I. INTRODUCTION

Much attention has been given recently to the calculation of the energy dependence of the resonant interactions between light and liquids or solids. These lineshape studies differ from those designed to explain the nonresonant collision broadening of optical transitions in dilute gases for, in a dilute gas, the time between collisions is very much longer than the duration of a collision, so that multiple interactions may be decomposed into sequences of two-body interactions. In condensed media, both in liquids and in solids, the interactions between molecules are of sufficient strength and duration that we may no longer realistically consider an electronic excitation to be localized at one site and to be lifetime broadened by a series of two-body collisions. The relevant interactions in these cases are between the collective electronic and nuclear modes of the condensed system. The

influence of this class of interactions on a transition lineshape is not included in the treatments developed to describe gas phase collision broadening of transitions.

The time dependent Green's function method, which has been discussed in detail in several review articles and books, has become popular as a formal tool for the description of optical absorption profiles.[1,2] Closely allied with the Green's function method is the correlation function method; the connection between these two forms of analysis is described in Ref. 1. In this paper we examine one particular exact method of describing the optical absorption profile function by the use of time dependent correlations between second quantized operators. We illustrate our treatment with descriptions of the absorption profiles in an impure crystal, a pure crystal, and a pure fluid. The technique employed is based on the projection operator method introduced by Zwanzig[3] in a similar context, and used recently by Wilson, King, and Kim.[4] This technique is shown to shift the emphasis of the calculation from a determination of the frequency dependence of the absorption profile function to a determination of a "self-energy" function whose frequency dependence is weaker.

This shift in focus is also precisely what is achieved by the use of the variational method introduced by Schwinger[5] for evaluation of the frequency-dependent Green's function. In the Schwinger variational method one introduces an external source of potential energy and then finds that the "self-energy" is related to the functional derivative of the Green's function with respect to the external potential, evaluated at zero potential. Whether the variational method of treating Green's functions or the projection operator method of treating correlation functions is the more suitable choice for a given problem depends upon the inevitable subsequent approximations which are required to reduce the self-energy function to a manageable form. Until more problems have been solved using both techniques, and a careful comparison of results made, it is not possible to decide in advance which is the more useful of these techniques.

As already mentioned, to demonstrate the potentialities of the projection operator method we herein apply it to the calculation of the optical absorption profiles corresponding to excitation of an impurity molecule in a crystalline host, the exciton states of a crystalline solid, and the exciton states of a liquid. From our analyses we find several new results and also show how older results are limiting cases of the ones which we obtain.

It should be noted that the projection operator method described in this paper is by no means restricted to use in optical absorption calculations, but may also be employed for a variety of problems in statistical physics.

II. OPTICAL ABSORPTION PROFILES CORRESPONDING TO TRANSITIONS BETWEEN BORN-OPPENHEIMER IMPURITY STATES OF A CRYSTAL

In this section we consider an impurity molecule imbedded in a host crystal and derive expressions for the lineshape of an electronic transition localized essentially on the impurity site. The formalism is sufficiently general to apply not only to *F*-centers,[6] from which the treatment is borrowed, but also to molecular Shopl'skii[7] crystals. We use the familiar Born-Oppenheimer[8] approximation in this section to reveal the rather complex line structure that results even in this simple limiting situation. We defer consideration of the complications arising from non-adiabatic transitions to the next section, in which the entire problem of optical absorption in impure crystals is reformulated in terms of statistical time dependent correlation functions. In this section we assume that the electronic energy surface deforms adiabatically as the nuclei move. In turn, the electronic energy surface so generated acts as the potential energy function in the nuclear Hamiltonian. To further simplify the calculation it is usually assumed that the adiabatic potential may be expanded in a Taylor series in the nuclear displacements, and the expansion terminated after the quadratic term. The resulting Hamiltonian may then be transformed by a suitable unitary matrix to a diagonal form which describes a set of uncoupled harmonic oscillators, or to the second quantized representation to describe a gas of noncolliding particles (phonons).[9] The coordinates appearing in the harmonic oscillator Hamiltonian are the crystal normal coordinates appropriate to the electronic state to which the adiabatic potential pertains. In general, different electronic states support different normal coordinates with different frequencies, but the analysis is greatly simplified if it is assumed that the ground and excited state potentials under investigation possess the same normal coordinates and frequencies, but do not have the same minima. This is the linear coupling approximation which has been exhaustively treated by many authors for the case of *F*-center absorption.[6,10] We reformulate their results in a form suitable to our needs.

The final approximation which is incorporated into our theory is the neglect of interaction between the impurity crystal state and the host electronic states or other impurity states. Given this approximation we may neglect exitation exchange between different crystal sites in that which follows.

In the Born-Oppenheimer linear coupling approximation, the nuclear Hamiltonians appropriate to the ground and excited electronic states are given by

$$H_f = T + \sum_I M\omega_I^2 X_I^f Q_I + \frac{1}{2}\sum_I M\omega_I^2 Q_I^2 + \hbar\omega'_f$$
$$H_0 = T + \frac{1}{2}\sum_I M\omega_I^2 Q_I^2 \tag{1}$$

in which T is the nuclear kinetic energy operator, ω_I is the frequency of the Ith normal mode with normal coordinate Q_I, X_I^f is the linear coupling coefficient for the fth electronic state and the Ith phonon mode, M is the oscillator reduced mass, and $\hbar\omega'_f$ is the energy difference between the fth electronic state and the ground state. We can display the Hamiltonians in a modified form to indicate how linear coupling leads to a normal coordinate shift and energy displacement.

$$H_f = T + \frac{1}{2}\sum_I M\omega_I^2(Q_I + X_I^f)^2 + \hbar\omega'_f - \frac{1}{2}\sum_I M\omega_I^2 (X_I^f)^2$$
$$H_0 = T + \frac{1}{2}\sum_I M\omega_I^2 Q_I^2 \tag{2}$$

Transitions between all of the vibrational levels appropriate to the ground electronic state and those of the excited electronic state can occur for a given normal coordinate but, because of the Born-Oppenheimer separation which has been assumed, they contribute delta functions to the absorption profile. The intensity distribution as a function of an applied electromagnetic field of frequency ω can then be described by the following function, if we invoke the Condon approximation in which the electronic transition matrix element is independent of the nuclear coordinates:

$$\mathscr{I}_{0f}(\omega) = \frac{1}{\mathrm{Tr}[\exp(-\beta H_0)]} \sum_{\{n_J;\, m_J\}=0}^{\infty}\sum^{\infty} \delta\left(\omega - \omega_{0f} - \sum_{J=1}^{N}(m_J - n_J)\omega_J\right)$$
$$\prod_{J=1}^{N} \exp\left[-\beta\hbar\omega_J(n_J + \tfrac{1}{2})\right] |\langle \chi_{n_J}{}^0(Q_J) \,|\, \chi_{m_J}{}^f(Q_J + X_J^f)\rangle|^2 \tag{3}$$

In Eq. (3) $\mathscr{I}_{0f}(\omega)$ is the frequency dependent intensity profile,

$$\hbar\omega_{0f} = \hbar\omega'_f - \tfrac{1}{2}\sum_J M\omega_J^2 (X_J^f)^2$$

and $\chi_{m_J}{}^f$ is the harmonic oscillator wavefunction for the m_Jth vibrational state of the Jth normal mode belonging to the fth electronic state. As usual,

$$\chi_{m_J}{}^f(\xi) = \left[\left(\frac{M\omega_J}{\hbar}\right)^{1/2} \frac{1}{2^{m_J}(\pi)^{1/2} m_J!}\right]^{1/2} \times \exp\left[-\frac{1}{2}\left(\frac{M\omega_J}{\hbar}\right)\xi^2\right] H_{m_J}\left[\left(\frac{M\omega_J}{\hbar}\right)^{1/2}\xi\right] \tag{4}$$

where $H_n(z)$ is a Hermite polynomial.

The overlap integrals in Eq. (3) may be evaluated analytically in the linear coupling approximation. It is found that[11]

$$|\langle\chi_{n_J}{}^0(Q_J)\,|\,\chi_{m_J}{}^f(Q_J + X_J{}^f)\rangle|^2 = \exp(-S_J)\begin{cases}\dfrac{(n_J)!}{(m_J)!}\, S_J{}^{m_J-n_J}[L_{n_J}{}^{m_J-n_J}(S_J)]^2 & n_J \leqslant m_J \\ \dfrac{(m_J)!}{(n_J)!}\, S_J{}^{n_J-m_J}[L_{m_J}{}^{n_J-m_J}(S_J)]^2 & n_J > m_J\end{cases} \tag{5}$$

where $S_J = (M\omega_J/2\hbar)(X_I{}^f)^2$, and $L_m{}^n(x)$ is a Laguerre polynomial.[12]

A rather lengthy algebraic manipulation produces the following expression for the intensity profile:

$$\mathcal{I}_{0f}(\omega) = \mathcal{I}_{0f}{}^{(0)}(\omega) + \mathcal{I}_{0f}{}^{\text{high}}(\omega) + \mathcal{I}_{0f}{}^{\text{low}}(\omega) \tag{6}$$

In the above equation $\mathcal{I}_{0f}{}^{(0)}(\omega)$ is the profile of the zero phonon line, which is a delta function centered at $\omega = \omega_{0f}$ and is constructed from a superposition of all vibronic transitions which involve no change in the quantum numbers of the phonon states of the ground and excited electronic states, i.e., $\{n_J\}^0 \rightarrow \{n_J\}^f$. The remaining terms in Eq. (6) describe the multiphonon sideband structure associated with the electronic transition. $\mathcal{I}_{0f}{}^{\text{high}}(\omega)$ is the absorption profile to the high energy side of $\omega = \omega_{0f}$, and $\mathcal{I}_{0f}{}^{\text{low}}(\omega)$ contains the low energy (hot band) structure of the absorption band. That these last two terms contain multiphonon structure is clear from the following decomposition in which the one, two, ..., phonon contributions are separated and made explicit:

$$\mathcal{I}_{0f}{}^{(0)}(\omega) = \exp(-S^f)\prod_{J=1}^{N} I_0(\lambda_J)\delta(\omega - \omega_{0f})$$

$$\mathcal{J}_{0f}^{\text{high}\atop\text{low}}(\omega) = \exp(-S^f)\Bigg[\sum_{J=1}^{N}\delta(\omega-\omega_{0f}\mp\omega_J)\exp(\pm\tfrac{1}{2}\hbar\beta\omega_J)I_1(\lambda_J)$$

$$\times\prod_{K\neq J}^{N}I_0(\lambda_K)$$

$$+\sum_{J=1}^{N}\delta(\omega-\omega_{0f}\mp 2\omega_J)\exp(\pm\hbar\beta\omega_J)I_2(\lambda_J)$$

$$\times\prod_{K\neq J}^{N}I_0(\lambda_K)+\sum_{\substack{J,K=1\\(J\neq K)}}^{N}\sum^{N}\delta(\omega\mp\omega_{0f}\mp\omega_J\to\omega_K)$$

$$\times\exp[\pm\tfrac{1}{2}\hbar\beta(\omega_J+\omega_K)]I_1(\lambda_J)I_1(\lambda_K)\prod_{\substack{L\neq J\\\neq K}}I_0(\lambda_L)$$

$$+\text{three phonon terms}+\cdots\Bigg] \tag{7}$$

In the above expression $I_J(z)$ is the modified Bessel function of the first kind,[12]

$$S^f=\sum_J S_J(2\langle n_J\rangle+1)$$

$$\lambda_J=S_J\,\operatorname{csch}(\tfrac{1}{2}\beta\hbar\omega_J)$$

and

$$\langle n_J\rangle=[\exp(\beta\hbar\omega_J)-1]^{-1} \tag{8}$$

Because the lattice phonon states almost form a continuum, it is convenient to replace all the sums over lattice modes by integrals and to introduce a phonon density of states function. Then

$$\sum_J A_J\,\delta(\omega-\omega_J)\to\int d\omega'\rho(\omega')A(\omega')\delta(\omega-\omega') \tag{9}$$

The density function $\rho(\omega)$ will be continuous for the acoustic modes and have delta-function peaks at frequencies corresponding to intramolecular vibrational energies which, of course, are also crystal phonon eigenstates in our general scheme. Of particular experimental interest is the form Eq. (7) assumes at zero degrees Kelvin if we introduce the phonon density of states from Eq. (9):

$$\mathcal{J}_{0f}^{\text{low}}(\omega)=0$$

$$\mathcal{J}_{0f}^{(0)}(\omega)=\exp(-\sum_J S_J)\delta(\omega-\omega_{0f})$$

$$\mathscr{J}_{0f}^{\text{high}}(\omega) = \exp\left(-\sum_J S_J\right)\Big\{S(\omega-\omega_{0f})\rho(\omega-\omega_{of}) + \frac{1}{2}\int_0^\infty d\omega'\rho(\omega')\rho(\omega-\omega_{0f}-\omega')S(\omega')S(\omega-\omega_{0f}-\omega') + \text{three phonon terms} + \cdots\Big\} \tag{10}$$

The only unknowns appearing in Eq. (10) are the phonon density of states and the coupling function

$$S(\omega) = \frac{M\omega}{2\hbar}[X^f(\omega)]^2 \tag{11}$$

Given the phonon density of states and the optical absorption profile extrapolated to $T = 0°$, one can calculate from the the one phonon peak the coupling function $S(\omega)$ as a function of frequency from Eq. (10). Maradudin[10] suggests that $S(\omega) \propto 1/\omega$ for the nonlocal phonon modes of *F*-centers, and Fitchen[6] has employed this suggestion to compute the density of states required to reproduce the observed lineshapes in *LiF*. It is unfortunate that more data are not presently available for the phonon densities of states of impure crystals, including molecular crystals of the Shpol'skii type.[7] Note added in proof: Recently R. Ostertag and H. C. Wolf [*Phys. Stat. Sol.* **31** 139 (1969)] have analyzed the emission spectra of several doped naphthalene crystals and have obtained results consistent with Eq. (7) from which they have deduced S^f.

As the final and most important result in this section, we obtain the Fourier transform of the intensity function. We do not present this result for merely pedantic reasons since, if we are to confine ourselves to the Born-Oppenheimer approximation, the expressions derived in the first part of this section are much more suitable for a discussion of the actual lineshape than are the Fourier transforms. We display the time-dependent Fourier transform of $\mathscr{J}_{0f}(\omega)$ because it will reoccur in connection with our discussion of the time-dependent correlation functions in the next section. Proceeding, then, a generating function is formally defined by the following expressions:

$$\begin{aligned}\mathscr{J}_{0f}(\omega) &= \frac{1}{2\pi}\int_{-\infty}^{\infty} dt\, e^{-i\omega t}\mathscr{F}_{0f}(t)\\ \mathscr{F}_{0f}(t) &= \int_{-\infty}^{\infty} d\omega\, e^{i\omega t}\mathscr{J}_{0f}(\omega)\end{aligned} \tag{12}$$

Beginning with Eq. (3) and introducing the integral representation for the delta function,

$$\delta(\omega - \omega') = \frac{1}{2\pi} \int_{-\infty}^{\infty} dt\, e^{-i(\omega-\omega')t} \tag{13}$$

one can show[13] that the generating function is given by

$$\mathscr{F}_{0f}(t) = \exp\left[i\omega_{0f} t - S^f + \sum_J S_J(\langle n_J \rangle + 1) \exp(i\omega_J t) + \sum_J S_J \langle n_J \rangle \exp(-i\omega_J t) \right] \tag{14}$$

III. CORRELATION FUNCTION TREATMENT OF OPTICAL LINESHAPES

One-particle time-dependent Green's functions are useful for a wide range of problems in quantum statistical mechanics, as the review article by Zubarev[1] amply demonstrates. Recently the technique has begun to be applied to the description of exciton-phonon interactions.[14] Now, at present there are two ways in which the statistical Green's functions may be calculated and used to describe a physical situation. One is the Schwinger variational method[5] which, as we mentioned in the Introduction, gives exact representations of the Green's function which are in a very appealing form. Another is the coupled hierarchy method, in which time derivatives of Green's functions are related to Green's functions of higher order in an infinite hierarchy.[1] Some decoupling approximation is then required to break into the chain of equations and allow the Green's function to be computed. We demonstrate in this section the use of a projection operator method in obtaining the correlation function appropriate to the description of the interaction of an excited impurity with a surrounding crystal lattice.

The spectral function (i.e., absorption line profile) may be formally calculated from the Fourier transform of a time-dependent correlation function or from the jump discontinuity in the Green's function across the real energy axis.[1] If the analysis is exact, both techniques yield the same solution. We choose to focus attention on the time-dependent correlation function method. Actually, if one bases an analysis upon equations of motion, as we do, there is very little difference between the solutions for the correlation function and its corresponding Green's function, since the two equations of motion differ by only a delta function in time.

In the linear coupling approximation the Hamiltonian for the impurity-host crystal system may be written in terms of second quantized operators:

$$H = \sum_f \mathscr{E}_f a_f^+ a_f + \sum_J \hbar\omega_J (b_J^+ b_J + \tfrac{1}{2}) + \sum_J \sum_f \hbar\omega_J (S_J^f)^{1/2} (b_J^+ + b_J) a_f^+ a_f$$
$$\times \sum_J \sum_{\substack{f,g \\ (f \neq g)}}{}' \hbar F_J^{fg} (b_J^+ + b_J) a_f^+ a_g + \sum_J \sum_f \hbar T_J^f (b_J^+ + b_J)(a_f^+ + a_f) \tag{15}$$

The operators a_f^+ and a_f respectively create and destroy an exicted state f of the crystal and satisfy the Bose-Einstein commutation relations

$$[a_f, a_{f'}^+] = \delta_{ff'}$$
$$[a_f, a_{f'}] = [a_f^+, a_{f'}^+] = 0 \tag{16}$$

in the limit that $\langle a_f^+ a_f \rangle \ll 1$. At low temperatures this inequality is satisfied. The operators b_J^+ and b_J create and destroy lattice phonons of index J and also satisfy the Bose-Einstein commutation relations. In Eq. (15) the linear coupling coefficient S_J^f is the same as the coefficient with the same symbol in Section II, Eq. (5) or (Eq. (11).

The Hamiltonian (15) describes the effects of phonons on the energy of each electronic state through the part of the Hamiltonian containing S_J^f, and includes non-adiabatic scattering terms which we denote by

$$H_{\text{int}}^{(1)} = \sum_J \sum_{\substack{f,g \\ (f \neq g)}} \hbar F_J^{fg} (b_J^+ + b_J) a_f^+ a_g \tag{17}$$

and

$$H_{\text{int}}^{(2)} = \sum_J \sum_f \hbar T_J^f (b_J^+ + b_J)(a_f^+ + a_f) \tag{18}$$

As is well known, $H_{\text{int}}^{(1)}$ gives rise to lifetime broadening of the Born-Oppenheimer states obtained from a diagonalization of $H - H_{\text{int}}^{(1)} + H_{\text{int}}^{(2)}$ by scattering of electronic excitations. In Eq. (18) $H_{\text{int}}^{(2)}$ does not conserve the number of excited electronic states but rather describes the phonon-induced destruction or creation of an electronic state f via coupling of the state f with the ground electronic state through the matrix element $\hbar T_J^f$.

We now apply a canonical transformation to the Hamiltonian in Eq. (15):

$$\begin{aligned}
\tilde{H} &= e^A H e^{-A} \\
&= \sum_f \hbar\omega_f a_f^+ a_f + \sum_J \hbar\omega_J (b_J^+ b_J + \tfrac{1}{2}) \\
&\quad + \sum_J \sum_f \sum_{f \neq g} \hbar F_J^{fg} B_f^+ (b_J^+ + b_J) B_g a_f^+ a_g \\
&\quad + \sum_J \sum_f \hbar T_J (B_f^+ a_f^+ + B_f a_f)(b_J^+ + b_J) - 2 \sum_J \sum_{f,g} \hbar T_J^f (S_J^g)^{1/2} \\
&\quad \times (B_f^+ a_f^+ + B_f a_f) a_g^+ a_g
\end{aligned} \tag{19}$$

where

$$A = \sum_J \sum_f (S_J{}^f)^{1/2}(b_J^+ - b_J)a_f^+ a_f$$

$$\hbar\omega_f = \varepsilon_f - \sum_J \hbar\omega_J S_J{}^f$$

and

$$B_f = \exp\left[-\sum_J (S_J{}^f)^{1/2}(b_J^+ - b_J)\right] \tag{20}$$

In the derivation of Eq. (19) we have assumed the validity of a one-particle model in which only one excited state resides at an impurity site (i.e., we have neglected multiple excitation terms). This transformation is similar to that used by Rashba,[14] Kudinov and Firsov,[15] and Fisher, Grover, Rice and Silbey,[16] for excitons in pure crystals. The transformed operators now are

$$\begin{aligned} \tilde{a}_f^+ &= e^A a_f^+ e^{-A} = B_f^+ a_f^+ \\ \tilde{a}_f &= e^A a_f e^{-A} = B_f a_f \end{aligned} \tag{21}$$

To proceed we introduce the one-particle time-dependent correlation function $\mathscr{G}_f(t)$, and describe its relationship with the complex frequency dependent conductivity. The time-dependent function is defined as

$$\mathscr{G}_f(t) = \langle \tilde{a}_f \tilde{a}_f^+(t)\rangle \tag{22}$$

where the expectation value in Eq. (22) is taken with respect to the equilibrium canonical ensemble defined by the Hamiltonian H,

$$\langle \mathscr{O}\rangle = \frac{\mathrm{Tr}\{\rho\mathscr{O}\}}{\mathrm{Tr}\{\rho\}}$$

$$\rho = \exp\{-\beta\tilde{H}\}$$

and

$$\mathscr{O}(t) = e^{i\tilde{H}t/\hbar}\mathscr{O}(0)\, e^{-i\tilde{H}t/\hbar} \tag{23}$$

Now, Kubo's linear response analysis[17] of the complex conductivity of a system, for the case of interaction between the system and a periodic plane wave field in the optical region, yields the following:

$$\sigma(\omega) = \mathrm{Re}\ \omega \int_0^\infty dt\, e^{-i\omega t}\langle M(0)M(t)\rangle \tag{24}$$

In (24) the dipole moment operator $M(t)$ is that induced by the field. To insure convergence of the integral transform, the frequency ω in Eq. (24) can be considered complex, with an infinitesimal negative imaginary part which is set equal to zero after the integration is performed. To use (24) we evaluate $\langle M(0)M(t)\rangle$ by writing the dipole moment in second quantized form:

$$M(t) = \frac{n}{V}\left[M_{0f}\,\tilde{a}_f^{+}(t) + M_{f0}\,\tilde{a}_f(t)\right] \tag{25}$$

In Eq. (25) V is the crystal volume, n is the number of impurity molecules, and M_{0f} is the dipole matrix element between the ground and fth excited electronic states.

If we assume that $\langle a_f^{+} a_f\rangle \ll 1$ as we must in order for the Bose-Einstein relations in Eq. (16) to be valid, we obtain for the dipole correlation function

$$\begin{aligned}\langle M(0)M(t)\rangle &= \frac{n}{V}\,|M_{0f}|^2\,\langle \tilde{a}_f\, a_f^{+}(t)\rangle \\ &= \frac{n}{V}\,|M_{0f}|^2\,\mathcal{G}_f(t)\end{aligned} \tag{26}$$

Introducing the Laplace transform of the time dependent correlation function by the relation

$$\hat{\mathcal{G}}_f(\omega) = \int_0^{\infty} dt\, e^{-i\omega t}\mathcal{G}_f(t), \qquad \operatorname{Im}\omega < 0 \tag{27}$$

we find that the conductivity is simply

$$\sigma(\omega) = \frac{\omega n}{V}\,|M_{0f}|^2\,\operatorname{Re}\hat{\mathcal{G}}_f(\omega) \tag{28}$$

an expression which justifies our introduction of the correlation function $\mathcal{G}_f(t)$.

For completeness we here reproduce expressions which show the connection between conductivity, the dielectric function $\varepsilon(\omega)$, and the real and imaginary parts of the refractive index, $\eta(\omega)$ and $\kappa(\omega)$, respectively:[18]

$$\begin{aligned}\varepsilon(\omega) &= \varepsilon_0 + i\,\frac{\sigma(\omega)}{\omega}, \\ \varepsilon(\omega) &= \eta^2(\omega) - \kappa^2(\omega) + 2i\eta(\omega)\kappa(\omega)\end{aligned} \tag{29}$$

If we now assume that the residual interaction term in the transformed Hamiltonian is small, we can decouple the averages over electron and phonon operators by the approximation

$$\langle \tilde{a}_f \tilde{a}_f^+(t)\rangle \simeq \langle a_f a_f^+(t)\rangle\langle B_f B_f^+(t)\rangle \tag{30}$$

With the aid of the definitions

$$\begin{aligned} G_f(t) &= \langle a_f a_f^+(t)\rangle \\ D_{0f}(t) &= \langle B_f B_f^+(t)\rangle \end{aligned} \tag{31}$$

and the transforms

$$\hat{G}_f(\omega) = \int_0^\infty dt\, e^{-i\omega t} G_f(t)$$

$$\tilde{D}_{0f}(\omega) = \frac{1}{2\pi}\int_{-\infty}^{\infty} dt\, e^{-i\omega t} D_{0f}(t) \tag{32}$$

we may write

$$\hat{\mathscr{G}}_f(\omega) = \int_{-\infty}^{\infty} d\xi\, \hat{G}_f(\omega - \xi)\tilde{D}_{0f}(\xi) \tag{33}^*$$

Furthermore, if we assume free propagation of the phonons in order to evaluate $D_{0f}(t)$, i.e., if

$$\begin{aligned} b_J^+(t) &= \exp(i\omega_J t) b_J^+ \\ b_J(t) &= \exp(-i\omega_J t) b_J \end{aligned} \tag{34}$$

we find that

$$\begin{aligned} D_{0f}(t) &= \exp\left\{-\sum_J S_J(2\langle n_J\rangle + 1)\right. \\ &\qquad \left. + \sum_J S_J[(\langle n_J\rangle + 1)\exp(i\omega_J t) + \langle n_J\rangle \exp(-i\omega_J t)]\right\} \\ &= \exp(-i\omega_f t)\mathscr{F}_{0f}(t) \end{aligned} \tag{35}$$

where $\mathscr{F}_{0f}(t)$ is the generating function introduced in Eq. (12). Thus by Eqs. (12) and (32)

$$\tilde{D}_{0f}(\omega) = \mathscr{J}_{0f}(\omega + \omega_f) \tag{36}$$

* Throughout this paper the symbols $\wedge$ and $\sim$ will denote the Laplace and Fourier transforms, respectively.

and the frequency-dependent correlation function $\hat{\mathscr{G}}_f(\omega)$ is simply the convolution of $\hat{G}_f(\omega)$ with the Born-Oppenheimer intensity distribution:

$$\hat{\mathscr{G}}_f(\omega) = \int_{-\infty}^{\infty} d\xi\, \hat{G}_f(\omega - \xi)\mathscr{I}_{0f}(\omega_f + \xi) \tag{37}$$

If we also assume free propagation of the electronic excited state,

$$\begin{aligned} a_f^+(t) &= \exp(i\omega_f t)a_f^+ \\ a_f(t) &= \exp -i\omega_f t)a_f \end{aligned} \tag{38}$$

we can easily show that

$$\operatorname{Re} \hat{\mathscr{G}}_f(\omega) = \pi \mathscr{I}_{0f}(\omega) \tag{39}$$

by using the relation

$$\frac{1}{\omega \pm i\varepsilon} = \text{P.P.}\,\frac{1}{\omega} \mp i\pi\delta(\omega), \qquad \text{as } \varepsilon \to 0^+ \tag{40}$$

where P.P. means the Cauchy principal part. Indeed, it is the real part of $\hat{G}_{0f}(\omega)$ which is of interest for a calculation of the dissipative part of the dielectric function in Eq. (29).

However, in the following we will not assume that the fth excited state propagates freely, but rather that it is scattered in accordance with the interaction term of the full linear coupling Hamiltonian. Of course it is not true that the phonon states have infinite lifetimes either, but we will concentrate only upon electronic scattering by phonons in order to keep the analysis simple. Thus, the function whose time development we desire is $G_f(t)$.

First we obtain the equation of motion for $G_f(t)$:

$$\begin{aligned} \dot{G}_f(t) = \frac{d}{dt} G_f(t) &= \langle a_f \dot{a}_f(t)\rangle \\ &= i\langle a_f L a_f^+(t)\rangle \end{aligned} \tag{41}$$

where the Liouville operator is defined as

$$\begin{aligned} LY &= \frac{1}{\hbar}[\tilde{H}, Y] \\ \mathrm{W}(t) &= e^{i\tilde{H}t/\hbar}\mathrm{W}(0)\, e^{-i\tilde{H}t/\hbar} = e^{iLt}\mathrm{W}(0) \end{aligned} \tag{42}$$

for any operators W, Y.

The hierarchy method[1] would have us evaluate the commutator and obtain equations of motion for the resulting higher order correlation function, ad infinitum. Instead of this method we will use the projection operator method. The operator which we want is one which acts upon the space of second quantized creation and destruction operators and projects out only the relevant part of the second quantized operators. Such an operator is the one used by Wilson, King, and Kim[2] for the calculation of the infrared lineshape of a U-center, It has the form

$$\mathscr{P}_f Y = a_f^+ \frac{\langle a_f Y \rangle}{\langle a_f a_f^+ \rangle} \tag{43}$$

This projection operator possesses the usual properties, i.e., it is idempotent.

$$\begin{aligned} \mathscr{P}_f{}^2 &= \mathscr{P}_f \\ \mathscr{P}_f(1 - \mathscr{P}_f) &= (1 - \mathscr{P}_f)\mathscr{P}_f = 0 \end{aligned} \tag{44}$$

Moreover, we note that by definition (43) the operator has no effect upon $G_f(t)$ or its time derivatives,

$$\begin{aligned} G_f(t) &= \langle a_f \mathscr{P}_f a_f^+(t) \rangle \\ \dot{G}_f(t) &= \left\langle a_f \frac{d}{dt} \mathscr{P}_f a_f^+(t) \right\rangle \\ &= \langle a_f \mathscr{P}_f \dot{a}_f^+(t) \rangle \end{aligned} \tag{45}$$

The introduction of an operator which seems to do nothing may appear odd, but in fact its introduction allows us to generate an exact solution for $\hat{G}_f(\omega)$ which is in a most useful form. We proceed by noting from (42) that

$$a_f^+(t) = e^{iLt} a_f^+ \tag{46}$$

Thus,

$$\mathscr{P}_f \dot{a}_f^+(t) = i\mathscr{P}_f L \mathscr{P}_f a_f^+(t) + i\mathscr{P}_f L(1 - \mathscr{P}_f) a_f^+(t) \tag{47a}$$

$$(1 - \mathscr{P}_f)\dot{a}^+(t) = i(1 - \mathscr{P}_f)L\mathscr{P}_f a_f^+(t) + i(1 - \mathscr{P}_f)L(1 - \mathscr{P}_f) a_f^+(t) \tag{47b}$$

The last equation may be solved formally to give

$$\begin{aligned} (1 - \mathscr{P}_f) a_f^+(t) = \exp\,[i(1 - \mathscr{P}_f)Lt](1 - \mathscr{P}_f) a_f^+ \\ + i \int_0^t dt' \exp\,[i(1 - \mathscr{P}_f)Lt'](1 - \mathscr{P}_f) L \mathscr{P}_f a_f^+(t - t') \end{aligned} \tag{48}$$

Upon substitution of Eq. (48) into the right-hand side of Eq. (47a) and insertion of the result of such an operation into (45), we find the integro-differential equation:

$$\dot{G}_f(t) = -ig_f G_f(t) - \int_0^t dt' K_f(t') G_f(t - t') \tag{49}$$

where

$$g_f = \langle a_f L a_f^+ \rangle$$

In Eq. (49) the kernel $K_f(t)$ is given formally by

$$K_f(t) = -\langle (La_f) \exp [i(1 - \mathscr{P}_f)Lt](1 - \mathscr{P}_f)La_f^+ \rangle \tag{50}$$

The value of this particular form of the derivative becomes immediately obvious when the Laplace transform convolution theorem is invoked.[19] We find

$$\hat{G}_f(\omega) = \frac{1}{i(\omega - g_f) + \hat{K}_f(\omega)} \tag{51}$$

where

$$\hat{K}_f(\omega) = \int_0^\infty dt\, e^{-i\omega t} K_f(t) \tag{52}$$

We are only interested in the real part of Eq. (51) because of Eqs. (28) and (29). The real part is

$$\operatorname{Re} \hat{G}_f(\omega) = \frac{\operatorname{Re} \hat{K}_f(\omega)}{[\omega - g_f + \operatorname{Im} \hat{K}_f(\omega)]^2 + [\operatorname{Re} \hat{K}_f(\omega)]^2} \tag{53}$$

This form for $\hat{G}_f(\omega)$ is convenient because the task of calculating observables is now reduced to finding the self-energy $\hat{K}_f(\omega)$. If $\hat{K}_f(\omega)$ is a complex number independent of ω in the vicinity of $\omega \simeq g_f$, we retrieve the familiar Lorentzian profile for the absorption lineshape. The frequency dependence of $\hat{K}_f(\omega)$ therefore gives the observed lineshape its asymmetry.

The commutators appearing in Eq. (50) may be evaluated by using (42) and (19):

$$\begin{aligned} La_f = &-\omega_f a_f - \sum_I \sum_{g \neq f} F_I^{fg} B_f^+ (b_I^+ + b_I) B_g a_g \\ &- \sum_I T_I^f B_f^+ (b_I^+ + b_I) + 2 \sum_{I,g} T_I^f (S_I^f)^{1/2} B_g^+ a_g^+ a_f \\ &+ 2 \sum_{I,g} T_I^f (S_I^g)^{1/2} B_f^+ a_g^+ a_g + 2 \sum_{I,g} T_I^g (S_I^f)^{1/2} B_g a_g a_f \end{aligned} \tag{54}$$

$$La_f^+ = \omega_f a_f^+ + \sum_J \sum_{g\neq f}' F_J^{gf} B_g^+ (b_J^+ + b_J) B_f a_g^+ + \sum_J T_J^f B_f (b_J^+ + b_J) - 2\sum_{J,g} T_J^g (S_J^f)^{1/2} B_g^+ a_g^+ a_f - 2\sum_{J,g} T_J^g (S_J^f)^{1/2} B_g a_g a_f^+ - 2\sum_{J,g} T_J^g (S_J^g)^{1/2} B_f a_g^+ a_g \quad (55)$$

One should now substitute (54) into (50) and replace $\exp[i(1-P_f)Lt]$ by the power series for which it is symbolic and carry out all the commutations and projections until the operator P_f no longer appears explicitly in $K_f(t)$. Unfortunately, the resulting infinite series is not a very useful form for further calculations, so we are forced to resort to approximations in order to reduce the kernel $K_f(t)$ to a manageable and physically transparent form. The approximations which we use are:

(*a*) Averages over phonon and excited electronic state operators are separated into two distinct averages, as already assumed in Eq. (30).

(*b*) The operators P_f and L are assumed to commute. This is strictly true only if the Hamiltonian is diagonal in $a_f^+ a_f$, but is approximately correct if the coupling terms are small.

(*c*) Averages of operators containing different electronic state operators are separated into independent averages.

(*d*) Products of operators describing multiple excitations are neglected.

Along with these assumptions we also use the following exact relations

$$\langle Z(1-P_f)a_f^+\rangle = 0$$
$$\langle a_f(1-P_f)Z\rangle = 0 \quad (56)$$
$$\langle a_f \exp[i(1-P_f)Lt](1-P_f)Z\rangle = 0$$

for any operator Z.

Using the exact and approximate relations cited, we obtain.

$$K_f(t) = \sum_{g\neq f}' \sum_{I,J} F_I^{fg} F_J^{gf} G_g(t) \langle B_f^+ Q_I B_g B_g^+(t) Q_J(t) B_f(t)\rangle + \sum_{I,J} T_I^f T_J^f \langle B_f^+ Q_I Q_J(t) B_f(t)\rangle + 4\sum_{g\neq f}' \sum_{I,J} T_I^g T_J^g (S_I^f S_J^f)^{1/2} G_g(t) G_f(t) \langle B_g B_g^+(t)\rangle \quad (57)$$

where

$$Q_J(t) \equiv b_J^+ \exp(i\omega_J t) + b_J \exp(-i\omega_J t)$$

In the same approximation scheme

$$g_f = \langle a_f La_f^+\rangle \simeq \omega_f \quad (58)$$

The time-dependent correlation functions may be explicitly evaluated for a harmonic lattice. It is found that

$$\begin{aligned}
&\langle B_f^+ Q_I B_g B_g^+(t) Q_J(t) B_f(t)\rangle \\
&\quad = \langle B_f^+ B_g Q_I Q_J(t) B_g^+(t) B_f(t)\rangle \\
&\qquad + 4(S_I^g)^{1/2}\{(S_J^f)^{1/2}[1-(S_J^g)^{1/2}\cos(\omega_J t)]\}\langle B_f^+ B_g B_g^+(t) B_f(t)\rangle \\
&\qquad - 2(S_J^g)^{1/2}\langle Q_I B_f^+ B_g B_g^+(t) B_f(t)\rangle \\
&\qquad - 2(S_J^g)^{1/2}\langle Q_J(t) B_f^+ B_g B_g^+(t) B_f(t)\rangle
\end{aligned} \tag{59}$$

where

$$\begin{aligned}
&\langle Q_J(t) B_f^+ B_g^+(t) B_f(t)\rangle \\
&\quad = \{(S_J^f)^{1/2} - (S_J^g)^{1/2}\} \\
&\qquad \times [(\langle n_J\rangle + 1)\exp(-i\omega_J t) + \langle n_J\rangle \exp(\omega i_J t) - 1] \\
&\qquad \times \langle B_f^+ B_g B_g^+(t) B_f(t)\rangle
\end{aligned} \tag{60}$$

and

$$\begin{aligned}
&\tfrac{1}{2}\langle B_f^+ B_g[Q_I Q_J(t) + Q_J Q_I(t)] B_g^+(t) B_f(t)\rangle \\
&\quad = \delta_{IJ}[(\langle n_J\rangle + 1)\exp(i\omega_J t) + \langle n_J\rangle \exp(-i\omega_J t)] \\
&\qquad \times \langle B_f^+ B_g B_g^+(t) B_f(t)\rangle + \{(S_J^f)^{1/2} - (S_J^g)^{1/2}\}\{(S_I^f)^{1/2} - (S_I^g)^{1/2}\} \\
&\qquad \times [\exp(i\omega_f t)(\tfrac{3}{2} - \langle n_J\rangle - \langle n_I\rangle) \\
&\qquad + \exp(-i\omega_J t)(\tfrac{1}{2} - \langle n_I\rangle - \langle n_J\rangle) + \exp(i\omega_I t)(\tfrac{3}{2} - \langle n_J\rangle - \langle n_I\rangle) \\
&\qquad + \exp(-i\omega_I t)(\tfrac{1}{2} - \langle n_J\rangle - \langle n_I\rangle) - \tfrac{1}{2}(\exp[i(\omega_I - \omega_J)t] \\
&\qquad + \exp[-i(\omega_I - \omega_J)t]) \times \{\langle n_J\rangle\langle n_I\rangle(1 + \exp[\beta\hbar(\omega_I + \omega_J)])\} \\
&\qquad + \tfrac{1}{2}(\exp[i(\omega_I + \omega_J)t] + \exp[-i(\omega_I + \omega_J)t]) \\
&\qquad \times \{1 - \langle n_I\rangle\langle n_J\rangle(1 + \exp[\beta\hbar(\omega_I + \omega_J)])\} \\
&\qquad - 1]\langle B_f^+ B_g B_g^+(t) B_f(t)\rangle
\end{aligned} \tag{61}$$

Equations (59) through (61) contain the time-dependent contributions to the lineshape from interelectronic scattering processes. These processes are, in general, multiphonon induced, but reduce to the familiar one-phonon scattering expressions when $S_J^f = S_J^g$, i.e., when the potential minima for electronic states f and g are the same.

The time-dependent contributions to the absorption profile function from relaxation (exciton nonconserving) processes are given by:

$$\sum_{I,J} T_I^f T_J^f \langle B_f^+ Q_J Q_I(t) B_f(t)\rangle$$

$$= \sum_{I,J} T_I^f T_J^f \delta_{IJ}[(\langle n_J\rangle + 1)\exp(i\omega_J t) + \langle n_J\rangle \exp(-i\omega_J t)]$$

$$\times \langle B_f B_f^+(t)\rangle + \sum_{I,J} T_I^f T_J^f (S_I^f S_J^f)^{1/2}$$

$$\times [(\exp(i\omega_J t) + \exp(i\omega_I t))(\tfrac{3}{2} - \langle n_J\rangle - \langle n_I\rangle)$$

$$+ (\exp(-i\omega_J t) + \exp(-i\omega_I t))(\tfrac{1}{2} - \langle n_J\rangle - \langle n_I\rangle)$$

$$- \tfrac{1}{2}(\exp[i(\omega_I - \omega_J)t] + \exp[-i(\omega_I - \omega_J)t])$$

$$\times \{\langle n_J\rangle\langle n_I\rangle(1 + \exp[\beta\hbar(\omega_I + \omega_J)])\}$$

$$+ \tfrac{1}{2}(\exp[i(\omega_I + \omega_J)t] + \exp[-i(\omega_I + \omega_J)t])\{1 - \langle n_I\rangle\langle n_J\rangle$$

$$\times (1 + \exp[\beta\hbar(\omega_I + \omega_J)])\} - 1] \tag{62}$$

The time-dependent correlation functions

$$\langle B_f^+ B_g B_g^+(t) B_f(t)\rangle \qquad \text{and} \qquad \langle B_f^+ B_f(t)\rangle$$

are easily evaluated and are related to the Fourier transforms of the Born-Oppenheimer absorption functions $\mathscr{J}_{f\to g}(\omega)$ and $\mathscr{J}_{f\to 0}(\omega)$, respectively, They are, in fact,

$$\langle B_f^+ B_f(t)\rangle = \exp\{-\sum_J S_J^f(2\langle n_J\rangle + 1) + \sum_J S_J^f[(\langle n_J\rangle + 1)$$

$$\times \exp(i\omega_J t) + \langle n_J\rangle \exp(-i\omega_J t)]\} \tag{63}$$

and

$$\langle B_f^+ B_g B_g^+(t) B_f(t)\rangle$$

$$= \exp\left\{-\sum_J \{(S_J^f)^{1/2} - (S_J^g)^{1/2}\}^2(2\langle n_J\rangle + 1)\right.$$

$$+ \sum_J \{(S_J^f)^{1/2} - (S_J^g)^{1/2}\}^2$$

$$\left.\times [(\langle n_J\rangle + 1)\exp(i\omega_J t) + \langle n_J\rangle \exp(-i\omega_J t)]\right\} \tag{64}$$

The relation between $\langle B_f^+ B_f(t)\rangle$ and $\mathscr{J}_{0f}(\omega)$ is given by Eqs. (31), (32), and (36). A similar relation exists between $\langle B_f^+ B_g B_g^+(t) B_f(t)\rangle$ and

$\mathscr{J}_{fg}(\omega)$. Since we are interested in the one-sided Fourier (complex Laplace) transform of the time-dependent functions we will use this relationship.

All of the frequency-dependent contributions to $K(\omega)$ will be of the following form

$$\int_0^\infty dt \exp(-i\omega' t)\langle B_f^+ B_f(t)\rangle \equiv \mathrm{A}_f(\omega') \tag{65}$$

or

$$\int_0^\infty dt \exp(-i\omega' t)\langle B_f^+ B_g B_g^+(t) B_f(t)\rangle \equiv \mathrm{A}_{fg}(\omega') \tag{66}$$

for various choices of ω' (which may depend on the normal mode index J and I). By simple manipulations we can show that

$$\mathrm{A}_f(\omega') = \pi \mathscr{J}_{0f}(\omega' - \omega_f) - i\mathrm{P.P.} \int_{-\infty}^{\infty} d\xi \frac{\mathscr{J}_{0f}(\omega' - \omega_f + \xi)}{\omega' - \xi} \tag{67}$$

$$\mathrm{A}_{fg}(\omega') = \pi \mathscr{J}_{fg}(\omega' + \omega_g - \omega_f) - i\mathrm{P.P.} \int_{-\infty}^{\infty} d\xi \frac{\mathscr{J}_{fg}(\omega' + \omega_g - \omega_f + \xi)}{\omega' - \xi} \tag{68}$$

We note that the real and imaginary parts of $A_f(\omega')$ and $A_{fg}(\omega')$ satisfy Kramers-Kronig relations, so that one needs to know only the real part in order to obtain the imaginary part.

The contribution to $\hat{K}_f(\omega)$ from the relaxation term

$$\sum_g{}' \sum_{I,J} T_I^g T_J^g (S_I^f S_J^f)^{1/2} G_g(t) G_f(t) \langle B_g B_g^+(t)\rangle \tag{69}$$

arises from an interesting, albeit quite negligible, source, This term describes relaxation of the fth electronic state to the ground state via intermediary electronic states. The Laplace transform of Eq. (69), with the extra assumption that

$$G_g(t) = \langle a_g a_g^+(t)\rangle \simeq \exp(i\omega_g t) \tag{70}$$

is

$$\sum_g{}' \sum_{I,J} T_J^g T_I^g [(S_I^f)(S_J^f)]^{1/2} \int_{-\infty}^{\infty} d\xi \hat{G}_f(\omega - \xi) \mathscr{J}_{0g}(\xi) \tag{71}$$

which is entirely negligible since $G_f(\omega - \xi)$ and $\mathscr{J}_{0g}(\xi)$ have almost zero differential overlap at $\omega \simeq \omega_f$.

The Laplace transform $\hat{K}_f(\omega)$ is

$$
\begin{aligned}
&\frac{1}{\pi}\,\mathrm{Re}\,\hat{K}_f(\omega+\omega_f)\\
&\quad=\sum_g{}'\sum_J |F_J^{fg}|^2\,[(\langle n_J\rangle+1)\mathscr{J}_{fg}(\omega-\omega_J)\\
&\qquad+\langle n_J\rangle\mathscr{J}_{fg}(\omega+\omega_J)]+\sum_g{}'\sum_{I,J}F_J^{fg}F_I^{gf}\\
&\qquad\times\{[(S_I^f)^{1/2}-(S_I^g)^{1/2}][(S_J^f)^{1/2}-(S_J^g)^{1/2}][(\tfrac{1}{2}-\langle n_J\rangle-\langle n_I\rangle)\\
&\qquad\times\{\mathscr{J}_{fg}(\omega-\omega_J)+\mathscr{J}_{fg}(\omega-\omega_I)\}\\
&\qquad+(\tfrac{1}{2}-\langle n_J\rangle-\langle n_I\rangle)\{\mathscr{J}_{fg}(\omega+\omega_I)+\mathscr{J}_{fg}(\omega+\omega_I)\}\\
&\qquad+\tfrac{1}{2}[1-\langle n_I\rangle\langle n_J\rangle(1+\exp[\beta\hbar(\omega_I+\omega_J)])]\\
&\qquad\times\{\mathscr{J}_{fg}(\omega-\omega_I-\omega_J)+\mathscr{J}_{fg}(\omega+\omega_I+\omega_J)\}\\
&\qquad-\tfrac{1}{2}\langle n_I\rangle\langle n_J\rangle(1+\exp[\beta\hbar(\omega_I+\omega_J)])\{\mathscr{J}_{fg}(\omega+\omega_I-\omega_J)\\
&\qquad+\mathscr{J}_{fg}(\omega-\omega_I+\omega_J)]\}-\mathscr{J}_{fg}(\omega)\}\\
&\qquad+2\sum_{I,J}\sum_g{}'F_I^{fg}F_J^{gf}(S_I^g)^{1/2}\{(S_J^f)^{1/2}-(S_J^g)^{1/2}\}[(2-\langle n_I\rangle-\langle n_J\rangle)\\
&\qquad\times\mathscr{J}_{fg}(\omega-\omega_J)+(1-\langle n_J\rangle-\langle n_I\rangle)\mathscr{J}_{fg}(\omega+\omega_J)+\mathscr{J}_{fg}(\omega)]\\
&\qquad+4\sum_g{}'\sum_{I,J}F_I^{fg}F_J^{gf}(S_I^gS_J^g)^{1/2}\mathscr{J}_{fg}(\omega)\\
&\qquad+\sum_J|T_J^f|^2\,[(\langle n_J\rangle+1)\mathscr{J}_{f0}(\omega-\omega_J)+\langle n_J\rangle\mathscr{J}_{f0}(\omega+\omega_J)]\\
&\qquad+\sum_{J,I}T_J^fT_I^f\{(S_I^fS_J^f)^{1/2}[(\tfrac{1}{2}-\langle n_J\rangle-\langle n_I\rangle)\{\mathscr{J}_{f0}(\omega-\omega_J)\\
&\qquad+\mathscr{J}_{f0}(\omega-\omega_I)\}+(\tfrac{1}{2}-\langle n_J\rangle-\langle n_I\rangle)\{\mathscr{J}_{f0}(\omega+\omega_J)\\
&\qquad+\mathscr{J}_{f0}(\omega+\omega_I)\}+\tfrac{1}{2}[1-\langle n_J\rangle\langle n_I\rangle(1+\exp[\beta\hbar(\omega_I+\omega_J)])\\
&\qquad\times\{\mathscr{J}_{f0}(\omega-\omega_I-\omega_J)+\mathscr{J}_{f0}(\omega+\omega_I+\omega_J)\}\\
&\qquad-\tfrac{1}{2}\langle n_I\rangle\langle n_J\rangle(1+\exp[\beta\hbar(\omega_I+\omega_J)])\{\mathscr{J}_{f0}(\omega+\omega_I+\omega_J)\\
&\qquad+\mathscr{J}_{f0}(\omega-\omega_I+\omega_J)\}]-\mathscr{J}_{f0}(\omega)\}\\
&\qquad+\sum_{I,J}\sum_g{}'T_I^gT_J^g(S_I^fS_J^f)^{1/2}\int_{-\infty}^{\infty}d\xi\,\hat{G}_f(\xi)\mathscr{J}_{0g}(\omega-\xi)
\end{aligned}
\tag{72}
$$

The imaginary part of $\hat{K}_f(\omega)$ is formally obtainable through

$$
\mathrm{Im}\,\hat{K}_f(\omega)=-\frac{1}{\pi}\,\mathrm{P.P.}\int_{-\infty}^{\infty}d\xi\,\frac{\mathrm{Re}\,\hat{K}_f(\xi)}{\omega-\xi}
\tag{73}
$$

Equation (53) reveals that the real part of $\hat{K}_f(\omega)$ is associated with the line width of state f while the imaginary part gives the spectral shift.

We have used Eq. (72) as a basis for the calculation of the thermal-dependence of the line profile width for various numerical choices of the coupling parameters. A detailed discussion of the numerical calculation is given in the Appendix.

If we pass to the limit in which all potential curves possess minima at the same values of the normal coordinates, i.e., at $\{Q_J\} = 0$, only the familiar one-phonon scattering contribution remains.[20] This is

$$\begin{aligned}\frac{1}{\pi}\operatorname{Re}\hat{K}_f(\omega+\omega_f) &= \sum_g{}' \sum_J |F^{fg}|^2 [(\langle n_J\rangle + 1)\delta(\omega - \omega_J + \omega_f - \omega_g) \\ &\quad + \langle n_J\rangle\delta(\omega + \omega_J - \omega_f + \omega_g)] \\ &\quad + \sum_J (T_J^f)^2[(\langle n_J\rangle + 1)\delta(\omega + \omega_f - \omega_J) \\ &\quad + \langle n_J\rangle\delta(\omega + \omega_f + \omega_J)] \end{aligned} \tag{74}$$

To conclude this section we mention the shortcomings and omissions in our treatment of the optical lineshape corresponding to the absorption of light by a nonresonant impurity molecule in a host crystal. Because we have assumed harmonic potentials for the electronic states in question, the overlap of vibrational wavefunctions in one electronic manifold with almost isoenergetic vibrational wave-functions of another electronic manifold is misrepresented if not actually seriously in error when this model is compared to real crystals.

Because of the misrepresentation of such vibrational overlaps the radiationless transitions described are fictitious. It would be interesting to incorporate anharmonicities into the vibrational manifolds if one is interested in focusing attention on the details of radiationless transitions of a realistic nature.

We have also omitted the effect of phonon clothing of intramolecular mixing of states and have chose to use basis functions for the electronic states which are appropriate to a static rather than a dynamic lattice. If we wish to include dynamical state mixing, we must include a term in the untransformed Hamiltonian in Eq. (15) of the general form.

$$H' = \sum_{\substack{f,g \\ g\neq f}} \sum \hbar W_{fg} a_g^+ a_g \tag{75}$$

corresponding to which there will appear an extra term in Eq. (19) after

$$\tilde{H}' = e^{A}H'e^{-A} = \sum_{f,g}{}' \hbar W_{fg} B_f^{+} B_g a_f^{+} a_g \tag{76}$$

transformation: Note added in proof: A recent theoretical study of radiationless transitions in large molecules by Engleman and Jortner (*Mol. Phys.* in press) uses such a Hamiltonian, although the language of their paper more closely resembles that of Section II than that of Section III.

This term is of the same structure as the excitation transfer term in the pure crystal Hamiltonian to be described in the next section.[16]

Throughout these calculations we have used the linear coupling approximation; inclusion of terms quadratic in the phonon creation and destruction operators would lead to phonon frequency shifts in each electronic state. We have also omitted this effect for simplicity.

With respect to the linear coupling Hamiltonian which we have used and to the projection operator technique, more thought needs to be given to better approximations than the one which we have used in reducing the exact result in Eq. (50) to the simplified form of Eq. (57). The way in which we have used the techniques is the same as that from a simplified solution to the variational method, so it is merely a matter of taste as to which one is used. However, it may be that one is better suited to subsequent approximation schemes than is the other. To that interesting possibility we have no answer at present.

IV. PURE MOLECULAR CRYSTALS

In a pure molecular crystal there exist resonant interactions between the molecules. Because of these interactions, there exist in the crystal bands, electronic states whose parentages are single molecular electronic states. There will, of course, be as many states in each band as there are molecules in the crystal. In the static lattice approximation, each crystal state of one of the aforementioned bands is characterized by a quantum number (or wave vector), $\mathbf{k}$, which is interpreted as the pseudomomentum associated with that state. If the lattice is vibrating, $\mathbf{k}$ is no longer a good quantum number, and the real crystal eigenstates can be represented as a mixture of all the static lattice states. One way to analyse the absorption profile in a pure crystal is to assume that the states labelled by $\mathbf{k}$ are almost good eigenstates, and that a perturbation in the form of phonon scattering occurs, much as in the impurity case we have already studied. In a pure molecular crystal, however, scattering can occur within the same band (i.e., $\mathbf{k}' \rightarrow \mathbf{k}$) as

well as between bands. Thus, the accoustic phonons play a larger role in determining the characteristic features of the absorption spectrum of a pure crystal than they do in the case of impurity absorption. In this section we derive expressions for the optical lineshape of an absorbing pure molecular crystal, paying special attention to the effects of phonon–exciton clothing and phonon–exciton intra- and interband scattering. We shall, in all that follows, only consider crystals with one molecule per unit cell. Thus, we do not consider any of the interesting aspects related to phonon-induced scattering between Davydov components in a crystal with more than one molecule per unit cell.

The linear coupling Hamiltonian appropriate to the pure crystal with one molecule per unit cell is[21]

$$H = H_{\text{ex}} + H_{\text{ph}} + H_{\text{int}}, \tag{77}$$

where

$$H_{\text{ex}} = \sum_{n,f} E_f a_{nf}^{+} a_{nf} + \sum_{n,m,f} \hbar K_{nm}{}^{f} a_{nf}^{+} a_{mf}$$

$$H_{\text{ph}} = \sum_{\mathbf{q},j} \hbar\Omega_j(\mathbf{q})(b_{\mathbf{q}j}^{+} b_{\mathbf{q}j} + \tfrac{1}{2})$$

and

$$\begin{aligned} H_{\text{int}} = &\sum_{n,f} \sum_{\mathbf{q},j} \hbar\Omega_j(\mathbf{q})(S_{\mathbf{q}j}{}^{fn})^{1/2}(b_{\mathbf{q}j}^{+} + b_{-\mathbf{q}j}) a_{nf}^{+} a_{nf} \\ &+ \sum_{n,f} \sum_{\substack{m,g \\ (n\neq m)}} \sum_{\mathbf{q},j} \hbar F_{\mathbf{q}j}{}^{nm}(f,g)(b_{\mathbf{q}j}^{+} + b_{-\mathbf{q}j}) a_{nf}^{+} a_{mg} \end{aligned} \tag{78}$$

Most of the parameters appearing in Eq. (78) have already been defined in Section III, except that they have been generalized to refer to the more complex case of the pure crystal. Thus, E_f is the molecular fth excited state energy, as altered by the static crystal field, and the summation indices n and f refer to the crystal sites and electronic states, respectively, where $n = 1, 2, \ldots, N$. The parameter $K_{nn}{}^{f}$ is an excitation transfer matrix element which describes excitation transfer of electronic state f from site n' to n. The diagonal term $K_{nn}{}^{f}$ is the contribution of the static lattice crystal field to the excited state energy, and is independent of the site index.

In the phonon Hamiltonian of Eq. (78) $\Omega_i(\mathbf{q})$ is the frequency of a phonon belonging to the ith branch with wave-vector $\mathbf{q}$. The reciprocal lattice vector $\mathbf{q}$ is defined as usual, and is confined to the first Brillouin zone, in which there are N values of $\mathbf{q}$. The branch index i has $3s$ values, corresponding to s atoms per molecule. In the case of molecular crystals, to which this discussion is restricted, in the first approximation the $3sN$

crystal vibration may be factored into $3s - 6$ crystal symmetrized intramolecular vibrations and 6 intermolecular vibrations, each of which has N values of $\mathbf{q}$ associated with it.

The last term in Eq. (78) is the phonon–exciton interaction. $S_{\mathbf{q}i}^{nf}$ describes the $\mathbf{q}i$th phonon-induced deformation of the lattice at site n when the fth excited state is there, while $F_{\mathbf{q}i}^{nn'}(f,f')$ describes the effect of scattering of electronic states $f' \to f$, $n' \to n$ by a phonon of index $\mathbf{q}i$.

In order for H to be Hermitian, $[S_{\mathbf{q}j}]^{1/2} = [S_{-\mathbf{q}j}]^{1/2*}$, and $F_{\mathbf{q}i} = (F_{-\mathbf{q}i})^*$. In explicit form, $(S_{\mathbf{q}i}{}^{nf})^{1/2} = \gamma_{\mathbf{q}i}{}^{f} \exp\{i\mathbf{q} \cdot \mathbf{X}_n\}$, where $\gamma_{\mathbf{q}i}{}^{f}$ is a real number. It is assumed here, as in Section III, that interaction terms linear in the phonon normal coordinates are dominant, and that phonon frequency changes upon electronic excitation are negligibly small.

In order to partially diagonalize the Hamiltonian to remove the deformation term we define

$$A \equiv \sum_{n,f} \sum_{\mathbf{q},j} (S_{\mathbf{q}j}{}^{nf})^{1/2} (b_{\mathbf{q}j}^{+} - b_{-\mathbf{q}j}) a_{nf}\, a_{nf} \tag{79}$$

We now transform the Hamiltonian as follows:

$$\begin{aligned} \tilde{H} &= e^{+A} H e^{-A} \\ &= \tilde{H}^{(0)} + \tilde{H}_{\text{int}} \end{aligned}$$

where

$$\begin{aligned} \tilde{H}^{(0)} = \sum_{n,f} \Bigg\{ & E_f - \sum_{\mathbf{q}j} \hbar\Omega_j(\mathbf{q})(\gamma_{\mathbf{q}j}{}^{f})^2 \Bigg\} a_{nf}^{+} a_{nf} \\ & + \sum_{n,f} \sum_{m} \hbar K_{nm}{}^{f} B_{nf}^{+} B_{mf}\, a_{nf}^{+} a_{mf} \\ & + \sum_{\mathbf{q}j} \hbar\Omega_j(\mathbf{q})(b_{\mathbf{q}j}^{+} b_{\mathbf{q}j} + \tfrac{1}{2}) \end{aligned} \tag{80}$$

and

$$\tilde{H}_{\text{int}} = \sum_{nf} \sum_{mg} \sum_{\mathbf{q}j} \hbar F_{\mathbf{q}j}{}^{nm}(f,g) B_{nf}^{+} (b_{\mathbf{q}j}^{+} + b_{-\mathbf{q}j}) B_{mg}\, a_{nf}^{+}\, a_{mg} \tag{81}$$

The operator B_{nf} is defined by

$$B_{nf} = \exp\left\{ -\sum_{\mathbf{q}j} (S_{\mathbf{q}j}{}^{fn})^{1/2} (b_{\mathbf{q}j}^{+} - b_{-\mathbf{q}j}) \right. \tag{82}$$

and the clothed exciton operators are

$$\begin{aligned} \tilde{a}_{nf} &= e^{A} a_{nf}\, e^{-A} = B_{nf}\, a_{nf} \\ \tilde{a}_{nf}^{+} &= e^{A} a_{nf}^{+}\, e^{-A} = B_{nf}^{+}\, a_{nf}^{+} \end{aligned} \tag{83}$$

We are, of course, interested in the states characterized by the wave-

vector $\mathbf{k}$. The static lattice one site operators a_{nf}^{+}, a_{nf} are related to the $\mathbf{k}$-dependent operators by the Fourier transforms:

$$a_{nf}^{+} = \left(\frac{1}{N}\right)^{1/2} \sum_{\mathbf{k}} \exp(i\mathbf{k}\cdot\mathbf{X}_n) a_{\mathbf{k}f}^{+}$$
$$a_{nf} = \left(\frac{1}{N}\right)^{1/2} \sum_{\mathbf{k}} \exp(-i\mathbf{k}\cdot\mathbf{X}_n) a_{\mathbf{k}f} \tag{84}$$

With the use of Eq. (84) and the translational invariance of the crystal, i.e.,

$$\frac{1}{N}\sum_{n} \exp[i(\mathbf{k}-\mathbf{q})\cdot\mathbf{X}_n] = \delta_{\mathbf{k}-\mathbf{q}} \tag{85}$$

the Hamiltonian may be written in the form

$$\tilde{H} = \sum_{f,\mathbf{k}} \hbar\omega_f(\mathbf{k}) a_{\mathbf{k}f}^{+} a_{\mathbf{k}f} + \sum_{\mathbf{q}j} \hbar\Omega_j(\mathbf{q})(b_{\mathbf{q}j}^{+} b_{\mathbf{q}j} + \tfrac{1}{2})$$
$$+ \sum_{\mathbf{k},\mathbf{k}'} \sum_{f,g} \hbar C_{\mathbf{k}\mathbf{k}'}^{fg} a_{\mathbf{k}f}^{+} a_{\mathbf{k}'g} \tag{86}$$

where

$$\hbar\omega_f(\mathbf{k}) = E_f - \sum_{\mathbf{q}j} \hbar\Omega_j(\mathbf{q})(\gamma_{\mathbf{q}j}^{nf})^2 + \frac{\hbar}{N}\sum_{n,m} \exp[i\mathbf{k}\cdot(\mathbf{X}_n - \mathbf{X}_m)] K_{nm}^{f} B_{nf}^{+} B_{mf}$$
$$+ \frac{1}{N}\sum_{\mathbf{q}j}\sum_{n,m} \hbar F_{\mathbf{q}j}^{nm}(f,f) B_{nf}^{+}(b_{\mathbf{q}j}^{+} + b_{-\mathbf{q}j}) B_{mf} \exp[i\mathbf{k}\cdot(\mathbf{X}_n - \mathbf{X}_m)]$$

and

$$C_{\mathbf{k}\mathbf{k}'}^{fg} = \frac{1}{N}\sum_{n,m} \exp(i\mathbf{k}\cdot\mathbf{X}_n - i\mathbf{k}'\cdot\mathbf{X}_m)\Big\{K_{nm}^{f} B_{nf}^{+} B_{mf}$$
$$+ \sum_{\mathbf{q}j} F_{\mathbf{q}j}^{nm}(f,g) B_{nf}^{+}(b_{\mathbf{q}j}^{+} + b_{-\mathbf{q}j}) B_{mg}\Big\}$$

Since the operator product $B_{nf}^{+} B_{mf}$ does not depend on $\mathbf{X}_n - \mathbf{X}_m$, we cannot simplify the expressions above by the use of (85), as we could when considering a static undeformed lattice.

The average energy of the $f\mathbf{k}$th state may be approximated by the first (diagonal) term in Eq. (86) if the exciton-phonon interaction is weak and the exciton and phonon averages may be separated as follows:

$$\langle\omega_f(\mathbf{k})\rangle = \frac{1}{N}\sum_{n,m} \exp[i\mathbf{k}\cdot(\mathbf{X}_n - \mathbf{X}_m)]\{K_{nm}^{f}\langle B_{nf}^{+} B_{mf}\rangle$$
$$+ \sum_{\mathbf{q}j} F_{\mathbf{q}j}^{nm}(f,f)\langle B_{nf}^{+}(b_{\mathbf{q}j}^{+} + b_{-\mathbf{q}j}) B_{mf}\rangle\}$$
$$+ \frac{1}{\hbar} E_f - \sum_{\mathbf{q}j} \Omega_j(\mathbf{q})(\gamma_{\mathbf{q}j}^{f})^2 \tag{88}$$

The correlation functions appearing in Eq. (88) may be evaluated in the harmonic lattice approximation. It is found that

$$\langle B_{nf}^{+} B_{mf} \rangle = \exp \left\{ -2 \sum_{\mathbf{q}j} (\gamma_{\mathbf{q}j}{}^{f})^2 \sin^2 [\tfrac{1}{2}\mathbf{q} \cdot (\mathbf{X}_n - \mathbf{X}_m)] \times (2\langle n_{\mathbf{q}j} \rangle + 1) \right\} \tag{89}$$

and

$$\langle B_{nf}^{+}(b_{\mathbf{q}j}^{+} + b_{-\mathbf{q}j}) B_{mf} \rangle = -\gamma_{\mathbf{q}j}{}^{f} [\exp(-i\mathbf{q} \cdot \mathbf{X}_n) + \exp(-i\mathbf{q} \cdot \mathbf{X}_m)] \langle B_{nf}^{+} B_{mf} \rangle \tag{90}$$

Therefore the average energy of the $f\mathbf{k}$th exciton state is

$$\begin{aligned} \langle \omega_f(\mathbf{k}) \rangle = {} & \frac{1}{\hbar} E_f - \sum_{\mathbf{q}j} \Omega_j(\mathbf{q}) (\gamma_{\mathbf{q}j}{}^{f})^2 \\ & + \sum_{(n-m)} \exp [i\mathbf{k} \cdot (\mathbf{X}_n - \mathbf{X}_m)] K_{n-m}^{f} \langle B_{nf}^{+} B_{mf} \rangle \\ & - \frac{1}{N} \sum_{\mathbf{q}j} (\gamma_{\mathbf{q}j}{}^{f}) \sum_{n,m} \exp [i\mathbf{k} \cdot (\mathbf{X}_n - \mathbf{X}_m)] \\ & \times [\exp(-i\mathbf{q} \cdot \mathbf{X}_n) + \exp(-i\mathbf{q} \cdot \mathbf{X}_m)] F_{\mathbf{q}j}{}^{nm}(f, f) \langle B_{nf}^{+} B_{mf} \rangle \end{aligned} \tag{91}$$

where use was made of the fact that $K_{nn'}^{f} \langle B_{nf}^{+} B_{n'f} \rangle$ depends on $\mathbf{X}_n$ and $\mathbf{X}_{n'}$ only through their difference whereas the last term in Eq. (91) does not. In the limit as $\gamma_{\mathbf{q}j}{}^{f}$ goes to zero, Eq. (91) reduces to the well-known undeformed static lattice result.[22]

As in Section III, we now solve for the frequency-dependent correlation function

$$\hat{G}_{\mathbf{k}f}(\omega) = \int_0^\infty dt\, e^{-i\omega t} G_{\mathbf{k}f}(t)$$

where

$$G_{\mathbf{k}f}(t) = \langle a_{\mathbf{k}f}\, a_{\mathbf{k}f}^{+}(t) \rangle \tag{92}$$

We use exactly the same procedure as before, introducing here the projection operator $P_{\mathbf{k}f}$:

$$P_{\mathbf{k}f}\, Y \equiv a_{\mathbf{k}f}^{+} \frac{\langle a_{\mathbf{k}f}\, Y \rangle}{\langle a_{\mathbf{k}f}\, a_{\mathbf{k}f}^{+} \rangle} \tag{93}$$

Proceeding as in Section III, we express the correlation function in the following form:

$$\hat{G}_{\mathbf{k}f}(\omega) = \frac{1}{i(\omega - \langle \omega_f(\mathbf{k}) \rangle) + \hat{R}_{\mathbf{k}f}(\omega)} \tag{94}$$

where

$$\hat{R}_{\mathbf{k}f}(\omega) = \int_0^\infty dt\, e^{-i\omega t} R_{\mathbf{k}f}(t)$$

and

$$R_{\mathbf{k}f}(t) = \sum_{\mathbf{k}',\mathbf{k}''} \sum_{g,h} (1 - \delta_{kk'})(1 - \delta_{kk''}) \langle C^{fg}_{\mathbf{k}\mathbf{k}'} a_{\mathbf{k}'g} \exp[i(1 - P_{\mathbf{k}f})Lt](1 - P_{\mathbf{k}f}) C^{hf}_{\mathbf{k}''\mathbf{k}} a^{+}_{\mathbf{k}''h} \rangle \tag{95}$$

The approximation we use to reduce $R_{\mathbf{k}f}(t)$ to a more manageable form is the same as that introduced in Section III, that is,

$$[P_{\mathbf{k}f}, L] \cong 0$$

and

$$\exp(iP_{\mathbf{k}f} L) \cong \exp(iP_{\mathbf{k}f} L_0)$$

where

$$L_0 Z = \frac{1}{\hbar}[\tilde{H}^{(0)}, Z].$$

Equation (95) now becomes

$$R_{\mathbf{k}f}(t) = \sum_{\mathbf{k}',f'} (1 - \delta_{\mathbf{k}\mathbf{k}'}) G_{\mathbf{k}'f'}(t) \langle C^{ff'}_{\mathbf{k}\mathbf{k}'} C^{f'f}_{\mathbf{k}'\mathbf{k}}(t) \rangle \tag{96}$$

which in turn yields

$$\hat{R}_{\mathbf{k}f}(\omega) = \sum_{\mathbf{k}',f'} \int_{-\infty}^{\infty} d\xi\, \hat{G}_{\mathbf{k}'f'}(\omega - \xi) C^{ff'}_{\mathbf{k}\mathbf{k}'}(\xi)(1 - \delta_{\mathbf{k}\mathbf{k}'}) \tag{97}$$

where

$$\tilde{C}^{ff'}_{\mathbf{k}\mathbf{k}'}(\omega) = \frac{1}{2\pi} \int_{-\infty}^{\infty} dt\, e^{-i\omega t} \langle C^{ff'}_{\mathbf{k}\mathbf{k}'} C^{f'f}_{\mathbf{k}'\mathbf{k}}(t) \rangle \tag{98}$$

The correlation function $\langle C^{ff'}_{k'k}.\ C^{f'f}_{k'k}(t)\rangle$ is evaluated with the assumption given in Eq. (65) and found to be

$$
\begin{aligned}
&\langle C^{ff'}_{\mathbf{kk}'} C^{f'f}_{\mathbf{k}'\mathbf{k}}(t)\rangle \\
&= \frac{1}{N^2}\sum_{n,m}\sum_{n',m'} \exp\left[i\mathbf{k}\cdot(\mathbf{X}_n - \mathbf{X}_{n'}) - i\mathbf{k}'\cdot(\mathbf{X}_m - \mathbf{X}_{m'})\right] \\
&\times \{K_{nm}{}^{f}\langle B^{+}_{nf} B_{mf}\, B^{+}_{m'f}(t) B_{n'f}(t)\rangle K^{f}_{m'n'} + \sum_{\mathbf{q}j} F_{\mathbf{q}j}{}^{m'-n'}(f', f) K_{nm}{}^{f} \\
&\times \langle B^{+}_{nf} B_{mf}\, B^{+}_{m'f'}(t) B_{n'f}(t)\rangle [-2\gamma_{\mathbf{q}j}{}^{f'} \exp(-i\mathbf{q}\cdot\mathbf{X}_{m'}) \\
&- \gamma_{\mathbf{q}j}{}^{f}(\exp[-i\mathbf{q}\cdot\mathbf{X}_n] - \exp[-i\mathbf{q}\cdot\mathbf{X}_m])(\exp[i\Omega_j(\mathbf{q})t] \\
&+ \exp[-i\Omega_j(\mathbf{q})t]) + \langle n_{\mathbf{q}j}\rangle[\gamma_{\mathbf{q}j}{}^{f}(\exp[-i\mathbf{q}\cdot\mathbf{X}_n] - \exp[-i\mathbf{q}\cdot\mathbf{X}_m] \\
&- \exp[-i\mathbf{q}\cdot\mathbf{X}_{n'} - i\Omega_j(\mathbf{q})t]) + \gamma_{\mathbf{q}j}{}^{f'} \exp[-i\mathbf{q}\cdot\mathbf{X}_{m'} + i\Omega_j(\mathbf{q})t] \\
&\times (\exp[i\Omega_j(\mathbf{q})t] + \exp[-i\Omega_j(\mathbf{q})t + \beta\hbar\Omega_j(\mathbf{q})])] \\
&+ \sum_{\mathbf{q}j} F_{\mathbf{q}j}{}^{n-m}(f, f') K^{f}_{m'n'}\langle B^{+}_{nf} B_{mf'}\, B_{m'f}(t) B_{n'f}(t)\rangle \\
&\times [-2\gamma_{\mathbf{q}j}{}^{f} \exp(-i\mathbf{q}\cdot\mathbf{X}_n) + \gamma_{\mathbf{q}j}{}^{f}\{\exp(-i\mathbf{q}\cdot\mathbf{X}_n) \\
&+ \exp[i\Omega_j(\mathbf{q})t](\exp[-i\mathbf{q}\cdot\mathbf{X}_{m'}] - \exp[-i\mathbf{q}\cdot\mathbf{X}_{n'}])\} \\
&+ \gamma_{\mathbf{q}j}{}^{f'} \exp[-i\mathbf{q}\cdot\mathbf{X}_{m'} + i\Omega_j(\mathbf{q})t]] \\
&+ \sum_{\mathbf{q}j}\sum_{\sigma l} F_{\sigma l}{}^{n-m}(f, f') F_{\mathbf{q}j}{}^{m'-n'}(f', f) \\
&\times \langle B^{+}_{nf} B_{mf'}\, B^{+}_{m'f'}(t) B_{n'f}(t)\rangle [-2\gamma_{\sigma l}{}^{f} \exp(-i\sigma\cdot\mathbf{X}_n) \\
&\times \{-2\gamma_{\mathbf{q}j}{}^{f'} \exp(-i\mathbf{q}\cdot\mathbf{X}_m) - \gamma_{\mathbf{q}j}{}^{f}(\exp[-i\mathbf{q}\cdot\mathbf{X}_n] - \exp[-i\mathbf{q}\cdot\mathbf{X}_m) \\
&\times (\exp[i\Omega_j(\mathbf{q})t] + \exp[-i\Omega_j(\mathbf{q})t]) + \langle n_{\mathbf{q}j}\rangle[\gamma_{\mathbf{q}j}{}^{f} \\
&\times (\exp[-i\mathbf{q}\cdot\mathbf{X}_m] - \exp[-i\mathbf{q}\cdot\mathbf{X}_{n'} - i\Omega_j(\mathbf{q})t]) \\
&+ \gamma_{\mathbf{q}j}{}^{f'}(\exp[-i\mathbf{q}\cdot\mathbf{X}_{m'} + i\Omega_j(\mathbf{q})t] - \exp(-i\mathbf{q}\cdot\mathbf{X}_m))] \\
&\times (\exp[i\Omega_j(\mathbf{q})t] + \exp[-i\Omega_j(\mathbf{q})t + \beta\hbar\Omega_j(\mathbf{q})])\} \\
&- \{\gamma_{\sigma l}{}^{f}(\exp[-i\sigma\cdot\mathbf{X}_n] - \exp[-i\sigma\cdot\mathbf{X}_{n'} - i\Omega_l(\sigma)t]) \\
&- \gamma_{\sigma l}{}^{f'}(\exp[-i\sigma\cdot\mathbf{X}_m] - \exp[-i\sigma\cdot\mathbf{X}_{m'} - i\Omega_l(\sigma)t])\} \\
&\times \{-2\gamma_{\mathbf{q}j}{}^{f'} \exp(-i\mathbf{q}\cdot\mathbf{X}_n) - (\gamma_{\mathbf{q}j}{}^{f} \exp[-i\mathbf{q}\cdot\mathbf{X}_n] \\
&- \gamma_{\mathbf{q}j}{}^{f'} \exp[-i\mathbf{q}\cdot\mathbf{X}_m])(\exp[i\Omega_j(\mathbf{q})t] + \exp[-i\Omega_j(\mathbf{q})t])\} \\
&+ \langle n_{\mathbf{q}j}\rangle\langle n_{\sigma l}\rangle\{\gamma_{\sigma l}{}^{f}(\exp[-i\sigma\cdot\mathbf{X}_n] - \exp[i-\sigma\cdot\mathbf{X}_{n'} - i\Omega_l(\sigma)t]) \\
&- \gamma_{\sigma l}{}^{f'}(\exp[-i\sigma\cdot\mathbf{X}_m] - \exp[-i\sigma\cdot\mathbf{X}_{m'} - i\Omega_l(\sigma)t])]
\end{aligned}
$$

$$\times [\gamma_{\mathbf{q}j}{}^{f}(\exp[-i\mathbf{q}\cdot\mathbf{X}_n] - \exp[-i\mathbf{q}\cdot\mathbf{X}_{n'} - i\Omega_j(\mathbf{q})t])$$
$$- \gamma_{\mathbf{q}j}{}^{f'}(\exp[-i\mathbf{q}\cdot\mathbf{X}_m] - \exp[-i\mathbf{q}\cdot\mathbf{X}_{m'} - i\Omega_j(\mathbf{q})t])]$$
$$\times \{\exp[i\Omega_j(\mathbf{q})t] + \exp[-i\Omega_j(\mathbf{q})t + \beta\hbar(\Omega_j(\mathbf{q}) + \Omega_i(\sigma))]$$
$$- \exp[-i\Omega_j(\mathbf{q})t + \beta\Omega_j(\mathbf{q})\hbar] - \exp[i\Omega_j(\mathbf{q})t + \beta\hbar\Omega_i(\sigma)]\}$$
$$+ \delta_{i,j}\delta_{\mathbf{q}+\sigma}[(\langle n_{i\sigma}\rangle + 1)\exp[i\Omega_i(\sigma)t]$$
$$+ \langle n_{\sigma i}\rangle \exp[-i\Omega_i(\sigma)t]]\} \tag{99}$$

Finally, the correlation function on the right-hand side of Eq. (99) may be evaluated exactly for a harmonic lattice. It is found that

$$\langle B_{nf}^{+} B_{m'f'} B_{mf'}^{+}(t) B_{m'f}(t)\rangle$$
$$= \exp(-2\sum_{\mathbf{q}j}\gamma_{\mathbf{q}j}{}^{f}\gamma_{\mathbf{q}j}{}^{f'}[(2\langle n_{\mathbf{q}j}\rangle + 1)(\sin^2[\tfrac{1}{2}\mathbf{q}\cdot(\mathbf{X}_n - \mathbf{X}_{n'})]$$
$$+ \sin^2[\tfrac{1}{2}\mathbf{q}\cdot(\mathbf{X}_m - \mathbf{X}_{m'})]) + [(\langle n_{\mathbf{q}j}\rangle + 1)\exp[i\Omega_j(\mathbf{q})t] + \langle n_{\mathbf{q}j}\rangle$$
$$\times \exp[-i\Omega_j(\mathbf{q})t]] \times \{[\cos[\mathbf{q}\cdot(\mathbf{X}_m - \mathbf{X}_n)]$$
$$+ \cos[\mathbf{q}\cdot(\mathbf{X}_m - \mathbf{X}_{n'})] + \cos(\mathbf{q}\cdot(\mathbf{X}_n - \mathbf{X}_{m'})]$$
$$+ \cos[\mathbf{q}\cdot(\mathbf{X}_{m'} - \mathbf{X}_{n'})]]\}) \tag{100}$$

Given numerical or analytical values for the coupling constants, and a knowledge of the crystal phonon dispersion relations, Eqs. (94) through (100) can be used to calculate the lineshape, at least in principle. Further approximations, such as the assumption that all exciton states $\mathbf{k}'f' \neq \mathbf{k}f$ have infinite lifetimes, yield results analogous to those quoted in Section III. None of the results of this section are really any different from those obtained by Fischer, Grover, Rice, and Silbey[16] using the variational technique, except for a trivial extension arising from the inclusion of interband scattering and the use of phonon branch indices in this paper. What is different is the method used to obtain the results.

As in Section III we have assumed that the excited state operators create excited states of the static crystal with the crystal field mixing effects already included. No account is taken herein of the phonon clothing effect on crystal field mixing of free molecule states, or mixing of free molecule states with charge-transfer crystal states.

V. TRANSITIONS IN A SIMPLE FLUID

Several recent papers have discussed the properties of the exciton states of simple fluids[23] and disordered semiconductors.[24] It has been shown that an exciton can exist in a disordered system if the wave vector associated

with the excited state is small relative to the reciprocal of the local ordering distance, σ. That is to say, exciton states with small $\mathbf{k}$ are not effectively mixed by perturbations arising from disorder in the fluid; dynamical perturbations do, however, lead to state mixing, just as in a pure crystal. We note that the effect of disorder on those fluid states for which $|\mathbf{k}|$ is of the order of magnitude of σ^{-1} is severe enough to prevent characterization of such states by a single real vector $\mathbf{k}$.

Fischer and Rice[25] have discussed the line shape coresponding to an optical transition in a simple fluid, using as the principle analytical tool the theory of one particle Green's functions. These investigators obtained an expression for the energy dependence of the optical resonance by truncating a hierarchy of coupled equations. In this section we use the Hamiltonian introduced by Fischer and Rice, and solve for the frequency-dependent absorption profile function with the projection operator method.

To start with we write the Hamiltonian for a fluid consisting of N particles, each of mass M in the form

$$H = H_{\text{fluid}} + H_{\text{ex}} + H_{\text{int}} \tag{101}$$

where

$$H_{\text{fluid}} = -\frac{\hbar^2}{2M}\sum_n \nabla_n^2 + U$$

$$H_{\text{ex}} = E\sum_n a_n^+ a_n + \sum_{\mathbf{k}} F(\mathbf{k}) a_{\mathbf{k}}^+ a_{\mathbf{k}}$$

and

$$H_{\text{int}} = \frac{1}{N}\sum_{\mathbf{k},\mathbf{q}} \left(\frac{\hbar}{M}\mathbf{q}\cdot\mathbf{J}_{\mathbf{q}-\mathbf{k}} + \frac{\hbar^2 q^2}{2M}\rho_{\mathbf{q}-\mathbf{k}}\right) a_{\mathbf{k}}^+ a_{\mathbf{q}} \tag{102a}$$

The various functions appearing in Eq. (102) are defined as follows: U is the total potential of interaction between all fluid atoms and is dependent upon the configuration of all the atoms; E is the energy of the electronic state in question, and has been suitably adjusted to take account of the average fluid field acting on a given atom; $F(\mathbf{k})$ is given by

$$F(\mathbf{R}) = \frac{1}{N}\sum_{\mathbf{k}} F(\mathbf{k}) e^{i\mathbf{k}\cdot\mathbf{R}}$$

where $F(\mathbf{R})$ is the excitation exchange matrix element for two atoms separated by a distance $\mathbf{R}$ in the fluid. In the interaction Hamiltonian, H_{int}, the quantity

$$\mathbf{J}_{\mathbf{k}} = \sum_n e^{i\mathbf{k}\cdot\mathbf{R}_n}(-i\hbar\nabla_n) \tag{102b}$$

is the **k**th Fourier component of the fluid momentum, and

$$\rho_{\mathbf{k}} = \sum_n e^{i\mathbf{k}\cdot\mathbf{R}n} \tag{102c}$$

is the **k**th Fourier component of the atomic density fluctuation. Finally, a_k^+ and a_k are exciton creation and destruction operators defined on a Born-Oppenheimer basis set. In the derivation of (102) the dependence of the electronic state at each site on nuclear displacements has been neglected.

Given the Hamiltonian (101), the calculation of the absorption lineshape is carried out exactly as before. The function of interest is

$$\hat{G}_{\mathbf{k}}(\omega) = \int_0^\infty dt\, e^{-i\omega t} G_{\mathbf{k}}(t) \tag{103}$$

where

$$G_{\mathbf{k}}(t) = \langle a_{\mathbf{k}}\, a_{\mathbf{k}}^+(t)\rangle$$

The use of the projection operator P_k defined by

$$P_{\mathbf{k}}\, Y = a_{\mathbf{k}}^+ \frac{\langle a_{\mathbf{k}}\, Y\rangle}{\langle a_{\mathbf{k}}\, a_{\mathbf{k}}^+\rangle} \tag{104}$$

yields the following representation of $\hat{G}_{\mathbf{k}}(\omega)$:

$$\hat{G}_{\mathbf{k}}(\omega) = \frac{1}{i(\omega - \langle\omega_{\mathbf{k}}\rangle) + \hat{R}_{\mathbf{k}}(\omega)} \tag{105}$$

where

$$\langle\omega_{\mathbf{k}}\rangle = E + F(\mathbf{k}) + \hbar^2 k^2/2M$$

and

$$\hat{R}_{\mathbf{k}}(\omega) = \int_0^\infty dt\, e^{-i\omega t} R_{\mathbf{k}}(t)$$

Finally,

$$R_{\mathbf{k}}(t) = \frac{1}{N^2} \sum_{\mathbf{q}} \sum_{\mathbf{q}'} (1 - \delta_{\mathbf{kq}})(1 - \delta_{\mathbf{kq}'}) \times \langle W_{\mathbf{kq}}\, a_{\mathbf{q}} \exp\,[i(1 - P_{\mathbf{k}})Lt](1 - P_{\mathbf{k}}) W_{\mathbf{q}'\cdot\mathbf{k}}\, a_{\mathbf{q}'}^+\rangle \tag{106}$$

with

$$W_{\mathbf{kq}} = \frac{1}{M}\,\mathbf{q}\cdot\mathbf{J}_{\mathbf{q}-\mathbf{k}} + \frac{\hbar\mathbf{q}^2}{2M}\,\rho_{\mathbf{q}-\mathbf{k}}$$

Again, introducing the simplifying assumptions

$$[P_{\mathbf{k}}, L] \simeq 0$$

$$\exp(iP_{\mathbf{k}} Lt) \simeq \exp(iP_{\mathbf{k}} L_0 t)$$

where

$$L_0 Z = \frac{1}{\hbar}[H_{ex}, Z]$$

we find that

$$R_{\mathbf{k}}(t) = \frac{1}{N^2}\sum_{\mathbf{q}}(1 - \delta_{\mathbf{kq}})G_{\mathbf{q}}(t)\langle W_{\mathbf{kq}}(0)W_{\mathbf{qk}}(t)\rangle \tag{107}$$

The correlation function in Eq. (107) may be expressed in the form

$$\begin{aligned}\langle W_{\mathbf{kq}} W_{\mathbf{qk}}(t)\rangle = {} & \frac{\hbar^2 q^2 k^2}{4M^2}\int_{-\infty}^{\infty} d\omega\, e^{i\omega t} S(\mathbf{k} - \mathbf{q}, \omega) \\ & + \frac{1}{M^2}\mathbf{kq} : \langle \mathbf{J}_{\mathbf{q}-\mathbf{k}} \mathbf{J}_{\mathbf{k}-\mathbf{q}}(t)\rangle \\ & + \frac{\hbar q^2}{2M^2}\mathbf{k} \cdot \langle \rho_{\mathbf{q}-\mathbf{k}} \mathbf{J}_{\mathbf{k}-\mathbf{q}}(t)\rangle \\ & + \frac{\hbar k^2}{2M^2}\mathbf{q} \cdot \langle \mathbf{J}_{\mathbf{q}-\mathbf{k}} \rho_{\mathbf{k}-\mathbf{q}}(t)\rangle \end{aligned} \tag{108}$$

where $S(\mathbf{k},\omega)$ is the Van Hove structure factor[26] defined by

$$S(\mathbf{k}, \omega) = \frac{1}{2\pi}\int_{-\infty}^{\infty} dt\, e^{-i\omega t}\langle \rho_{-\mathbf{k}} \rho_{\mathbf{k}}(t)\rangle \tag{109}$$

In principle $S(\mathbf{k},\omega)$ may be obtained from measurements of the differential cross section for x-ray or neutron scattering from the fluid.[26]

The remaining correlation functions of Eq. (108) must be evaluated through some approximation scheme. The one we employ was also used by Fisher and Rice,[25] and was first suggested in an important paper by Zwanzig.[27] The assumption is that $\mathbf{J}_{\mathbf{k}}(t)$ satisfies a damped oscillator equation of motion:

$$\frac{d^2}{dt^2}\mathbf{J}_{\mathbf{k}}(t) + \Omega_{\mathbf{k}}{}^2 \mathbf{J}_{\mathbf{k}}(t) + \frac{1}{\tau_{\mathbf{k}}}\frac{d}{dt}\mathbf{J}_{\mathbf{k}}(t) = 0 \tag{110}$$

Eq. (110) has the general solution

$$\mathbf{J}_{\mathbf{k}}(t) = \left[\mathbf{J}_{\mathbf{k}}(0) - \frac{\dot{\mathbf{J}}_{\mathbf{k}}(0) - \alpha_{\mathbf{k}}\mathbf{J}_{\mathbf{k}}(0)}{(\xi_{\mathbf{k}} - \alpha_{\mathbf{k}})}\right] \exp\{\alpha_{\mathbf{k}} t\} + \left[\frac{\dot{\mathbf{J}}_{\mathbf{k}}(0) - \alpha_{\mathbf{k}}\mathbf{J}_{\mathbf{k}}(0)}{(\xi_{\mathbf{k}} - \alpha_{\mathbf{k}})}\right] \exp\{\xi_{\mathbf{k}} t\} \tag{111a}$$

where the dot signifies a time derivative and

$$\begin{aligned} \alpha_{\mathbf{k}} &= -\frac{1}{2\tau_{\mathbf{k}}} + \left[\left(\frac{1}{2\tau_{\mathbf{k}}}\right)^2 - \Omega_{\mathbf{k}}^2\right]^{1/2} \\ \xi_{\mathbf{k}} &= -\frac{1}{2\tau_{\mathbf{k}}} - \left[\left(\frac{1}{2\tau_{\mathbf{k}}}\right)^2 - \Omega_{\mathbf{k}}^2\right]^{1/2} \end{aligned} \tag{111b}$$

In order to facilitate the remainder of the calculations, classical mechanics is used to evaluate the correlation functions of Eq. (108). That is to say, $-i\hbar\nabla_n = \mathbf{P}_n =$ momentum of nth atom, and the canonical ensemble averages are performed according to the prescription:

$$\langle A\rangle = \frac{\int d\{\mathbf{P}\}\, d\{\mathbf{R}\} \exp\left(-\beta\left[\sum_{n=1}^{N} P_n^2/2M + \mathrm{U}\{\mathbf{R}\}\right]\right) A(\{\mathbf{P}, \mathbf{R}\})}{\int d\{\mathbf{P}\}\, d\{\mathbf{R}\} \exp\left(-\beta\left[\sum_n P_n^2/2M + \mathrm{U}\{R\}\right]\right)} \tag{112}$$

The expression for $\mathbf{J}_{\mathbf{k}}(t)$ in Eq. (111) is incomplete since the initial conditions on $\mathbf{J}_{\mathbf{k}}(0)$ and $\dot{\mathbf{J}}_{\mathbf{k}}(0)$ are not specified. However, we do have expressions for these functions for $t = 0$ from Eq. (102b).

Classical mechanical averaging of the correlation functions appearing in Eq. (108) yields

$$\begin{aligned} \langle \mathbf{J}_{\mathbf{k}}(0)\mathbf{J}_{-\mathbf{k}}(t)\rangle &= \frac{MN}{\beta}\mathbf{1}(\xi_{\mathbf{k}} \exp(\alpha_{\mathbf{k}} t) - \alpha_{\mathbf{k}} \exp(\xi_{\mathbf{k}} t)) \\ \langle \rho_{\mathbf{k}}(0)\mathbf{J}_{-\mathbf{k}}(t)\rangle &= -i\mathbf{k}\frac{MNS(\mathbf{k})}{\beta(\xi_{\mathbf{k}} - \alpha_{\mathbf{k}})}(\exp(\xi_{\mathbf{k}} t) - \exp(\alpha_{\mathbf{k}} t)) \\ \langle \mathbf{J}_{\mathbf{k}}(0)\rho_{-\mathbf{k}}(t)\rangle &= i\mathbf{k}\frac{MNS(\mathbf{k})}{\beta(\xi_{\mathbf{k}} - \alpha_{\mathbf{k}})}(\exp(\xi_{\mathbf{k}} t) - \exp(\alpha_{\mathbf{k}} t)) \end{aligned} \tag{113}$$

As usual $S(\mathbf{k})$ is the static structure factor,

$$\begin{aligned} S(\mathbf{k}) &= \int_{-\infty}^{\infty} d\omega\, S(\mathbf{k}, \omega) \\ &= \langle \rho_{\mathbf{k}}(0)\rho_{-\mathbf{k}}(0)\rangle \end{aligned} \tag{114}$$

In the derivation of Eq. (113), we have set equal to zero the average of the Fourier transform of the force acting on a particle. This force term appears in the calculation of $\langle \rho_{\mathbf{k}} \mathbf{J}_{-\mathbf{k}}(t) \rangle$ and $\langle \mathbf{J}_{\mathbf{k}} \rho_{-\mathbf{k}}(t) \rangle$.

That there is some error in using classical mechanics for the evaluation of these integrals can be best seen by the following example in which $\langle \rho_{\mathbf{k}}(0) \rho_{-\mathbf{k}}(0) \rangle$ is presented. From Eq. (109) and use of the identity.

$$\int d\omega \, \omega S(\mathbf{k},\omega) = \frac{\hbar k^2}{2M} \tag{115}$$

we find that

$$\langle \rho_{\mathbf{k}}(0) \dot{\rho}_{-\mathbf{k}}(0) \rangle = \frac{-i\hbar k^2}{2M} \tag{116}$$

From classical mechanics, with the use of (102c) and (112), we find

$$\langle \rho_{\mathbf{k}}(0) \dot{\rho}_{-\mathbf{k}}(0) \rangle = 0 \tag{117}$$

In the limit as $\hbar \to 0$, the two expressions in Eqs. (116) and (117) agree for any $\mathbf{k}$. Clearly, if we restrict attention to small values of $|\mathbf{k}|$, approximate agreement is also insured. This example shows that having used a classical averaging procedure, our calculations are restricted to the range where $|\mathbf{k}|$ is small. Since the quantum states of the fluid can be labelled with a real quasimomentum $\mathbf{k}$ only if $|\mathbf{k}|$ is small compared to σ^{-1}, this is no further restriction on our analysis.

With the help of Eq. (113) we can now write an explicit expression for $\hat{R}_{\mathbf{k}}(\omega)$. That expression is

$$\hat{R}_{\mathbf{k}}(\omega) = \frac{1}{N^2} \sum_{q} \int_{-\infty}^{\infty} d\omega' \, \hat{G}_{\mathbf{q}}(\omega - \omega') \tilde{W}_{\mathbf{kq}}(\omega')(1 - \delta_{\mathbf{kq}}) \tag{118}$$

where

$$\tilde{W}_{\mathbf{kq}}(\omega) = \frac{1}{2\pi} \int_{-\infty}^{\infty} dt \, e^{-i\omega t} \langle W_{\mathbf{kq}} W_{\mathbf{qk}}(t) \rangle \tag{119}$$

The correlation function in (119) is

$$\begin{aligned} \langle W_{\mathbf{kq}} W_{\mathbf{qk}}(t) \rangle = {} & \frac{\mathbf{k} \cdot \mathbf{q}}{\beta M} (\xi_{\mathbf{k}} \exp(\alpha_{\mathbf{k}} t) - \exp(\xi_{\mathbf{k}} t)) \\ & + \frac{\hbar^2 q^2 k^2}{4M^2} \int_{-\infty}^{\infty} d\omega \, e^{i\omega t} S(\mathbf{k} - \mathbf{q}, \omega) \\ & + \frac{i\hbar}{2\beta M} S(\mathbf{k} - \mathbf{q}) \frac{1}{\xi_{\mathbf{k}} - \alpha_{\mathbf{k}}} (\exp(\xi_{\mathbf{k}} t) - \exp(\alpha_{\mathbf{k}} t)) \end{aligned} \tag{120}$$

so that, after integration,

$$\tilde{W}_{\mathbf{kq}}(\omega) = \frac{\hbar^2 q^2 k^2}{4M^2} S(\mathbf{k}-\mathbf{q},\omega) + \frac{\mathbf{k}\cdot\mathbf{q}}{2\pi m\beta}\left(\frac{1}{\tau_{\mathbf{k}-\mathbf{q}}}\right)$$
$$\times\left[\frac{-\frac{1}{2\tau_{\mathbf{k}-\mathbf{q}}} - i\Omega_{\mathbf{k}-\mathbf{q}}}{(\omega-\Omega_{\mathbf{k}-\mathbf{q}})^2 + \left(\frac{1}{2\tau_{\mathbf{k}-\mathbf{q}}}\right)^2} + \frac{\frac{1}{2\tau_{\mathbf{k}-\mathbf{q}}} - i\Omega_{\mathbf{k}-\mathbf{q}}}{(\omega+\Omega_{\mathbf{k}-\mathbf{q}})^2 + \left(\frac{1}{2\tau_{\mathbf{k}-\mathbf{q}}}\right)^2}\right]$$
$$+\frac{i\hbar S(\mathbf{k}-\mathbf{q})}{8\pi M\beta}\left(\frac{1}{\tau_{\mathbf{k}-\mathbf{q}}}\right)[2q^2k^2 - \mathbf{k}\cdot\mathbf{q}(k^2+q^2)]$$
$$\times\left[\frac{1}{(\omega-\Omega_{\mathbf{k}-\mathbf{q}})^2 + \left(\frac{1}{2\tau_{\mathbf{k}-\mathbf{q}}}\right)^2} + \frac{1}{(\omega+\Omega_{\mathbf{k}-\mathbf{q}})^2 + \left(\frac{1}{2\tau_{\mathbf{k}-\mathbf{q}}}\right)^2}\right] \tag{121}$$

If it is assumed that the damping is very small compared to the eigenfrequency $\Omega_{\mathbf{k}}$ corresponding to a collective translational excitation of the fluid, we find that

$$\begin{aligned} \text{Im}\,\xi_{\mathbf{k}} &= -\text{Im}\,\alpha_{\mathbf{k}} = \Omega_{\mathbf{k}} \\ \text{Re}\,\xi_{\mathbf{k}} &= \text{Re}\,\alpha_{\mathbf{k}} = \tfrac{1}{2}\tau_{\mathbf{k}} \end{aligned} \tag{122}$$

and we obtain for $\hat{R}_{\mathbf{k}}(\omega)$ the lengthy formula:

$$\hat{R}_{\mathbf{k}}(\omega) = \frac{1}{N}\sum_{\mathbf{q}}\int_{-\infty}^{\infty} d\omega' \hat{G}_{\mathbf{q}}(\omega')$$
$$\times\left\{\frac{\hbar^2 q^2 k^2}{4M^2} S(\mathbf{k}-\mathbf{q},\omega') + \frac{\mathbf{k}\cdot\mathbf{q}}{2\pi\beta M}\left(\frac{1}{\tau_{\mathbf{k}-\mathbf{q}}}\right)\right.$$
$$\times\left[\frac{-(1/2\tau_{\mathbf{k}-\mathbf{q}}) - i\Omega_{\mathbf{k}-\mathbf{q}}}{(\omega-\Omega_{\mathbf{k}-\mathbf{q}})^2 + \frac{1}{4}(1/\tau_{\mathbf{k}-\mathbf{q}})^2} + \frac{(1/2\tau_{\mathbf{k}-\mathbf{q}}) - i\Omega_{\mathbf{k}-\mathbf{q}}}{(\omega+\Omega_{\mathbf{k}-\mathbf{q}})^2 + \frac{1}{4}(1/\tau_{\mathbf{k}-\mathbf{q}})^2}\right]$$
$$+\frac{i\hbar S(\mathbf{k}-\mathbf{q})}{8\pi\beta M}\left(\frac{1}{\tau_{\mathbf{k}-\mathbf{q}}}\right)[2q^2k^2 - \mathbf{k}\cdot\mathbf{q}(k^2+q^2)]$$
$$\left.\times\left[\frac{1}{(\omega+\Omega_{\mathbf{k}-\mathbf{q}})^2 + \frac{1}{4}(1/\tau_{\mathbf{k}-\mathbf{q}})^2} - \frac{1}{(\omega-\Omega_{\mathbf{k}-\mathbf{q}})^2 + \frac{1}{4}(1/\tau_{\mathbf{k}-\mathbf{q}})^2}\right]\right\} \tag{123}$$

The spectral shift may be evaluated from the imaginary part of $\hat{R}_{\mathbf{k}}(\omega)$ and the linewidth from the real part (see Eq. (53)). All of the parameters in Eq. (123) may be obtained from experimental scattering and lifetime data.

Note that our treatment of optical absorption in fluids omits interband scattering and any effects of nuclear motion on the internal electronic states of an atom in the fluid.

In the limit of infinitely large systems, we desire to replace the sum over $\mathbf{q}$ by an integral. In order to do so we need to know the density of states in $\mathbf{q}$-space. If we assume that the density of fluid states is the same as that of a solid, i.e., is equal to the fluid volume, we simply replace

$$\frac{1}{N}\sum_{\mathbf{q}} \rightarrow \frac{V}{N}\int d\mathbf{q}$$

We repeat once more, however, that the $\mathbf{q}$-states may not bunch together with a uniform density as in a crystal, nor is $\mathbf{q}$ restricted to the real axis.

VI. SUMMARY AND DISCUSSION

The preceding sections have been devoted to a detailed derivation of expressions for the optical absorption profile function, $\hat{G}(\omega)$, appropriate to transitions in several types of condensed media. A particular approach which involved the use of a projection operator, was employed to develop a formal solution for the complex Laplace transform of the time dependent correlation function of interest. To then reduce the formal expressions to tractable forms, several simplifying approximations were introduced. These approximations implied that the coupling between the electronic state of interest and the lattice or fluid "bath" was weak. For the purposes of convenience and discussion the final results obtained in each preceding section are reproduced in this final section. Even after reduction by approximation our results are formidably formal: at present, in only one instance, the case of an impurity molecule in a crystal lattice, have we completed some numerical calculations. The other two situations considered, that of light absorption in a pure crystal and in a pure fluid, may also be studied further by the use of numerical calculations, but we have not attempted such a study in this work.

A. Impurity Absorption

The conductivity of a crystal containing a small fraction of nonresonant impurity molecules of number density n/v is given by

$$\sigma(\omega) = \omega \frac{n}{V} |M_{0f}|^2 \operatorname{Re} \mathscr{G}_f(\omega) \tag{124}$$

where the function $\mathscr{G}_f(\omega)$ is the convolution of the B-O intensity function $\mathscr{I}_{0f}(\omega)$ and the electronic spectral function $\hat{G}_f(\omega)$:

$$\mathscr{G}_f(\omega) = \int_{-\infty}^{\infty} d\xi\, \hat{G}_f(\omega - \xi)\mathscr{I}_{0f}(\xi + \omega_f) \tag{125}$$

By the use of the projection operator and subsequent simplifying approximations, the profile function $\hat{G}_f(\omega)$ is found to be

$$\operatorname{Re} \hat{G}_f(\omega) = \frac{\operatorname{Re} \hat{K}_f(\omega)}{[\omega - \omega_f + \operatorname{Im} \hat{K}_f(\omega)]^2 + [\operatorname{Re} \hat{K}_f(\omega)]^2} \tag{126}$$

where the width function, or self-energy term, $\hat{K}_f(\omega)$ is

$$\begin{aligned}
&\frac{1}{\pi} \operatorname{Re} \hat{K}_f(\omega + \omega_f) \\
&\quad = \sum_g{}' \sum_J |F_J{}^{fg}|^2 [(\langle n_J \rangle + 1) \mathcal{J}_{fg}(\omega - \omega_J) + \langle n_J \rangle \mathcal{J}_{fg}(\omega + \omega_J)] \\
&\quad + \sum_g{}' \sum_{I,J} F_J{}^{fg} F_I{}^{gf} \{[(S_I{}^f)^{1/2} - (S_I{}^g)^{1/2}][(S_J{}^f)^{1/2} - (S_J{}^g)^{1/2}] \\
&\quad \times [(\tfrac{3}{2} - \langle n_J \rangle - \langle n_I \rangle)\{\mathcal{J}_{fg}(\omega - \omega_J) + \mathcal{J}_{fg}(\omega - \omega_I)\} \\
&\quad + (\tfrac{1}{2} - \langle n_J \rangle - \langle n_I \rangle)\{\mathcal{J}_{fg}(\omega + \omega_I) + \mathcal{J}_{fg}(\omega + \omega_J)\} \\
&\quad + \tfrac{1}{2}[1 - \langle n_I \rangle \langle n_J \rangle (1 + \exp[\beta\hbar(\omega_I + \omega_J)])]\{\mathcal{J}_{fg}(\omega - \omega_I - \omega_J) \\
&\quad + \mathcal{J}_{fg}(\omega + \omega_I + \omega_J)\} - \tfrac{1}{2}\langle n_J \rangle \langle n_I \rangle (1 + \exp[\beta\hbar(\omega_I + \omega_J)]) \\
&\quad \times \{\mathcal{J}_{fg}(\omega + \omega_J - \omega_J) + \mathcal{J}_{fg}(\omega - \omega_I + \omega_J)\}] - \mathcal{J}_{fg}(\omega)\} \\
&\quad + 2 \sum_{I,J} \sum_g{}' F_I{}^{fg} F_J{}^{fg} (S_I{}^g)^{1/2} \{(S_J{}^f)^{1/2} - (S_J{}^g)^{1/2}\}[(2 - \langle n_I \rangle - \langle n_J \rangle) \\
&\quad \times \mathcal{J}_{fg}(\omega - \omega_J) + (1 - \langle n_J \rangle - \langle n_I \rangle)\mathcal{J}_{fg}(\omega + \omega_J) + \mathcal{J}_{fg}(\omega)] \\
&\quad + 4 \sum_g{}' \sum_{I,J} F_I{}^{gf} F_J{}^{fg} (S_I{}^g S_J{}^g)^{1/2} \mathcal{J}_{fg}(\omega) \\
&\quad + \sum_J |T_J{}^f|^2 [(\langle n_J \rangle + 1)\mathcal{J}_{f0}(\omega - \omega_J) + \langle n_J \rangle \mathcal{J}_{f0}(\omega + \omega_J)] \\
&\quad + \sum_{I,J} T_J{}^f T_I{}^f \{(S_I{}^f S_J{}^f)^{1/2}[(\tfrac{1}{2} - \langle n_J \rangle - \langle n_I \rangle)\{\mathcal{J}_{f0}(\omega - \omega_J) \\
&\quad + \mathcal{J}_{f0}(\omega - \omega_I)\} + (\tfrac{1}{2} - \langle n_J \rangle - \langle n_I \rangle)\{\mathcal{J}_{f0}(\omega + \omega_J) \\
&\quad + \mathcal{J}_{f0}(\omega + \omega_I)\} + \tfrac{1}{2}[1 - \langle n_J \rangle \langle n_I \rangle (1 + \exp[\beta\hbar(\omega_I + \omega_J)]) \\
&\quad \times \{\mathcal{J}_{f0}(\omega - \omega_I - \omega_J) + \mathcal{J}_{f0}(\omega + \omega_I + \omega_J)\} - \tfrac{1}{2}\langle n_J \rangle \langle n_I \rangle \\
&\quad \times (1 + \exp[\beta\hbar(\omega_I + \omega_J)])\{\mathcal{J}_{f0}(\omega + \omega_I - \omega_J) + \\
&\quad + \mathcal{J}_{f0}(\omega - \omega_I + \omega_J)\} - \mathcal{J}_{f0}(\omega)\} \\
&\quad + \sum_{I,J} \sum_g{}' T_I{}^g T_J{}^g (S_I{}^f S_J{}^f)^{1/2} \int_{-\infty}^{\infty} d\xi \hat{G}_f(\xi) \mathcal{J}_{0g}(\omega - \xi)
\end{aligned} \tag{127}$$

In the Appendix we have outlined the model calculation of the real part of $\hat{K}_f(\omega)$ under the Lorentzian approximation in which $\hat{K}_f(\omega)$ is independent

of frequency in the vicinity of $\omega = \omega_f$. The dominant contributions to the linewidth arise from dynamical processes in which the electronic state of interest relaxes to a lower lying electronic state and emits phonons into the lattice. The line width associated with this type of scattering shows a slight tendency to decrease as the temperature is raised but is, roughly speaking, essentially constant over a wide range of temperature. The temperature narrowing cited is associated with a redistribution of the B.-O. intensity with temperature for electronic states whose potential curves possess different minima along a given normal coordinate. Our calculations show that the larger the separation between the electronic states between which scattering occurs, and the larger the difference in the positions of the potential minima, the more rapid is the rate of change of the linewidth with respect to temperature.

We expect, therefore, from our numerical results that the non-Born-Oppenheimer scattering terms in the Hamiltonian will determine the zero temperature linewidth, while higher order B.-O. interactions, such as quadratic coupling, determine the temperature behavior of the observed lineshapes.

The process in which energy is absorbed from the lattice to promote an electron from the state of interest to a higher electronic state is shown to be negligible in its contribution to the linewidth. While it is true that this phonon absorption type of scattering exhibits a contribution to the increase in linewidth with increasing temperature, the numerical values of such contributions are less than those due to photon–matter lifetime broadening.

The behavior of the scattering contributions to the impurity lineshape bears an interesting analogy to the behavior of macroscopic thermodynamic systems. We may reword the description of temperature narrowing of the relaxation processes in which phonons are generated in the lattice to say that as the temperature is raised and, hence, as the number of phonons present at equilibrium in the lattice is increased, the lattice shows a greater resistance to absorbing more phonons created by a relaxation of the excited electronic state to a lower lying electronic state.

The greater feasibility of electronic relaxation with phonon generation as opposed to electronic excitation with phonon absorption describes a situation in which the total energy associated with the coupled impurity-lattice system tends to be preferentially distributed among as many normal modes as possible.

B. Absorption in a Pure Crystal

The expression for the crystal conductivity of a pure crystal is formally the same as that for an impure crystal if we interpret the number density

n/V as the number of molecules per unit volume instead of the number of impurity molecules per unit volume. The conductivity now, however, is nonlocal, that is **k**-dependent, since we are interested in the static crystal states of index **k**. The absorption spectral function of interest is

$$\mathscr{G}_{\mathbf{k}f}(\omega) = \frac{1}{N}\sum_{\mathbf{q}}\int_{-\infty}^{\infty} d\xi\, \hat{G}_{\mathbf{q}f}(\omega - \xi)\mathscr{J}_{\mathbf{k}-\mathbf{q}f}(\xi + \omega_{\mathbf{k}-\mathbf{q}}) \tag{128}$$

where $\hat{G}_{\mathbf{k}f}(\omega)$ is

$$\operatorname{Re}\hat{G}_{\mathbf{k}f}(\omega) = \frac{\operatorname{Re}\hat{R}_{\mathbf{k}f}(\omega)}{(\omega - \omega_{\mathbf{k}f} + \operatorname{Im}\hat{R}_{\mathbf{k}f}(\omega))^2 + (\operatorname{Re}\hat{R}_{\mathbf{k}f}(\omega))^2}$$

and

$$\mathscr{J}_{\mathbf{k}-\mathbf{q}f}(\omega) = \frac{1}{2\pi}\int_{-\infty}^{\infty} dt \exp\left[-i(\omega - \omega_{\mathbf{k}-\mathbf{q}})t\right]\langle B_{\mathbf{k}-\mathbf{q}f} B^{+}_{\mathbf{k}-\mathbf{q}f}(t)\rangle \tag{129}$$

where

$$B^{+}_{\mathbf{k}} = \left(\frac{1}{N}\right)^{1/2}\sum_{n}\exp(i\mathbf{k}\mathbf{X}_n)B^{+}_{nf}$$

The linewidth function $\hat{R}_{\mathbf{k}f}(\omega)$ may be shown to assume the following approximate form in a harmonic lattice:

$$\hat{R}_{\mathbf{k}f}(\omega) = \int_{0}^{\infty} dt\, e^{-i\omega t}R_{\mathbf{k}f}(t)$$

where

$$R_{\mathbf{k}f}(t) = \sum_{\mathbf{k}'f'}(1 - \delta_{k'k})G_{\mathbf{k}'f'}(t)\langle C^{ff'}_{\mathbf{k}\mathbf{k}'}C^{f'f}_{\mathbf{k}'\mathbf{k}}(t)\rangle$$

and finally,

$$\begin{aligned}
&\langle C^{ff'}_{\mathbf{k}\mathbf{k}'}C^{f'f}_{\mathbf{k}'\mathbf{k}}(t)\rangle \\
&= \frac{1}{N^2}\sum_{n,m}\sum_{n',m'}\exp\left[i\mathbf{k}\cdot(\mathbf{X}_n - \mathbf{X}_{n'}) - i\mathbf{k}'\cdot(\mathbf{X}_m - \mathbf{X}_{m'})\right] \\
&\quad\times\{K^{f}_{n-m}\langle B^{+}_{nf}B_{mf}B^{+}_{m'f}(t)B_{n'f}(t)\rangle K^{f}_{m'-n'} + \sum_{\mathbf{q}j}F^{m'-n'}_{\mathbf{q}j}(f', f)K^{f}_{n-m} \\
&\quad\times\langle B^{+}_{nf}B_{mf}B^{+}_{m'f'}(t)B_{n'f}(t)\rangle[-2\gamma_{\mathbf{q}j}{}^{f'}\exp(-i\mathbf{q}\cdot\mathbf{X}_{m'}) \\
&\quad-\gamma_{\mathbf{q}j}{}^{f}(\exp[-i\mathbf{q}\cdot\mathbf{X}_n] - \exp[-i\mathbf{q}\cdot\mathbf{X}_m]) \\
&\quad\times(\exp[i\Omega_j(\mathbf{q})t] + \exp[-i\Omega_j(\mathbf{q})t]) \\
&\quad+\langle n_{\mathbf{q}j}\rangle[\gamma_{\mathbf{q}j}{}^{f}(\exp[-i\mathbf{q}\cdot\mathbf{X}_n] - \exp[-i\mathbf{q}\cdot\mathbf{X}_m]
\end{aligned}$$

$$
\begin{aligned}
&- \exp[-i\mathbf{q}\cdot\mathbf{X}_{n'} - i\Omega_j(\mathbf{q})t]) + \gamma_{\mathbf{q}j}{}^{f'} \exp[-i\mathbf{q}\cdot\mathbf{X}_{m'} + i\Omega_j(\mathbf{q})t] \\
&\times (\exp[i\Omega_j(\mathbf{q})t] + \exp[-i\Omega_j(\mathbf{q})t + \beta\hbar\Omega_j(\mathbf{q})]) \\
&+ \sum_{\mathbf{q}j} F^{n-m}_{\mathbf{q}j}(f, f') K^{f}_{m'-n'} \langle B^{+}_{nf} B_{mf'} B^{+}_{m'f}(t) B_{n'f}(t)\rangle \\
&\times [-2\gamma_{\mathbf{q}j}{}^{f} \exp(-i\mathbf{q}\cdot\mathbf{X}_n) + \gamma_{\mathbf{q}j}{}^{f} \{\exp(-i\mathbf{q}\cdot\mathbf{X}_n) + \exp[i\Omega_g(\mathbf{q})t] \\
&\times (\exp[-i\mathbf{q}\cdot\mathbf{X}_{m'}] - \exp[-i\mathbf{q}\cdot\mathbf{X}_{n'}])\} \\
&+ \gamma_{\mathbf{q}j}{}^{f'} \exp[-i\mathbf{q}\cdot\mathbf{X}_{n'} + i\Omega_j(\mathbf{q})t]] + \sum_{\mathbf{q}j}\sum_{\sigma l} F^{n-m}_{\sigma l}(f, f') F^{m'-n'}_{\mathbf{q}j}(f', f) \\
&\times \langle B^{+}_{nf} B_{mf'} B^{+}_{m'f'}(t) B_{n'f}(t)\rangle [-2\gamma_{\sigma l}{}^{f} \exp(-i\boldsymbol{\sigma}\cdot\mathbf{X}_n) \\
&\times \{-2\gamma_{\mathbf{q}j}{}^{f'} \exp(-i\mathbf{q}\cdot\mathbf{X}_{m'}) - \gamma_{\mathbf{q}j}{}^{f} (\exp[-i\mathbf{q}\cdot\mathbf{X}_n] \\
&- \exp[-i\mathbf{q}\cdot\mathbf{X}_m])(\exp[i\Omega_j(\mathbf{q})t] + \exp[-i\Omega_j(\mathbf{q})t]) \\
&+ \langle n_{\mathbf{q}j}\rangle [\gamma_{\mathbf{q}j}{}^{f} (\exp[-i\mathbf{q}\cdot\mathbf{X}_n] - \exp[-i\mathbf{q}\cdot\mathbf{X}_{n'} - i\Omega_j(\mathbf{q})t]) \\
&+ \gamma_{\mathbf{q}j}{}^{f'} (\exp[-i\mathbf{q}\cdot\mathbf{X}_{m'} + i\Omega_j(\mathbf{q})t] - \exp[-i\mathbf{q}\cdot\mathbf{X}_m])] \\
&\times (\exp[i\Omega_j(\mathbf{q})t] + \exp[-i\Omega_j(\mathbf{q})t + \beta\hbar\Omega_j(\mathbf{q})])\} \\
&- \{\gamma_{\sigma l}{}^{f} (\exp[-i\boldsymbol{\sigma}\cdot\mathbf{X}_n] - \exp[-i\boldsymbol{\sigma}\cdot\mathbf{X}_{n'} - i\Omega_j(\boldsymbol{\sigma})t]) \\
&- \gamma_{\sigma l}{}^{f'} (\exp[-i\boldsymbol{\sigma}\cdot\mathbf{X}_m] + \exp[-i\boldsymbol{\sigma}\cdot\mathbf{X}_{m'} - i\Omega_l(\boldsymbol{\sigma})t])\} \\
&\times \{-2\gamma_{\mathbf{q}j}{}^{f'} \exp(-i\mathbf{q}\cdot\mathbf{X}_{n'}) - (\gamma_{\mathbf{q}j}{}^{f} \exp[-i\mathbf{q}\cdot\mathbf{X}_n] \\
&- \gamma_{\mathbf{q}j}{}^{f'} \exp[-i\mathbf{q}\cdot\mathbf{X}_m])(\exp[i\Omega_j(\mathbf{q})t] + \exp[-i\Omega_j(\mathbf{q})t])\}] \\
&+ \langle n_{\mathbf{q}j}\rangle\langle n_{\sigma l}\rangle \{\gamma_{\sigma l}{}^{f} (\exp[-i\boldsymbol{\sigma}\cdot\mathbf{X}_n] - \exp[-i\boldsymbol{\sigma}\cdot\mathbf{X}_{n'} - i\Omega_l(\boldsymbol{\sigma})t]) \\
&- \gamma_{\sigma l}{}^{f'} (\exp[-i\boldsymbol{\sigma}\cdot\mathbf{X}_m] - \exp[-i\boldsymbol{\sigma}\cdot\mathbf{X}_{m'} - i\Omega_l(\boldsymbol{\sigma})t])\} \\
&\times \{\gamma_{\mathbf{q}j}{}^{f} (\exp[-i\mathbf{q}\cdot\mathbf{X}_n] - \exp[-i\mathbf{q}\cdot\mathbf{X}_{n'} - i\Omega_j(\mathbf{q})t]) \\
&\times \gamma_{\mathbf{q}j}{}^{f'} (\exp[-i\mathbf{q}\cdot\mathbf{X}_m] - \exp[-i\mathbf{q}\cdot\mathbf{X}_{m'} - i\Omega_j(\mathbf{q})t])\} \\
&\times \{\exp[i\Omega_j(\mathbf{q})t] + \exp[-i\Omega_j(\mathbf{q})t + \beta\hbar(\Omega_j(\mathbf{q}) + \Omega_i(\boldsymbol{\sigma}))] \\
&- \exp[-i\Omega_j(\mathbf{q})t + \beta\hbar\Omega_j(\mathbf{q})] - \exp[i\Omega_j(\mathbf{q}) + \beta\hbar\Omega_i(\boldsymbol{\sigma})]\} \\
&+ \delta_{j,l}\delta_{\mathbf{q}-\boldsymbol{\sigma}} \{(\langle n_{\sigma l}\rangle + 1) \exp[i\Omega_l(\boldsymbol{\sigma})t] + \langle n_{\sigma l}\rangle \exp[-i\Omega_l(\boldsymbol{\sigma})t]\}].
\end{aligned}
\tag{130}
$$

We note that the expression for the lineshape of a transition originating on an impurity molecule in a lattice and the corresponding lineshape for a transition in a pure crystal are very similar in structure, although the low frequency phonon modes of the pure crystal are much more important for

dynamical state mixing than they are in the doped crystal. The pure crystal linewidth expressions cited do not include terms which cause relaxation of the exciton state back to the crystal ground state, under the assumption that the dominant contribution to the linewidth is from intraband **k**-mixing.

C. Absorption in a Pure Liquid

Our theoretical analysis of the lineshape of optical absorption in a semiclassical fluid stressed the dynamical effects and assumed that the mixing of states due to fluid disorder was negligible. Other authors have discussed how **k**-mixing due to disorder becomes small as $\mathbf{k} \to \mathbf{0}$. On the other hand, the dynamical state mixing contribution to the linewidth also vanishes as $\mathbf{k} \to \mathbf{0}$ as is seen from an examination of our final expressions in Section IV (which are reproduced below). It would seem that a combination theory which contained disorder and dynamical state mixing is called for.

In our calculations the electronic states of the fluid are coupled to the momentum and density excitations of the fluid. The lineshape function is defined in analogy to the crystal spectral function, Eq. (129), with the self-energy given by

$$\begin{aligned}\hat{R}_{\mathbf{k}}(\omega) = \frac{v}{N}\int d\mathbf{q} \int_{-\infty}^{\infty} d\xi\, \hat{G}_{\mathbf{q}}(\omega - \xi)\Bigg[& \frac{\hbar^2 q^2 k^2}{4M^2} S(\mathbf{k}-\mathbf{q}, \xi) \\ & + \frac{\mathbf{k}\cdot\mathbf{q}}{2\pi M\beta}\left(\frac{1}{\tau_{\mathbf{k}-\mathbf{q}}}\right)\Bigg[\frac{-\left(\frac{1}{2\tau_{\mathbf{k}-\mathbf{q}}}\right) - i\Omega_{\mathbf{k}-\mathbf{q}}}{(\xi - \Omega_{\mathbf{k}-\mathbf{q}})^2 + \left(\frac{1}{2\tau_{\mathbf{k}-\mathbf{q}}}\right)^2} \\ & + \frac{\left(\frac{1}{2\tau_{\mathbf{k}-\mathbf{q}}}\right) - i\Omega_{\mathbf{k}-\mathbf{q}}}{(\xi + \Omega_{\mathbf{k}-\mathbf{q}})^2 + \left(\frac{1}{2\tau_{\mathbf{k}-\mathbf{q}}}\right)^2}\Bigg] \\ & + \frac{i\hbar S(\mathbf{k}-\mathbf{q})}{8\pi M\beta}\left(\frac{1}{\tau_{\mathbf{k}-\mathbf{q}}}\right)[2q^2k^2 - \mathbf{k}\cdot\mathbf{q}(k^2+q^2)] \\ & \times\left[\frac{1}{(\xi + \Omega_{\mathbf{k}-\mathbf{q}})^2 + \left(\frac{1}{2\tau_{\mathbf{k}-\mathbf{q}}}\right)^2} - \frac{1}{(\xi - \Omega_{\mathbf{k}-\mathbf{q}})^2 + \left(\frac{1}{2\tau_{\mathbf{k}-\mathbf{q}}}\right)^2}\right]\Bigg]\end{aligned} \tag{131}$$

We may describe the linewidth or self-energy term $\hat{R}_{\mathbf{k}}(\omega)$ as the convolution of the spectral functions for momentum and density excitations of the fluid with the profile function of the states belonging to the exciton band, omitting only $\mathbf{k}$ itself. We have introduced the assumption that the momentum excitations possess Lorentzian spectral functions, but we have retained the general liquid dynamical structure function $S(\mathbf{k},\omega)$. If $\hat{R}_{\mathbf{k}}(\omega)$ is independent of ω in the vicinity of $\omega = \omega_{\mathbf{k}}$ the resulting lineshape is a simple Lorentzian. If the derivative $(d/d\omega)R_{\mathbf{k}}(\omega)$ in the vicinity of the absorption peak is large, the resulting band shape will depart considerably from a Lorentzian. From Eq. (131) we see that this would require a rapid change of the spectral functions for density and momentum excitations in passing from negative to positive frequencies. This is possible since the equation of detailed balance requires that

$$S(\mathbf{k},-\omega) = e^{-\beta\hbar\omega} S(\mathbf{k},\omega) \tag{132}$$

Our argument suggests that if we could observe a liquid at low temperatures, when β is large, the lineshape for the fluid would be non-Lorentzian but would tend to a Lorentzian as the temperature was raised. Of course, in any real system we are restricted to the range of β for which the fluid is still a fluid, and this effect may not be observable.

APPENDIX. Numerical Calculations of the Lineshape of a Transition in a Doped Crystal

A general expression for the shape of the absorption profile corresponding to an optical transition in an impurity molecule imbedded in a crystal is given in Eq. (72). In order to evaluate the profile function Re $\hat{G}_f(\omega)$ we require a knowledge of the coupling parameters $\{S_J^g\}_{J,g}$ and $\{F_J^{fg}\}_{J,g}$. Instead of a first principles evaluation of these parameters for a particular guest–host system, we present a simple model calculation of the linewidth in which S and F are variable parameters. With these results we can examine the general behavior of the absorption profile as a function of temperature.

The simple model system has the impurity molecule coupled to only two crystal modes, of energy 100 and 1000 cm^{-1}. The same values of S and F are associated with each mode. Only one other excited electronic state, g, is close enough to the state of interest, labeled f, to participate in phonon scattering. The gth electronic state is assumed to possess the same potential minima along each normal coordinate as does the ground state, i.e., $S_J^g = 0$.

In brief, we are calculating the linewidth of the fth electronic state caused by phonon assisted scattering of the excitation from f to a nearby

state g which may lie above or below f in energy. The feasibility of this process is measured by the parameter F. The parameter S measures the displacement on the minima of the potential curves along the normal coordinates corresponding to the modes of energy 100 and 1000 cm^{-1} (see Eq. (11)).

These choices of phonon energies were made because they are representative of a low frequency lattice mode (100 cm^{-1}) and an optical or intramolecular vibrational mode.

The half-width of the profile at half-height is simply Re $\hat{K}_f(\omega_f)$, and the spectral shift is formally available from Im $\hat{K}_f(\omega_f)$ via the relation cited in Eq. (73). In this model calculation we assume that the Re $\hat{K}_f(\omega)$ is a constant in the vicinity of ω_f (Lorentzian approximation), so the values of the half-widths are all evaluated at $\omega = \omega_f$.

If we denote the two modes by ω_1 and ω_2 the line shape half-width is given by

$$\begin{aligned}
&\frac{1}{\pi F^2}\,\mathrm{Re}\,\hat{K}_f(\omega_f) \\
&\quad = S\mathscr{J}_{fg}(0)[-1-\langle n(\omega_1)\rangle^2(1+\exp[2\beta\hbar\omega_1]) - \langle n(\omega_2)\rangle^2 \\
&\qquad \times (1+\exp[2\beta\hbar\omega_2])] + \sum_{j=1}^{2} \tfrac{1}{2}S\{\mathscr{J}_{fg}(2\omega_j) + \mathscr{J}_{fg}(-2\omega_j)\} \\
&\qquad \times \{1-\langle n(\omega_j)\rangle^2(1+\exp[2\beta\hbar\omega_j])\} \\
&\qquad + \sum_{j=1}^{2} \mathscr{J}_{fg}(\omega_j)[\langle n(\omega_j)\rangle + S(1-4\langle n(\omega_j)\rangle)] \\
&\qquad + \sum_{j=1}^{2} \mathscr{J}_{fg}(-\omega_j)[\langle n(\omega_j)\rangle + 1 + S(3-4\langle n(\omega_j)\rangle)] \\
&\qquad + S\{\mathscr{J}_{fg}(\omega_1-\omega_2) + \mathscr{J}_{fg}(\omega_2-\omega_1)\} \\
&\qquad \times \{-\langle n(\omega_1)\rangle\langle n(\omega_2)\rangle(1+\exp[\beta\hbar(\omega_1+\omega_2)])\} \\
&\qquad + S\{\mathscr{J}_{fg}(\omega_1+\omega_2) + \mathscr{J}_{fg}(-\omega_1-\omega_2)\} \\
&\qquad \times \{1-\langle n(\omega_1)\rangle\langle n(\omega_2)\rangle(1+\exp[\beta\hbar(\omega_1+\omega_2)])\} \qquad (A1)
\end{aligned}$$

We found that if the state g lies above f in energy, the scattering cited gives negligible contributions to the linewidth. This contribution increases as the temperature increases but is far too small to be observed.

On the other hand, if g is lower in energy than f, the contribution of the scattering process to the linewidth may be observable for an appropriate choice of S, F, and the energy of separation between f and g. The coupling

parameter F may be removed by an evaluation of the ratio of the linewidths at two different temperatures. Tables I and II show how slightly this ratio changes over a wide temperature range. Also given in these tables is the value of the linewidth at zero degrees. Choices of F in the range of 10 cm^{-1} give linewidths ranging from the negligible up to values of about 10 cm^{-1}.

Because of the crudeness of the model calculations, the results are meant to be used in only a qualitative or suggestive sense.

TABLE I[a]

Tabulation of the Ratio $[\mathrm{Re}\ \hat{K}_f(\omega_f)]_{T\cdot K}/[\mathrm{Re}\ \hat{K}_f(\omega_f)]_{0\cdot K}$. Separation of Electronic States = 4000 cm^{-1}.

	T					
S	0°	20°	50°	75°	105°	$[\mathrm{Re}\ \hat{K}_f(\omega_f)]_{0\cdot K}$ (cm^{-1})
0.1	1.0	1.0	1.0	1.0	0.98	$5.2 \times 10^{-4} F^2$
0.3	1.0	1.0	1.0	0.99	0.89	$1.2 \times 10^{-2} F^2$
0.7	1.0	1.0	0.99	0.84	0.65	$9.5 \times 10^{-2} F^2$
1.5	1.0	0.72	0.58	0.35	0.05	$0.31 F^2$

[a] Tabulation of the ratio of the line widths of various temperatures to those at zero degrees Kelvin for a range of choices of S. The linewidth at $T = 0°K$ requires F to be expressed in units of cm^{-1}.

TABLE II[a]

Tabulation of the Ratio $[\mathrm{Re}\ \hat{K}_f(\omega_f)]_{T\cdot K}/[\mathrm{Re}\ \hat{K}_f(\omega_f)]_{0\cdot K}$. Separation of Electronic States = 8000 cm^{-1}.

	T					
S	0°	20°	50°	75°	105°	$[\mathrm{Re}\ \hat{K}_f(\omega_f)]_{0\cdot K}$ (cm^{-1})
0.1	1.0	1.0	1.0	0.99	0.96	$6.39 \times 10^{-11} F^2$
0.3	1.0	1.0	1.0	0.94	0.84	$1.27 \times 10^{-7} F^2$
0.7	1.0	1.0	0.96	0.83	0.66	$3.02 \times 10^{-5} F^2$
1.5	1.0	0.85	0.74	0.57	0.36	$1.78 \times 10^{-3} F^2$

[a] Tabulation of the ratio of linewidths at various temperatures to those at zero degrees Kelvin for a range of choices of S. The linewidth at $T = 0°K$ requires F to be expressed in units of cm^{-1}.

Acknowledgments

This research was supported by the Directorate of Chemical Sciences, Air Force Office of Scientific Research. We have also benefited from the use of facilities supported by the Advanced Research Projects Agency for materials research at the University of Chicago.

References

1. D. N. Zubarev, *Usp. Fiz. Nauk*, **71**, 71 (1960) [*Soviet Phys. Usp.*, **3**, 320 (1960)]; D. ter Haar, in *Fluctuations, Relaxation and Resonance in Magnetic Systems*, D. ter Haar, Ed., Oliver and Boyd, London, 1962, p. 119.
2. A. A. Abrikosov, L. P. Gorkov, and I. E. Dzhaloshinski, *Methods of Quantum Field Theory in Statistical Physics*, Prentice-Hall, Englewood Cliffs, N.J., 1963.
3. R. Zwanzig, *J. Chem. Phys.*, **33**, 1338 (1960).
4. R. S. Wilson, W. T. King, and S. K. Kim, *Phys. Rev.*, **175**, 1164 (1968).
5. J. Schwinger, *Proc. Natl. Acad. Sci. U.S.*, **37**, 452 (1951); L. P. Kadanoff and G. Baym, *Quantum Statistical Mechanics*, Benjamin, New York 1962, and references therein.
6. See, for example, the review article by D. B. Fitchen in *Physics of Color Centers*, W. B. Fowler, Ed., Academic Press, New York, 1968, p. 293.
7. E. V. Shpol'skii, *Usp. Fiz. Nauk*, **77**, 321 (1962) [*Soviet Phys. Usp.*, **5**, 522 (1962)]; *Usp. Fiz. Nauk*, **71**, 215 (1960) [*Soviet Phys. Usp.*, **3**, 372 (1960)]; *Usp. Fiz. Nauk.*, **80**, 255 (1963) [*Soviet Phys. Usp.*, **6**, 411 (1963)].
8. For example, M. Born and K. Huang, *Dynamical Theory of Crystal Lattices*, Oxford Univ. Press, 1952.
9. A concise discussion of these two transformations is given by H. H. Jensen in *Phonons and Phonon Interactions*, T. Bak, Ed., Benjamin, New York, 1964, p. 1.
10. K. Huang and A. Rhys, *Proc. Royal Soc. (London)*, **204A**, 406 (1950); M. Lax, *J. Chem. Phys.*, **20**, 1752 (1952); R. C. O'Rourke, *Phys. Rev.* **91**, 265 (1953); A. A. Maradudin, *Solid State Phys.*, **18**, 273 (1966); D. E. McCumber, *J. Math. Phys.*, **5**, 221, 508 (1964); *Ibid.*, *Phys. Rev.*, **135**, A1676 (1964); Y. Toyozawa in *Dynamical Processes in Solid State Optics*, R. Kubo and H. Kaminura, Eds., Benjamin, New York, 1968, p. 90; A. E. Hughes, *Phys. Rev.*, **173**, 860 (1968).
11. T. H. Keil, *Phys. Rev.*, **140**, A605 (1965).
12. All the necessary definitions of polynomials and evaluation of integrals or infinite series which appear in these calculations are found in Gradsteyn and Ryzhik, *Table of Integrals, Series and Products*, Academic Press, New York, 1965.
13. The details of this derivation are given best by O'Rourke in Ref. 10 if one rewrites his final answer slightly.
14. A. Suna, *Phys. Rev.*, **135**, A111 (1964): E. I. Rashba, *Zh. Eksperim. i Teor. Fiz.*, **50**, 1064 (1966). [*Soviet Phys. JETP*, **23**, 708 (1966)]; A. S. Davydov, *Phys. Status Solidi*, **20**, 143 (1967); A. S. Davydov and B. M. Nitsovich, *Fiz. Tverd. Tela*, **9**, 2230 (1967) [*Soviet Phys.-Solid State*, **9**, 1749 (1968)]; S. Takeno, *J. Chem. Phys.*, **44**, 853 (1966); *Ibid.*, **46**, 2481 (1967); B. S. Sommer and J. Jortner, *J. Chem. Phys.*, **50**, 187, 822 829 (1969).
15. E. K. Kudinov and Yu. A. Firsov, *Zh. Eksperim. i Teor. Fiz.*, **47**, 601 (1964) [*Soviet Phys. JETP*, **20**, 400 (1965)].
16. S. Fischer, and S. A. Rice, *J. Chem. Phys.* in press.
    M. K. Grover, and R. Silbey, *J. Chem. Phys.* in press.

17. R. Zwanzig, *Ann. Rev. Phys. Chem.*, **16,** 67 (1965); R. Kubo, *J. Phys. Soc. Japan*, **12,** 570 (1957).
18. See, for example, M. Born and E. Wolf, *Principles of Optics*, Pergamon Press, New York, 1965.
19. Fourier and Laplace transforms are discussed in detail in P. M. Morse and H. Feshbach, *Methods of Theoretical Physics, Part I*, McGraw-Hill, New York, 1953.
20. Y. Toyozawa, *Progr. Theoret. Phys. (Kyoto)*, **27,** 89 (1962).
21. Most of the papers of Ref. 14 discuss this.
22. A. S. Davydov, *Usp. Fiz. Nauk*, **82,** 393 (1964) [*Soviet Phys., Usp.*, **7,** 145 (1964)].
23. S. A. Rice and J. Jortner, *J. Chem. Phys.*, **44,** 4470 (1966); G. Nicolis and S. A. Rice, *J. Chem. Phys.*, **46,** 4445 (1967); J. Popielawski and S. A. Rice, *J. Chem. Phys.*, **47,** 2292 (1967); S. A. Rice, G. Nicolis, and J. Jortner, *J. Chem. Phys.*, **48,** 2484 (1968); G. Nicolis, S. A. Rice, and J. Jortner, *J. Chem. Phys.*, **48,** 3544 (1968); S. A. Rice, *Accts. Chem. Res.*, **1,** 81 (1968).
24. L. Fiermans and P. Phariseau, *Physica*, **32,** 1966 (1968); W. Christiaens and P. Phariseau, *Physica*, **38,** 155 (1968).
25. S. Fischer and S. A. Rice, *Phys. Rev.*, **176,** 409 (1968).
26. L. Van Hove, *Phys. Rev.*, **95,** 249 (1954).
27. R. Zwanzig, *Phys. Rev.*, **156,** 190 (1967).

Advance in Chemical Physics, Volume XVII
Edited by I. Prigogine, Stuart A. Rice

AUTHOR INDEX

Numbers in parentheses are reference numbers and show that an author's work is referred to although his name is not mentioned in the text. Numbers in *italics* indicate the pages on which the full references appear.

Advance in Chemical Physics, Volume XVII
Edited by I. Prigogine, Stuart A. Rice

SUBJECT INDEX